Dissertation zur Erlangung des Doktorgrades
der Fakultät für Chemie und Pharmazie
der Ludwig-Maximilians-Universität München

Syntheses of Multinary Lithium (Oxo)nitridosilicates

Saskia Lupart

aus

Augsburg, Deutschland

2012

Erklärung

Diese Dissertation wurde im Sinne von § 7 der Promotionsordnung vom 28. November 2011 von Herrn Prof. Dr. W. Schnick betreut.

Eidesstattliche Versicherung

Diese Dissertation wurde eigenständig und ohne unerlaubte Hilfe erarbeitet.

München, 30.03.2012

.....

(Saskia Lupart)

Dissertation eingereicht am	30.03.2012
1. Gutacher	Prof. Dr. W. Schnick
2. Gutachter	Prof. Dr. O. Oeckler
Mündliche Prüfung am	26.04.2012

Meiner Familie

Acknowledgement

First of all, I would like to express my gratitude to Prof. Wolfgang Schnick for offering me this extremely interesting research project in his group. Especially I would like to thank him for the nice working atmosphere, the freedom in research, the trust he puts into his coworkers, his always open ear, the helpful and sometimes very funny discussions (because he obviously can make sense) and the continuing encouragement and support during this work.

For being my second referee, I thank Prof. O. Oeckler. Furthermore, I would like to thank him for support in almost all situations during my PhD as well as inspiring discussions and help with crystallographic questions.

I am thankful to Prof. H.-C. Böttcher, Prof. D. Johrendt, Prof. K. Karaghiosoff and Prof. W. Schmahl for being available as examiners in my *viva-voce*.

For analytical measurements and help with the hardware I would like to thank the following persons (in alphabetical order): Dr. P. Mayer, T. Miller, C. Minke, Prof. O. Oeckler, W. Wünschheim, and Dr. J. Schmedt auf der Günne.

For the conduction of lithium ion conductivity measurements and helpful discussions about this subject I would like to thank Prof. Dr. J. Maier and especially Dr. G. Gregori (both MPI Stuttgart) who is the best cooperation partner.

I am indebted to my research students: S. Johansson, K. Fenzke, D. Durach, E. Flügel and A. Zimpel. I want to thank especially D. Durach and wish her all the best for her master thesis and the following PhD thesis.

Special thanks to my lab-mates and the nice working atmosphere in lab D2.100. Especially to T. Schröder with whom I had the honor to share a bench although after all this time I am still not able to distinguish between all the metal-music styles; for me he is the best melodic death metal guy in the world. Furthermore, I would like to thank M. Seibald and F. Hintze for all the fun we had.

I would like to thank all my colleagues of the solid-state group for the nice working atmosphere and countless helpful discussions.

In detail I would like to thank Dr. S. Pagano who started the research field of lithium nitridosilicates (and the countless smoothies to activate my grey cells) and left some things to do for me. Great thanks go to Dr. M. Tegel who helped me a lot starting in the solid-state group. To Dr. S. Sedlmaier I am indebted for interesting discussions about almost everything, preferable accompanied by a good dinner with good wine. Dr. C. Höller I want to thank for all his encouraging “telephone-jokes”. Furthermore, I would like to thank Dr. A. Zurawski, with whom I had helpful discussions, but also a lot of fun. T. Rosenthal I thank for his always open ear. Thanks also go to F. Pucher who shares my hobby and joined me early Sunday mornings at the fish-market.

D. Baumann I thank for being my Glovebox-Buddy and the interesting discussions about the wonderful world of nitrogen. N. Braml, S. Schmiechen and P. Pust I would like to thank for the lunch pauses. S. Schmiechen I would like to thank further for trying out my ideas, although he had great doubts at first.

I would like to thank Matthias in whom I found true love and who supported and encouraged me during my thesis.

Above all I would like to thank my mother without her love, understanding and help in every situation I wouldn’t be here. Great thanks go to my sister, the best sister on the world.

I am among those who think that science has great beauty.

A scientist in his laboratory is not only a technician:

he is also a child placed before natural phenomena

which impress him like a fairy tale.

(Marie Curie)

1 Introduction 1

2 Lithium Alkaline-Earth Nitridosilicates 8

2.1 Overview 8

2.2 Tuning the Dimensionality of Nitridosilicates in Lithium Melts 13

2.2.1 Introduction 14

2.2.2 Results and Discussion 14

2.2.3 Conclusion 20

2.2.4 Experimental Section 20

2.2.4.1 X-ray diffraction 20

2.2.4.2 Solid-state MAS NMR 21

2.2.4.3 Microanalysis 21

2.2.4.4 Synthesis 21

2.2.5 References 22

2.3 $Li_4Ca_3Si_2N_6$ and $Li_4Sr_3Si_2N_6$ – Quaternary Lithium Nitridosilicates with Isolated $[Si_2N_6]^{10-}$ Ions 26

2.3.1 Introduction 27

2.3.2 Results and Discussion 27

2.3.3 Conclusions 31

2.3.4 Experimental Section 31

2.3.4.1 Synthesis 31

2.3.4.2 X-ray Diffraction 32

2.3.4.3 Microanalysis 32

2.3.5 References 33

2.4 $LiCa_3Si_2N_5$ – A Lithium Nitridosilicate with a $[Si_2N_5]^{7-}$ double-chain 34

2.4.1 Introduction 35

2.4.2 Results and Discussion 35

2.4.2.1 Crystal Structure Description 35

2.4.2.2 Lattice Energy Calculations According to the MAPLE Concept 39

2.4.2.3 Solid-state MAS NMR 40

2.4.3 Conclusions 42

2.4.4 Experimental Section 42

2.4.4.1 Synthesis 42

2.4.4.2 Chemical Analyses 43

2.4.4.3 Single Crystal X-ray Analysis 43

2.4.4.4 X-ray Powder Diffraction 43

2.4.4.5 Solid-state MAS NMR 44

2.4.5 References 44

2.5 $Li_2Sr_4[Si_2N_5]N$ – A Layered Lithium Nitridosilicate Nitride 46

2.5.1 Introduction 47

2.5.2 Results and Discussion 48

2.5.2.1 Synthetical Approach 48

2.5.2.2 Data Collection 48

2.5.2.3 Crystal Structure Description 49

2.5.2.4 Lattice Energy Calculations According to the MAPLE Concept 52

2.5.2.5 DFT Calculations 55

2.5.2.6 Comparison between Lattice Energy Calculations and DFT Calculations 56

2.5.3 Conclusions 56

2.5.4 Experimental Section 57

2.5.4.1 Synthesis 57

2.5.4.2 Chemical Analyses 59

2.5.4.3 Single Crystal X-ray Analysis 59

2.5.4.4 Computational Methods 59

2.5.5 References 60

3 Lithium Rare-Earth Nitridosilicates 63

3.1 Overview 63

3.2 Chain-Type Lithium Rare-Earth Nitridosilicates – $Li_5Ln_5Si_4N_{12}$ with Ln = La, Ce. 67

3.2.1 Introduction 68

3.2.2 Results and Discussion 69

3.2.2.1 Synthetical Approach 69

3.2.2.2 Crystal Structure 70

3.2.2.3 Solid-State MAS NMR 75

3.2.2.4 Lattice Energy Calculations According to the MAPLE Concept 76

3.2.3 Conclusions 77

3.2.4 Experimental Section 77

3.2.4.1 Synthesis 77

3.2.4.2 Chemical Analyses 78

3.2.4.3 Single Crystal X-ray Analysis 78

3.2.4.4 X-ray Powder Diffraction 79

3.2.4.5 Solid-State MAS NMR 80

3.2.5 References 81

3.3 $LiLa_5Si_4N_{10}O$ and $LiPr_5Si_4N_{10}O$ – Chain Type Oxonitridosilicates 83

3.3.1 Introduction 84

3.3.2 Results and Discussion 84

3.3.2.1 Synthesis and Crystal Structure 84

3.3.2.2 Solid-state MAS NMR 88

3.3.2.3 Lattice Energy Calculations According to the MAPLE Concept ... *89*
3.3.3 Conclusions ... 90
3.3.4 Experimental Section ... 91
3.3.4.1 Synthesis ... *91*
3.3.4.2 Chemical Analyses ... *91*
3.3.4.3 Single Crystal X-ray Analysis ... *92*
3.3.4.4 X-ray Powder Diffraction ... *92*
3.3.4.5 Solid-state MAS NMR ... *93*
3.3.5 References ... 94

3.4 $Li_{14}Ln_5[Si_{11}N_{19}O_5]O_2F_2$ with Ln = Ce, Nd – Representatives of a Family of Potential Lithium Ion Conductors ... 96
3.4.1 Introduction ... 97
3.4.2 Experimental Section ... 98
3.4.2.1 Synthesis ... *98*
3.4.2.2 Chemical Analysis ... *99*
3.4.2.2 Single Crystal X-ray Analysis ... *99*
3.4.2.3 X-ray Powder Diffraction ... *100*
3.4.2.4 Electrical Conductivity Measurements ... *101*
3.4.3 Results and Discussion ... 101
3.4.3.1 Synthesis and Crystal Structure ... *101*
3.4.3.2 Structural Analysis of Possible Lithium Migration Pathways ... *105*
3.4.3.3 Electrical Conductivity Measurements ... *105*
3.4.4 Conclusion ... 109
3.4.5 References ... 109

3.5 $Li_{35}Ln_9Si_{30}N_{59}O_2F$ with Ln = Ce, Pr - Highly Condensed Nitridosilicates ... 112
3.5.1 Introduction ... 113
3.5.2 Results and Discussion ... 114
3.5.2.1 Crystal structure description ... *114*
3.5.2.2 Lattice Energy Calculations According to the MAPLE Concept ... *117*
3.5.3 Conclusions ... 118
3.5.4 Experimental Section ... 119
3.5.4.1 Syntheses ... *119*
3.5.4.2 X-ray Diffraction ... *119*
3.5.4.3 Microanalysis ... *120*
3.5.5 References ... 120

4 Outlook ... 122

5 Summary ... 126

6 Appendix 131

6.1 Supporting Information for Chapter 2.2 ..... **131**

6.2 Supporting Information for Chapter 3.3 ..... **135**

6.3 Supporting Information for Chapter 3.4 ..... **137**

6.4 Supporting Information for Chapter 3.5 ..... **144**

7 Publications 148

8 Curriculum Vitae 152

1 Introduction

Almost two centuries ago, in 1817, the Swedish scientist Johann August Arfvedson discovered a new element in the mineral petalite ($LiAl(Si_2O_5)_2$).[1-3] As he found it in a silicate, he named it after the Greek word for stone (λίθος), lithium. Although he was not able to isolate lithium, one year later William Thomas Brande and Sir Humphrey Dave were able to extract smaller amounts of elemental lithium by electrolysis of Li_2O.[1,2] In the first years after its discovery lithium was more or less treated as a new curiosity in the periodic table of elements with no obvious applications. However, in 1855 larger amounts of the alkali metal became available by electrolysis of LiCl, and early experiments did yield first indications of the latter importance of lithium for mankind.[2] Not only its very low density (0.534 g/ cm) and high specific heat were discovered, but in addition first experiments to use lithium as additive for ceramics were conducted. However, these early applications were far away from broad industrial applications.

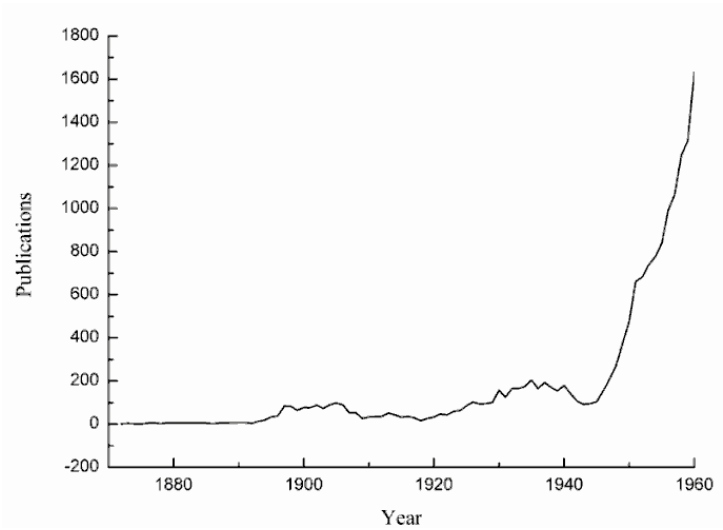

Figure 1. Publications per year, which contain the keyword „lithium“.[4]

With the beginning of World War II lithium got in the focus of research for novel materials and a systematic investigation of lithium compounds began (Figure 1).[2] Especially with the upraising of rocketry the need for new grease materials, which resist extreme temperatures, came along and lithium stearates proved to be excellent for this purpose and are still in use (Figure 2).[2] In the last years of World War II the race for the nuclear bomb began and – as lithium is needed for the safe storage of heavy hydrogen (^6LiD) in nuclear weapons and for the reaction to tritium - with it the rapidly increasing importance of lithium and its compounds.[5,6] This trend lasts until nowadays, where due to the question of energy management in our society a search for alternative energies and storage systems began. Lithium batteries moved into the focus of research as their efficiency makes them promising candidates for the solution of the problem of energy storage.[7-9] In addition, lithium is used for manifold applications as shown in

Figure 2. Therefore, lithium is currently one of the elements with the fastest growing demand rate.

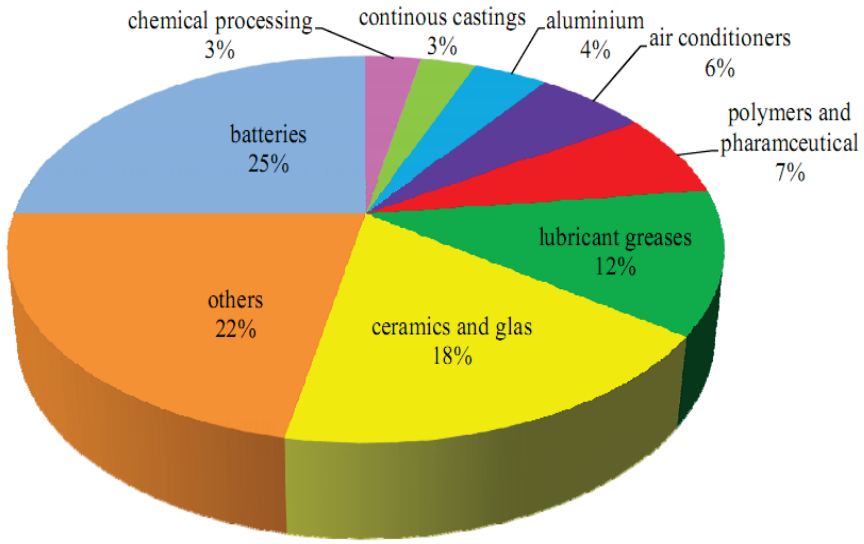

Figure 2. Utilization of lithium compounds (situation in 2007).[10]

When lithium started to gain importance Juza et al. studied 1953 the quasi binary system LiN_3-Si_3N_4.[11] During this research he discovered a novel compound class, namely the first nitridosilicates. However, only with the growing technological relevance of non-oxidic materials such as Si_3N_4 and AlN as high performance ceramics decades later, nitridosilicates and other nitridic compounds gained again focus in the scientific world and a systematic investigation of nitridosilicates took place.[12-14]

As a direct consequence of the abundance of oxygen in our world, nitridosilicates do not occur naturally. The only exception is the mineral sinoite which has however meteoritic origin.[15,16] The difference between oxo- and nitridosilicates is not a simple substitution of O by N. On the one hand Si-N bonding is generally weaker than Si-O, which is also the reason why a lot of nitridosilicates hydrolyze in air, if they are not kinetically hindered. On the other hand the covalent character of nitridosilicates is higher compared to oxosilicates and therefore other bonding situations occur.

From a structural point of view nitridosilicates could exhibit a higher structural diversity as oxosilicates. Oxosilicates are limited to terminally ($O^{[1]}$) or simply bridging ($O^{[2]}$) positions. In contrast to that nitrogen can also connect three tetrahedra centers ($N^{[3]}$) and even four tetrahedra ($N^{[4]}$) by adopting ammonia character.[17,18] Moreover, both edge-sharing and corner-sharing of [SiN_4] tetrahedra can occur in nitridosilicates.[17,19] In oxosilicates edge

sharing has only been postulated for so-called fibrous SiO_2 but has not been unequivocally proven, yet.[20] The different connectivities do not exclude each other, hence they can be observed side by side in nitridosilicate structures.[19,21] As a direct consequence of the structural variety of nitridosilicates a higher degree of condensation (κ) can be achieved. Whereas in oxosilicates κ has an upper limit of ½ as in SiO_2 in nitridosilicates κ can reach values up to ¾, e.g. in Si_3N_4. The lowest value of κ is ¼ which corresponds to isolated $[SiO_4]^{4-}$ and $[SiN_4]^{8-}$, respectively.[17,22]

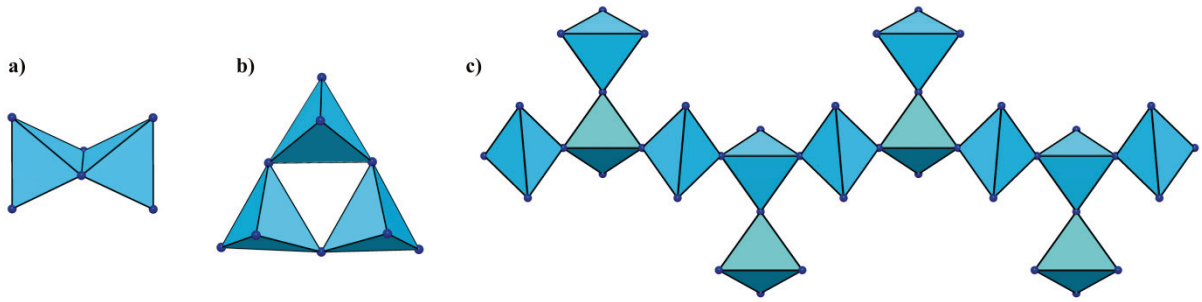

Figure 3. a) Bow-tie units $[Si_2N_6]^{10-}$ of $Ba_5Si_2N_6$; b) isolated *dreier* rings of $Pr_9Se_6Si_3N_9$; c) branched chain in $Ln_5Si_3N_9$ (Ln = La, Ce, Pr). $[SiN_4]$ tetrahedra blue, nitrogen atoms dark blue.

This higher structural diversity and different bonding characteristics of nitridosilicates compared to oxosilicates can lead to interesting properties. For example, nitridosilicates can exhibit a great hardness due to higher covalency of bonds, e.g. $SrSi_7N_{10}$ exhibits a Vickers hardness of 16.1(5) GPa.[23] Furthermore, nitridosilicates can be applied as heat sink materials owing to their high thermal conductivity[24,25] or in optical devices due to nonlinear optical properties.[26,27] One of the most important recent applications of nitridosilicates is the utilization as inorganic phosphors.[17,28] Several (oxo)nitridosilicates are highly efficient phosphors upon doping with Eu^{2+} or Ce^{3+}.[29-32] Due to their properties (oxo)nitridosilicates are an ideal compound class for utilization in phosphor converted (pc)-LEDs.[17] As these materials exhibit high chemical and thermal stability and a high luminous efficacy, some (oxo)nitridosilicates such as $M_2Si_5N_8$ (M = Ca, Sr, Ba)[32] and $MSi_2O_2N_2$ (M = Ca, Sr, Ba)[30,33] already have industrial application.[28,29] Tailor-made tuning of the emission wavelength is possible, by either applying solid solutions or co-doping of the materials. As a plethora of different structures in this compound class exists, the whole visible spectrum is accessible.[17]

However, until recently primarily highly condensed nitridosilicates ($\kappa > 0.5$) were known. Some of the rare exceptions were $Ln_5Si_3N_9$ with Ln = La, Ce, Pr (chain-type silicate; Figure 3c),[34,35] $Pr_9Se_6Si_3N_9$ (ring-type silicate; Figure 3b),[36] and $Ba_5Si_2N_6$ which contains bow-tie units of edge-sharing $[Si_2N_6]^{10-}$ tetrahedra (Figure 3a).[37] The latter has been synthesized at moderate temperatures (750 °C) in liquid sodium as fluxing agent combined with NaN_3 – a route which has been initially established for the syntheses of AlN and GaN.[38] This leads to the implication that with the "classical" synthesis conditions which require high temperatures (> 1200 °C) mainly thermodynamic stable phases with highly condensed nitridosilicate networks result. The use of fluxing agents, in contrast, allows for the reduction of the synthesis temperatures as atomic mobility is facilitated in the flux. Hence, access to kinetically controlled products and low condensed silicate substructures might be expected from this synthetic approach. However, in contrast to e.g. barium various metals and especially silicon exhibit a bad solubility in liquid sodium at moderate temperatures.[39] In contrast, various metals, silicon and nitrogen are adequately soluble in lithium rich systems at moderate temperatures.[6] The stability of the binary nitrides of sodium and lithium is also rather different. Whereas Na_3N is not formed under normal conditions, Li_3N is an easily accessible compound. This implies that lithium can be regarded as nitride acceptor which might be one of the reasons that lithium is often a reactive flux concerning syntheses of nitridic compounds, resulting in lithium containing products.

Due to the reasons mentioned above lithium flux is ideally suitable for the synthesis of novel lithium containing and also low condensed nitridosilicates, which might combine the excellent properties of nitridosilicates with the properties of lithium compounds. Since the syntheses of the first ternary lithium nitridosilicates by Juza et al. the system Li-Si-N has been well investigated and nowadays several lithium nitridosilicates are known, e.g. $LiSi_2N_3$,[40] Li_2SiN_2,[41-43] Li_5SiN_3,[11,44] Li_8SiN_4,[45] $Li_{18}Si_3N_{10}$ and $Li_{21}Si_3N_{11}$,[45] which all exhibit lithium ion conductivity.[46] Recently, doping of $LiSi_2N_3$ with Ca^{2+} showed that the Li^+ ion conductivity can be enhanced with increasing calcium content.[47] Therefore, not only from a structural point of view but also concerning applications multinary lithium nitridosilicates might be very promising.

The first part of this thesis deals with the synthesis of novel quaternary alkaline-earth nitridosilicates with different dimensionalities concerning the silicate substructure. In the second part the synthetical route using liquid lithium as fluxing agent has been extended to lithium rare-earth (oxo)nitridosilicates including also highly condensed silicate structures with

triply bridging $N^{[3]}$ synthesized at moderate temperatures. The completion of this work is the further extension of lithium flux away from closed reaction systems (e.g. tantalum ampoules) to open systems to obtain higher amounts of the samples and an investigation of the lithium ion conductivity of the novel compound $Li_{14}Ln_5[Si_{11}N_{19}O_5]O_2F_2$.

References

[1] H. H. Binder, *Lexikon der chemischen Elemente: das Periodensystem in Fakten, Zahlen und Daten*, S. Hirzel, Stuttgart, **1999**.

[2] P. Enhag, *Encyclopedia of the Elements*, Wiley-VCH, Weinheim, **2004**.

[3] Q.-S. Hans-Jürgen, *Die Welt der Elemente - die Elemente der Welt*, Wiley-VCH, Weinheim, **2006**.

[4] Publication numbers are given as results according to a keyword search ("lithium") on the SciFinder database (http:www.scifinder.cas.org); visited 19th October 2011.

[5] R. Rhodes, *The Making of the Atomic Bomb*, Simon & Schuster, New York, **1986**.

[6] R. J. Pulham, P. Hubberstey, *J. Nucl. Mater.* **1983**, *115*, 239-250.

[7] A. D. Robertson, A. R. West, A. G. Ritchie, *Solid State Ionics* **1997**, *104*, 1-11.

[8] M. S. Whittingham, *Chem. Rev.* **2004**, *104*, 4271-4301.

[9] J. F. M. Oudenhoven, L. Baggetto, P. H. L. Notten, *Adv. Energy Mater.* **2011**, *1*, 10-33.

[10] Scheme according to the data of: L. Gaines, P. Nelson, *Fact Sheet: Lithium-Ion Batteries: Possible Material Demand Issues*, Argonne National Laboratory, Argonne, IL, **2009**.

[11] R. Juza, H. H. Weber, E. Meyer-Simon, *Z. Anorg. Allg. Chem.* **1953**, *273*, 48-64.

[12] H. Lange, G. Wötting, G. Winter, *Angew. Chem.* **1991**, *103*, 1606-1625; *Angew. Chem., Int. Ed. Engl.* **1991**, 16*30*, 1579-1597.

[13] K. Kim, W. R. L. Lambrecht, B. Segall, *Phys. Rev. B* **1996**, *53*, 16310-16326.

[14] W. Schnick, *Angew. Chem.* **1993**, *105*, 846-858; *Angew. Chem., Int. Ed. Engl.* **1993**, *33*, 806-818.

[15] A. Bischoff, T. Grund, T. Jording, B. Heying, R.-D. Hoffmann, U. C. Rodewald, R. Pöttgen, *Z. Naturforsch. B* **2005**, *60*, 1231-1234.

[16] W. H. Baur, *Nature* **1972**, *240*, 461-462.

[17] M. Zeuner, S. Pagano, W. Schnick, *Angew. Chem.* **2011**, *123*, 7898-7920; *Angew. Chem. Int. Ed*. **2011**, 78*50*, 7754-7775.

[18] W. Schnick, H. Huppertz, *Chem. Eur. J.* **1997**, *3*, 679-683.

[19] H. Huppertz, W. Schnick, *Chem. Eur. J.* **1997**, *3*, 249-252.

[20] A. Weiss, A. Weiss, *Z. Anorg. Allg. Chem.* **1954**, *276*, 95-112.

[21] F. Ottinger, R. Nesper, *Z. Anorg. Allg. Chem.* **2005**, *631*, 1597-1602.

[22] F. Liebau, *Naturwissenschaften* **1962**, *49*, 481-490.

[23] G. Pilet, H. A. Höppe, W. Schnick, S. Esmaeilzadeh, *Solid Sate Sci.* **2005**, *7*, 391-396.

[24] G. A. Slack, *J. Phys. Chem. Solids* **1973**, *34*, 321-335.

[25] M. Kitayama, K. Hirao, K. Watari, M. Toriyama, S. Kanzaki, *J. Am. Ceram. Soc.* **2001**, *84*, 353-358.

[26] S. R. Marder, G. D. Stucky, J. E. Sohn, *Materials for Nonlinear Optics: Chemical Perspectives*, ACS Symp. Ser., **1991**.

[27] H. Lutz, S. Joosten, J. Hoffmann, P. Lehmeier, A. Seilmeier, H. A. Höppe, W. Schnick, *J. Phys. Chem. Solids* **2004**, *65*, 1285-1290.

[28] W. Schnick, *Phys. Status Solidi RRL A* **2009**, *3*, 113-114.

[29] R. Mueller-Mach, G. Mueller, M. R. Krames, H. A. Höppe, F. Stadler, W. Schnick, T. Juestel, P. Schmidt, *Phys. Status Solidi A* **2005**, *202*, 1727-1732.

[30] V. Bachmann, C. Ronda, O. Oeckler, W. Schnick, A. Meijerink, *Chem. Mater.* **2009**, *21*, 316-325.

[31] R.-J. Xie, N. Hirosaki, *Sci. Technol. Adv. Mater.* **2007**, *8*, 588-600.

[32] H. A. Höppe, H. Lutz, P. Morys, W. Schnick, A. Seilmeier, *J. Phys. Chem. Solids* **2000**, *61*, 2001-2006.

[33] Y. Q. Li, G. deWith, H. T. Hintzen, *J. Solid State Chem.* **2008**, *181*, 515-524.

[34] C. Schmolke, D. Bichler, D. Johrendt, W. Schnick, *Solid State Sci.* **2009**, *11*, 389-394.

[35] S. Lupart, W. Schnick, *Acta Crystallogr. E* **2009**, *65*, i43.

[36] F. Lissner, T. Schleid, *Z. Anorg. Allg. Chem.* **2004**, *630*, 2226-2230.

[37] H. Yamane, F. J. DiSalvo, *J. Alloys Compd.* **1996**, *240*, 33-36.

[38] M. G. Kanatzidis, R. Pöttgen, W. Jeitschko, *Angew. Chem.* **2005**, *117*, 7156-7184; *Angew. Chem., Int. Ed.* **2005**, 71*43*, 6996-7023.

[39] P. Hubberstey, P. G. Roberts, *J. Chem. Soc. Dalton Trans.* **1994**, 667-673.

[40] M. Orth, W. Schnick, *Z. Anorg. Allg. Chem.* **1999**, *625*, 1426-1428.

[41] S. Pagano, M. Zeuner, S. Hug, *Eur. J. Inorg. Chem.* **2009**, 1579-1584.

[42] B. Song, J. K. Jian, G. M. Cai, M. Lei, H. Q. Bao, H. Li, Y. P. Xu, W. Y. Wang, J. C. Han, X. L. Chen, *Solid State Ionics* **2009**, *180*, 29-35.

[43] A. J. Anderson, R. G. Blair, S. M. Hick, R. B. Kaner, *J. Mater. Chem.* **2006**, *16*, 1318-1322.

[44] A. T. Dadd, P. Hubberstay, *Dalton Trans.* **1982**, 2175-2179.

[45] J. Lang, J.-P. Charlot, *Rev. Chim. Miner.* **1970**, *7*, 121-131.

[46] H. Yamane, S. Kikkawa, M. Koizumi, *Solid State Ionics* **1987**, *25*, 183-191.

[47] E. Narimatsu, Y. Yamamoto, T. Takeda, T. Nishimura, N. Hirosaki, *J. Mater. Res.* **2011**, *26*, 1133-1142.

2 Lithium Alkaline-Earth Nitridosilicates

2.1 Overview

The compound class of alkaline-earth nitridosilicates has been thoroughly investigated in the last years. In this context, the series $MSiN_2$ with M = Zn, Mn, Be, Mg, Ca, Sr, and Ba could be structurally elucidated.[1-6] Although all members of this series exhibit the same sum formula and therefore a condensation-degree of $\kappa = ½$, which would indicate a three-dimensional network in oxosilicates, the structural chemistry is rather diverse. With the heavier alkaline-earth elements Sr and Ba layer-like silicates with edge-sharing tetrahedra are formed.[1] $SrSiN_2$ and $BaSiN_2$ exhibit similar layers, which are distorted in the case of $SrSiN_2$ due to the smaller ionic radius of Sr^{2+} compared to Ba^{2+}. The lighter homologues $MSiN_2$ with M = Zn, Be, Mg, Ca, Mn exhibit a three-dimensional network with exclusively corner-sharing $[SiN_4]$ tetrahedra. $CaSiN_2$ can be derived from the (distorted) β-cristobalite-type,[1] whereas $MSiN_2$ with M = Zn, Be, Mg, Mn crystallize in a cation-ordered wurtzite-type structure.[2-5] Another important representative of alkaline-earth nitridosilicates is the so-called 2-5-8 family, $M_2Si_5N_8$ with M = Ca, Ba, Sr, and Eu.[7,8,9] These materials gained industrial application due to their remarkable luminescence properties upon doping with Eu^{2+} (Chapter 1).[10,11] In this family the heavier analogues (Sr^{2+} and Ba^{2+}) and Eu^{2+}, the latter exhibiting a similar ionic radius as Sr^{2+}, also crystallize in isotypic structures. The networks consist of corner-sharing $[SiN_4]$ tetrahedra, where half of the nitrogen atoms connect two ($N^{[2]}$) and the other half three ($N^{[3]}$) tetrahedral centers. The smaller ionic radius of Ca^{2+} causes a diferent topology, where the distribution of the ring sizes (Si/N) in the networks differs significantly. The isotypic compounds MSi_6N_8 with M = Sr, Ba contain Si-Si bonds and represent therefore nitridosilicates with Si in the oxidation states +III and +IV. These first examples of reduced nitridosilicates contain a three-dimensional network with corner sharing $[SiN_4]$ tetrahedra and $N_3Si\text{-}SiN_3$ units.[12,13]

These examples may clarify the fact, that alkaline-earth nitridosilicates exhibit a high structural diversity, however, low condensed alkaline-earth nitridosilicates are scarcely known. One of the rare exceptions is Li_8SiN_4, for which isolated $[SiN_4]^{8-}$ tetrahedra are postulated, however, the crystal structure has not been unequivocally proven, yet.[14] The only structurally verified examples with low condensed silicate substructures contain bow-tie units $[Si_2N_6]^{10-}$ of edge-sharing double tetrahedra. This structural feature has been identified in

$M_5Si_2N_6$ with M = Ca, Ba,[15,16] $Ca_7[NbSi_2N_9]$[17] and $Li_4M_3Si_2N_6$ with M = Ca, Sr.[18] The latter compounds are also topics of this thesis, as the Ca-compound has been investigated in this work (Chapter 2.3).

It is assumed that the group of mostly only highly condensed nitridosilicates (2D and 3D) in conventional syntheses is due to the necessary high temperatures (> 1200 °C). To obtain also low condensed nitridosilicates the use of lithium as fluxing agent in closed systems like Nb or Ta ampoules is very promising. Due to the high solubility of alkaline-earth elements in lithium at moderate temperatures, it is possible to apply reaction temperatures below 1000 °C, but still obtain high atomic mobility necessary to form novel compounds. Both alkaline-earth elements Ca and Sr can be dissolved in lithium at 300 °C in melts containing over 60 atom% Li, as indicated by the binary phase diagrams shown in Figure 1.

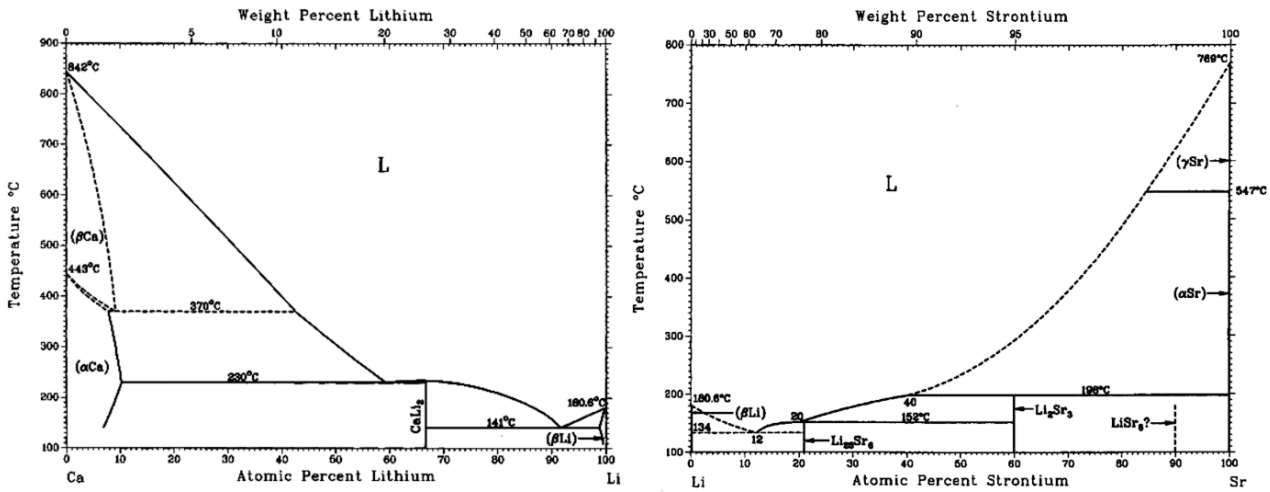

Figure 1. Phase diagrams for the system Li-Ca (left) and Li-Sr (right).[19,20]

Table 1 shows an overview of lithium alkaline-earth nitridosilicates, which were synthesized utilizing lithium as fluxing agent. With this synthetic route, now the whole range of dimensionality can be accessed. Additionally, according to our experience, the degree of condensation can be controlled by the atomic ratio of Li/ Li_3N/ LiN_3 (Chapter 2.2). The compounds $Li_4M_3Si_2N_6$ (M = Ca, Sr) and $LiCa_3Si_2N_5$ were both synthesized at 900 °C without LiN_3. However, for the synthesis of $Li_4M_3Si_2N_6$ with (M = Ca, Sr) a higher atomic ratio Li_3N : Li is necessary, which seems to suppress the one-dimensional structure of $LiCa_3Si_2N_5$ (Chapter 2.4). The addition of LiN_3 raises the nitrogen pressure inside the

ampoules (as LiN_3 decomposes into Li and N_2 at temperatures between 185-220 °C)[21] and favors the three-dimensional structures of $Li_2MSi_2N_4$ with M = Ca, Sr (Figure 2).[22]

Table 1. Overview of structurally elucidated lithium alkaline-earth nitridosilicates synthesized in lithium as fluxing agent. Written in italics are the compounds, which were synthesized during this thesis. The other compounds were described by *Pagano* and *Zeuner*.

0D	1D	2D	3D
$Li_4Ca_3Si_2N_6$	*$LiCa_3Si_2N_5$*	*$Li_2Sr_4[Si_2N_5]N$*	$Li_2CaSi_2N_4$[22]
$Li_4Sr_3Si_2N_6$[18]			$Li_2SrSi_2N_4$[22]
			$Li_2Sr_4Si_4N_8O$[23]

Annealing experiments with the band-silicate $LiCa_3Si_2N_5$ revealed that after several days at 900 °C only $Li_4Ca_3Si_2N_6$ (0D) and $Li_2CaSi_2N_4$ (3D) could be obtained. This leads to the conclusion, that $LiCa_3Si_2N_5$ is metastable in the thermodynamic series $Li_4Ca_3Si_2N_6$ - $LiCa_3Si_2N_5$ - $Li_2CaSi_2N_4$. This seems not surprising as the usage of fluxing agents gives access to thermodynamic as well as kinetic products. It could also be shown, that upon applying pressure (5 GPa) on $Li_4Ca_3Si_2N_6$ or $LiCa_3Si_2N_5$ the three-dimensional nitridosilicate $Li_2CaSi_2N_4$ can be obtained.

The layer nitridosilicate nitride $Li_2Sr_4[Si_2N_5]N$ (Chapter 2.5) has been synthesized using CsI as catalyst. In contrast, $Li_2Sr_4Si_4N_8O$ (Figure 2) has been synthesized by *Pagano* with additional Li_2O, which is incorporated in the crystal structure. Due to the syntheses in lithium flux, the exact reaction mechanism for the compounds is hard to predict. However, the comparison of these two examples shows that the possibilities of this synthetic route are enormous.

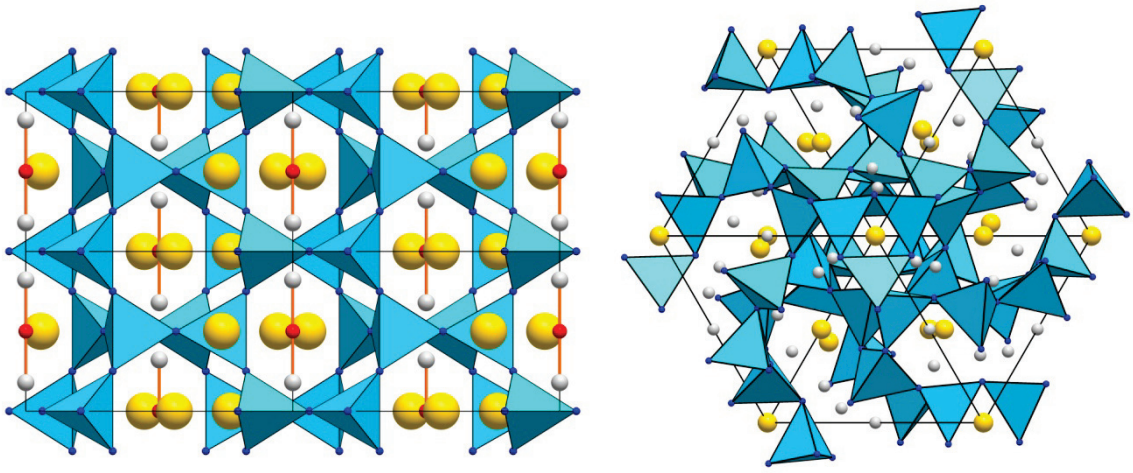

Figure 2. Crystal structure of $Li_2Sr_4Si_4N_8O$ (left), and $Li_2MSi_2N_4$ with M = Ca, Sr (right). $[SiN_4]$ tetrahedra light blue; Sr, Ca yellow, oxygen red and lithium light gray.

References

[1] Z. A. Gál, P. M. Mallinson, H. J. Orchard, S. J. Clarke, *Inorg. Chem.* **2004**, *43*, 3998-4006.

[2] T. Endo, Y. Sato, H. Takizawa, M. Shimada, *J. Mater. Sci. Lett.* **1992**, *11*, 424-426.

[3] M. Winterberger, R. Marchand, M. Maunaye, *Solid State Commun.* **1977**, *21*, 733-735.

[4] P. Eckerlin, A. Rabenau, H. Nortmann, *Z. Anorg. Allg. Chem.* **1967**, *353*, 113-121.

[5] P. Eckerlin, A. Rabenau, H. Nortmann, *Z. Anorg. Allg. Chem.* **1967**, *353*, 225-235.

[6] J. David, Y. Laurent, J. Lang, *Bull. Soc. Fr. Mineral. Cristallogr.* **1970**, *93*, 153-159.

[7] T. Schlieper, W. Schnick, *Z. Anorg. Allg. Chem.* **1995**, *621*, 1037-1041.

[8] T. Schlieper, W. Milius, W. Schnick, *Z. Anorg. Allg. Chem.* **1995**, *621*, 1380-1384.

[9] H. Huppertz, W. Schnick, *Acta Crystallogr., Sect. C: Cryst. Struct. Commun.* **1997**, *53*, 1751-1753.

[10] W. Schnick, *Phys. Status Solidi RRL* **2009**, *3*, A113-A114.

[11] R. Mueller-Mach, G. Mueller, M. R. Krames, H. A. Höppe, F. Stadler, W. Schnick, T. Juestel, P. Schmidt, *Phys. Status Solidi A* **2005**, *202*, 1727-1732.

[12] F. Stadler, O. Oeckler, J. Senker, H. A. Höppe, P. Kroll, W. Schnick, *Angew. Chem.* **2005**, *117*, 573-576; *Angew. Chem., Int. Ed.* **2005**, **20***44*, **2**567-**2**570.

[13] F. Stadler, W. Schnick, *Z. Anorg. Allg. Chem.* **2007**, *633*, 589-592.

[14] J. Lang, J.-P. Charlot, *Rev. Chim. Miner.* **1970**, *7*, 121-131.

[15] F. Ottinger, R. Nesper, *Z. Anorg. Allg. Chem.* **2005**, *631*, 1597-1602.

[16] H. Yamane, F. J. DiSalvo, *J. Alloys Compd.* **1996**, *240*, 33-36.

[17] F. Ottinger, R. Nesper, *Z. Anorg. Allg. Chem.* **2005**, *631*, 1597-1602.

[18] S. Pagano, S. Lupart, S. Schmiechen, W. Schnick, *Z. Anorg. Allg. Chem.* **2010**, *636*, 1907-1909.

[19] C. W. Bale, A. D. Pelton, *J. Phase Equilib.* **2003**, *24*, 296-298.

[20] C. W. Bale, A. D. Pelton, *J. Phase Equilib.* **1987**, *8*, 125-127.

[21] E. G. Prout, V. C. Liddiard, *J. Inorg. Nucl. Chem.* **1973**, *35*, 2183-2193.

[22] M. Zeuner, S. Pagano, S. Hug, P. Pust, S. Schmiechen, C. Scheu, W. Schnick, *Eur. J. Inorg. Chem.* **2010**, 4945-4951.

[23] S. Pagano, S. Lupart, M. Zeuner, W. Schnick, *Angew. Chem.* **2009**, *121*, 6453-6456; *Angew. Chem., Int. Ed. Engl.* **2009**, *48*, 6335-6338.

2.2 Tuning the Dimensionality of Nitridosilicates in Lithium Melts

published in Sandro Pagano, Saskia Lupart, Martin Zeuner, and Wolfgang Schnick

Angew. Chem. **2009**, *121* (34), 6453-6456;
Angew. Chem. Int. Ed. **2009**, *48* (34), 6335-6338;
DOI: 10.1002/ange.200902594
Copyright © 2009 WILEY-VCH Verlag GmbH & Co. KGaA, Weinheim
http://onlinelibrary.wiley.com/doi/10.1002/ange.200902594/abstract
http://onlinelibrary.wiley.com/doi/10.1002/anie.200902594/abstract

Convenient access to nitridosilicates with the whole range of dimensionality known for silicates is provided by synthesis in molten lithium in welded-shut tantalum ampoules. For example, $Li_4Ca_3Si_2N_6$ consists of edge-sharing "bow-tie" $[Si_2N_6]^{10-}$ units, $LiCa_3Si_2N_5$ has an edge-sharing double-chain and channels occupied by Li^+ ions, and $Li_2Sr_4Si_4N_8O$ exhibits a zeolite-analogous structure due to inclusion of Li_2O (see picture).

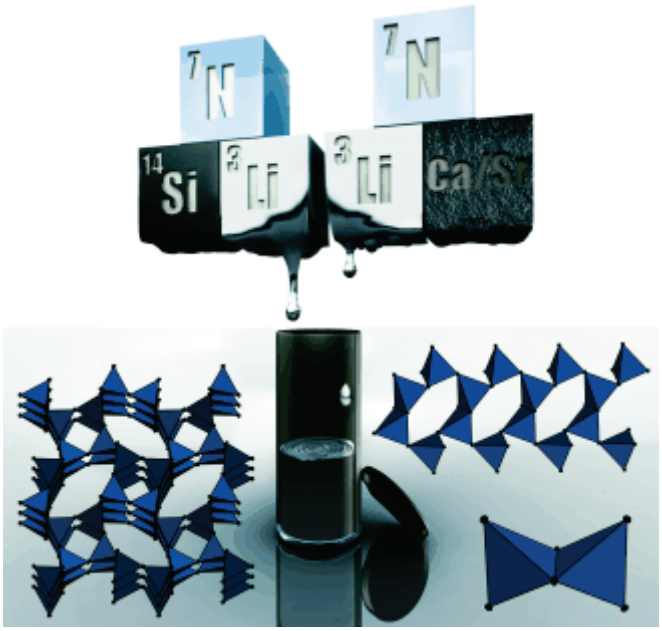

2.2.1 Introduction

Owing to their large scope of materials properties, such as luminescence, lithium ion conductivity, and nonlinear optical properties, nitridosilicates have attracted broad academic and industrial interest.[1–6] In particular, doping of alkaline earth metal nitridosilicates (e.g., $M_2Si_5N_8$, $MSi_2N_2O_2$; M = Ca, Sr, Ba) with Eu^{2+} has pushed the borders of luminescent materials industrially used in phosphor-converted warmwhite LEDs.[7–10] The majority of hitherto-investigated nitridosilicates are three-dimensional framework silicates, obtained by high-temperature reactions starting from the respective metals and silicon nitride or silicon diimide ($Si(NH)_2$).[2,11,12] Introduction of oxygen into nitridosilicates seems to favor layer-like oxonitridosilicates (e.g., $MSi_2N_2O_2$,[7,13] $Ba_3Si_6N_4O_9$).[14] However, there is still a significant lack of less condensed or even metal-rich nitridosilicates. In this context $RE_5Si_3N_9$ (RE=La, Ce) is the only chain-type[15] and $Pr_9Se_6[Si_3N_9]$ the only ring-type[16] nitridosilicate reported so far. The predominance of highly condensed Si/N substructures may be a consequence of the high-temperature reactions that have been mostly employed for the synthesis of nitridosilicates. Under such conditions, highly condensed nitridosilicates seem to be energetically or kinetically favored over less condensed substructures. Accordingly, it is not surprising that the first group-type nitridosilicate, namely, $Ba_5Si_2N_6$, was synthesized in sodium melts at surprisingly low temperature (760 °C).[17] This synthetic approach employing liquid sodium as a flux and decomposition of sodium azide as nitrogen source has also afforded structurally elucidated $MSiN_2$ (M = Ca, Sr, Ba).[18]

2.2.2 Results and Discussion

During our search for a complementary approach and low-temperature routes to less condensed nitridosilicates, we targeted a series of precursor compounds[19,20] and flux methods,[21] ending up with the idea to utilize liquid lithium, which has been effectually used for the synthesis of borides and carbides.[22–24] Interest in liquid lithium incipiently stems from its proposed use as a tritium breeder and/or primary coolant in several designs of the deuterium/tritium-fuelled thermonuclear reactor.[25] Thus, substantial knowledge is available about the reactivity of lithium melts with silicon and/or nitrogen.[26] According to these investigations silicon and nitrogen dissolve to a comparable extent in lithium at elevated temperatures.[26] Systematic investigations in the system Li/Si/N already have afforded a number of ternary lithium nitridosilicates with interesting material properties, for example,

lithium ion conductivity.[3,26–28] These findings distinguish nitride chemistry in lithium from nitride chemistry in sodium, in which silicon and nitrogen are only sparingly soluble. The nitrogen uptake of liquid sodium is improved if alkaline earth metals are added, as reported by Simon and coworkers during their studies on subnitrides (e.g., $NaBa_3N$).[29] In an investigation of the reaction between liquid lithium containing dissolved alkaline earth metals and low nitrogen contents, a homogenous solution of Li/M/N (M = Ca, Sr, Ba) was found.[30] In summary, applicable solubility has been reported in the systems Li/Si/N and Li/M/N. Thus, it was intriguing to combine these systems and utilize the solubilities for the synthesis of quaternary lithium alkaline earth nitridosilicates. Although the addition of Li to sodium melts has led to quaternary phases in the field of nitridogallates and -germanates (e.g., $LiCaGaN_2$,[31] $Li_4Sr_3Ge_2N_6$),[32] no lithium alkaline earth metal nitridosilicates are known so far.

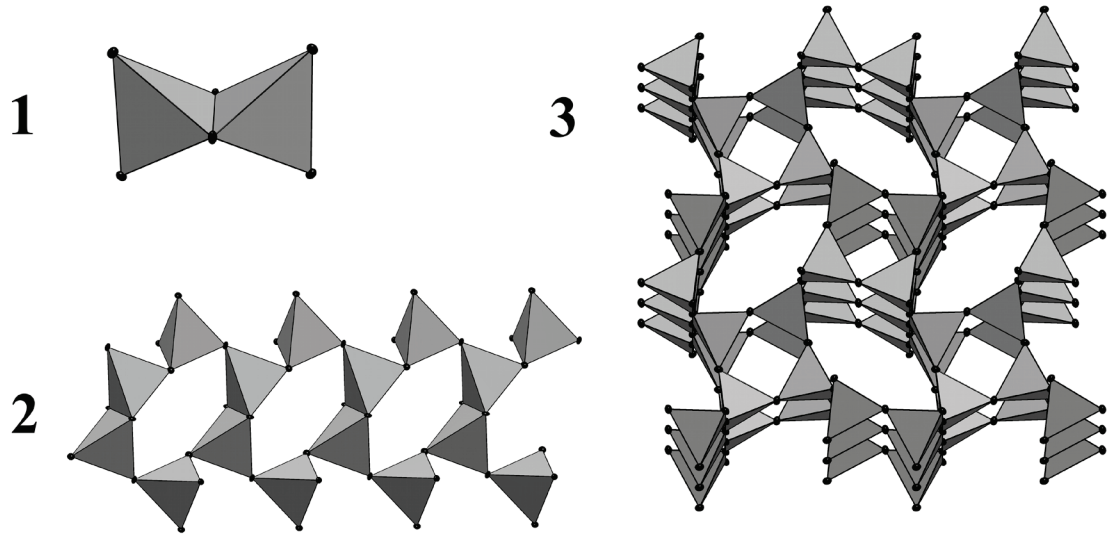

Figure 1. $[SiN_4]$ substructures: double tetrahedra (1) in **I** ($Li_4Ca_3Si_2N_6$), double-chain (2) in **II** ($LiCa_3Si_2N_5$), and framework (3) in **III** ($Li_2Sr_4Si_4N_8O$).

Our experiments were conducted in closed tantalum crucibles, heated to 900 °C under argon atmosphere, and used $Si(NH)_2$ as reactive Si precursor, Ca or Sr metal, LiN_3 or Li_3N as additional nitrogen source, and Li as flux (detailed experimental data for the synthesis of single crystals and bulk samples are given in the Experimental Section). Systematic investigations in this system led to the discovery of novel compounds covering the whole range of dimensionality of $[SiN_4]$ building blocks from group-type ions through chains and sheets up to frameworks. The diversity known for oxosilicate chemistry, which has also been reported for nitridometalates,[33, 34] is now accessible for nitridosilicates. Three new nitridosilicates are briefly presented to illustrate the structural variety accessible by the

lithium-flux method and new structural features resulting from the incorporation of Li^+ or Li_2O.

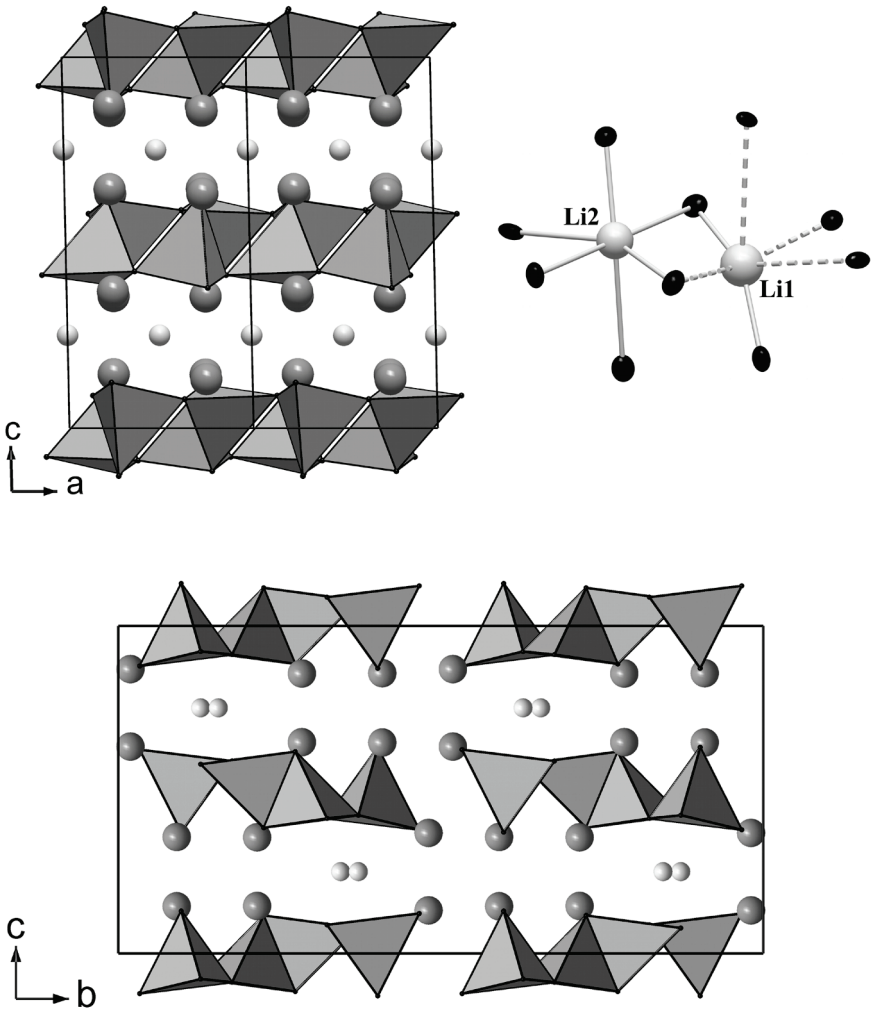

Figure 2. Unit cell of $LiCa_3Si_2N_5$ (**II**) along [010] (top) and along [100] (bottom). Coordination spheres of the Li^+ ions in **II** (top right, ellipsoids at 90% probability). $[SiN_4]$ units are depicted as filled gray tetrahedra, N atoms black, Ca ions dark gray, and Li ions light gray.

The compound with the less condensed $[SiN_4]$ building blocks is $Li_4Ca_3Si_2N_6$ (**I**).[35] It consists of edge-sharing "bowtie" $[Si_2N_6]^{10-}$ units and is isotypic with $Li_4Sr_3Ge_2N_6$.[32] The group-like silicate $[Si_2N_6]^{10-}$, known from $Ba_5Si_2N_6$ and $Ca_5Si_2N_6$ has the lowest degree of condensation of structurally characterized nitridosilicates.[17,36] By adding sufficient Li_3N to the reaction mixture higher condensation of the $[SiN_4]$ network can be suppressed and **I** is isolated. Hitherto-unknown intermediates such as double-chain-like silicates can be obtained when an appropriate amount of Li_3N is added to the reaction mixture. $LiCa_3Si_2N_5$ (**II**) exhibits two zweier single-chains, connected through common edges along [001] (Figures 1 and 2).[37] The formula $[Si_2N_5]^{7-}$ could be indicative of a layer silicate, but due to edge sharing of the

[SiN_4] tetrahedra, which is unprecedented for oxosilicates, **II** is the first double-chain-like nitridosilicate. Interestingly, the structure exhibits an infinite chain of Li^+ ions running along the *a* axis (Figure 2). The structure contains two crystallographically independent Li^+ positions, and the coordination spheres of the lithium ions were assigned by lattice energy calculations (MAPLE: Madelung part of lattice energy).[38, 39]

Accordingly, Li2 is octahedrally coordinated by nitrogen, whereas Li1 exhibits only two close nitrogen contacts relevant to the lattice energy and four elongated Li-N distances. If both lithium polyhedra are interpreted in terms of distorted octahedra, as illustrated in Figure 2, the polyhedra share one edge, and Li^+ ion conductivity along the a axis seems likely. This assumption is supported by our observation that the line width at half-maximum (FWHM) of the ^{7}Li solid-state MAS NMR of **II** at room temperature is halved compared to **I**, although **I** exhibits solely one crystallographically independent lithium position. The ^{7}Li solid-state NMR spectra of **I** and **II** (see Figure 3 (**I**) and Figure 4 (**II**)) consist of an intense isotropic peak centered at 2.0 ppm (FWHM: 7.9 ppm) for **I** and 2.7 ppm (FWHM: 2.9 ppm) for **II**. The chemical shifts are comparable to those of $LiSi_2N_3$ (1.3 ppm) and Li_2SiN_2 (1.7 ppm).[20, 40] The applicability of **II** as Li^+ ion conductor is currently being investigated.

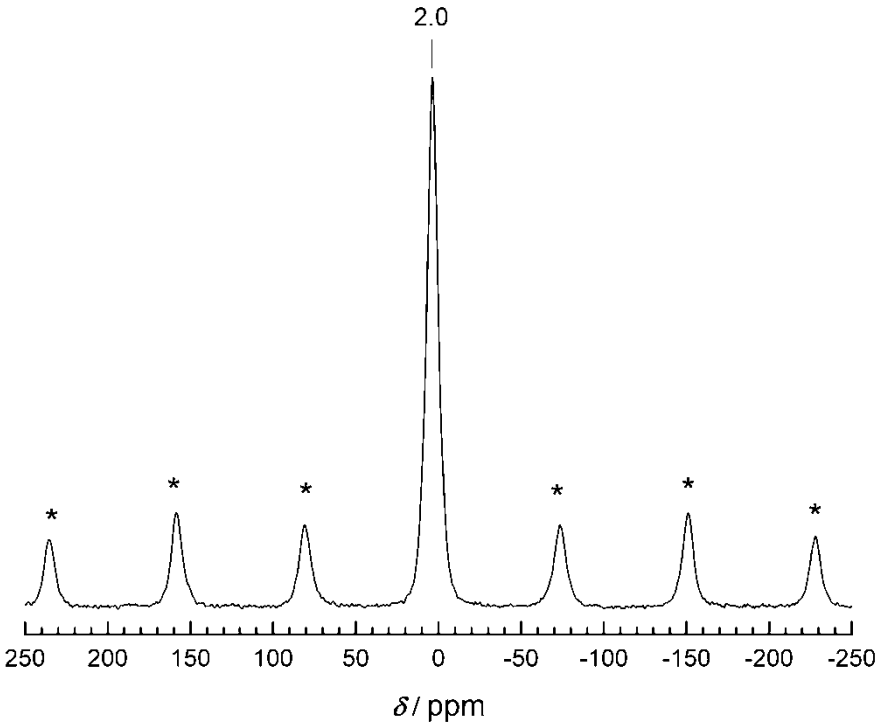

Figure 3. ^{7}Li Solid-state MAS NMR spectrum of $Li_4Ca_3Si_2N_6$. Rotation bands are indicated by asterisks (rotation frequency 15 kHz). The one-dimensional ^{7}Li NMR spectrum was acquired with a 90° pulse length of 1.5 μs and a recycle delay of 64 s.

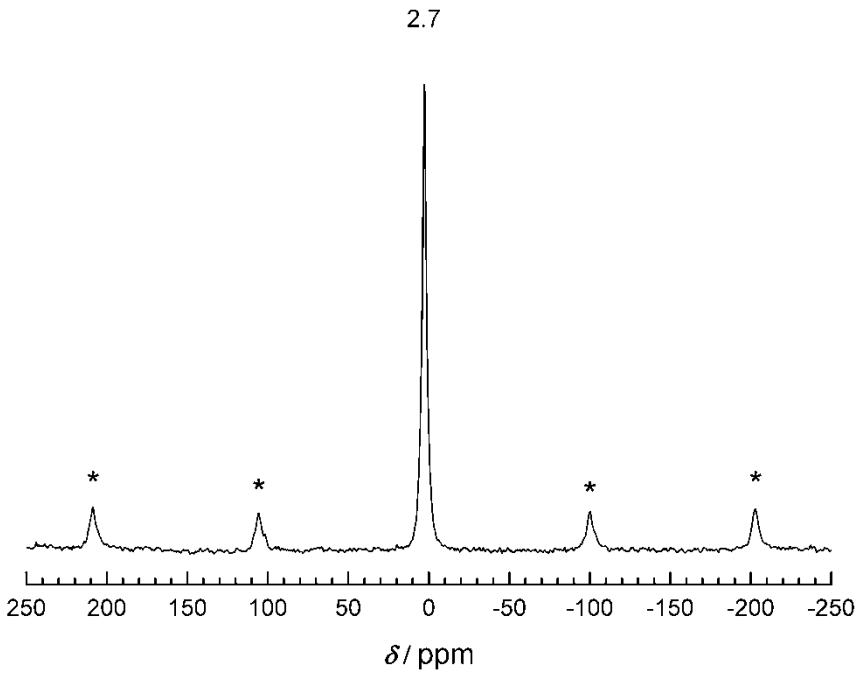

Figure 4. ^{7}Li Solid-state MAS NMR spectrum of $LiCa_3Si_2N_5$. Rotation bands are indicated by asterisks (rotation frequency 20 kHz). The one-dimensional ^{7}Li NMR spectrum was acquired with a 90° pulse length of 1.5 µs and a recycle delay of 64 s.

From a series of new Sr compounds, we present $Li_2Sr_4Si_4N_8O$ (**III**) exemplarily, as it exhibits a zeolite-analogous $[SiN_2]^{2-}$ framework incorporating Li_2O.[41] It was synthesized from Li_2O, Sr, $Si(NH)_2$, and LiN_3 in liquid lithium. As **III** is resistant to oxygen and water, the colorless crystals can be isolated from side products by washing with EtOH. Compound **III** can be formulated as $L_{i2}O@[SrSiN_2]_4$, as oxygen is located in channels together with the Li^+ ions along [001] and is not bound to any silicon atoms (Figure 5). The $[SiN_2]^{2-}$ framework is made up exclusively of vertex-sharing vierer rings, condensed analogously to the BCT zeolite framework type.[42] Characteristic for the BCT structure are vierer ring and achter ring channels along [001] and sechser ring channels along [100] and [010], respectively (Figure 1 and Figure 5). In contrast to the BCT-type structures reported so far, the achter rings are distorted and evocative of the layer silicate apophyllite.[43] Therefore, the structure could also be described by the condensation of apophyllite-like layers along [001]; especially the rather rare space group P4/mnc is typical for this mineral. The Sr^{2+} ions are centered in the sechser ring channels, whereas Li_2O is positioned in a strand-like fashion in the vierer ring channels (Figure 5, top right). The Li-O and Sr-O distances are significantly shorter than the Li-N and Sr-N distances and correspond well to the data found in the literature.

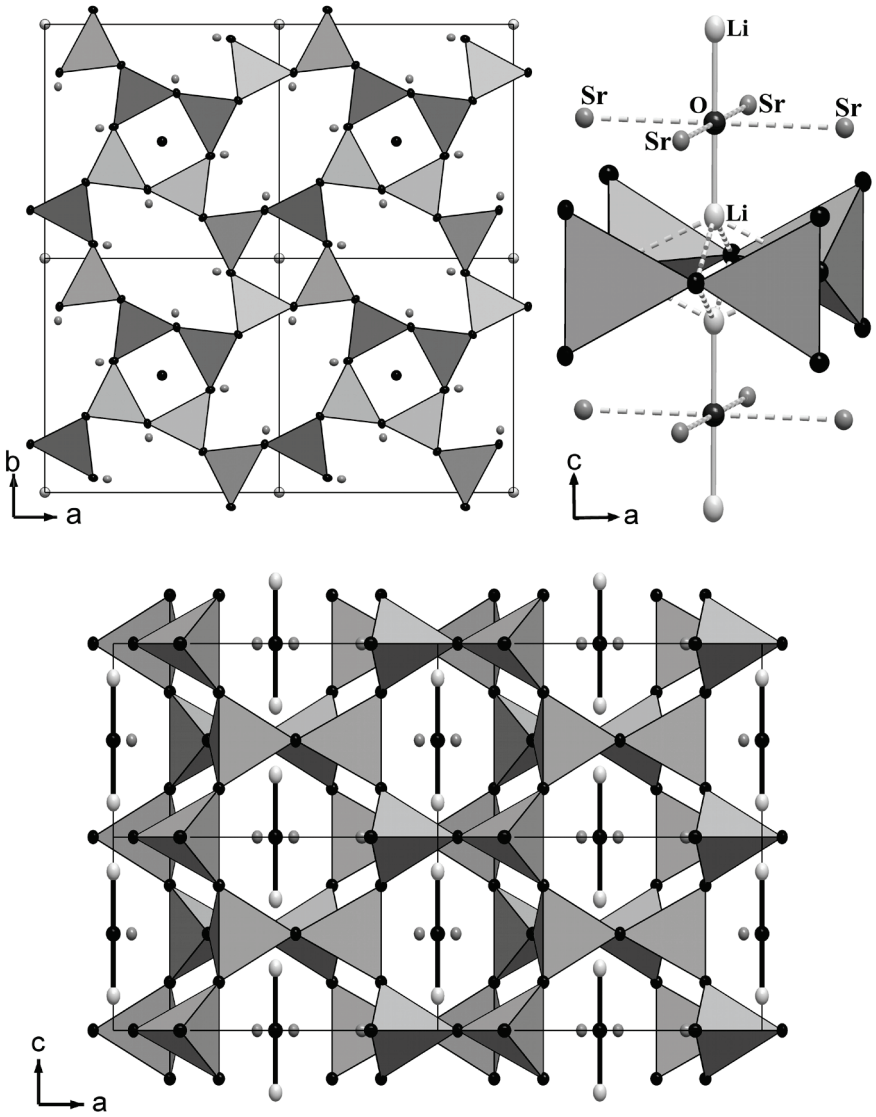

Figure 5. 2x2x2 unit cell of $Li_2Sr_4Si_4N_8O$ along [001] (top left) and along [010] (bottom, Li_2O illustrated by black bonds). Top right: Li_2O unit in $Li_2Sr_4Si_4N_8O$. [SiN_4] units are depicted as filled gray tetrahedra, N/O atoms black, Sr ions dark gray and Li ions light gray. Ellipsoids at 50% probability.

Compound **III** underlines the wide structural variety for nitridosilicates with a molar ratio Si:N=1:2 (c.f. $MSiN_2$, Li_2SiN_2).[18, 20] Interestingly, **III** has the lowest framework density[44] (16.7) and additionally it is the first nitridosilicate having a zeolite-type framework, which already has been found in oxosilicate chemistry. This may arise from Li_2O, if it is interpreted in terms of a molecule-like inorganic template. A template effect of Li_2O has already been discussed for the compound $Li_6B_{18}(Li_2O)_x$, where Li_2O was essential for formation of the zeolite-analogous boride framework.[22] This observation is consistent with our finding that other lithium strontium nitridosilicates are formed if no Li_2O is present. Inclusion of Li_2O is supported by ^{7}Li solid-state MAS NMR spectroscopy and Raman measurements.

2.2.3 Conclusion

The ability of liquid lithium to dissolve a variety of metals, inorganic salts, and even complex anions (e.g., CN_2^{2-})[25] opens the door to a plethora of new nitridosilicates. Preliminary experiments with lanthanides or other alkali metal salts as templates point in this direction.

In summary, the lithium-flux method allows control of the dimensionality of $[SiN_4]$ substructures, from group-type silicates through chainlike anions to frameworks, by simply adjusting the Li_3N content, the nitrogen pressure (LiN_3), and the reaction temperature. Furthermore, chemical screening of suitable materials for lithium ion conductivity or luminescence can now be facilitated by this versatile synthetic approach.

2.2.4 Experimental Section

All manipulations were performed with rigorous exclusion of oxygen and moisture in flame-dried Schlenk-type glassware on a Schlenk line interfaced to a vacuum (10^{-3} mbar) line or in an argon-filled glovebox (Unilab, MBraun, Garching, $O_2 < 0.1$ ppm, $H_2O < 0.1$ ppm). Argon (Messer-Griessheim, 5.0) was purified by passage through columns of silica gel (Merck), molecular sieve (Fluka, 4 Å), KOH (Merck, ≥ 85 %), P_4O_{10} (Roth, ≥ 99 %, granulate) and titanium sponge (Johnson Matthey, 99.5 %, grain size ≤ 0.8 cm) at 700 °C. Li_3N (99.4 %, metal based) and Li (99.9 %, metal based) were purchased from Alfa Aesar. LiN_3[45] and $Si(NH)_2$[46] were synthesized according to the literature. Calcium and Strontium were purchased from Sigma-Aldrich (99.99 %, metal based).

For the synthesis tantalum tubes (wall thickness 0.5 mm, internal diameter 10 mm, length 300 mm) were cleaned in a mixture of HNO_3 (conc.) and HF (40 %). They were weld shut under a pressure of 1 bar purified Argon in an arc furnace. The crucible holder was water cooled in order to avoid starting of the reaction during welding.

2.2.4.1 X-ray diffraction

By inspection under a microscope integrated in a glove-box, colorless single crystals of the title compounds were isolated from residual lithium and enclosed in glass capillaries. Single-crystal X-ray diffraction data were collected on a STOE IPDS I diffractometer ($Mo_{K\alpha}$ radiation). The program package SHELX97 was used for structure solution and refinement.[47]

Powder diffraction data were collected in Debye-Scherrer geometry on a STOE Stadi P powder diffractometer with Ge(111)-monochromatized Cu-$K_{\alpha 1}$ radiation (λ = 1.5406 Å) for $Li_4Ca_3Si_2N_6$ (**I**) and $Li_2Sr_4Si_4N_8O$ (**III**) and with Mo-$K_{\alpha 1}$ radiation (λ = 0.7104 Å) for $LiCa_3Si_2N_5$ (**II**). The Rietveld refinements were performed with the TOPAS package[48] using the fundamental parameters approach as reflection profiles (convolution of appropriate source emission profiles with equatorial and axial instrument contributions as well as crystallite microstructure effects). All diffractograms were measured without an internal standard, so the absolute lattice parameters might be slightly offset.

2.2.4.2 Solid-state MAS NMR

Solid-state MAS NMR experiments were performed at 11.74 T on a Bruker DSX 500 spectrometer equipped with a commercial 2.5 mm triple-resonance MAS probe at the ^{7}Li frequencies of 194.399 MHz. All experiments were performed in ZrO_2 rotors at room temperature. The chemical shifts of ^{7}Li are reported using the frequency ratios published by IUPAC (δ scale relative to 1 % tetramethylsilane (TMS) in $CDCl_3$).[49]

2.2.4.3 Microanalysis

EDX spectra of selected crystals were obtained using a JSM 6500F scanning electron microscope (JEOL) equipped with an EDX detector 7418 (Oxford Instruments).

2.2.4.4 Synthesis

$Li_4Ca_3Si_2N_6$ (I): Single crystals were isolated by reacting 20 mg (2.88 mmol) Li, 53.8 mg (1.50 mmol) $Si(NH)_2$ 20.1 mg (0.50 mmol) Ca and 23.2 mg (0.66 mmol) Li_3N in closed tantalum crucibles placed in silica tubes. The silica tube (under argon) was placed in the middle of a tube furnace. The temperature was raised to 900 °C (rate 120 °C h^{-1}), maintained for 17 h, subsequently cooled to 500 °C (rate 8 °C h^{-1}) and finally quenched to room temperature by switching off the furnace. Bulk samples of **I** for solid-state MAS NMR and the Rietveld refinement were synthesized from 35.8 mg $Si(NH)_2$ (0.62 mmol), 40.0 mg Ca (1.00 mmol) and 26.0 mg Li_3N (0.75 mmol). The temperature was raised with a rate of 300 °C h^{-1} to 900 °C, maintained for 24 h, cooled down to 450 °C within 1.5 h and quenched to room temperature by switching off the furnace. The molar ratio of heavy atoms Ca : Si was found to be 22(2) : 14(2) (average from 3 independent measurements) by microanalysis

$LiCa_3Si_2N_5$ (II): Single crystals were isolated by reacting 50 mg (7.2 mmol) Li, 45.0 mg (0.77 mmol) $Si(NH)_2$, 33.5 mg (0.84 mmol) Ca and 19.4 mg (0.56 mmol) Li_3N in closed tantalum crucibles placed in silica tubes. The silica tube (under argon) was placed in the middle of a tube furnace. The temperature was raised to 900 °C (rate 120 °C h^{-1}), maintained for 12 h, subsequently cooled to 500 °C (rate 8 °C h^{-1}) and finally quenched to room temperature by switching off the furnace. Bulk samples of **II** for solid-state MAS NMR and the Rietveld refinement were synthesized from 35.8 mg $Si(NH)_2$ (0.62 mmol), 40.0 mg (1.0 mmol) Ca and 15.5 mg (0.45 mmol) Li_3N. The crucible was heated to 900 °C within 3 h, maintained at this temperature for 24 h, cooled down at 450 °C (rate 300 °C h^{-1}) and quenched to room temperature after 3 h annealing. The molar ratio of heavy atoms Ca : Si was found to be 32(1) : 20(1) (average from 3 independent measurements).

$Li_2Sr_4Si_4N_8O$ (III): Single crystals were isolated by reacting 24 mg (3.5 mmol) Li, 40.7 mg (0.7 mmol) $Si(NH)_2$, 61.3 mg (0.7 mmol) Sr, 5.3 mg (0.18 mmol) Li_2O and 17.1 mg (0.35 mmol) LiN_3 in closed tantalum crucibles placed in silica tubes. The silica tube (under argon) was placed in the middle of a tube furnace. The temperature was raised to 900 °C (rate 120 °C h^{-1}), maintained for 24 h, subsequently cooled to 500 °C (rate 5 °C h^{-1}) and finally quenched to room temperature by switching off the furnace. Bulk samples of **III** for solid-state MAS NMR and the Rietveld refinement were synthesized from 12 mg (1.75 mmol) Li, 40.7 mg (0.7 mmol) $Si(NH)_2$, 61.3 mg (0.7 mmol) Sr, 5.3 mg (0.18 mmol) Li_2O and 17.1 mg (0.35 mmol) LiN_3. The temperature was raised to 900 °C (rate 300 °C h^{-1}), maintained for 24 h, subsequently cooled to 500 °C (rate 10 °C h^{-1}) and finally quenched to room temperature by switching off the furnace. The product was washed several times with ethanol to remove residual lithium. The molar ratio of heavy atoms Sr : Si was found to be 20(4):21(2) (average from 3 independent measurements) by microanalysis.

2.2.5 References

[1] R.-J. Xie, N. Hirosaki, N. Kimura, K. Sakuma, M. Mitomo, *Appl. Phys. Lett.* **2007**, *90*, 191101.

[2] W. Schnick, H. Huppertz, *Chem. Eur. J.* **1997**, *3*, 679-683.

[3] H. Yamane, S. Kikkawa, M. Koizumi, *Solid State Ionics* **1987**, *25*, 183-191.

[4] H. A. Höppe, *Angew. Chem.* **2009**, *121*, 3626 – 3636; *Angew. Chem. Int. Ed*. **2009**, *48*, 3572-3582.

[5] Y. Q. Li, G. deWith, H. T. Hintzen, *J. Solid State Chem*. **2008**, *181*, 515-524.

[6] H. Lutz, S. Joosten, J. Hoffmann, P. Lehmeier, A. Seilmeier, H. A. Höppe, W. Schnick, *J. Phys. Chem. Solids* **2004**, *65*, 1285-1290.

[7] V. Bachmann, C. Ronda, O. Oeckler, W. Schnick, A. Meijerink, *Chem. Mater*. **2009**, *21*, 316-325.

[8] R. Mueller-Mach, G. Mueller, M. R. Krames, H. A. Höppe, F. Stadler, W. Schnick, T. Juestel, P. Schmidt, *Phys. Status Solidi A* **2005**, *202*, 1727-1732.

[9] M. Yamada, T. Naitou, K. Izuno, H. Tamaki, Y. Murazaki, M. Kameshima, T. Mukai, *Jpn. J. Appl. Phys. Part 1* **2003**, *42*, L20.

[10] H. A. Höppe, H. Lutz, P. Morys, W. Schnick, A. Seilmeier, *J. Phys. Chem. Solids* **2000**, *61*, 2001-2006.

[11] H. Huppertz, W. Schnick, *Acta Crystallogr. Sect. C* **1997**, *53*, 1751-1753.

[12] T. Schlieper, W. Milius, W. Schnick, *Z. Anorg. Allg. Chem.* **1995**, *621*, 1380-1384.

[13] H. A. Höppe, F. Stadler, O. Oeckler, W. Schnick, *Angew. Chem*. **2004**, *116*, 5656-5659; *Angew. Chem. Int. Ed*. **2004**, *43*, 5540-5542.

[14] F. Stadler, W. Schnick, *Z. Anorg. Allg. Chem*. **2006**, *632*, 949-954.

[15] C. Schmolke, D. Bichler, D. Johrendt, W. Schnick, *Solid State Sci.* **2009**, *11*, 389-394.

[16] F. Lissner, T. Schleid, *Z. Anorg. Allg. Chem*. **2004**, *630*, 2226-2230.

[17] H. Yamane, F. J. DiSalvo, *J. Alloys Compd*. **1996**, *240*, 33-36.

[18] Z. A. Gál, P. M. Mallinson, H. J. Orchard, S. J. Clarke, *Inorg. Chem*. **2004**, *43*, 3998-4006.

[19] M. Zeuner, F. Hintze, W. Schnick, *Chem. Mater.* **2009**, *21*, 336-342.

[20] S. Pagano, M. Zeuner, S. Hug, *Eur. J. Inorg. Chem*. **2009**, 1579-1584.

[21] S. Pagano, O. Oeckler, T. Schröder, W. Schnick, *Eur. J. Inorg. Chem.* **2009**, 2678-2683.

[22] R. Nesper, M. Wörle, G. Mair, H. G. von Schnering, *Solid State Sci*. **2007**, *9*, 459-464.

[23] M. G. Kanatzidis, R. Pöttgen, W. Jeitschko, *Angew. Chem*. **2005**, *117*, 7156-7184; *Angew. Chem. Int. Ed.* **2005**, *44*, 6996-7023.

[24] F. Kawamura, T. Ogura, M. Imade, M. Yoshimura, Y. Kitaoka, Y. Mori, T. Sasaki, *Mater. Lett*. **2008**, *62*, 1048-1051.

[25] R. J. Pulham, P. Hubberstey, *J. Nucl. Mater.* **1983**, *115*, 239-250.

[26] A. T. Dadd, P. Hubberstey, *J. Chem. Soc. Dalton Trans.* **1982**, 2175-2179.

[27] R. Juza, H. H. Weber, E. Meyer-Simon, *Z. Anorg. Allg. Chem.* **1953**, *273*, 48-64.

[28] B. Song, J. K. Jian, G. M. Cai, M. Lei, H. Q. Bao, H. Li, Y. P. Xu, W. Y. Wang, J. C. Han, X. L. Chen, *Solid State Ionics* **2009**, *180*,29-35.

[29] P. E. Rauch, A. Simon, *Angew. Chem.* **1992**, *104*, 1505-1506; *Angew. Chem. Int. Ed. Engl.* **1992**, *31*, 1519-1521.

[30] P. Hubberstey, P. G. Roberts, *J. Chem. Soc. Dalton Trans.* **1994**, 667-673.

[31] M. S. Bailey, F. J. DiSalvo, *J. Alloys Compd.* **2006**, *417*, 50-54.

[32] D. G. Park, Z. A. Gál, F. J. DiSalvo, *J. Solid State Chem.* **2003**, *172*, 166-170.

[33] R. Niewa, H. Jacobs, *Z. Anorg. Allg. Chem.* **1996**, *622*, 881-884.

[34] R. Niewa, H. Jacobs, *Chem. Rev.* **1996**, *96*, 2053-2062.

[35] Crystal structure data for $Li_4Ca_3Si_2N_6$ (**I**) (288.24 gmol $^{-1}$) at 293(2) K: monoclinic, C2/m (No. 12), *a*=5.7873(12), *b*=9.7045(19), *c*=5.9771(12) Å, V=335.68(12) Å^3, Z=2; diffractometer: STOE IPDS I ($Mo_{K\alpha}$ radiation, graphite monochromator); 0.08 x 0.05 x 0.02 mm; ρ_{calcd}=2.852; μ=2.751 mm^{-1}; $2\theta_{max}$=618; 1787 observed intensities; 505 unique; multi-scan absorption correction; least-squares refinement (all atoms anisotropic) SHELXL-97; 40 free variables; GOF=1.117; *R* values [$I \geq 2\sigma(I)$]: *R*1=0.0219, *wR*2=0.0566; max./min. residual electron density: 0.512/-0.457 eÅ^{-3}. Further details of the crystal structure investigations may be obtained from the Fachinformationszentrum Karlsruhe, 76344 Eggenstein-Leopoldshafen, Germany (fax: (+49)7247-808-666; e-mail: crysdata@fiz-karlsruhe.de), on quoting the depository number CSD-420675.

[36] F. Ottinger, R. Nesper, *Z. Anorg. Allg. Chem.* **2005**, *631*, 1597-1602.

[37] Crystal structure data for $LiCa_3Si_2N_5$ (**II**) (253.41 gmol $^{-1}$) at 140(2) K: monoclinic, C2/c (No. 15), *a*=5.1454(10), *b*=20.380(4), *c*=10.357(2) Å, V=1085.8(4) Å^3, Z=8; diffractometer: STOE IPDS I ($Mo_{K\alpha}$ radiation, graphite monochromator); 0.09 x 0.06 x 0.04 mm; ρ_{calcd}=3.100; μ =3.382 mm^{-1}; $2\theta_{max}$ =558; 4447 observed intensities; 1244 unique; numerical absorption correction; least-squares refinement (all atoms anisotropic except Li) SHELXL-97; 96 free variables; GOF=1.135; *R* values [$I \geq 2\sigma(I)$]: *R*1=0.0442, *wR*2=0.1084; max./min. residual electron density: 1.182/-0.677 eÅ^{-3}. Pseudomerohedral twinning: twin law 001 0-10 00-1 BASF=0.0414. Further details of the crystal structure investigations may be obtained from the Fachinformationszentrum Karlsruhe, 76344 Eggenstein-Leopoldshafen, Germany (fax: (+49)7247-808-666; e-mail: crysdata@fiz-karlsruhe.de), on quoting the depository number CSD-420676

[38] R. Hübbenthal, Programm zur Berechnung des Madelunganteils der Gitterenergie, Vers. 4, Universität Gießen, **1993**.

[39] R. D. Shannon, *Acta Crystallogr. Sect. A* **1976**, *32*, 751-767.

[40] P. Kempgens, R. K. Robin, D. P. Thompson, *Solid State Nucl. Magn. Reson.* **1999**, *15*, 109-118.

[41] Crystal structure data for $LiSr_4Si_4N_8O$ (**III**) (604.76 $gmol^{-1}$) at 293(2) K: tetragonal, P4/mnc (no. 128), a=9.2957(13), c=5.5528(11) Å, V=479.82(13) $Å^3$, Z=2; diffractometer: STOE IPDS I ($Mo_{K\alpha}$ radiation, graphite monochromator); 0.2 x 0.15 x 0.11 mm; ρ_{calcd} =4.186; μ =22.606 mm^{-1}; $2\theta_{max}$ =608; 4575 observed intensities; 358 unique; numerical absorption correction; least-squares refinement (all atoms anisotropic) SHELXL- 97; 30 free variables; GOF=1.071; *R* values [$I \geq 2\sigma(I)$]: $R1$= 0.0336, $wR2$=0.0805; max./min. residual electron density: 1.046/-1.163 $eÅ^{-3}$. Further details of the crystal structure investigations may be obtained from the Fachinformationszentrum Karlsruhe, 76344 Eggenstein-Leopoldshafen, Germany (fax: (+49)7247-808-666; e-mail: crysdata@fiz-karlsruhe.de), on quoting the depository number CSD-420677

[42] W. A. Dollase, C. R. Ross, *Am. Mineral.* **1993**, *78*, 627-632.

[43] F. Liebau, *Structural Chemistry of Silicates*, Springer, Berlin, **1985**.

[44] A measure for the microporosity of a zeolite-analogous structure is the framework density, which indicates the number of tetrahedral centers in a volume of 1000 $Å^3$.

[45] H. D. Fair, R. F. Walker, *Energetic Materials 1, Physics and Chemistry of the Inorganic Azides*, Plenum Press, New York, London, **1977**, pp. 32.

[46] H. Lange, G. Wötting, G. Winter, *Angew. Chem.* **1991**, *103*, 1606-1625; *Angew. Chem. Int. Ed.* **1991**, *30*, 1579-1597.

[47] G. M. Sheldrick, *Acta Crystallogr., Sect. A: Cryst. Found. Crystallogr.* **2008**, *64*, 112-122.

[48] R. W. Cheary, A. A. Coelho, J. P. Cline, *Res. Natl. Inst. Stand. Technol.* **2004**, *109*, 1.

[49] R. K. Harris, E. D. Becker, S. M. Cabral de Menezes, R. Goodfellow, P. Granger, *Solid State Nucl. Magn. Reson.* **2002**, *22*, 458-483.

2.3 $Li_4Ca_3Si_2N_6$ and $Li_4Sr_3Si_2N_6$ – Quaternary Lithium Nitridosilicates with Isolated $[Si_2N_6]^{10-}$ Ions

published in Sandro Pagano, Saskia Lupart, Sebastian Schmiechen, and Wolfgang Schnick

Z. Anorg. Allg. Chem. **2010**, *636* (11), 1907-1909
DOI: 10.1002/zaac.201000163
Copyright © 2010 WILEY-VCH Verlag GmbH & Co. KGaA, Weinheim
http://onlinelibrary.wiley.com/doi/10.1002/zaac.201000163/abstract

Abstract. The isotypic nitridosilicates $Li_4Ca_3Si_2N_6$ and $Li_4Sr_3Si_2N_6$ were synthesized by reaction of strontium or calcium with $Si(NH)_2$ and additional excess of Li_3N in weld shut tantalum ampoules. The crystal structure, which has been solved by single-crystal X-ray diffraction ($Li_4Sr_3Si_2N_6$: $C2/m$, Z = 2, a = 6.1268(12), b = 9.6866(19), c = 6.2200(12) Å, β = 90.24(3)°, $wR2$ = 0.0903) is made up from isolated $[Si_2N_6]^{10-}$ ions and is isotypic to $Li_4Sr_3Ge_2N_6$. The bonding angels and distances within the edge-sharing $[Si_2N_6]^{10-}$ double-tetrahedra are strongly dependent on the lewis acidity of the counterions. This finding is discussed in relation to the compounds $Ca_5Si_2N_6$ and $Ba_5Si_2N_6$, which also exhibit isolated $[Si_2N_6]^{10-}$ ions.

2.3.1 Introduction

Recently, we have reported on the utilization of liquid lithium for the synthesis of quaternary lithium nitridosilicates. The ability of liquid lithium to dissolve a variety of metals, silicon, and nitrogen allows for a controlled synthesis of group-type silicates, chain-like anions up to frameworks by simply adjusting the Li_3N content, the nitrogen pressure (LiN_3) and the reaction temperature.[1] By adding an excess of Li_3N to the reaction mixture higher condensation of the $[SiN_4]$ tetrahedra network is suppressed and the lowest degree of condensation for nitridosilicates is observed. Orthosilicate-like isolated $[SiN_4]^{8-}$ tetrahedra, which might occur in the compound Li_8SiN_4 are not yet structurally verified.[2,3] Consequently, up to now group-type silicates made up from edge-sharing $[Si_2N_6]^{10-}$ double-tetrahedra represent nitridosilicates with the lowest degree of condensation characterized by single-crystal X-ray diffraction so far. Identical building blocks have already been reported for $Ba_5Si_2N_6$ synthesized by *DiSalvo* et al. in a sodium flux and $Ca_5Si_2N_6$ obtained by solid-state reaction of Ca_2N and silicon.[4,5]

In this contribution we report on synthesis and structural features of $Li_4Ca_3Si_2N_6$ and on the isotypic Sr-phase.

2.3.2 Results and Discussion

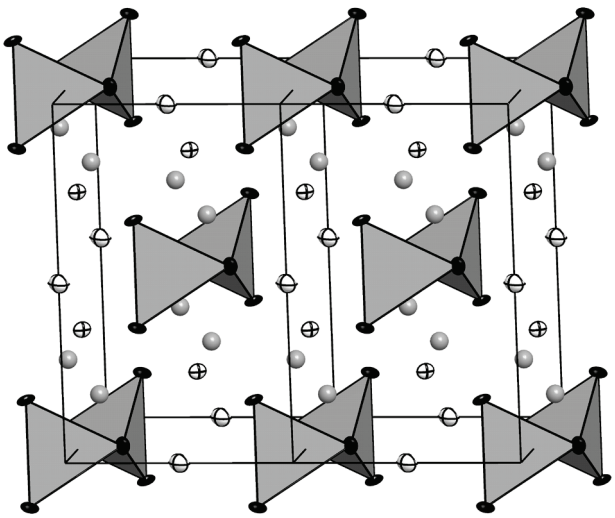

Figure 1. Two unit cells of $Li_4Sr_3Si_2N_6$ along [00-1]. Ellipsoids at 90 % probability level. $[SiN_4]$ units are depicted as closed gray tetrahedra, N atoms black, Sr ions white/black and Li ions gray.

Table 1. Crystallographic data of $Li_4Ca_3Si_2N_6$ and $Li_4Sr_3Si_2N_6$.

Formula	$Li_4Ca_3Si_2N_6$	$Li_4Sr_3Si_2N_6$
Formula mass / g · mol^{-1}	288.24	430.86
Crystal system	monoclinic	
Space group	*C*2/*m* (no. 12)	
Cell parameters / Å, °	*a* = 5.7873(12) *b* = 9.7045(19) *c* = 5.9771(12) *β* = 90.45(3)	*a* = 6.1268(12) *b* = 9.6866(19) *c* = 6.2200(12) *β* = 90.24(3)
Cell volume / 10^6 pm^3	*V* = 335.68(12)	*V* = 369.14(12)
Formula units / cell	2	
Crystal size / mm^3	0.08 · 0.05 · 0.02	0.14 · 0.12 · 0.05
$\rho_{calcd.}$ / g · cm^{-3}	2.852	3.876
μ / mm^{-1}	2.751	21.86
F(000)	284	392
Diffractometer	Stoe IPDS I	Oxford Diffraction XCalibur
Temperature / K	295(2)	200(2)
Radiation, monochromator	Mo-K$_\alpha$, (λ = 71.073 pm), graphite	
Absorption correction	multi-scan	numerical
min. /max. transmission	0.726 / 0.946	0.0467 / 0.466
θ range / °	2.3 – 30.5	3.89 – 29.99
Measured reflections	1787	1221
Independent reflections	505	539
Observed reflections	450	456
Refined parameters	36	36
GoF	1.117	1.122
R indices ($F_o^2 \geq 2\sigma (F_o^2)$)	*R*1 = 0.0219 *wR*2 = 0.0566	*R*1 = 0.0314 *wR*2 = 0.0903
R indices (all data)	*R*1 = 0.0252 *wR*2 = 0.0572[a)]	*R*1 = 0.0370 *wR*2 = 0.0935[b)]
Max. / min. residual electron density/ eÅ^{-3}	0.512 / -0.457	1.816 / -1.741

a) $w = [\sigma^2(F_o^2) + (0.0347\ P)^2 + 0.00\ P]^{-1}$ where $P = (F_o^2 + 2\ F_c^2)/3$

b) $w = [\sigma^2(F_o^2) + (0.0595\ P)^2 + 0.00\ P]^{-1}$ where $P = (F_o^2 + 2\ F_c^2)/3$

$Li_4Ca_3Si_2N_6$ and $Li_4Sr_3Si_2N_6$ were synthesized from the corresponding metals, $Si(NH)_2$ and an excess of Li_3N in weld shut tantalum ampoules at 900 °C. Addition of lithium metal as a fluxing agent was not essential for the synthesis of suitable single crystals. This might be due to Li_3N acting as a flux as it melts above 815 °C under autogenously nitrogen pressure in

closed systems.[6] The title compounds are not stable against air and moisture and were handled under inert gas atmosphere. The approximate atomic ratio of heavy elements (Ca/Sr and Si) was determined by energy dispersive X-ray microanalysis. $Li_4Ca_3Si_2N_6$ and $Li_4Sr_3Si_2N_6$ crystallize in the monoclinic space group *C*2/*m* with two formula units per unit cell (for details see Table 1).

The unit cell and coordination spheres of $Li_4Sr_3Si_2N_6$ are depicted in Figure 1 and Figure 2, respectively. The asymmetric unit consists of two strontium and nitrogen sites, one silicon and lithium site named according to Figure 2. The structure is built up from isolated $[Si_2N_6]^{10-}$ ions and is isotypic to that of the nitridogermanate.[7] Group-like $[Si_2N_6]^{10-}$ ions have already been reported for $Ca_5Si_2N_6$ and $Ba_5Si_2N_6$.[4,5] Due to the edge-sharing of $[SiN_4]$ tetrahedra, the tetrahedra angels are distorted to values of 91–96° (N2–Si1–N2) for all compounds (cf. Table 2). The corresponding Si1–N2 bonds are elongated from 1.74 Å to 1.81–1.85 Å, resulting in quite short Si1–Si1 distances ranging from 2.40(1) Å in $Ca_5Si_2N_6$ to 2.556(7) Å in $Ba_5Si_2N_6$.[4,5] The Si1–Si1 distances of $Li_4Ca_3Si_2N_6$ and $Li_4Sr_3Si_2N_6$ are ranging in between these values (cf. Table 2). Regarding the series of isolated $[Si_2N_6]^{10-}$ ions one could assume that the distortion of the square built up from Si1 and N2 is dependent on the Lewis acidity of the surrounding metal ions. The smaller ionic radius of Ca^{2+} compared to Sr^{2+} and Ba^{2+} leads to shorter N–metal distances and the higher Lewis acidity results in a displacement of N2 from the ideal square built up from Si1 and N2. Consequently, the angels Si–N2–Si are increasing from 91.1(1)° in $Ba_5Si_2N_6$ and 93.2(3)° in $Li_4Sr_3Si_2N_6$ to 96.7(1)° in $Ca_5Si_2N_6$.[4,5] Presumably, this effect is responsible for the decrease of the distances Si1–Si1 in the sequence Ba^{2+}, Sr^{2+} to Ca^{2+} (Table 2). The distances N–*AE* (*AE* = alkaline earth) in $Li_4Ca_3Si_2N_6$ and $Li_4Sr_3Si_2N_6$ are in the typical range for alkaline earth nitrides.[8] In $Li_4Ca_3Si_2N_6$ both metal sites are coordinated by six nitrogen atoms, whereas in $Li_4Sr_3Si_2N_6$ Sr1 exhibits a 6+2 coordination. The coordination spheres (cf. Figure 2) were assigned by lattice energy calculations (MAPLE; Madelung part of lattice energy).[9,10] In both compounds, Li1 is coordinated by four nitrogen atoms in distorted tetrahedral fashion (105–123°) with typical distances Li–N (values within the sum of the ionic radii).[9,11] The smaller lattice parameters of $Li_4Ca_3Si_2N_6$ also lead to significantly shorter Li–N distances [Li1–N1: 1.968(3), 2.072(3), 2.123(3) Å, Li1–N2: 2.259(3) Å]. Edge-sharing of $[LiN_4]$ polyhedra along [100] causes chains of Li^+ ions with quite short Li1–Li1 distances [$Li_4Ca_3Si_2N_6$: 2.213(6), 2.447(6) Å; $Li_4Sr_3Si_2N_6$: 2.273(18), 2.487(19) Å]. The lithium ion conductor Li_2SiN_2 exhibits comparable chains of $[LiN_x]$ polyhedra with analogous Li–Li distances.[12] It may be noted that the

addition of 1 % of europium to the reaction mixture yielded red single crystals, which, however showed no fluorescence under UV light at room temperature.

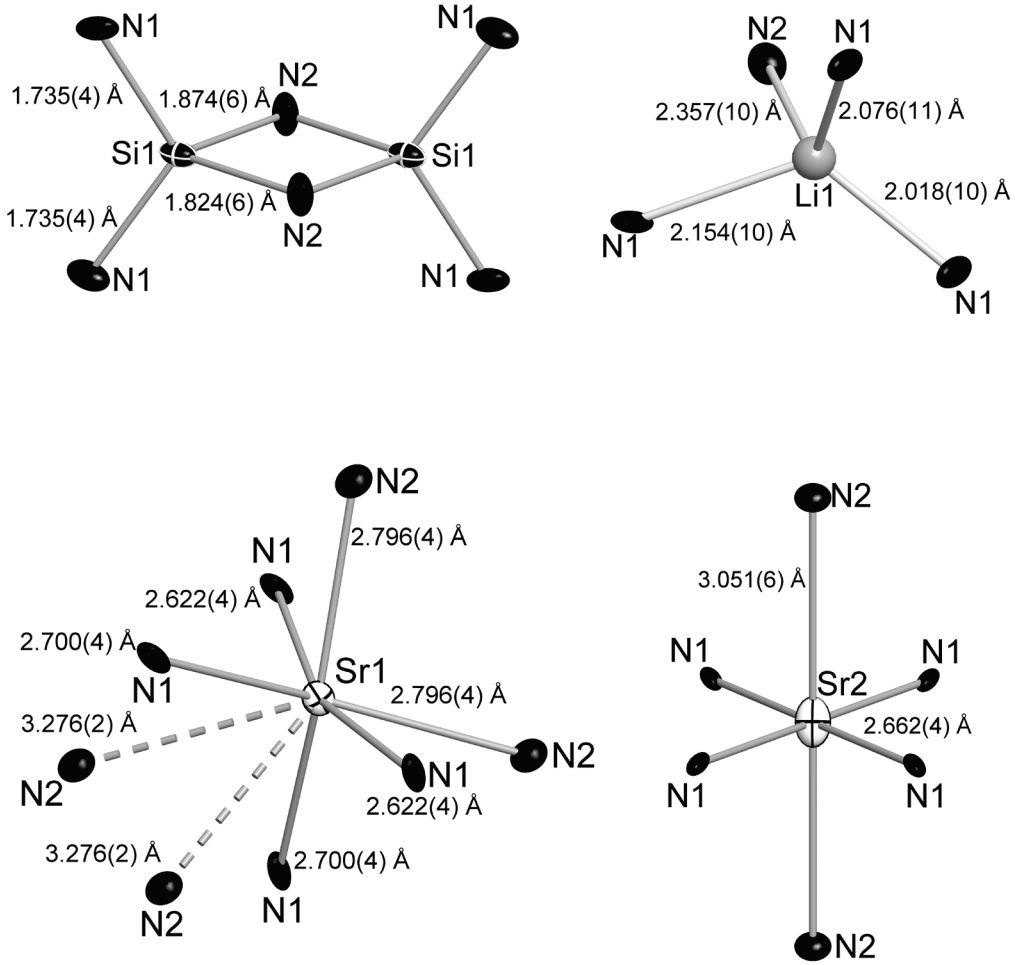

Figure 2. Coordination spheres in $Li_4Sr_3Si_2N_6$. N atoms black, Sr ions white and Li ions gray.

Table 2. Comparison of compounds exhibiting isolated $[Si_2N_6]^{10-}$ ions.

	$Ba_5Si_2N_6$[3]	$Ca_5Si_2N_6$[4]	$Li_4M_3Si_2N_6$	
			Ca	Sr
Synthesis	Na-Flux	solid-state	Li-Flux	Li-Flux
Space group	$P2_12_12_1$	$C2/c$	$C2/m$	$C2/m$
X-ray T /K	293	293	293	200
Si-Si /Å	2.556(7)	2.40(1)	2.453(1)	2.540(4)
Si-N2 /Å	1.83(2)[a)]	1.81(1)[a)]	1.83(1)[a)]	1.85(1)[a)]
Si-N1 /Å	91.1(1)[a)]	96.7(1)[a)]	95.9(1)	93.2(3)
Si-N2-Si /°	1.75(2)[a)]	1.73(1)[a)]	1.711(2)	1.735(4)

a) Averaged values because of more than one set of symmetry independent bonds/angles.

2.3.3 Conclusions

In this contribution, we demonstrate that addition of an excess of Li_3N to the reaction mixture of Ca/Sr and $Si(NH)_2$ suppresses the higher condensation of $[SiN_4]$ tetrahedra and a low degree of condensation for nitridosilicates is achieved. The isotypic compounds $Li_4Ca_3Si_2N_6$ and $Li_4Sr_3Si_2N_6$ are the third and fourth example of nitridosilicates containing isolated $[Si_2N_6]^{10-}$ ions, respectively. Presumably, the lengths of the distances Si–Si within the $[Si_2N_6]^{10-}$ ions is dependent on the Lewis acidity of the counterions. It may be noted that the presence of $[LiN_4]$ polyhedra chains along [100] might be an interesting feature for lithium ion conductivity.

2.3.4 Experimental Section

2.3.4.1 Synthesis

All manipulations were performed with rigorous exclusion of oxygen and moisture in flame-dried Schlenk-type glassware on a Schlenk line interfaced to a vacuum (10–3 mbar) line or in an argon-filled glove box (Unilab, MBraun, Garching, O_2 < 0.1 ppm, H_2O < 0.1 ppm). Li_3N

was purchased from Alfa Aesar (99.4 %), calcium and strontium from Sigma–Aldrich (99.99 %) and $Si(NH)_2$ was synthesized according to the literature.[13] For the reactions, tantalum crucibles (wall thickness 0.5 mm, internal diameter 10 mm, length 300 mm) were cleaned in a mixture of HNO_3 (conc.) and HF (40 %). They were arc-welded under a pressure of 1 bar purified argon. The crucible holder was water cooled in order to avoid decomposition reactions during welding.

Single crystals of $Li_4Ca_3Si_2N_6$ and $Li_4Sr_3Si_2N_6$ were synthesized from Li_3N (60 mg, 1.72 mmol), $Si(NH)_2$ (50 mg, 0.86 mmol) and calcium (34 mg, 0.86 mmol) or strontium (75 mg, 0.86 mmol) in closed tantalum crucibles placed in silica tubes. The silica tube (under argon) was placed in the middle of a tube furnace. The temperature was raised to 900 °C (rate 180 $°C \cdot h^{-1}$), maintained for 48 h, subsequently cooled to 500 °C (rate 5 $°C \cdot h^{-1}$) and finally quenched to room temperature by switching off the furnace.

2.3.4.2 X-ray Diffraction

By inspection under a microscope integrated in a glove box, colorless single crystals of the title compounds were isolated from residual Li_3N and enclosed in glass capillaries. Single-crystal X-ray diffraction data were collected with a Stoe IPDS I for $Li_4Ca_3Si_2N_6$ and with an Oxford Diffraction XCalibur for $Li_4Sr_3Si_2N_6$ (Mo-*K*α radiation). The program package SHELX97 was used for structure solution and refinement.[14] Further details of the crystal structure investigations can be obtained from the Fachinformationszentrum Karlsruhe, 76344 Eggenstein-Leopoldshafen, Germany (Fax: +49-7247-808-666; crysdata@fizkarlsruhe.de) on quoting the depository numbers CSD-420675 ($Li_4Ca_3Si_2N_6$) and CSD-421259 ($Li_4Sr_3Si_2N_6$), the names of the authors and citation of the publication.

2.3.4.3 Microanalysis

EDX spectra of selected crystals were obtained using a JSM 6500F scanning electron microscope (JEOL) equipped with an EDX detector 7418 (Oxford Instruments). The approximate molar ratio of the elements Ca:Si was found to be 22(2):14(2) (average from 3 independent measurements) for $Li_4Ca_3Si_2N_6$ and Sr:Si was found to be 19(2):13(2) (average from 3 independent measurements) for $Li_4Sr_3Si_2N_6$.

2.3.5 References

[1] S. Pagano, S. Lupart, M. Zeuner, W. Schnick, *Angew. Chem.* **2009**, *121*, 6453–6456; *Angew. Chem. Int. Ed.* **2009**, *48*, 6335–6338.

[2] J. Lang, J.-P. Charlot, *Rev. Chim. Miner.* **1970**, *7*, 121–131.

[3] H. Yamane, S. Kikkawa, M. Koizumi, *Solid State Ionics* **1987**, *25*, 183–191.

[4] F. Ottinger, R. Nesper, *Z. Anorg. Allg. Chem.* **2005**, *631*, 1597–1602.

[5] H. Yamane, F. J. DiSalvo, *J. Alloys Compd.* **1996**, *240*, 33–36.

[6] R. P. Elliot, *Constitution of Binary Alloys*, McGraw-Hill Book Company, New York, **1965**.

[7] D. G. Park, Z. A. Gal, F. J. DiSalvo, *J. Solid State Chem.* **2003**, *172*, 166–170.

[8] P. Hoehn, S. Hoffmann, J. Hunger, S. Leoni, F. Nitsche, W. Schnelle, R. Kniep, *Chem. Eur. J.* **2009**, *15*, 3419–3425.

[9] R. D. Shannon, *Acta Crystallogr., Sect. A* **1976**, *32*, 751–767.

[10] R. Hubbenthal, *MAPLE*, Programm zur Berechnung des Madelunganteils der Gitterenergie, Vers. 4; Universitat Giesen, **1993**.

[11] H. Baur, *Crystallogr. Rev.* **1987**, *1*, 59–83.

[12] S. Pagano, M. Zeuner, S. Hug, W. Schnick, *Eur. J. Inorg. Chem.* **2009**, 1579–1584.

[13] H. Lange, G. Wotting, G. Winter, *Angew. Chem.* **1991**, *103*, 1606–1625; *Angew. Chem. Int. Ed. Engl.* **1991**, *30*, 1579–1597.

[14] G. M. Sheldrick, *Acta Crystallogr., Sect. A* **2008**, *64*, 112–122.

2.4 $LiCa_3Si_2N_5$ – A Lithium Nitridosilicate with a $[Si_2N_5]^{7-}$ double-chain

published in

Saskia Lupart and Wolfgang Schnick

Z. Anorg. Allg. Chem. **2012**, (in print)
DOI: 10.1002/zaac.201200106
Copyright © 2012 WILEY-VCH Verlag GmbH & Co. KGaA, Weinheim
http://onlinelibrary.wiley.com/doi/10.1002/zaac.201200106/abstract

Abstract. The lithium nitridosilicate $LiCa_3Si_2N_5$ was synthesized by the reaction of calcium with $Si(NH)_2$ and Li_3N in weld shut tantalum ampoules at 900 °C. The structure of $LiCa_3Si_2N_5$ (space group C2/c (no. 15, $a = 5.1454(10)$, $b = 20.380(4)$, $c = 10.357(2)$ Å, $\beta = 91.24(3)°$; $wR2 = 0.1084$, 863 data,102 parameters)) consists of $[Si_2N_5]^{7-}$ double-chains including edge-sharing tetrahedra. The lithium atoms in the crystal structure are situated in strands along the crystallographic *b*-axis. Lattice energy calculations (MAPLE) and EDX measurements confirmed the electrostatic bonding interactions and the chemical composition. The ^{29}Si and ^{7}Li solid-state MAS NMR investigations are reported.

2.4.1 Introduction

Nitridosilicates are an interesting class of materials due to their outstanding chemical and physical properties as described in a recent review article (e.g. luminescence, non-linear optical properties or lithium ion conductivity).[1] Formally, they can be derived from oxosilicates by substituting N for O, which implies also an enhanced structural diversity. Whereas oxosilicates are limited to terminal $O^{[1]}$ or simply bridging $O^{[2]}$ positions,[2] in nitridosilicates, N can connect up to four neighboring tetrahedral centers ($N^{[4]}$).[1,3] Moreover, edge-sharing tetrahedra have often been observed in nitridosilicates.[4-6] However, only few less condensed nitridosilicates have been reported compared to the plethora of known higher condensed ones. This finding is probably due to the high temperatures applied typically in classical syntheses of nitridosilicates (> 1200 °C).[1, 7] In this context, we reported recently a synthetic approach utilizing liquid lithium as fluxing agent to access also less condensed nitridosilicates. Thus, due to the fluxing medium the reaction temperature can be decreased to 900 °C. It could be shown that by altering the nitrogen pressure inside the tantalum ampoule by varying the content of Li_3N/LiN_3, different degrees of condensation seem to be accessible.[7] For instance, the compounds $Li_2Sr_4Si_4N_8O$[7] and $Li_2CaSi_2N_4$,[8] which both exhibit three-dimensional nitridosilicate substructures were synthesized utilizing LiN_3 to increase the pressure inside the ampoules. Whereas, the low dimensional nitridosilicates $Li_4Ca_3Si_2N_6$ (0D)[4] and $LiCa_3Si_2N_5$ (1D) were both synthesized at 900 °C with only Li_3N.

In this contribution we report about the crystal structure of $LiCa_3Si_2N_5$. This compound has already been mentioned as example for the possibilities of the synthetic approach of utilizing lithium as fluxing agent.[7] However, the crystal structure, which exhibits the remarkable feature of a silicate substructure consisting of unbranched double-chains interconnected via edge-sharing tetrahedra, has not been discussed, yet.

2.4.2 Results and Discussion

2.4.2.1 Crystal Structure Description

The compound $LiCa_3Si_2N_5$ has been synthesized starting from Ca, silicon diimide and Li_3N in weld shut tantalum ampoules at 900 °C. Single crystals could be obtained by adding lithium as fluxing agent to the reaction mixture. X-ray structure analysis of $LiCa_3Si_2N_5$ revealed a monoclinic space group with a pseudo-meroedric twinning. Due to the monoclinic angle of

91.24°, only high angle data of the two individuals split up in reciprocal space. Therefore, it was possible to integrate with larger profiles and treat the twin-parts as meroedric. In the space group *C*2/*c* (no. 15) with the twin-law 100 0-10 00-1 the crystal structure could be solved and refined with satisfying R-values. Details of the crystal structure determination are listed in Table 1. All atoms were refined anisotropically except for the Li positions (see Table 2).

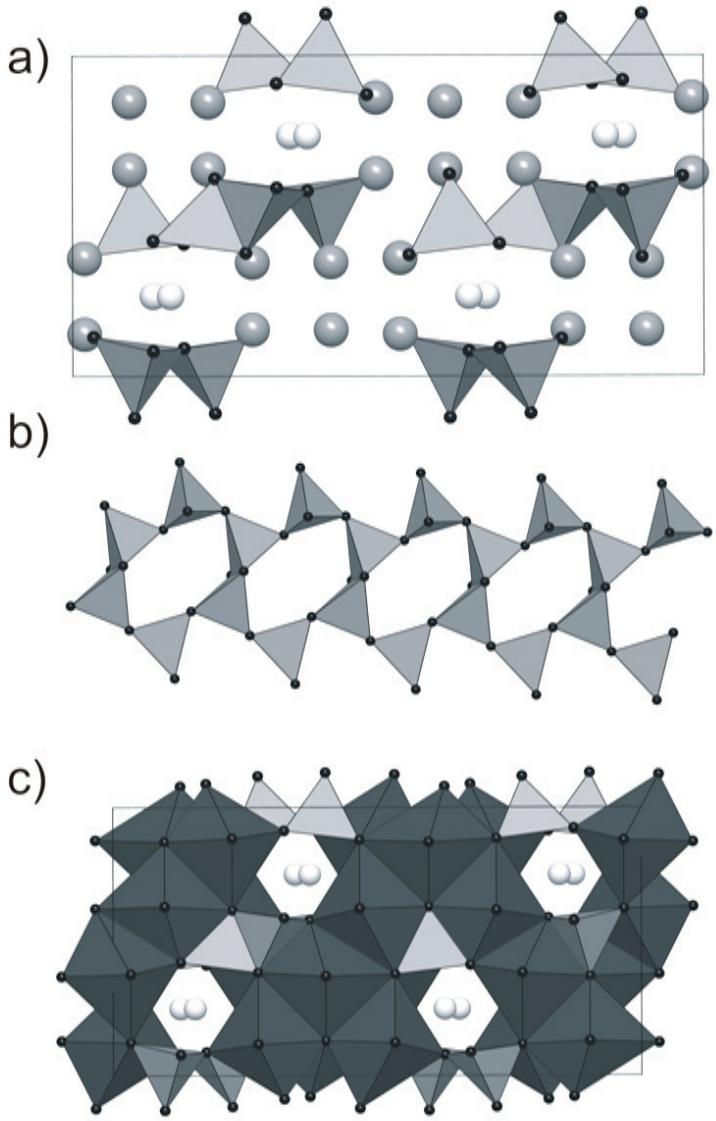

Figure 1. Crystal structure of $LiCa_3Si_2N_5$ a) view along [100]; b) $[Si_2N_5]^{7-}$ double-chain; c) unit cell with depicted SiN_4-tetrahedra (light gray) and CaN_6-octahedra (dark gray); Li atoms light gray, Ca atoms dark gray and nitrogen atoms black spheres.

The crystal structure of $LiCa_3Si_2N_5$ is depicted in Figure 1. The silicate substructure consists of a double-chain interconnected via common edges along the crystallographic *a*-axis, an unprecedented structural motif (see Figure 1b). The degree of condensation $\kappa = 0.40$ is due the edge-sharing slightly higher than expected for double-chain silicates ($\kappa = 0.36$). The Si-N distances range between 1.716(6) and 1.807(5) Å and thus are slightly elongated compared to the sum of the ionic radii (1.72 Å).[9] This is due to the edge-sharing of the $[SiN_4]$ tetrahedra. Investigations about edge-sharing tetrahedra in nitridosilicates revealed an elongation of the distances Si-N up to 1.85 Å, combined with rather short interatomic Si-Si distances (≈ 2.4-2.5 Å).[4-6,10] In $LiCa_3Si_2N_5$ the Si-Si distance of 2.4594(4) Å is therefore in the expected range of an edge-sharing unit.

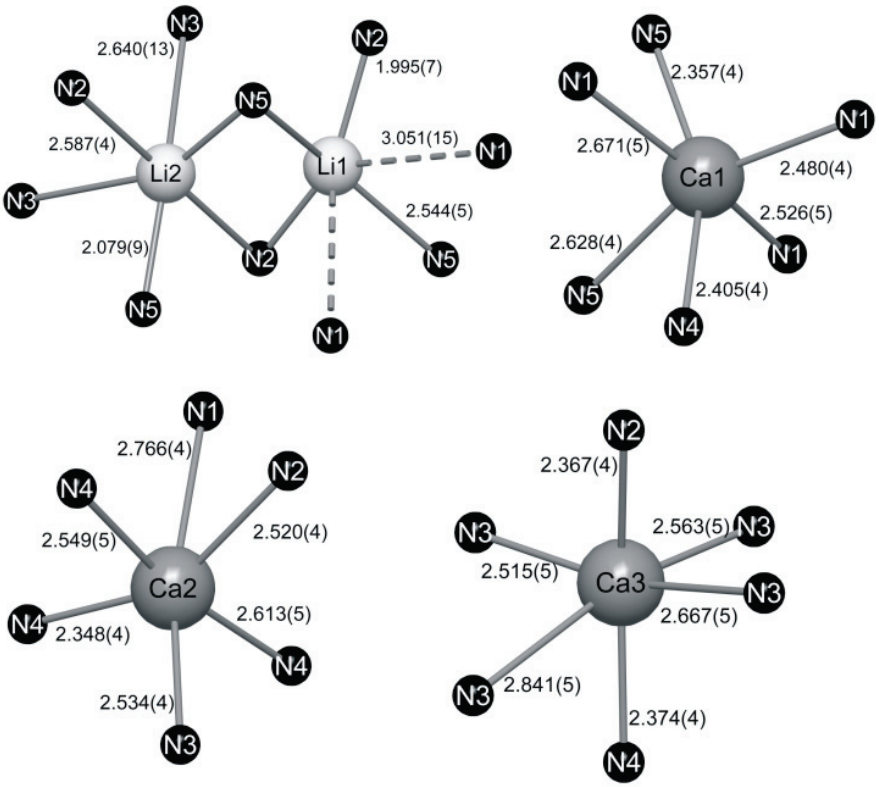

Figure 2. Coordination spheres of the Li and Ca atoms (distances in Å), Li atoms light gray, Ca atoms dark gray and nitrogen atoms black.

The crystal structure comprises three crystallographic independent Ca^{2+} positions, which are all coordinated by six N building distorted octahedra (see Figure 2). The distances in these octahedra vary between 2.344(5) Å and 2.834(5) Å and are in agreement with other calcium compounds and with the sum of the ionic radii (2.46 Å).[4,5,8,12-14] These octahedra are interconnected via common edges resulting in helices (see Figure 1c).

Table 1. Crystallographic data of $LiCa_3Si_2N_5$.

Formula	$LiCa_3Si_2N_5$
Formula mass /g · mol^{-1}	253.41
Crystal system	monoclinic
Space group	*C*2/*c* (no. 15)
Cell parameters / Å	a = 5.1454(10), b = 20.380(4), c = 10.357(2)
	β = 91.24(3)
Cell volume / 10^6 Å^3	V = 1085.8(4)
Formula units / cell	8
Crystal size / mm^3	0.04 x 0.06 x 0.09
$\rho_{calcd.}$ / g · cm^{-3}	3.100
μ / mm^{-1}	3.382
F(000)	1008.0
Diffractometer	Stoe IPDS I
Temperature / K	140(2)
Radiation, monochr.	Mo-K_α, (λ = 0.71073 Å), graphite
Absorption correction	semi-empirical[11]
θ range / °	3.9 - 27.5
Measured reflections	4453
Independent reflections	1246
Observed reflections	863
Refined parameters	102
Twinlaw	100 0-10 00-1
BASF	0.0414
GoF	1.135
R indices ($F_o^2 \geq 2\sigma (F_o^2)$)	R_1 = 0.0442, $wR2$ = 0.1084
R indices (all data)	R_1 = 0.0751, $wR2$ = 0.1222 [a]
Max. / min. residual electron density/ eÅ^{-3}	1.18/-0.68

[a] $w=1/[\sigma^2(F_o^2) +(0.0533\ P)^2+14.1412\ P]^{-1}$ where $P=(F_o^2+2F_c^2)/3$

Table 2. Atomic coordinates and equivalent displacement parameters [Å²] for $LiCa_3Si_2N_5$.

		x	*y*	*z*	U_{iso}/U_{eq}[a]
Ca1	*8f*	0.2458(2)	0.21530(6)	0.6453(2)	0.0058(3)
Ca2	*8f*	0.2547(2)	0.09060(6)	0.8557(2)	0.0065(3)
Ca3	*8f*	0.7514(3)	-0.01885(6)	0.8681(2)	0.0096(3)
Si1	*8f*	0.2030(3)	010486(7)	0.4619(2)	0.0034(4)
Si2	*8f*	-0.1914(3)	0.30338(7)	0.5477(2)	0.0060(4)
N1	*8f*	0.2694(11)	0.2256(2)	0.8835(5)	0.0062(10)
N2	*8f*	0.8723(10)	0.1278(3)	0.4225(5)	0.0084(10)
N3	*8f*	0.7335(11)	-0.0332(2)	0.624(5)	0.0089(11)
N4	*8f*	0.2389(10)	0.0976(2)	0.6298(4)	0.0064(9)
N5	*8f*	0.1312(11)	0.3236(3)	0.5873(5)	0.0087(10)
Li1	*4e*	½	0.3446(11)	¾	0.030(5)
Li2	*4e*	0	0.3727(10)	¾	0.020(4)

[a] U_{eq} is defined as 1/3 of the trace of the orthogonalized U_{ij} tensors; U_{eq} for Li.

The CaN_6 octahedra and SiN_4 tetrahedra enclose channels along the crystallographic *a*-axis, in which the two crystallographic independent lithium positions are situated. These lithium positions Li1 and Li2 are coordinated by 4+2 and six nitrogen atoms, respectively. The resulting highly distorted octahedra are connected by common edges and form zigzag strands along the crystallographic *a*-axis. The Li-N distances for Li2 range between 2.370(5) and 2.843(5) Å, whereas the distances in the 4+2 coordination of Li1 range between 1.998(8) and 3.044(16) Å (see Figure 2).

2.4.2.2 Lattice Energy Calculations According to the MAPLE Concept

Lattice energy calculations (MAPLE: Madelung part of lattice energy) were performed to prove the electrostatic consistency of the crystal structure.[15,16] Exclusively electrostatic interactions in an ionic crystal were taken into account, depending on the charge, distance and coordination spheres of the constituting ions. The calculated partial MAPLE values of the crystallographic atom positions are all within the typical ranges of the partial MAPLE values of comparable compounds (see Table 2). The minor deviation of 0.14 % of the total MAPLE sum compared to the MAPLE sum of the formally constituting compounds corroborates the crystal structure.

Table 2. Results of the MAPLE calculations [kJ/mol] for $LiCa_3Si_2N_5$; Δ = difference.[a]

	$LiCa_3Si_2N_5$
Ca^{2+}	1918, 2068, 2168
Si^{4+}	9090, 9794
$N^{[1]\,3-}$	4526, 4764
$N^{[2]\,3-}$	5589, 5602, 5639
Li^{+}	603, 614
Total MAPLE	51766
Δ	0.14 %
Total MAPLE (2/3 Si_3N_4 + 1 Ca_3N_2 +1/3 Li_3N: 1692 kJ/mol;	

[a] Typical partial MAPLE values [kJ/mol]: Ca^{2+}: 1700 - 2200; Si^{4+}: 9000 – 10200; $N^{[1]3-}$: 4300 – 5000; $N^{[2]3-}$4600 – 6000; Li^{+}: 550 -860.[1]

2.4.2.3 Solid-state MAS NMR

For a further corroboration of the crystal structure ^{29}Si and ^{7}Li solid-state MAS NMR measurements were conducted. For the measurements samples synthesized without lithium flux have been used (see experimental details). The ^{29}Si solid-state MAS NMR spectrum (see Figure X) shows two peaks at -50.9 and -54.1 ppm, which is in accordance with two crystallographic independent Si sites. For other (oxo)nitridosilicates a wide range for the chemical shift has been observed starting from -28 ppm (observed for $SrSi_6N_8$)[17] up to -68 ppm ($Ba_3Si_6O_9N_4$).[18] However, chemical shifts for ^{29}Si in $[SiN_4]$-tetrahedra occur most frequently in the region between -40 to -60 ppm,[17,19-22] which is in good accordance with chemical shifts observed for the title compound.

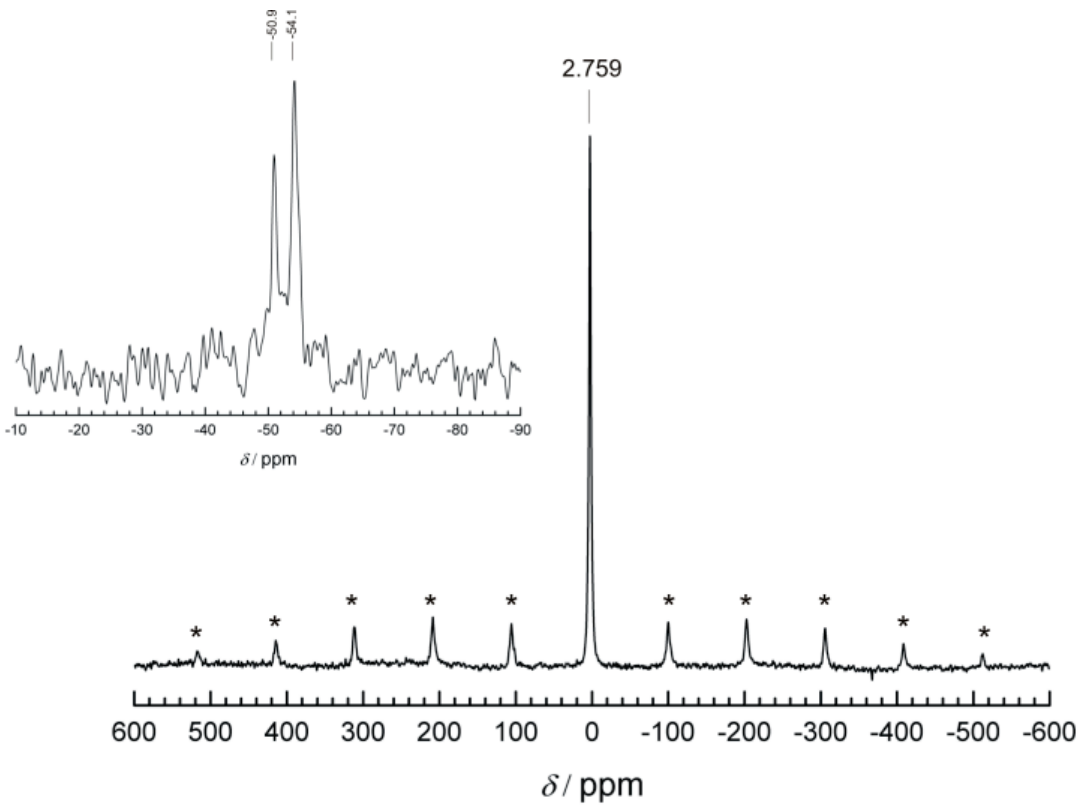

Figure 3. Solid-state MAS NMR spectra of ^{7}Li (rotation bands indicated by asterics) and ^{29}Si (inset) (rotation frequenz for both: 20 kHz).

The ^{7}Li solid-state MAS NMR spectrum of $LiCa_3Si_2N_5$ shows one isotropic signal at 2.7 ppm with a full width at half maximum (FWHM) of 2.9 ppm (see Figure 3). This chemical shift and the value for the full width at half maximum are in good accordance with other lithium nitridosilicates (e.g. Li_2SiN_2: $\delta = 1.7$ ppm, FWHM = 7.5;[23] $LiLa_5Si_4N_{10}O$, $\delta = 0.3$ ppm, FWHM = 8.6;[21] $Li_4Ca_3Si_2N_6$ $\delta = 2.0$ ppm, FWHM = 7.9).[4] The existence of only one signal in the ^{7}Li spectra can be assigned due to the bad resolution of ^{7}Li, which has also been observed e.g. for Li_2SiN_2, where eight crystallographic independent Li positions also result in only one signal in the solid-state MAS NMR.[23]

2.4.3 Conclusions

In this contribution we present the crystal structure of $LiCa_3Si_2N_5$. The compound has been synthesized utilizing liquid lithium at 900 °C in weld shut tantalum ampoules. The silicate substructure consists of $[Si_2N_5]^{7-}$ double-chains including edge-sharing tetrahedra. Although edge-sharing tetrahedra in nitridosilicates are still seldom observed, the deviations of the angles and distances in these units from the expected distances in corner-sharing tetrahedra seem, however, characteristic. The compound further corroborates that less condensed nitridosilicates are accessible via this synthetic approach.

2.4.4 Experimental Section

2.4.4.1 Synthesis

All manipulations were performed with rigorous exclusion of oxygen and moisture in flame-dried Schlenk-type glassware on a Schlenk line interfaced to a vacuum line (10^{-3} mbar) or in an argon-filled glove box (Unilab, MBraun, Garching, O_2 < 0.1 ppm, H_2O < 0.1 ppm). Argon (Messer-Griessheim, 5.0) was purified by passage through columns of silica gel (Merck), molecular sieve (Fluka, 4 Å), KOH (Merck, ≥ 85 %), P_4O_{10} (Roth, ≥ 99 %, granulate) and titanium sponge (Johnson Matthey, 99.5 %, grain size ≤ 0.8 cm) at 700 °C. For the synthesis of $LiCa_3Si_2N_5$ tantalum tubes (wall thickness 0.5 mm, internal diameter 10 mm, length 300 mm) were cleaned and their oxide layer removed by treating with a mixture of HNO_3 (conc.) and HF (40 %). The tubes were weld shut in an arc furnace under 1 bar purified argon. During this procedure, the crucible holder was water cooled in order to avoid chemical reactions during welding.

Single crystals were isolated by reacting 45.0 mg (0.77 mmol) $Si(NH)_2$,[24] 33.5 mg (0.84 mmol) Ca and 19.4 mg (0.56 mmol) Li_3N with 50 mg (7.2 mmol) Li as fluxing agent in closed tantalum ampoules. The sealed tantalum ampoule was placed in a silica tube under argon, which was placed in the middle of a tube furnace. The sample was heated to 900 °C (rate 120 °C h^{-1}), kept at this temperature for 12 h, subsequently cooled to 500 °C (rate 8 °C h^{-1}) and finally quenched to room temperature by switching off the furnace. The sample contained $LiCa_3Si_2N_5$ as colorless, air and moisture sensitive crystals.

Bulk samples were synthesized from 35.8 mg $Si(NH)_2$ (0.62 mmol), 40.0 mg (1.0 mmol) Ca and 15.5 mg (0.45 mmol) Li_3N. The crucible was heated to 900 °C within 3 h, maintained at this temperature for 24 h, cooled down to 450 °C (rate 300 °C h^{-1}) and quenched to room temperature after 3 h.

2.4.4.2 Chemical Analyses

Scanning electron microscopy was performed on a JEOL JSM-6500F equipped with a field emission gun at an acceleration voltage of 10 kV with a Si/Li EDX detector (Oxford Instruments, model 7418). Samples were prepared by placing single crystals on adhesive conductive pads and subsequently coating them with a thin conductive carbon film. Each EDX spectrum (Oxford Instruments) was recorded with the analyzed area limited onto one single crystal to avoid the influence of possible contaminating phases. Average analysis of three spots per crystallite showed an atomic ratio Ca/Si = 3.2 : 2.0 which corroborates the formation of $LiCa_3Si_2N_5$.

2.4.4.3 Single Crystal X-ray Analysis

Single crystals of $LiCa_3Si_2N_5$ were isolated under a microscope, which is integrated in a glove box, enclosed in glass capillaries (∅ 0.2 mm), and sealed under argon. Single-crystal X-ray diffraction data were collected at 140(2) K on a STOE IPDS I diffractometer (Stoe and Cie GmbH, Darmstadt) with Mo-K_α radiation (λ = 0.71073 Å, graphite monochromator). The structures were solved by direct methods after semi-empirical absorption correction. For the structure solution and refinement the program package SHELX97 was used.[25] Further details of the crystal structure investigations can be obtained from the Fachinformationszentrum Karlsruhe, 76344 Eggenstein-Leopoldshafen, Germany (fax: (+49)7247-808-666; e-mail: crysdata@fiz-karlsruhe.de) on quoting the depository number CSD-420676, the names of the authors and citation of the publication.

2.4.4.4 X-ray Powder Diffraction

X-ray powder diffraction data were collected on a STOE STADI P diffractometer with Ge(111)-monochromatized Mo-$K_{\alpha 1}$ radiation (λ = 0.71073 Å) in Debye-Scherrer geometry. The samples were enclosed in glass capillaries and sealed under argon.

2.4.4.5 Solid-state MAS NMR

Solid-state NMR experiments were performed on a Bruker Advance DSX 500 spectrometer with an external field of 11.75 T. The ^{7}Li and ^{29}Si spectra were recorded with direct excitation using a commercial 2.5 mm triple-resonance MAS probe at the frequency 194.415MHz. All experiments were carried out at room temperature in ZrO_2 rotors. The chemical shifts are reported using the frequency ratios published by IUPAC (δ scale relative to 1 % tetramethylsilane (TMS) in $CDCl_3$). Both spectra were recorded with a 90° pulse and at a spinning frequency of 20 kHz.

2.4.5 References

[1] M. Zeuner, S. Pagano, W. Schnick, *Angew. Chem.* **2011**, *123*, 7898-7920; *Angew. Chem. Int. Ed*. **2011**, 78*50*, 7754-7775.

[2] Superscript number specifies connectedness: number of directly connected silicon atoms.

[3] W. Schnick, *Int. J. Inorg. Mater.* **2001**, *3*, 1267-1272.

[4] S. Pagano, S. Lupart, S. Schmiechen, W. Schnick, *Z. Anorg. Allg. Chem.* **2010**, *636*, 1907-1909.

[5] F. Ottinger, R. Nesper, *Z. Anorg. Allg. Chem.* **2005**, *631*, 1597-1602.

[6] H. Huppertz, W. Schnick, *Chem. Eur. J.* **1997**, *3*, 249-252.

[7] S. Pagano, S. Lupart, M. Zeuner, W. Schnick, *Angew. Chem.* **2009**, *121*, 6453-6456; *Angew. Chem., Int. Ed. Engl.* **2009**, 64*48*, 6335-6338.

[8] M. Zeuner, S. Pagano, S. Hug, P. Pust, S. Schmiechen, C. Scheu, W. Schnick, *Eur. J. Inorg. Chem.* **2010**, 4945-4951.

[9] R. D. Shannon, *Acta Crystallogr., Sect. A: Cryst. Found. Crystallogr.* **1976**, *32*, 751-767.

[10] H. Yamane, F. J. DiSalvo, *J. Alloys Compd.* **1996**, *240*, 33-36.

[11] V. XPREP, Siemens Analytical X-ray Instruments Inc., Madison, Wisconsin, USA, **1996**.

[12] M. S. Bailey, F. J. DiSalvo, *J. Alloys Compd.* **2006**, *417*, 50-54.

[13] F. Ottinger, R. Nesper, *Z. Anorg. Allg. Chem.* **2005**, *631*, 1597-1602.

[14] Z. A. Gál, P. M. Mallinson, H. J. Orchard, S. J. Clarke, *Inorg. Chem.* **2004**, *43*, 3998-4006.

[15] R. Hoppe, *Angew. Chem.* **1970**, *82*, 7-16; *Angew. Chem. Int. Ed. Engl.* **1970**, *9*, 25-34.

[16] R. Hoppe, *Angew. Chem.* **1966**, *78*, 52-63; *Angew. Chem. Int. Ed. Engl.* **1966**, *5*, 95-106.

[17] F. Stadler, O. Oeckler, J. Senker, H. A. Höppe, P. Kroll, W. Schnick, *Angew. Chem.* **2005**, *117*, 573-576; *Angew. Chem., Int. Ed.* **2005**, *44*, 567-570.

[18] F. Stadler, W. Schnick, *Z. Anorg. Allg. Chem.* **2006**, *632*, 949-954.

[19] F. Stadler, R. Kraut, O. Oeckler, S. Schmid, W. Schnick, *Z. Anorg. Allg. Chem.* **2005**, *631*, 1773-1178.

[20] G. R. Hatfield, B. Li, W. B. Hammond, F. Reidinger, J. Yamanis, *J. Mater. Sci.* **1990**, *25*, 4032-4035.

[21] S. Lupart, W. Schnick, *Z. Anorg. Allg. Chem.* **2011**, *638*, 94-97.

[22] S. Lupart, M. Zeuner, S. Pagano, W. Schnick, *Eur. J. Inorg. Chem.* **2010**, 2636-2641.

[23] S. Pagano, M. Zeuner, S. Hug, *Eur. J. Inorg. Chem.* **2009**, 1579-1584.

[24] H. Lange, G. Wötting, G. Winter, *Angew. Chem.* **1991**, *103*, 1606-1625; *Angew. Chem., Int. Ed. Engl.* **1991**, *30*, 1579-1597.

[25] G. M. Sheldrick, *Acta Crystallogr. A* **2008**, *64*, 112-122.

2.5 $Li_2Sr_4[Si_2N_5]N$ – A Layered Lithium Nitridosilicate Nitride

published in

Saskia Lupart, Sandro Pagano, Oliver Oeckler, and Wolfgang Schnick

Eur. J. Inorg. Chem. **2011** (13), 2118-2123
DOI: 10.1002/ejic.201100115
Copyright © 2011 WILEY-VCH Verlag GmbH & Co. KGaA, Weinheim
http://onlinelibrary.wiley.com/doi/10.1002/ejic.201100115/abstract

Abstract. The quaternary alkaline earth nitridosilicate nitride $Li_2Sr_4[Si_2N_5]N$ has been synthesized at 900 °C using liquid lithium as fluxing agent in weld-shut tantalum ampoules. The structure of $Li_2Sr_4[Si_2N_5]N$ (space group $I\bar{4}m2$ [no. 119, a = 751.46(11), c = 1508.9(3) pm, Z = 4, $R1$ = 0.049, $wR2$ = 0.135, 499 data, 41 parameters]) is built up from vertex sharing $[SiN_4]$ tetrahedra forming layers which can be derived from the apophyllite structure type. According to the condensation degree of κ = 2:5 discrete N^{3-} ions which are coordinated by five Sr^{2+} and one Li^{+} site occur besides the silicate layers in the crystal structure. The electronic structure and chemical bonding in $Li_2Sr_4[Si_2N_5]N$ has been analyzed by Madelung calculations (MAPLE) and DFT (VASP) calculations.

2.5.1 Introduction

Both from an academic as well as an industrial point of view nitridosilicates and related compounds (e.g. SiONs and SiAlONs) are interesting materials due to their outstanding chemical and physical properties (e.g. luminescence or lithium ion conductivity).[1–3] Nitridosilicates can be formally derived from oxosilicates by substituting N for O, which allows more extended structural possibilities. As the structural chemistry of oxygen in silicates is limited to terminal $O^{[1]}$ or bridging $O^{[2]}$ atom positions,[4] a higher crosslinking can be achieved by substituting O for N, which allows connecting up to four neighboring tetrahedral centers yielding even ammonium type character for N. Typical structures with $N^{[1]}$, $N^{[2]}$, $N^{[3]}$ or $N^{[4]}$ functionalities have been summarized in a recent review and include examples such as $M_2Si_5N_8$ with M = Sr, Ba ($N^{[2]}$, $N^{[3]}$), $MSi_2O_2N_2$ with M = Ca, Sr, Ba ($N^{[3]}$), γ-Si_3N_4 ($N^{[4]}$) or $MYbSi_4N_7$ with M = Eu, Sr, Ba ($N^{[2]}$, $N^{[4]}$).[3] In addition, edge-sharing tetrahedra have been observed in nitridosilicates, whereas for oxosilicates they have exclusively been postulated for fibrous SiO_2.[5] However, the existence of the latter compound has been controversially discussed.

Most of the nitridosilicates reported so far, have been synthesized employing high temperatures (1400–1600 °C) and exhibit predominantly three-dimensional silicate networks made up of $[SiN_4]$ tetrahedra. This observation is probably due to the rather harsh syntheses conditions that favor formation of more stable network structures.[6–10] Recently, a novel synthetic approach has been reported using sodium melts as fluxing agent. Thereby, the nitridosilicate $Ba_5Si_2N_6$ which consists of exclusively edge-sharing $[Si_2N_6]^{10-}$ bow-tie units could be synthesized at lower temperatures.[11] The employment of liquid sodium as fluxing agent at lower temperatures also afforded the compounds $MSiN_2$ (M = Ca, Sr, Ba).[9] Recently, we reported about a variation of this method using liquid lithium in weld-shut tantalum ampoules, which exhibits several advantages compared to the use of sodium, such as higher solvability of lithium and higher melting point. As a result of the employment of lithium as tritium breeder and primary coolant in several designs of the deuterium fuelled thermonuclear reactor, the reactivity of lithium with other elements has been well investigated.[12–14] Accordingly, silicon, nitrogen, various metals as well as inorganic salts are soluble in liquid lithium at moderate temperatures,[13] which gives way to a promising approach to new nitridosilicates. Using this technique, we were able to synthesize a number of quaternary lithium nitridosilicates with varying degrees of condensation in lithium melts.[15–17] Group-like ($Li_4M_3Si_2N_6$ with M = Ca, Sr), chain-type ($LiCa_3Si_2N_5$, $Li_5Ln_5Si_4N_{12}$ with Ln =

La, Ce) and framework nitridosilicates ($Li_2Sr_4Si_4N_8O$) can be obtained and hence the whole range of dimensionality can be accessed.[15,16,18] The reactions were conducted at temperatures below 1250 °C in liquid lithium in closed tantalum ampoules. However, we assume that upon varying the pressure conditions inside the ampoules by the amount of lithium azide/lithium nitride, the degree of condensation is influenced.

In this contribution we present a further new quaternary lithium nitridosilicate nitride obtained using liquid lithium as fluxing agent. $Li_2Sr_4[Si_2N_5]N$ exhibits a two-dimensional $[Si_2N_5]^{7-}$ network and isolated N^{3-} ions, which have not been observed in nitridosilicates so far. However, they were found in nitridogallates, e.g. $Sr_6[GaN_3]N_2$ or nitridometallates, e.g. $Ca_6[MnN_3]N_2$.[19–21] Moreover, the nitridogermanate nitrides $M_7[GeN_4]N_2$ (M = Ca, Sr) have recently been structurally elucidated.[22]

2.5.2 Results and Discussion

2.5.2.1 Synthetical Approach

$Li_2Sr_4[Si_2N_5]N$ was obtained by the reaction of silicon diimide, lithium azide and strontium metal in liquid lithium in weld-shut tantalum ampoules at 900 °C. One equivalent cesium iodide is necessary for the reaction, probably acting as a catalyst for the formation of $Li_2Sr_4[Si_2N_5]N$. Cesium iodide might function as a template for the formation of the $[Si_2N_5]^{7-}$ network. The amount of CsI seems crucial as reactions with various other amounts do not lead to the slightly orange crystals of extremely air and moisture sensitive $Li_2Sr_4[Si_2N_5]N$.

2.5.2.2 Data Collection

Single-crystal X-ray structure analysis revealed a tetragonal body centered lattice. As Sr and Si atom positions can be described in a sub-cell, rather weak superstructure reflections in all three spatial directions had to be taken into account in the refinement, where the space group $I\bar{4}m2$ gave a reasonable structural model with satisfactory R values. Moreover, no evidence was found indicating a lower symmetry. In the tetragonal model, one nitrogen atom position is not included in the $[Si_2N_5]^{7-}$ silicate substructure, but corresponds to a discrete N^{3-} ion. The refinement of its site occupancy leads to an almost half-occupied site. In order to provide charge neutrality, the occupancy factor was fixed at a value of ½. There were no hints of a

possible superstructure concerning the half-occupied nitrogen in the Xray diffraction. Some details of the crystal structure determination are displayed in the experimental section. All atoms were refined anisotropically except the lithium and the half-occupied nitrogen atom position. Atomic coordinates and Wyckoff positions are listed in Table 1.

Table 1. Atomic coordinates and equivalent displacement parameters [Å^2] for $Li_2Sr_4[Si_2N_5]N$.

Atom		s.o.f	*x*	*y*	*z*	U_{eq}/ U_{iso}[a]
Sr1	8*i*		0.24803(10)	0	0.08320(12)	0.0090(5)
Sr2	8*i*		0.24535(11)	½	0.09867(11)	0.0127(6)
Si	8*i*		0	0.2262(4)	0.2005(3)	0.087(7)
N1	8*i*		0	0.251(11)	0.0840(8)	0.014(3)
N2	4*e*		0	0	0.2305(11)	0.021(3)
N3	8*h*		0.1957(10)	0.3043(10)	¼	0.025(2)
N4	8*i*	½	½	0.246(3)	0.090(2)	0.038(10)
Li	8*i*		½	0.2462(19)	0.2099(18)	0.011(5)

[a] U_{eq} is defined as 1/3 of the trace of the U_{ij} tensors; U_{eq} for N4 and Li.

2.5.2.3 Crystal Structure Description

The crystal structure of $Li_2Sr_4[Si_2N_5]N$ consists of loopbranched *dreier* single layers built up from $[Si_2N_5]^{7-}$ tetrahedra and can be derived from the apophyllite structure type ($KCa_4[Si_4O_{10}]_2(F,OH)\cdot 8H_2O$),[24,25] although the molar ratio Si/N = 1:3 does not indicate a layered structure. This discrepancy is due to the discrete N^{3-} ions. The silicate substructure itself exhibits a condensation degree κ = 2:5, which is in accordance with a layered silicate structure. The layers in $Li_2Sr_4[Si_2N_5]N$ exhibit *vierer* and *achter* rings in analogy to the apophyllite structure[26] (cf. Figure 1) and are situated parallel (110). However, due to the higher symmetry of $Li_2Sr_4[Si_2N_5]N$ these rings are more regular and not tilted as in apophyllite. The distances Si–N range between 175.1(5)–176.7(13) pm and are in good accordance with other nitridosilicates.[27,28]

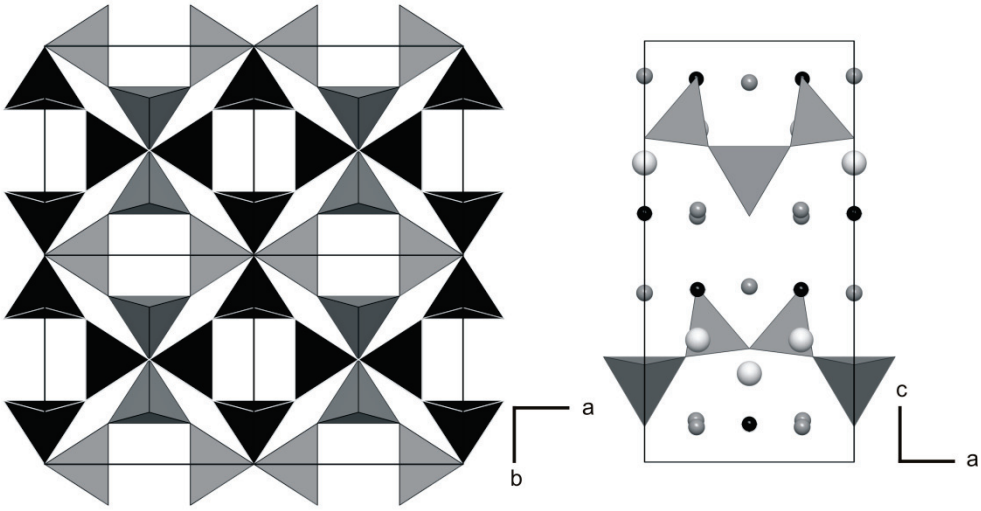

Figure 1. left: $[SiN_4]$ substructure along [001], black $[SiN_4]$ tetrahedra in the back, gray ones in the front; right: unit cell along [010], Sr dark gray, Li white, N black.

There are two crystallographically independent Sr^{2+} positions occupying Wyckoff sites 8*i* (cf. Figure 2). The Sr1 positions exhibit a distorted octahedral coordination made up of nitrogen atoms. The Sr2 are surrounded by seven nitrogen atoms building a monocapped distorted octahedron. The distances within these coordination polyhedra range between 252.2(12) and 290.4(13) pm for Sr1 and 263.4(6)–274.3(3) pm for Sr2, respectively (cf. Table 2). These distances and coordination spheres correspond well with other strontium containing nitridosilicates (e.g. $SrSiN_2$, $SrYSi_4N_7$ or $Sr_2Si_5N_8$)[7,9,29] and the sum of the ionic radii according to Shannon[30] (264 pm sixfold coordination, 267 pm sevenfold coordination), Baur[31] (273 pm) and Slater[32] (265 pm). The Sr1 and Sr2 polyhedra are situated alternately in the crystal structure, forming double layers between the $[Si_2N_5]^{7-}$ layers.

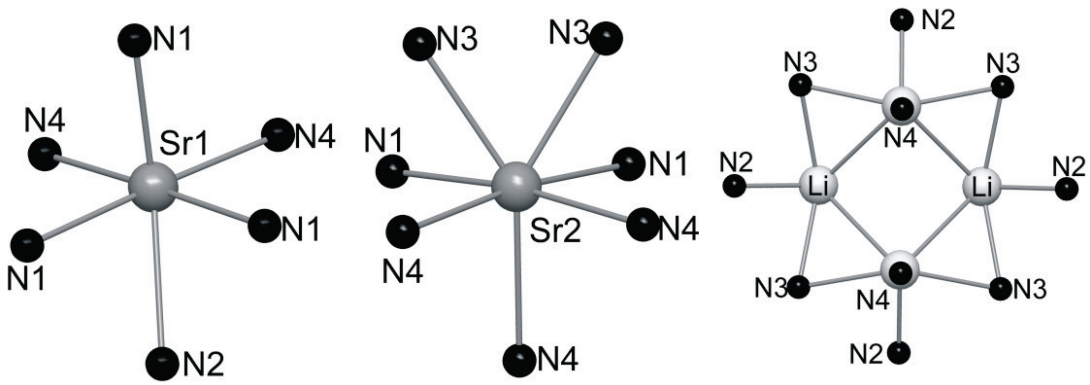

Figure 2. Coordination spheres of Sr1 (left), Sr2 (middle) and the Li atoms (right).

Table 2. Selected interatomic distances (pm) for $Li_2Sr_4[Si_2N_5]N$. Standard deviations are given in parentheses.

Sr1-N1		252.2(12)	Sr2-N1	(2x)	263.4(6)
Sr1-N4	(2x)	265.4(18)	Sr2-N4	(2x)	270.0(18)
Sr1-N1	(2x)	265.4(6)	Sr2-N3		274.3(4)
Sr1-N2		290.4(13)	Sr1-N3		274.3(3)
Si-N3	(2x)	175.3(5)	Li-N4		181(4)
Si-N2		176.0(6)	Li-N2	(2x)	210.5(17)
Si-N4		176.8(13)	Li-N3		240.1(11)

The Li^+ site is coordinated by four nitrogen atoms with distances Li–N in the range 181(4)–240.1(11) pm (cf. Table 2). These distances are in good accordance with previously reported lithium nitridosilicates and the sum of the effective ionic radii (205–212 pm).[17,30–33] The coordination sphere of Li is unusual, because all ligands are rather on one side of the ion. However, there are several other examples for such a coordination, e.g. Li_2SiN_2 or $LiMo_2Ba_5N_7Cl_2$.[33,34] In the second coordination sphere, the lithium ions form $[Li_4N_8]^{20-}$ building units, which are separated by nitrogen from each other (cf. Figure 2). The distances Li–Li amounts to 288(3) pm, therefore no reasonable short pathways between the polyhedra indicative of lithium ion mobility, as, for example, described for Li_2SiN_2, can be found.[33]

The discrete N^{3-} ions (N4) are coordinated in a pseudooctahedral way by five Sr^{2+} and one Li^+ (cf. Figure 3). The distances Sr–N^{3-} vary between 265.4(18) and 285(4) pm, which is within the range of comparable compounds[7,27] and correspond well with the sum of the ionic radii as described above.[30–32] The distance Li–N^{3-} of 181(4) pm is the shortest distance in the structure. Compared to the nitridogermanate nitride $Sr_7[GeN_4]N_2$, which exhibits discrete N^{3-} ions in addition to $[GeN_4]^{8-}$ tetrahedrons, the Sr–N^{3-} distances are in the same range.[22]

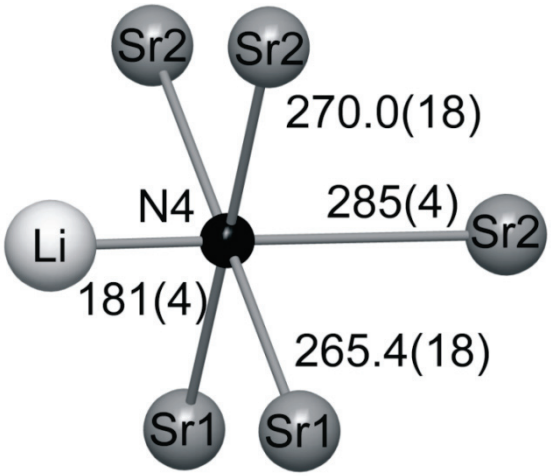

Figure 3. Coordination sphere of the half occupied N^{3-} site with distances in pm.

2.5.2.4 Lattice Energy Calculations According to the MAPLE Concept

Lattice energy calculations (MAPLE: Madelung part of lattice energy)[30,35–37] were performed to prove the electrostatic consistency of the crystal structure and especially the presence of discrete N^{3-} ions. Hereby, exclusively electrostatic interactions in an ionic crystal were considered, depending on the charge, distance and coordination spheres of the constituting atoms. As there is no possibility to deal with partially occupied positions with the MAPLE program, it is necessary to use subgroup models for this calculation with fully occupied N^{3-} sites, although there are no indications for ordering from the X-ray diffraction data. Refinements in appropriate subgroups did not yield ordered models. Two subgroups of $I\,4\bar{m}2$ (no. 119) exhibit a splitting of the Wyckoff position 8*i*, which is occupied by N^{3-}, into two fourfold positions, namely $P\bar{4}m2$ (no. 115; k1) and *Imm*2 (44, t1). In both space groups, MAPLE calculations were performed with one N^{3-} site fully occupied and the other void. However, only in *Imm*2 reasonable partial MAPLE values could be achieved. Other arrangements of the voids in *Imm*2 and models in $P\bar{4}m2$ lead to negative partial MAPLE values and were therefore neglected. In order to have a higher diversity for the defect sites also calculations with enlarged unit cells were performed. In this context, space group *Imm*2 (**a**, 3**b**, **c**) also led to reasonable MAPLE values, with different arrangement of the voids. All MAPLE calculations in the space group *Imm*2 and *Imm*2 (**a**, 3**b**, **c**) gave reasonable MAPLE values, which were all in the same range, therefore only the results of the model in *Imm*2 are listed in Table 3. The calculated partial MAPLE values of the crystallographically

independent atoms are in agreement with typical MAPLE ranges for different atom types of comparable compounds in the literature. Only the lithium position next to the defect sites is slightly below the expected range. The total MAPLE values correspond well with the sum of the total MAPLE values of the formally constituting compounds as can be seen in Table 3.

Table 3. Results of the MAPLE calculations [kJ/mol] for $Li_2Sr_4[Si_2N_5]N$ in space group *Imm*2 with half the isolated N^{3-} positions occupied, before and after optimization with VASP.

	$Li_2Sr_4[Si_2N_5]N$	$Li_2Sr_4[Si_2N_5]N$ (after GGA optimization)
Sr^{2+}	1415; 1548; 2051, 2307	1587; 2121; 1764; 1969
Si^{4+}	9896; 9932	9899; 9824
$N^{[1]\,3-}$	4449; 4571	4476; 4655
$N^{[2]\,3-}$	4974; 5339; 5414	5431; 5368; 5259
$N^{[0]3-}$	3183	3455
Li^{+}	360; 679	539; 761
Total MAPLE	28245	28501
Δ	1.01 %	0.10 %
Total MAPLE (1/2 $Li_4Sr_3Si_2N_6$ + 1/2 $SrSiN_2$ – 1/2 Li_2SiN_2): 28530 kJ/mol		

Typical partial MAPLE values [kJ/mol]: Sr^{2+}:1500-2300 Si^{4+}: 9000-10200; $N^{[0]3-}$: 3000-3500 $N^{[1]\,3-}$: 4300-5000; $N^{[2]\,3-}$: 4600-6000; Li^{+}: 550-860.[22,37-39]

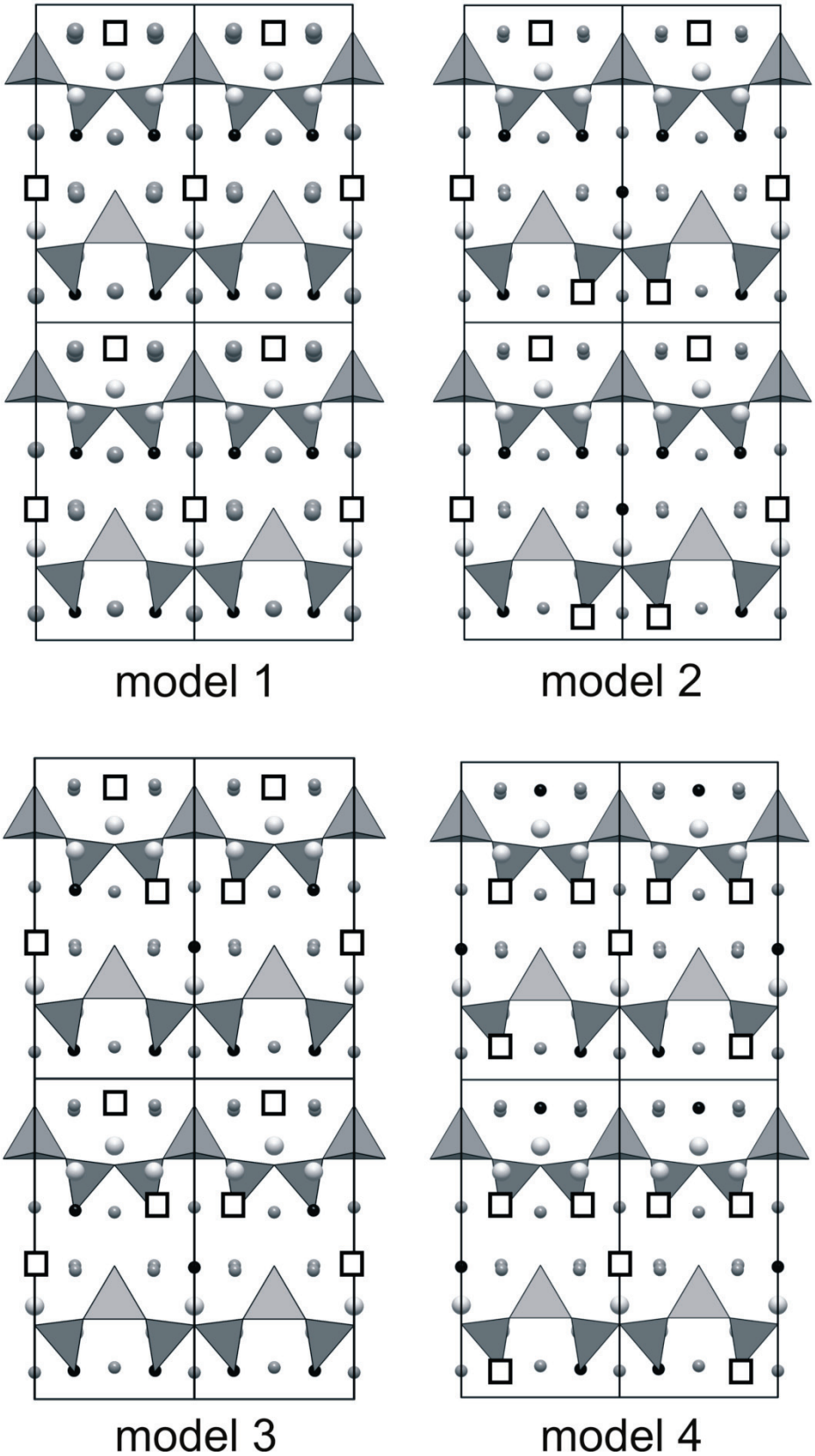

Figure 4. Depiction of the different models in the same unit cell for a better comparison. (Model 1: *Imm*2; model 2-4: *Imm*2 (**a**, 3**b**, **c**)).

2.5.2.5 DFT Calculations

Structural optimizations of the four best models according to MAPLE calculations were calculated within the density functional theory (DFT) using the Vienna ab initio Simulation Package (VASP). The four models vary in the arrangement of the voids as depicted in Figure 4. Structure optimizations of all four models show, that only minor deviations from the original cell and site parameters occurred during the optimizations. The optimized structures exhibit residual forces of less than 0.004 eV/Å. The cell volumes are in the same range for all models for the LDA as well as the GGA approximation. According to the lowest ground state energies, model 3, which exhibits the highest dispersion between the defect sites, is energetically favored (cf. Table 4). Also from a chemical point of view, this model is more likely, because an agglomeration of N^{3-} sites would lead to a high negatively charged location in the crystal structure, which is extremely unlikely to occur. However, the differences in energy are rather small and therefore indicate that all variants are likely to occur in the real structure.

Table 4. ΔE and V_0 of the optimized structural models compared to the MAPLE sums of the initial structures before optimization. The values of model 1 are adapted to the cells of the other models in *Imm*2_3*b* to have values better comparable.

	ΔE [eV][a]	V_0 [10^6pm^3]	ΔMAPLE [%][b]
model 1 (LDA)	1.511[c]	2517.15	1.01
model 2 (LDA)	3.539	2538.67	2.56
model 3 (LDA)	0	2521.90	1.34
model 4 (LDA)	3.832	2540.59	2.57
model 1 (GGA)	1.570[c]	2669.22	1.01
model 2 (GGA)	3.145	2694.07	2.56
model 3 (GGA)	0	2676.76	1.34
model 4 (GGA)	3.477	2696.23	2.57

[a] Relative energies compared to the lowest energy of LDA method (-1107.935 eV) and GGA (-1003.197 eV).

[b] Deviation from the theoretical MAPLE sums.

[c] Convergence test was performed with a *Imm*2_3*b* cell for model 1 resulting ΔE = 1.505 (LDA) and ΔE = 1.564 (GGA).

DOS calculations for model 1, which exhibits the smallest unit cell, reveal a band gap of 0.37 eV. The band gap for model 3, which is energetically favored, is 0.38 eV. Although the

models exhibit a different arrangement of the voids, the almost equal band gaps show, that it seems probable that in the real structure all models are present. The calculated band gaps are smaller than the expected ca. 2.2 eV corresponding to the slightly orange color and the transparency of the crystals. However, it is well known that band gaps are generally underestimated by DFT methods.[20,40]

2.5.2.6 Comparison between Lattice Energy Calculations and DFT Calculations

A comparison between the results of the DFT and the MAPLE calculations (cf. Table 4) leads to the conclusion that MAPLE can provide reasonable starting models, however, a prediction of the best model is not possible. MAPLE calculations of the optimized models revealed no significant differences. All LDA-optimized models had worse MAPLE values due to the fact that covalent bonding is overestimated by LDA and therefore slightly shorter, which has great influence on the MAPLE calculations. The GGA-optimized structures exhibit all less than 0.94% deviation from the theoretical MAPLE sums. In Table 3, the MAPLE values of the optimized model 1 are given in comparison to the values for the model derived by group-subgroup transformation. All partial values are in the expected range. Only the lithium position neighboring the void has a partial MAPLE value slightly below the expected range. However, respective values of other compounds, which exhibit low coordination for Li^+ range around 540 kJ/mol as well.[34,41]

2.5.3 Conclusions

In this contribution we present the first nitridosilicate nitride, namely $Li_2Sr_4[Si_2N_5]N$, with a layered $[Si_2N_5]^{7-}$ substructure, which can be derived from the apophyllite structure type. The title compound could be synthesized in closed tantalum ampoules using liquid lithium as fluxing agent. Apparently, the usage of cesium iodide as catalyst extends the spectrum of known quaternary lithium nitridosilicates. Therefore, we expect that a few more compounds can be afforded using lithium as fluxing agent and additional inorganic salts. To corroborate the half-occupied N^{3-} site MAPLE and DFT calculations were performed. In this context no higher ordering of the N^{3-} site could be found either in the X-ray diffraction or the DFT calculations. Moreover, $Li_2Sr_4[Si_2N_5]N$ is another example for the efficiency to develop new quaternary lithium nitridosilicates using liquid lithium. With respect to the highly anisotropic layered nitridosilicate structure and the concomitant presence of isolated N^{3-} ions, the high-

pressure behavior of $Li_2Sr_4[Si_2N_5]N$ is of special interest as it might lead to a nucleophilic attack of the nitride ions at the Si tetrahedral centers.

2.5.4 Experimental Section

2.5.4.1 Synthesis

All manipulations were performed with rigorous exclusion of oxygen and moisture in flame-dried Schlenk-type glassware on a Schlenk line interfaced to a vacuum line (10–3 mbar) or in an argon-filled glove box (Unilab, MBraun, Garching, $O_2 < 0.1$ ppm, H2O < 0.1 ppm). Argon (Messer–Griessheim, 5.0) was purified by passage through columns of silica gel (Merck), molecular sieves (Fluka, 4 Å), KOH (Merck ≥ 85 %), P_4O_{10} (Roth ≥ 99%, granulate) and titanium sponge (Johnson Matthey, 99.5%, grain size ≤ 0.8 cm) at 700 °C. For the syntheses of the title compound tantalum tubes (wall thickness 0.5 mm, internal diameter 10 mm, length 300 mm) were cleaned and the oxide layer removed by treatment with a mixture of HNO_3 (concd.) and aqueous HF (40 %). The tubes were weld-shut in an arc furnace under 1 bar of purified argon. During this procedure, the crucible holder was water cooled in order to avoid chemical reactions during welding.

For the synthesis of $Li_2Sr_4[Si_2N_5]N$, silicon diimide (38.7 mg, 0.67 mmol, synthesized according to literature[42]), LiN_3 (16.3 mg, 0.33 mmol, Sigma Aldrich 99.9 %), Sr (59.9 mg, 0.68 mmol, Sigma Aldrich, 99.99%) and CsI (43.0 mg, 0.17 mmol, Sigma Aldrich, dried under vacuum) were mixed in an agate mortar, filled in a tantalum ampoule and covered with lithium (12 mg, 1.7 mmol, Alfa Aesar, 99.9%) in a glove box. The sealed tantalum ampoule was placed into a silica tube under argon, which was placed in the middle of a tube furnace. The temperature was raised to 900 °C (rate 5 °C min^{-1}), maintained for 24 h and cooled down to 500 °C (rate 0.2 °C min^{-1}). Subsequently, the sample was quenched to room temperature by switching off the furnace. The sample contained $Li_2Sr_4[Si_2N_5]N$ as orange highly air - and moisture-sensitive crystals.

Table 5. Crystallographic data of $Li_2Sr_4[Si_2N_5]N$.

Formula	$Li_2Sr_4[Si_2N_5]N$
Formula mass /g · mol^{-1}	504.60
Crystal system	tetragonal
Space group	$I\bar{4}m2$ (no. 119)
Cell parameters / pm	a = 751.46(11)
	c = 1508.9(3)
Cell volume / 10^6 pm^3	V = 852.0(2)
Formula units / cell	4
Crystal size / mm^3	0.09 x 0.04 x 0.01
$\rho_{calcd.}$ / g · cm^{-3}	3.934
μ / mm^{-1}	25.136
F(000)	912
Diffractometer	Stoe IPDS I
Temperature / K	293(2)
Radiation, monochr.	Mo-K_α, (λ = 71.073 pm), graphite
Absorption correction	semi-empirical[21]
θ range / °	2.7 - 27.5
Measured reflections	3500
Independent reflections	554
Observed reflections	499
Refined parameters	41
Flack parameter	0.50(4)
GoF	1.091
R indices ($F_o^2 \geq 2\sigma (F_o^2)$)	R_1 = 0.0499, $wR2$ = 0.1364
R indices (all data)	R_1 = 0.0534, $wR2$ = 0.1413 [a]
Max. / min. residual electron density/ eÅ^{-3}	3.72/-2.26

[a] $w = 1/[\sigma^2(F_o^2) + (0.0980\,P)^2 + 0.00\,P]^{-1}$ where $P = (F_o^2 + 2\,F_c^2)\,/\,3$

2.5.4.2 Chemical Analyses

Scanning electron microscopy was performed on a JEOL JSM-6500F equipped with a field emission gun at an acceleration voltage of 10 kV with a Si/Li EDX detector (Oxford Instruments, model 7418). Samples were prepared by placing single crystals on adhesive conductive pads and subsequently coating them with a thin conductive carbon film. Each EDX spectrum (Oxford Instruments) was recorded with the analyzed area limited onto one single crystal to avoid the influence of possible contaminating phases. EDX-analysis showed an atomic ratio Sr/Si = 1:1.7 which corroborates the formation of $Li_2Sr_4[Si_2N_5]N$.

2.5.4.3 Single Crystal X-ray Analysis

Single crystals of $Li_2Sr_4[Si_2N_5]N$ were isolated under a microscope, which is integrated in a glove box, enclosed in glass capillaries (Ø = 0.3 mm), and sealed under argon. Single-crystal X-ray diffraction data were collected at room temperature on a STOE IPDS I diffractometer (Stoe and Cie GmbH, Darmstadt) with Mo-*K*α radiation (λ = 0.71073 Å, graphite monochromator). The structure was solved by direct methods after semi-empirical absorption correction. For the structure solution and refinement (see Table 5) the program package SHELX97 was used.[43] Further details on the crystal structure investigation may be obtained from the Fachinformationszentrum Karlsruhe, 76344 Eggenstein-Leopoldshafen, Germany (Fax: +49-7247-808-666; E-mail: crysdata@fiz-karlsruhe.de), on quoting the depository number CSD-422596.

2.5.4.4 Computational Methods

Structural optimizations, total energies and band structure calculations are calculated within density functional theory (DFT)[44] using the Vienna ab initio Simulation Package (VASP). Hereby, the total energy pseudopotential method is combined with a plane-wave basis set.[45–48] The electron exchange and correlation energy were treated within the local-density approximation (LDA)[49] as well as generalized-gradient approximation (GGA)[50] together with the project-augmented wave (PAW) method.[51,52] The cut-off energy for the expansion of the wave function into the plane wave basis was 500 eV. For the Brillouin zone integration the Monkhorst–Pack scheme was used.[53] All residual forces were converged below 5 x 10–3 eV/$Å^{-1}$. For structural optimizations all internal and cell parameters as well as the unit cell volumes were relaxed for all used models. For the model with 56 atoms per unit cell (*Imm*2) a

k-point mesh of 5 x 5 x 4 was used for the models with 168 atoms per unit cell (*Imm*2_3*b*) 5 x 3 x 4, respectively.

2.5.5 References

[1] W. Schnick, *Angew. Chem.* **1993**, *105*, 846–858; *Angew. Chem. Int. Ed. Engl.* **1993**, *32*, 806–818.

[2] R.-J. Xie, N. Hirosaki, N. Kimura, K. Sakuma, M. Mitomo, *Appl. Phys. Lett.* **2006**, *90*, 191101/191101-191101/191103.

[3] M. Zeuner, S. Pagano, W. Schnick, *Angew. Chem.* **2011**, *123*, 7898-7920; *Angew. Chem. Int. Ed.* **2011**, *50*, 7754-7775.

[4] Superscripted numbers specify connectedness: number of directly connected silicon atoms.

[5] A. Weiss, A. Weiss, *Z. Anorg. Allg. Chem.* **1954**, *276*, 95–112.

[6] W. Schnick, H. Huppertz, *Chem. Eur. J.* **1997**, *3*, 679–683.

[7] T. Schlieper, W. Milius, W. Schnick, *Z. Anorg. Allg. Chem.* **1995**, *621*, 1380–1384.

[8] M. Woike, W. Jeitschko, *Inorg. Chem.* **1995**, *34*, 5105–5108.

[9] Z. A. Gál, P. M. Mallinson, H. J. Orchard, S. J. Clarke, *Inorg. Chem.* **2004**, *43*, 3998–4006.

[10] S. Esmaeilzadeh, U. Halenius, M. Valldor, *Chem. Mater.* **2006**, *18*, 2713–2718.

[11] H. Yamane, F. J. DiSalvo, *J. Alloys Compd.* **1996**, *240*, 33–36.

[12] R. J. Pulham, P. Hubberstey, *J. Nucl. Mater.* **1983**, *115*, 239–250.

[13] A. T. Dadd, P. Hubberstey, *J. Chem. Soc., Dalton Trans.* **1982**, 2175–2179.

[14] P. Hubberstey, P. G. Roberts, *J. Chem. Soc., Dalton Trans.* **1994**, 667–673.

[15] S. Pagano, S. Lupart, M. Zeuner, W. Schnick, *Angew. Chem.* **2009**, *121*, 6453–6456; *Angew. Chem. Int. Ed.* **2009**, *48*, 6335–6338.

[16] S. Lupart, M. Zeuner, S. Pagano, W. Schnick, *Eur. J. Inorg. Chem.* **2010**, 2636–2641.

[17] M. Zeuner, S. Pagano, S. Hug, P. Pust, S. Schmiechen, C. Scheu, W. Schnick, *Eur. J. Inorg. Chem.* **2010**, 4945–4951.

[18] S. Pagano, S. Lupart, S. Schmiechen, W. Schnick, *Z. Anorg. Allg. Chem.* **2010**, *636*, 1907–1909.

[19] G. Cordier, P. Höhn, R. Kniep, A. Rabenau, *Z. Anorg. Allg. Chem.* **1990**, *591*, 58–66.

[20] D. G. Park, Z. A. Gál, F. J. DiSalvo, *Inorg. Chem.* **2003**, *42*, 1779–1785.

[21] D. H. Gregory, M. G. Barker, P. P. Edwards, D. J. Siddons, *Inorg. Chem.* **1995**, *34*, 5195–5198.

[22] S. C. Junggeburth, O. Oeckler, D. Johrendt, W. Schnick, *Inorg. Chem.* **2008**, *47*, 12018–12023.

[23] *X.PREP*, Siemens Analytical X-ray Instruments Inc., Madison, Wisconsin, USA, **1996**.

[24] D. Mittra, S. Z. Ali, *J. Appl. Crystallogr.* **1976**, *9*, 54–56.

[25] F. Pechar, *Cryst. Res. Technol.* **1987**, *22*, 1041–1046.

[26] The terms *dreier* and *achter* rings were coined by Liebau and are derived from the German words "drei" (three) and "acht" (eight). However, for example a *dreier* ring is not a three-membered ring, but a six-membered ring comprising *three* tetrahedra centers.

[27] F. Stadler, O. Oeckler, J. Senker, H. A. Höppe, P. Kroll, W. Schnick, *Angew. Chem.* **2005**, *117*, 573–576; *Angew. Chem. Int. Ed.* **2005**, *44*, 567–570.

[28] W. Schnick, *Int. J. Inorg. Mater.* **2001**, *3*, 1267–1272.

[29] C. M. Fang, Y. Q. Li, H. T. Hintzen, G. d. With, *J. Mater. Chem.* **2003**, *13*, 1480–1483.

[30] R. D. Shannon, *Acta Crystallogr., Sect. A: Cryst. Found. Crystallogr.* **1976**, *32*, 751–767.

[31] W. H. Baur, *Crystallogr. Rev.* **1987**, *1*, 59–83.

[32] J. C. Slater, *J. Chem. Phys.* **1964**, *41*, 3199–3204.

[33] S. Pagano, M. Zeuner, S. Hug, *Eur. J. Inorg. Chem.* **2009**, 1579–1584.

[34] A. Gudat, R. Kniep, J. Maier, *Z. Naturforsch., Teil B* **1992**, *47*, 1363–1366.

[35] R. Hübenthal, Vers. 4 ed., University of Gießen, **1993**.

[36] R. Hoppe, *Angew. Chem.* **1966**, *78*, 52–63; *Angew. Chem. Int. Ed. Engl.* **1966**, *5*, 95–106.

[37] R. Hoppe, *Angew. Chem.* **1970**, *82*, 7–16; *Angew. Chem. Int. Ed. Engl.* **1970**, *9*, 25–34.

[38] H. A. Höppe, Doctoral Thesis, University of Munich, **2003**.

[39] K. Köllisch, Doctoral Thesis, University of Munich, **2001**.

[40] C. Braun, M. Seibald, S. L. Börger, O. Oeckler, T. D. Boyko, A. Moewes, G. Miehe, A. Tücks, W. Schnick, *Chem. Eur. J.* **2010**, *16*, 9646–9657.

[41] R. Marx, R. M. Ibberson, *J. Alloys Compd.* **1997**, *261*, 123–131.

[42] H. Lange, G. Wötting, G. Winter, *Angew. Chem.* **1991**, *103*, 1606–1625; *Angew. Chem. Int. Ed. Engl.* **1991**, *30*, 1579–1597.

[43] G. M. Sheldrick, *Acta Crystallogr., Sect. A* **2008**, *64*, 112–122.

[44] P. Hohenberg, W. Kohn, *Phys. Rev. B* **1964**, *136*, 864–871.

[45] G. Kresse, J. Hafner, *Phys. Rev. B* **1996**, *47*, 558–561.

[46] G. Kresse, J. Hafner, *Phys. Rev. B* **1994**, *49*, 14251–15269.

[47] G. Kresse, J. Furthmüller, *Comput. Mater. Sci.* **1996**, *6*, 15–50.

[48] G. Kresse, J. Furthmüller, *Phys. Rev. B* **1996**, *54*, 11169–11186.

[49] J. P. Perdew, A. Zunger, *Phys. Rev. B* **1981**, *23*, 5048–5079.

[50] J. P. Perdew, J. A. Chevary, S. H. Vosko, K. A. Jackson, M. R. Pederson, D. J. Singh, C. Fiolhais, *Phys. Rev. B* **1992**, *46*, 6671–6687.

[51] P. E. Blöchl, *Phys. Rev. B* **1994**, *50*, 17953–17979.

[52] G. Kresse, J. Joubert, *Phys. Rev. B* **1999**, *59*, 1758–1775.

[53] H. J. Monkhorst, J. D. Pack, *Phys. Rev. B* **1976**, *13*, 5188–5192.

3 Lithium Rare-Earth Nitridosilicates

3.1 Overview

In Chapter 2 the possibilities of the synthesis route using lithium as fluxing agent in closed ampoules has been demonstrated in the field of alkaline-earth nitridosilicates. The logical next step is to extend this method to rare-earth elements. Analogously to the structural chemistry of alkaline-earth nitridosilicates, in the field of rare-earth (oxo)nitridosilicates only a few low condensed examples are known.[1] The only 0D rare-earth nitridosilicate is $Pr_9Se_6[Si_3N_9]$,[2] which comprises isolated *dreier* rings and can be synthesized at moderate temperatures (900 °C) in NaCl flux. The chain-type mixed valence europium nitridosilicate Eu_2SiN_3 has also been synthesized in a lithium flux at moderate temperatures.[3] However, the other examples for low condensed rare-earth nitridosilicates $Ln_5Si_3N_9$ with Ln = La-Pr[4,5] and $La_{16}[Si_8N_{22}][SiON_3]_2$[6] have been synthesized at high-temperatures in a radio-frequency furnace, which is rather surprising. The isostructural compounds $Ln_5Si_3N_9$ (Ln = La-Pr) are branched chain-type silicates, with intertwined zipper-like chains, building a pseudo three dimensional network (Figure 1). $La_{16}[Si_8N_{22}][SiON_3]_2$ is also a branched chain-type silicate, but exhibits edge-sharing as well as corner sharing $[SiN_4]$ tetrahedra in the strands. Additionally, isolated $[SiON_3]^{7-}$ tetrahedra are situated between the strands (Figure 1).

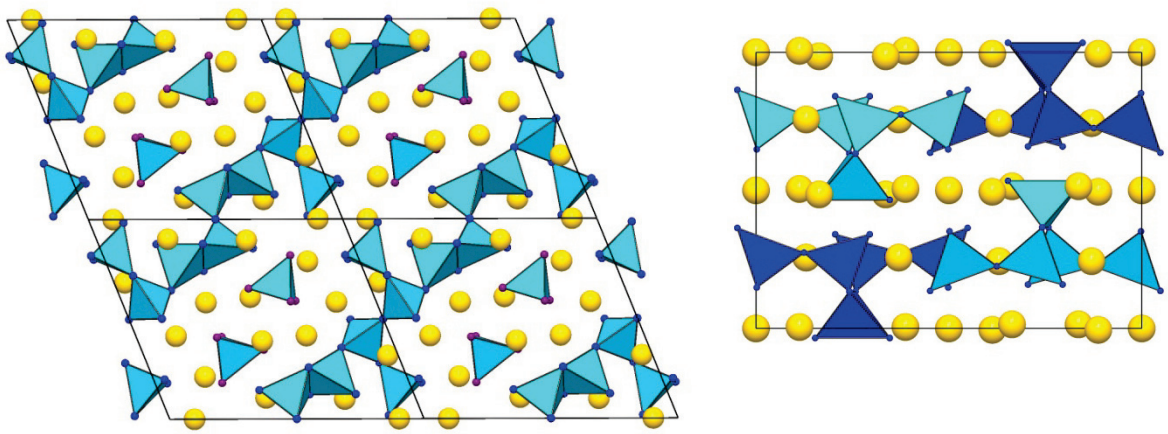

Figure 1. Crystal structure of $La_{16}[Si_8N_{22}][SiON_3]_2$ (left) and $Ln_5Si_3N_9$ with Ln = La-Pr (right). $[SiN_4]$ tetrahedra light blue (right: light and dark blue, to mark the separate single chains); nitrogen atoms dark blue, mixed occupied O/N violet and rare-earth atoms yellow.

In the beginning of this work no lithium rare-earth (oxo)nitridosilicates were known. An extension of the compound class of rare-earth to lithium rare-earth (oxo)nitridosilicates, however, may be interesting with respect to their structural chemistry as well as possible properties of such compounds. A possible and intriguing synthetic approach is of course the use of liquid lithium as fluxing agent, however the binary phase diagrams of rare-earth elements and Li show that they are only soluble at moderate temperatures with rather high lithium contents (Figure 2). As can be seen in Figure 2 this trend is even increasing in the series of the lanthanides. Furthermore the ionization energy for a RE^{3+} is about two times higher than for the formation of AE^{2+}.[7] Therefore the synthetic route of Chapter 2 had to be modified for the syntheses of novel lithium rare-earth (oxo)nitridosilicates by using rare-earth halogenides instead of the respective metals as starting materials.

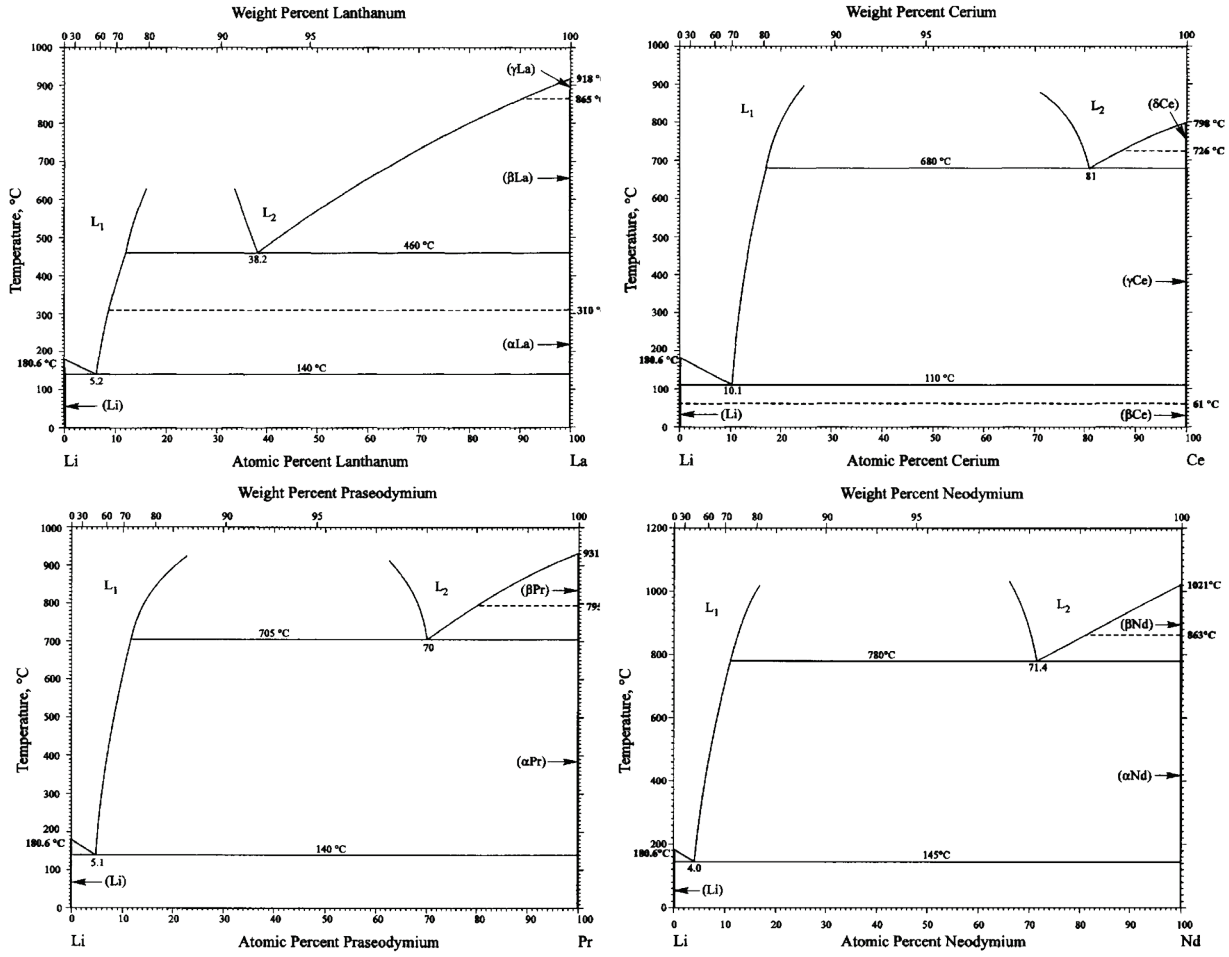

Figure 2. Phase diagrams for the system Li-La (top left), Li-Ce (top right), Li-Pr (bottom left) and Li-Nd (bottom right).[8-11]

Table 1. Overview of the known lithium rare-earth (oxo)nitridosilicates. In italics: compounds synthesized during this work; plain text: nitridosilicate synthesized in cooperation with *Zeuner*.[12]

1D	2D	3D
$Li_5La_5Si_4N_{12}$	$Li_{14}Ce_5[Si_{11}N_{19}O_5]O_2F_2$	$Li_{35}Ce_9Si_{30}N_{59}O_2F$
$Li_5Ce_5Si_4N_{12}$	$Li_{14}Nd_5[Si_{11}N_{19}O_5]O_2F_2$	$Li_{35}Pr_9Si_{30}N_{59}O_2F$
$LiLa_5Si_4N_{10}O$		
$LiPr_5Si_4N_{10}O$		

A plethora of different silicate structures from low condensed silicate structures in $Li_5Ln_5Si_4N_{12}$ (Ln = La, Ce) (cf. Chapter 3.3) and $LiLn_5Si_4N_{10}O$ (Ln = La, Pr) (Chapter 3.4) up to triply bridging nitrogen atoms ($N^{[3]}$) in $Li_{35}Ln_9Si_{30}N_{59}O_2F$ (Ln = Ce, Pr) (Chapter 3.6) were obtained in the course of this work using lithium as fluxing agent (Table 1). Moreover, the incorporation of lithium can result in compounds that combine the chemical and thermal resistivity of nitridosilicates, with the interesting material properties of lithium compounds, e.g. lithium ion conductivity (shown in Chapter 3.5). It could also be shown that this synthetic route can be transferred to open systems (tungsten crucible) in a radio-frequency furnace. Interestingly, hereby lower amounts of lithium flux have to be applied compared to the synthesis in closed tantalum or niobium ampoules. The synthesis in an open system yields higher amounts of the samples and impurities of the ampoule materials can be avoided. Therefore this transfer can give access to the development of novel materials.

References

[1] M. Zeuner, S. Pagano, W. Schnick, *Angew. Chem.* **2011**, *123*, 7898-7920; *Angew. Chem. Int. Ed.* **2011**, 78*50*, 7754-7775.

[2] F. Lissner, T. Schleid, *Z. Anorg. Allg. Chem.* **2004**, *630*, 2226-2230.

[3] M. Zeuner, S. Pagano, P. Matthes, D. Bichler, D. Johrendt, T. Harmening, R. Pöttgen, W. Schnick, *J. Am. Chem. Soc.* **2009**, *131*, 11242-11248.

[4] C. Schmolke, D. Bichler, D. Johrendt, W. Schnick, *Solid State Sci.* **2009**, *11*, 389-394.

[5] S. Lupart, W. Schnick, *Acta Crystallogr. E* **2009**, *65*, i43.

[6] C. Schmolke, S. Lupart, W. Schnick, *Solid State Sci.* **2009**, *11*, 305-309.

[7] A. F. Holleman, E. Wiberg, N. Wiberg, *Lehrbuch der Anorganischen Chemie, Vol. 102nd ed.*, W. de Gruyter, Berlin, **2007**.

[8] H. Okamoto, *J. Phase Equilib*. **1997**, *18*, 487.

[9] H. Okamoto, *J. Phase Equilib*. **1997**, *18*, 486.

[10] H. Okamoto, *J. Phase Equilib*. **1997**, *18*, 488.

[11] H. Okamoto, *J. Phase Equilib*. **1997**, *18*, 673.

[12] S. Lupart, M. Zeuner, S. Pagano, W. Schnick, *Eur. J. Inorg. Chem.* **2010**, 2636-2641.

3.2 Chain-Type Lithium Rare-Earth Nitridosilicates – $Li_5Ln_5Si_4N_{12}$ with Ln = La, Ce

published in

Saskia Lupart, Martin Zeuner, Sandro Pagano, and Wolfgang Schnick

Eur. J. Inorg. Chem. **2010** (18), 2636-2641
DOI: 10.1002/ejic.201000245
Copyright © 2010 WILEY-VCH Verlag GmbH & Co. KGaA, Weinheim
http://onlinelibrary.wiley.com/doi/10.1002/ejic.201000245/abstract

Abstract. The quaternary lithium rare-earth nitridosilicates $Li_5Ln_5Si_4N_{12}$ with Ln = La, Ce were synthesized at moderate temperatures below 900 °C in closed tantalum ampoules employing liquid lithium as a flux. Thereby, nitridosilicate substructures with a low degree of condensation were obtained. The air and moisture sensitive title compounds are the first representatives of quaternary lithium rare-earth nitridosilicates and crystallize in space group $P\bar{4}b2$ [$Li_5La_5Si_4N_{12}$: a = 1104.28(16), c = 557.30(11) pm, Z = 2, $R1$ = 0.0498, 873 data, 56 parameters; $Li_5Ce_5Si_4N_{12}$: a = 1097.78(16), c = 551.43(11) pm, Z = 2, $R1$ = 0.0334, 748 data, 56 parameters]. The nitridosilicate substructure consists of infinite non-branched *zweier* single-chains of vertex sharing SiN_4 tetrahedra running parallel to [001]. The chains exhibit a stretching factor f_S = 0.981 for La and 0.977 for Ce, respectively. The two crystallographically independent Li^+ sites are each coordinated by four nitrogen atoms. Lattice energy calculations (MAPLE) and EDX measurements confirmed the electrostatic bonding interactions and the chemical compositions. For the La containing compound ^7Li solid-state MAS NMR investigations are reported.

3.2.1 Introduction

Due to their remarkable properties (e.g. luminescence or lithium ion conductivity) nitridosilicates have become materials of broad academic and industrial interest.[1,2] In this context, doping of alkaline earth nitridosilicates (e.g. $M_2Si_5N_8$, M = Ca, Sr, Ba) with Eu^{2+} or Ce^{3+} lead to highly efficient host lattices for luminescent materials in phosphorconverted (pc)-LEDs.[2–6] Formally, nitridosilicates can be derived from oxosilicates by substituting N for O. Owing to the extended structural possibilities of nitrogen compared to oxygen, nitridosilicates feature a more variable degree of condensation and realize topologically new building blocks. For instance, fourfold coordinated $N^{[4]}$ has been observed in $BaYbSi_4N_7$ which exhibits a "star-shaped" $[N^{[4]}(SiN_3)_4]$ unit, where nitrogen adopts ammonium character.[7] Moreover, neighboring SiN_4 tetrahedra can share corners and even common edges.[8,9] However, most of the nitridosilicates characterized so far contain highly condensed frameworks which is probably due to the employment of high-temperature syntheses (>1300 °C).[10–12] Hence, only two chain-type nitridosilicates were obtained so far. Recently, $M_5Si_3N_9$ with M = La, Ce, Pr[13,14] has been described which exhibits zipper-like chains of vertex sharing SiN_4 tetrahedra due to additional Q1-type SiN_4 units[15] which are attached to every second tetrahedron of the chain. Quite recently, the mixed valence-type Eu_2SiN_3 has been synthesized by employment of a lithium flux technique at quite low temperatures. This nitridosilicate comprises nonbranched *zweier* chains of vertex sharing SiN_4 tetrahedra with a maximum stretching factor f_S = 1.0.[16,17] The use of molten sodium as flux agent for the synthesis of nitridosilicates was introduced by DiSalvo et al. in the case of $Ba_5Si_2N_6$.[18] An analogous synthetic approach resulted in structural characterization of a series of nitridosilicates, e.g. $MSiN_2$ (M = Ca, Sr, Ba),[19] though silicon and nitrogen are only sparingly soluble in liquid sodium.

Therefore, the use of lithium melts affords several advantages for the synthesis of nitridosilicates compared to sodium. Due to the broad spectrum of applications of lithium in radiochemistry the reactivity of liquid lithium with other elements has been well examined.[20–22] It has been shown that both nitrogen and silicon are soluble to a comparable extend in liquid lithium, and moreover, a variety of metals can be solved at moderate temperatures in lithium-rich systems as well.[21] Consequently, the use of lithium melts seemed to be a promising approach for the synthesis of novel nitridosilicates. Recently, we have been able to synthesize a number of quaternary lithium alkaline earth nitridosilicates with varying degrees of condensation employing closed tantalum ampoules.[23] The degree of condensation of the SiN_4 substructures could be directed by the pressure inside the ampoules. Within this context,

the structural elucidation of a group-like silicate, namely $Li_4Ca_3Si_2N_6$, with "bow tie" $[Si_2N_6]^{10-}$ units has been accomplished. Furthermore, hitherto unknown intermediates like double-chain nitridosilicates ($LiCa_3Si_2N_5$) could be synthesized using this synthetic approach.[23]

In this contribution we present the first quaternary lithium rare-earth nitridosilicates, namely $Li_5Ln_5Si_4N_{12}$ with Ln = La, Ce. Hence, the liquid lithium approach has been successfully extended to rare-earth materials, forming non-branched *zweier* single-chain nitridosilicates in closed tantalum ampoules at moderate temperatures.

3.2.2 Results and Discussion

3.2.2.1 Synthetical Approach

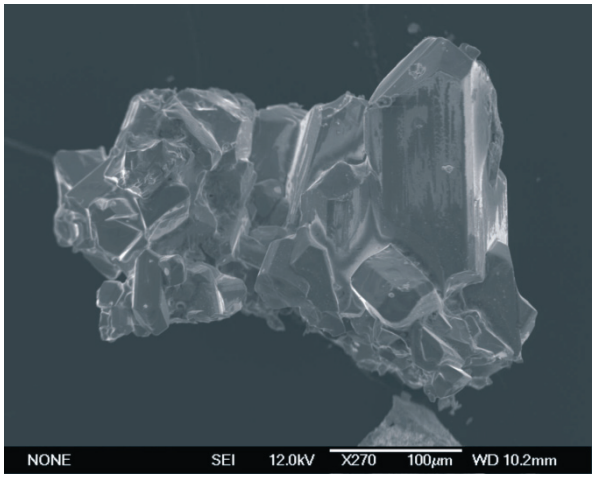

Figure 1. SEM image of $Li_5Ce_5Si_4N_{12}$.

The nitridosilicates $Li_5Ln_5Si_4N_{12}$ (Ln = La, Ce) were obtained by employment of two different synthesis routes. Both routes start from silicon diimide $[Si(NH)_2]$ and the corresponding rare-earth chlorides $LnCl_3$ (Ln = La, Ce). Single crystals (cf. Figure 1) of the title compounds could best be obtained by adding lithium as flux to the reaction mixture. Thereby, the amount of excessive lithium remaining in the sample cannot easily be controlled, because contamination occurs due to a certain amount of lithium adhering to the tantalum tube. Therefore, a second synthetic approach utilising LiN_3 as the only lithium source was developed, leading predominately to microcrystalline bulk samples of the title compounds. In contrast to recently reported lithium nitridosilicates ($Li_4Ca_3Si_2N_6$, $Li_2Sr_4Si_4N_8O$ or $LiCa_3Si_2N_5$)[23] no crystalline product was obtained when using Li_3N as the only lithium

source. Interestingly, a given nitrogen pressure is also needed for the formation of $Li_5Ln_5Si_4N_{12}$ (Ln = La, Ce). Therefore, the combination of NaN_3 and elemental lithium as starting materials yielded the title compounds, corroborating the necessity of a nitrogen pressure inside the ampoule. The obtained products exhibit air and moisture sensitivity, similar to related chain type nitridosilicates, probably due to their low condensation degree.[13,14,16]

3.2.2.2 Crystal Structure

X-ray structure analysis revealed two possible tetragonal space groups for the title compounds, namely *P*4/*nbm* (no. 125, centrosymmetric) and $P4\bar{b}2$ (no. 117, non-centrosymmetric). Solely the refinement in space group $P4\bar{b}2$ gave a reasonable structural model with satisfactory *R* values. The resulting flack parameters were indicative for inversion twinning, which was confirmed for both compounds. Details of the crystal structure determination are listed in Table 1. All atoms were refined anisotropically except for the Li positions.

The majority of nitridosilicates described so far exhibit highly condensed network structures with a degree of condensation $\kappa \geq 1{:}2$ (i.e. molar ratio Si/N). Less condensed nitridosilicate anions with $\kappa < 1{:}2$ are only scarcely known. Recently, we reported on Eu_2SiN_3, which consists of nonbranched *zweier* chains – a structural feature that has been unknown for nitridosilicates so far. $Li_5Ln_5Si_4N_{12}$ with Ln = La, Ce contain nonbranched *zweier* chains of corner sharing SiN_4 tetrahedra (cf. Figure 2) analogously to Eu_2SiN_3 and is therefore another rare example for nitridosilicates with a low degree of condensation. The single chains run along [001] and the four chains within the unit cell are rotated along the *c*-axis by 90°. Moreover, the nitridosilicate chains feature a stretching factor $f_S = 0.981$ for $Li_5La_5Si_4N_{12}$, and $f_S = 0.977$ for $Li_5La_5Si_4N_{12}$, respectively.[24] These values resemble that of the mineral johannsenite ($CaMn[Si_2O_6]$; $f_S = 0.98$).[17] In contrast, the stretching factor in Eu_2SiN_3 reaches a maximum value of $f_S = 1.0$. Distances Si–N range between 170.9(7)–174.9(4) pm for the cerium and 174.0(10)–176.3(7) pm for the $Li_5La_5Si_4N_{12}$ and $Li_5Ce_5Si_4N_{12}$, respectively. The values are in the typical range of nitridosilicates.[25]

Table 1. Crystallographic data of $Li_5Ln_5Si_4N_{12}$ with Ln = La, Ce.

Formula	$Li_5La_5Si_4N_{12}$	$Li_5Ce_5Si_4N_{12}$
Formula mass /g · mol^{-1}	1009.73	1015.78
Crystal system	tetragonal	
Space group	$P\bar{4}b2$ (no. 117)	
Cell parameters / pm	a = 1142.8(16) c = 557.30(11)	a = 1097.78(16) c = 551.43(11)
Cell volume / 10^6 pm^3	V = 679.59(19)	V = 664.54(19)
Formula units / cell	2	
Crystal size / mm^3	0.09 x 0.04 x 0.01	0.08 x 0.03 x 0.01
$\rho_{calcd.}$ / g · cm^{-3}	4.934	5.076
μ / mm^{-1}	15.74	17.151
F(000)	880	890
Diffractometer	Stoe IPDS 1	
Temperature / K	293(2)	293(2)
Radiation, monochr.	Mo-K$_\alpha$, (λ = 71.073 pm), graphite	
Absorption correction	multi scan	
θ range / °	2.3 - 30.5	
Measured reflections	6002	6615
Independent reflections	782	973
Observed reflections	748	873
Refined parameters	56	56
Flack parameter	0.41(8)	0.47(5)
GoF	1.233	1.097
R indices ($F_o^2 \geq 2\sigma(F_o^2)$)	R_1 = 0.0482, $wR2$ = 0.1278	R_1 = 0.0294, $wR2$ = 0.0749
R indices (all data)	R_1 = 0.0498, $wR2$ = 0.1293[a]	R_1 = 0.0334, $wR2$ = 0.0760[b]
Max. / min. residual electron density/ eÅ^{-3}	2.22/-1.50	1.273/-2.385

[a] $w = 1/[\sigma^2(F_o^2) + (0.0932\,P)^2 + 0.00\,P]^{-1}$ where $P = (F_o^2 + 2\,F_c^2)\,/\,3$.
[b] $w = 1/[\sigma^2(F_o^2) + (0.0473\,P)^2 + 0.00\,P]^{-1}$ where $P = (F_o^2 + 2\,F_c^2)\,/\,3$.

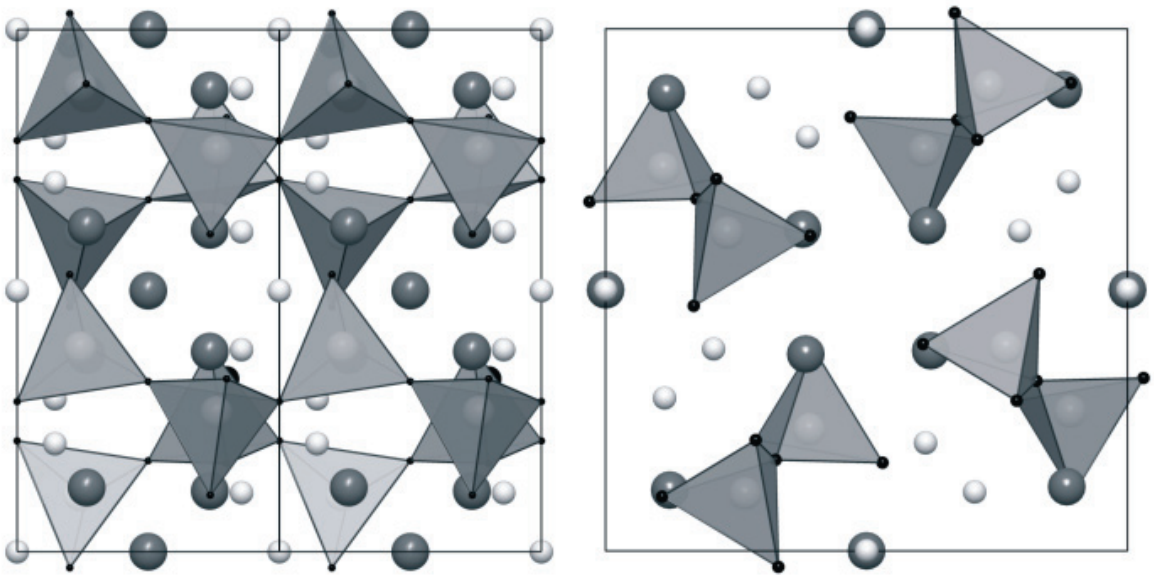

Figure 2: Crystal structure of $Li_5Ln_5Si_4N_{12}$ with Ln = La, Ce. Left: view along [100], Ln atoms dark gray, Li^+ white, SiN_4 tetrahedra gray. Right: View along [001], the tetrahedral tips of the chains are rotated clockwise by 90° relatively to each other.

There are two crystallographically independent Ln-sites occupying Wyckoff positions 8*i* (Ln1) and 2*d* (Ln2). The Ln1 atoms are surrounded by seven nitrogen atoms building a mono-capped distorted octahedron. The Ln2 positions exhibit a distorted octahedral coordination geometry made up of nitrogen (cf. Figure 3a). In the secondary coordination sphere Ln2 is coordinated by two Li2 atoms building alternating Ln–Li chains parallel to the *c*-axis. The interatomic distances for Ln1–N range between 249.9(9) to 292.3(9) pm and for Ln2–N between 251.6(9) and 270.6(11) pm [cf. Table 2; 247.8(8)–292.2(5) pm and 250.5(7)–270.4(9) pm for Ln = Ce, respectively]. These distances correspond well with other known lanthanum nitridosilicates (e.g. $La_3Si_6N_{11}$, $LaSi_3N_5$ or $La_5Si_3N_9$).[13,26] Analogously, the distances Ce–N are in the typical range of cerium containing nitridosilicates.[26]

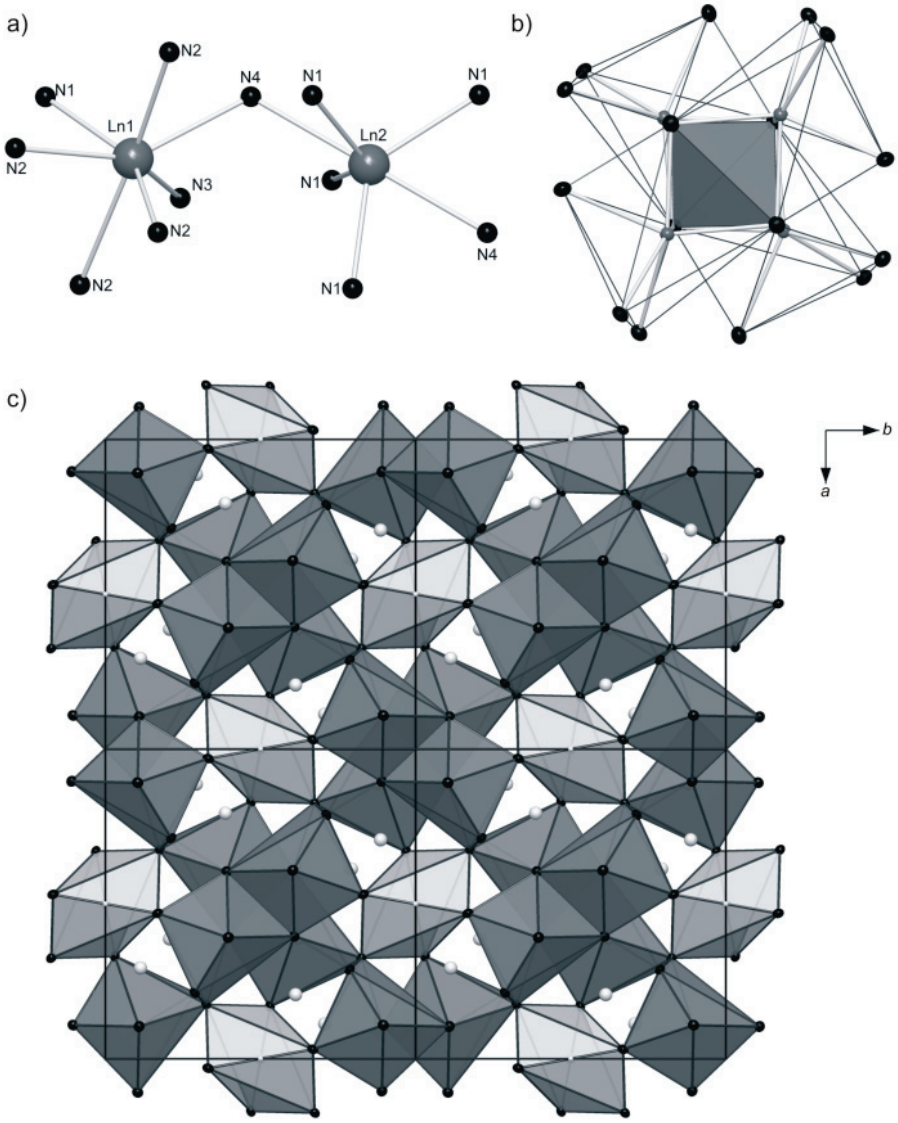

Figure 3. a) Coordination of Ln in $Li_5Ln_5Si_4N_{12}$ (Ln = La, Ce); b) Tetrahedral vacancy built up by four LnN_7-polyhedra; c) Depiction of the Ln-N polyhedra; dark gray LnN_7 polyhedra, light gray LnN_6 polyhedra. Li^+ positions are depicted in white, Si atoms omitted for clearity.

The Ln1 polyhedra are connected via common edges and corners, forming groups of four polyhedra, building up strands along [001]. Within these strands the polyhedra enclose nearly regular tetrahedral voids (cf. Figure 3b). The latter ones exhibit a distance of 210.3(2) pm between their centers and the surrounding N atoms. However, no residual electron density could be found within these voids. Moreover, occupying the voids with Li would lead to a charge within the compound, which cannot be counterbalanced by nitrogen. The LnN_7 strands are connected to each other via common corners and LnN_6 octahedra, which are depicted in light gray (cf. Figure 3c).

Table 2. Selected interatomic distances (pm) for $Li_5Ln_5Si_4N_{12}$ (Ln = La, Ce). Standard deviations are given in parentheses.

		La	Ce
Ln1-N2		249.9(9)	247.8(8)
Ln1-N2		253.2(10)	249.3(8)
Ln1-N3		257.7(4)	255.2(4)
Ln1-N1		260.1(9)	259.0(7)
Ln1-N2		266.4(9)	260.8(5)
Ln1-N4		266.9(5)	265.3(4)
Ln1-N2		292.3(9)	292.2(5)
Ln2-N1	(4x)	251.6(9)	250.5(7)
Ln2-N4	(2x)	270.6(11)	270.4(9)
Ln2-Li2	(2x)	278.7(2)	275.7(2)
Li1-N1		207(3)	205(2)
Li1-N2		210(3)	218(2)
Li1-N1		221(3)	215(2)
Li1-N3		225(3)	226(2)
Li2-N1	(4x)	221.7(10)	218.5(7)
Li1-Li2		281(3)	271(2)
Li1-Li1		225(6)	216(4)

The two crystallographically independent Li^+ sites are coordinated by nitrogen atoms in a distorted tetrahedral fashion, forming $[Li_5N_{10}]^{25-}$ building units. The distances Li–N vary between 210(3) and 221.7(10) pm for Ln = La, and 215(2)–225.6(19) pm for Ln = Ce, respectively (cf. Table 2). These distances are in good accordance with previously reported lithium containing nitridosilicates.[27,28] In the second coordination sphere five Li^+ ions form a "bowtie" arrangement (cf. Figure 4, left). Hereby, the Li2 positions are surrounded by Li1 atoms in a tetrahedrally distorted way. Interestingly, the Li1–Li1 distances are quite short [Li1–Li1: 225(6) pm for $Li_5La_5Si_4N_{12}$, 216(4) pm for $Li_5Ce_5Si_4N_{12}$]. However, the values exceed the range of the sum of the ionic radii.[29,30] Comparable distances Li–Li have been observed in other lithium nitridosilicates and lithium nitridophosphates [e.g. $Li_2Sr_4Si_4N_8O$: 199(3) pm; Li_7PN_4: 224.9 pm].[23,31] The planes spanned by Li1–Li1–Li2 enclose almost a right angle δ = 94.9(2)° for Ln = La, δ = 92.1(2)° for Ln = Ce (cf. Figure 4, right).

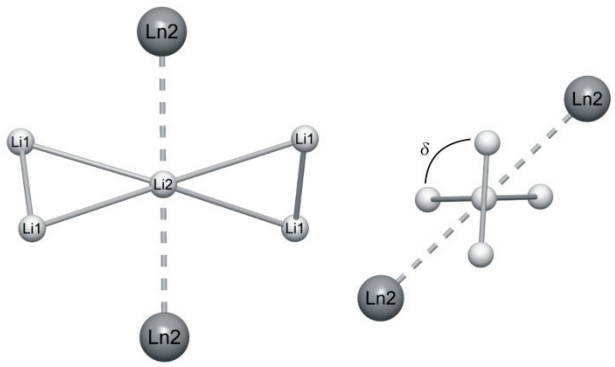

Figure 4. Lithium arrangement with coordinated Ln2. Right: Depiction of the angle δ spanned up by the two Li1-Li1-Li2 planes.

3.2.2.3 Solid-State MAS NMR

The ^{7}Li solid-state MAS NMR spectrum of $Li_5La_5Si_4N_{12}$ shows one isotropic intense peak at 1.6 ppm with a full width at half maximum (FWHM) of 3.5 ppm (Figure 5). This chemical shift is in good accordance with other lithium-containing nitridosilicates (e.g. Li_2SiN_2 δ = 1.7 ppm,[27] $LiSi_2N_3$, δ = 1.3 ppm,[28] $Li_4Ca_3Si_2N_6$ δ = 2.0 ppm).[23] Due to the low resolution of ^{7}Li solid-state MAS NMR no differentiation of the two crystallographically independent lithium sites can be observed in the spectrum. This is in accordance with other lithium nitridosilicates, e.g. Li_2SiN_2 exhibits eight crystallographically independent lithium sites, whereas only one sharp signal in the NMR spectrum can be found.[27]

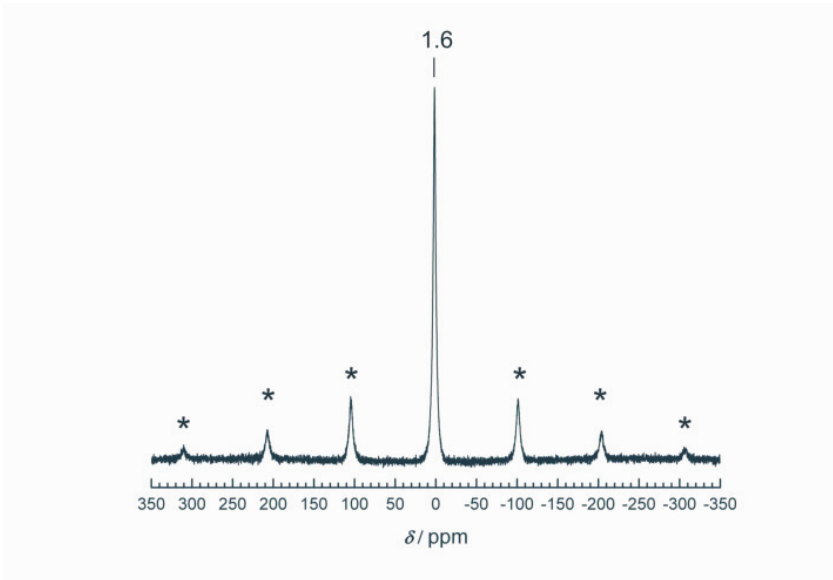

Figure 5. Solid-state MAS NMR of $Li_5La_5Si_4N_{12}$ of ^{7}Li. Rotation bands are indicated by asterisks (rotation frequency 20 kHz).

3.2.2.4 Lattice Energy Calculations According to the MAPLE Concept

Lattice energy calculations (MAPLE: Madelung part of lattice energy)[29,32–34] were performed to corroborate the crystal structures of $Li_5Ln_5Si_4N_{12}$ with Ln = La, Ce. Hereby, exclusively electrostatic interactions in an ionic crystal were considered, depending on the charge, distance and the coordination spheres of the constituting atoms. The total MAPLE values for the two title compounds correspond well with the sum of the total MAPLE values of the constituting binary nitrides (cf. Table 3). Furthermore, the calculated partial MAPLE values of the crystallographically different atoms are in good agreement with the atom type ranges from comparable compounds in the literature.[35,36] MAPLE calculations with a theoretically occupied tetrahedral void (built up by LnN_7 polyhedra, cf. Figure 3, b) were performed. However, the partial values for these hypothetical Li sites shift to anomalous MAPLE values, corroborating that the tetrahedral void are not occupied in accordance with the crystal structure determination.

Table 3. Results of the MAPLE calculations [kJ/mol] for $Li_5Ln_5Si_4N_{12}$ (Ln = La, Ce). Δ = difference.

	La	Ce
Ln^{3+}	4061; 3734	4079; 3884
Si^{4+}	9896	9988
$N^{[1]\,3-}$	4823; 4768	4850; 4842
$N^{[2]\,3-}$	5355; 5586	5451; 5586
Li^+ (8*i*)	700	727
Li^+ (2*b*)	784	775
Total MAPLE	123619	124800
Δ	0.75 %	0.16 %
Total MAPLE (5/3 Li_3N + 5 LaN + 4/3 Si_3N_4): 122698 kJ/mol		
Total MAPLE (5/3 Li_3N + 5 CeN + 4/3 Si_3N_4): 124997 kJ/mol		

Typical partial MAPLE values [kJ/mol]: La^{3+}: 3500-5000; Ce^{3+}: 3800-4800; Si^{4+}: 9000-10200; $N^{[1]\,3-}$: 4300-5000; $N^{[2]\,3-}$: 4600-6000; Li^+: 600-860.[35,36]

3.2.3 Conclusions

In this contribution, employment of lithium melts for the synthesis of lithium nitridosilicates could be expanded to compounds containing rare earth elements. Despite the higher melting points of the rare-earth metals compared to alkaline earth elements, rather low reaction temperatures of 900 °C can be applied. Two new less condensed lithium rare-earth nitridosilicates, namely $Li_5Ln_5Si_4N_{12}$ (Ln = La, Ce) have been synthesized, comprising the structural motif of nonbranched *zweier* chains – a structural feature for nitridosilicates hitherto only known for Eu_2SiN_3. Thus, the lithium flux method seems to be a promising approach for further extension to the synthesis of nitridosilicates of the late rare earth elements and gives access to compounds with a high metal content.

3.2.4 Experimental Section

3.2.4.1 Synthesis

All manipulations were performed with rigorous exclusion of oxygen and moisture in flame-dried Schlenk-type glassware on a Schlenk line interfaced to a vacuum line (10–3 mbar) or in an argon-filled glove box (Unilab, MBraun, Garching, O_2 < 0.1 ppm, H2O < 0.1 ppm). Argon (Messer-Griessheim, 5.0) was purified by passage through columns of silica gel (Merck), molecular sieves (Fluka, 4 Å), KOH (Merck, ≤ 85%), P_4O_{10} (Roth, ≤ 99%, granulate) and titanium sponge (Johnson Matthey, 99.5%, grain size ≥ 0.8 cm) at 700 °C. For the syntheses of the title compounds tantalum tubes (wall thickness 0.5 mm, internal diameter 10 mm, length 300 mm) were cleaned and their oxide layer removed by treating with a mixture of HNO_3 (concd.) and HF (40 %). The tubes were weld shut in an arc furnace under 1 bar purified argon. During this procedure, the crucible holder was water cooled in order to avoid chemical reactions during welding.

Synthesis of $Li_5La_5Si_4N_{12}$: For the synthesis of $Li_5La_5Si_4N_{12}$ silicon diimide (50 mg, 0.86 mmol; synthesized according to literature[37]), $LaCl_3$ (216 mg, 0.88 mmol) and NaN_3 (18.8 mg, 0.29 mmol, Acros, 99%) were mixed in an agate mortar, filled in a tantalum tube and covered with lithium (40 mg, 5.73 mmol, Alfa Aesar, 99.9%) in a glove box. The sealed tantalum ampoule was placed into a silica tube under argon, which was placed in the middle of a tube furnace. The temperature was raised to 900 °C (rate 2 °Cmin^{-1}), maintained for 24 h and cooled down to 500 °C (rate 0.09 °C min^{-1}). Subsequently, the sample was quenched

down to room temperature by switching off the furnace. The sample contained $Li_5La_5Si_4N_{12}$ as brownish, air- and moisture-sensitive crystals.

Synthesis of $Li_5Ce_5Si_4N_{12}$: $Li_5Ce_5Si_4N_{12}$ can be synthesized with an analogous approach, however, crystals of better quality can be obtained as follows. $Li_5Ce_5Si_4N_{12}$ was synthesized starting from silicon diimide[37] (23.3 mg, 0.39 mmol), $CeCl_3$ (74 mg, 0.30 mmol, Alfa Aesar, 99.99%) and LiN_3 (14 mg, 0.30 mmol). The starting materials were mixed in an agate mortar, filled in a tantalum tube and covered with lithium (14 mg, 20 mmol). The tantalum ampoule was placed in a silica tube under argon and heated to 900 °C (rate 5 °C min^{-1}). The temperature was kept for 12 h, subsequently, the tube was cooled down to 500 °C (rate 0.2 °C min^{-1}) and quenched to room temperature by switching off the furnace. The sample contained $Li_5Ce_5Si_4N_{12}$ as dark reddish, air- and moisture-sensitive crystals.

3.2.4.2 Chemical Analyses

Scanning electron microscopy was performed on a JEOL JSM-6500F equipped with a eld emission gun at an acceleration voltage of 10 kV with a Si/Li EDX detector (Oxford Instruments, model 7418). Samples were prepared by placing single crystals on adhesive conductive pads and subsequently coating them with a thin conductive carbon film. Each EDX spectrum (Oxford Instruments) was recorded with the analyzed area limited onto one single crystal to avoid the influence of possible contaminating phases. Analysis of three spots per crystallite showed average atomic ratio Ln/Si = 5:4 (Ln = La, Ce) which corroborates the formation of $Li_5Ln_5Si_4N_{12}$ (Ln = La, Ce). The determined compositions are in accordance to the structure model within the typical error ranges with regard to the fact that lithium cannot be detected by this method [calcd. (atom-%). Ln 19, Si 15, N 46; found (atom-%) La 20, Si 20, N 70; Ce 20, Si 11, N 62 O 2].

3.2.4.3 Single Crystal X-ray Analysis

Single crystals of $Li_5Ln_5Si_4N_{12}$ with Ln = La, Ce were isolated under a microscope, which is integrated in a glove box, enclosed in glass capillaries (Ø = 0.2 mm), and sealed under argon. Single-crystal X-ray diffraction data were collected at room temperature on a STOE IPDS I diffractometer (Stoe and Cie GmbH, Darmstadt) with Mo-$K\alpha$ radiation (λ = 0.71073 Å, graphite monochromator). The structures were solved by direct methods after semi-empirical absorption correction. For the structure solution and refinement the program package SHELX97 was used.[38] Further details on the crystal structure investigations may be obtained

from the Fachinformationszentrum Karlsruhe, 76344 Eggenstein-Leopoldshafen, Germany (Fax: +49-7247-808-666; E-mail: crysdata@fiz-karlsruhe.de), on quoting the depository number CSD-421528 (Ln = La) and -421527 (Ln = Ce).

3.2.4.4 X-ray Powder Diffraction

X-ray powder diffraction data were collected on a STOE STADI P diffractometer with Ge(111)-monochromatized Mo-*K*α1 radiation (λ = 0.71073 Å) in Debye–Scherrer geometry (cf. Figure 6 ($Li_5La_5Si_4N_{12}$) and Figure 7 ($Li_5Ce_5Si_4N_{12}$)). The samples were enclosed in silica tubes and sealed under argon.

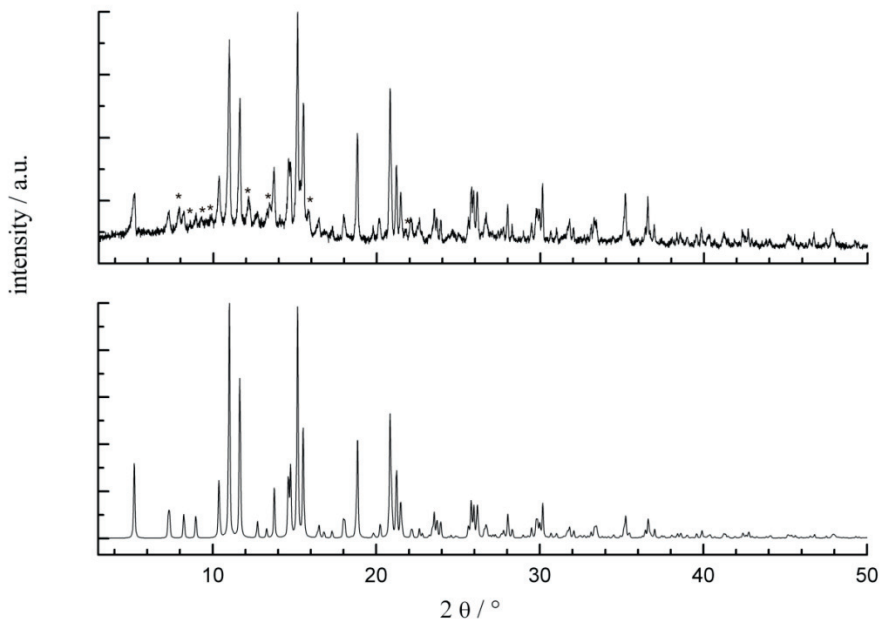

Figure 6. Measured PXRD pattern of $Li_5La_5Si_4N_{12}$ (top, MoKα1 radiation, λ = 71.073 pm) and simulated powder pattern $Li_5La_5Si_4N_{12}$ (below). With asterisks (*) marked peaks belong to an unknown phase.

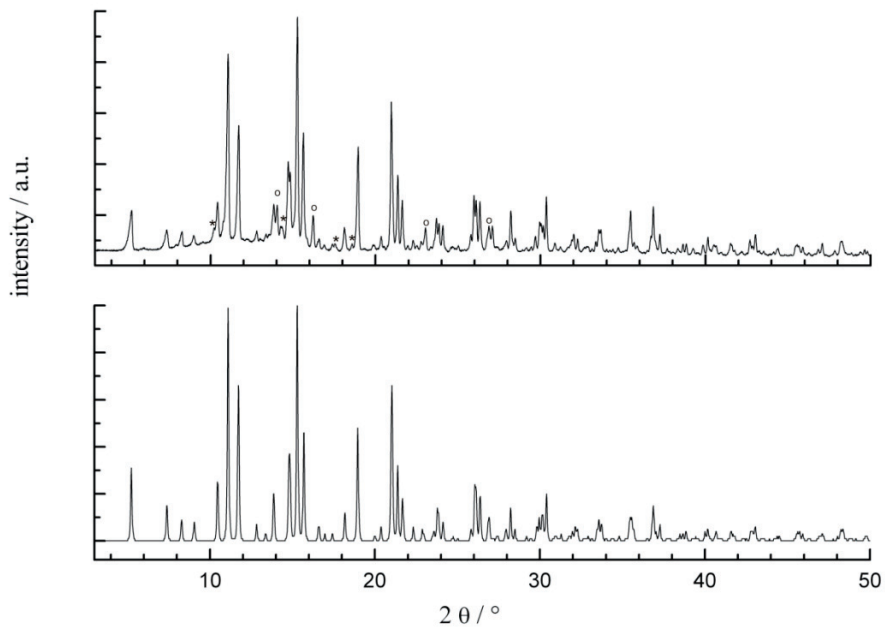

Figure 7. Measured PXRD pattern of $Li_5Ce_5Si_4N_{12}$ (top, $MoK_\alpha1$ radiation, λ = 71.073 pm) and simulated powder pattern $Li_5Ce_5Si_4N_{12}$ (below). With asterisks (*) marked peaks belong to an unknown phase; with circles (o) marked peaks belong to CeN.

3.2.4.5 Solid-State MAS NMR

Solid-state NMR experiments were performed on a Bruker Advance DSX 500 spectrometer with an external field of 11.75 T for $Li_5La_5Si_4N_{12}$. The ^7Li spectrum was recorded with direct excitation using a commercial 2.5 mm tripleresonance MAS probe at the frequency 194.415 MHz. All experiments were carried out at room temperature in ZrO_2 rotors. The chemical shifts of 7Li are reported using the frequency ratios published by IUPAC [δ scale relative to 1% tetramethylsilane (TMS) in $CDCl_3$]. The one-dimensional ^7Li NMR spectrum was acquired with a 90° pulse length of 3.0 µs, a recycle delay of 32 s and at a sample spinning frequency of 20 kHz.

3.2.5 References

[1] W. Schnick, *Angew. Chem.* **1993**, *105*, 846–858; *Angew. Chem. Int. Ed. Engl.* **1993**, *33*, 806–818.

[2] R.-J. Xie, N. Hirosaki, *Sci. Technol. Adv. Mater.* **2007**, *8*, 588–600.

[3] Y. Q. Li, G. deWith, H. T. Hintzen, *J. Solid State Chem.* **2008**, *181*, 515–524.

[4] R.-J. Xie, N. Hirosaki, N. Kimura, K. Sakuma, M. Mitomo, *Appl. Phys. Lett.* **2007**, *90*, 191101/1–191101/3.

[5] X. Piao, T. Horikawa, H. Hanzawa, K. Machida, *Appl. Phys. Lett.* **2006**, *88*, 161908/1–161908/3.

[6] R. Mueller-Mach, G. Mueller, M. R. Krames, H. A. Höppe, F. Stadler, W. Schnick, T. Juestel, P. Schmidt, *Phys. Status Solidi A* **2005**, *202*, 1727–1732.

[7] H. Huppertz, W. Schnick, *Angew. Chem.* **1996**, *108*, 2115–2116; *Angew. Chem. Int. Ed. Engl.* **1996**, *35*, 1983–1984.

[8] C. Schmolke, S. Lupart, W. Schnick, *Solid State Sci.* **2009**, *11*, 305–309.

[9] H. Huppertz, W. Schnick, *Chem. Eur. J.* **1997**, *3*, 249–252.

[10] M. Yamada, T. Naitou, K. Izuno, H. Tamaki, Y. Murazaki, M. Kameshima, T. Mukai, *Jpn. J. Appl. Phys.* **2003**, *42*, L20–L23.

[11] H. A. Höppe, H. Lutz, P. Morys, W. Schnick, A. Seilmeier, *J. Phys. Chem. Solids* **2000**, *61*, 2001–2006.

[12] W. Schnick, H. Huppertz, R. Lauterbach, *J. Mater. Chem.* **1999**, *9*, 289–296.

[13] C. Schmolke, D. Bichler, D. Johrendt, W. Schnick, *Solid State Sci.* **2008**, *10*, 389–394.

[14] S. Lupart, W. Schnick, *Acta Crystallogr., Sect. E* **2009**, *65*, i43.

[15] Q1-type SiN4 tetrahedra are connected with one vertex to the next tetrahedron, therefore representing a terminal unit.

[16] M. Zeuner, S. Pagano, P. Matthes, D. Bichler, D. Johrendt, T. Harmening, R. Pöttgen, W. Schnick, *J. Am. Chem. Soc.* **2009**, *131*, 11242–11248.

[17] F. Liebau, *Structural chemistry of Silicates*, Springer, Berlin, **1985**, p. 80 ff.

[18] H. Yamane, F. J. DiSalvo, *J. Alloys Compd.* **1996**, *240*, 33–36.

[19] Z. A. Gál, P. M. Mallinson, H. J. Orchard, S. J. Clarke, *Inorg. Chem.* **2004**, *43*, 3998–4006.

[20] R. J. Pulham, P. Hubberstey, *J. Nucl. Mater.* **1983**, *115*, 239–250.

[21] A. T. Dadd, P. Hubberstey, *J. Chem. Soc., Dalton Trans.* **1982**, 2175–2179.

[22] P. Hubberstey, P. G. Roberts, *J. Chem. Soc., Dalton Trans.* **1994**, 667–673.

[23] S. Pagano, S. Lupart, M. Zeuner, W. Schnick, *Angew. Chem.* **2009**, *121*, 6453–6456; *Angew. Chem. Int. Ed.* **2009**, *48*, 6335–6338.

[24] The stretching factor is defined by Liebau as $f_S = I_{chain}/(l_T \times P)$, with I_{chain}: the distance of one period; l_T: edge length of the tetrahedral; P: periodicity of the chain.

[25] F. Stadler, O. Oeckler, J. Senker, H. A. Höppe, P. Kroll, W. Schnick, *Angew. Chem.* **2005**, *117*, 573–576; *Angew. Chem. Int. Ed.* **2005**, *44*, 567–570.

[26] M. Woike, W. Jeitschko, *Inorg. Chem.* **1995**, *34*, 5105–5108.

[27] S. Pagano, M. Zeuner, S. Hug, W. Schnick, *Eur. J. Inorg. Chem.* **2009**, 1579–1584.

[28] M. Orth, W. Schnick, *Z. Anorg. Allg. Chem.* **1999**, *625*, 142631428.

[29] R. D. Shannon, *Acta Crystallogr., Sect. A: Cryst. Found. Crystallogr.* **1976**, *32*, 751–767.

[30] W. H. Baur, *Crystallogr. Rev.* **1987**, *1*, 59–83.

[31] W. Schnick, J. Lücke, *J. Solid State Chem.* **1990**, *87*, 101–106.

[32] R. Hübenthal, *Programm zur Berechnung des Madelunganteils der Gitterenergie*, version 4, University of Gießen, Germany, **1993**.

[33] R. Hoppe, *Angew. Chem.* **1966**, *78*, 52–63; *Angew. Chem. Int. Ed. Engl.* **1966**, *5*, 95–106.

[34] R. Hoppe, *Angew. Chem.*. **1970**, *82*, 7–16; *Angew. Chem. Int. Ed. Engl* **1970**, *9*, 25–34.

[35] H. A. Höppe, *Doctoral* Thesis, University of Munich, **2003**.

[36] K. Köllisch, *Doctoral* Thesis, University of Munich, **2001**.

[37] H. Lange, G. Wötting, G. Winter, *Angew. Chem. Int. Ed. Engl.* **1991**, *103*, 1606–1625; *Angew. Chem.* **1991**, *30*, 1579–1597.

[38] G. M. Sheldrick, *Acta Crystallogr., Sect. A* **2008**, *64*, 112.

3.3 $LiLa_5Si_4N_{10}O$ and $LiPr_5Si_4N_{10}O$ – Chain Type Oxonitridosilicates

published in Saskia Lupart and Wolfgang Schnick

Z. Anorg. Allg. Chem. **2011**, *638* (1), 94-97
DOI: 10.1002/zaac.201100381
Copyright © 2012 WILEY-VCH Verlag GmbH & Co. KGaA, Weinheim
http://onlinelibrary.wiley.com/doi/10.1002/zaac.201100381/abstract

Abstract. The isotypic lithium rare-earth oxonitridosilicates $LiLn_5Si_4N_{10}O$ with Ln = La, Pr were synthesized at temperatures of 1200 °C in weld shut tantalum ampoules employing liquid lithium as flux. Thereby, a silicate substructure with a low degree of condensation was obtained. $LiLa_5Si_4N_{10}O$ crystallizes in space group $P\bar{1}$ ($Z = 1$, $LiLa_5Si_4N_{10}O$: $a = 5.7462(11)$, $b = 6.5620(13)$, $c = 8.3732(17)$ Å, $\alpha = 103.54(3)$, $\beta = 107.77(3)$, $\gamma = 94.30(3)$, $wR2 = 0.0405$, 1315 data, 96 parameters). The nitridosilicate substructure consists of loop branched *dreier* single-chains of vertex sharing SiN_4 tetrahedra. Lattice energy calculations (MAPLE) and EDX measurements confirmed the electrostatic bonding interactions and the chemical compositions. The ^7Li solid-state MAS NMR investigation is reported.

3.3.1 Introduction

Nitridosilicates and oxonitridosilicates have gained increasing relevance due to broad academic as well as industrial interest.[1-3] In this class of compounds, remarkable properties such as luminescence, lithium ion conductivity or non-linear optical properties occur.[1,4-7] For example, doping of alkaline earth (oxo)nitridosilicates (e.g. $M_2Si_5N_8$, $MSi_2O_2N_2$ with M = Ca - Ba) with Eu^{2+} leads to highly efficient luminescent materials applicable in phosphor converted warm white light LEDs, which in the meantime attained industrial application.[8-10] Formally, nitridosilicates can be derived from oxosilicates by exchanging N for O, which allows extended structural possibilities with a more variable degree of condensation and new topological building blocks due to the higher connectivity of nitrogen compared to oxygen. Besides corner sharing, even edge sharing tetrahedra have frequently been observed in nitridosilicates.[11,12] However, probably due to the in general rather high synthesis temperatures (> 1300 °C) most nitridosilicates obtained so far exhibit highly condensed anionic network structures.[1,6,10] Similarly, for oxonitridosilicates only few less condensed species have been identified.[1] Recently, we have developed a synthetic approach using lithium melts in closed tantalum ampoules to obtain (oxo)nitridosilicates with a lower degree of condensation.[13] In this context, several quaternary lithium alkaline earth nitridosilicates were structurally elucidated, e.g. $Li_4M_3Si_2N_6$ with M = Ca, Sr, $LiCa_3Si_2N_5$ or $Li_2Sr_4[Si_2N_5]N$.[13-15] We were able to extend this synthetical route to rare earth elements using the respective halogenides and obtained the isotypic compounds $Li_5Ln_5Si_4N_{12}$ with Ln = La, Ce [16] and the nitridosilicates $Li_{35}Ln_9Si_{30}N_{59}O_2F$ with Ln = Ce, Pr.[17]

In this contribution we present a new lithium rare earth oxonitridosilicate, namely $LiLa_5Si_4N_{10}O$ and the isotypic Pr containing phase.

3.3.2 Results and Discussion

3.3.2.1 Synthesis and Crystal Structure

$LiLa_5Si_4N_{10}O$ was synthesized from LaF_3, $Si(NH)_2$ and LiN_3 with lithium as fluxing agent in weld shut tantalum ampoules at 1200 °C. The oxygen content stems probably from impurities in LaF_3. The title compound is sensitive against air and moisture and was therefore handled

under inert gas atmosphere. The approximate ratio of heavy elements (La : Si) was determined by energy dispersive X-ray microanalysis. $LiLa_5Si_4N_{10}O$ crystallizes in triclinic space group $P\bar{1}$ with one formula unit per cell (for details see Table 1 and Appendix 6.3). One mixed occupied N/O position has been assigned with respect to the shortest Si-(N/O) distance in the silicate substructure. The atomic ratio on this site has been fixed to O : N = 1 : 1 in order to achieve charge neutrality. Analogously, the isotypic Pr containing phase was synthesized. Lattice constants were determined by single-crystal X-ray diffraction as a = 5.6561(11), b = 6.4870(13), c = 8.2567(17) Å, = 103.13(3), β = 107.68(3), γ = 94.42(3)°.

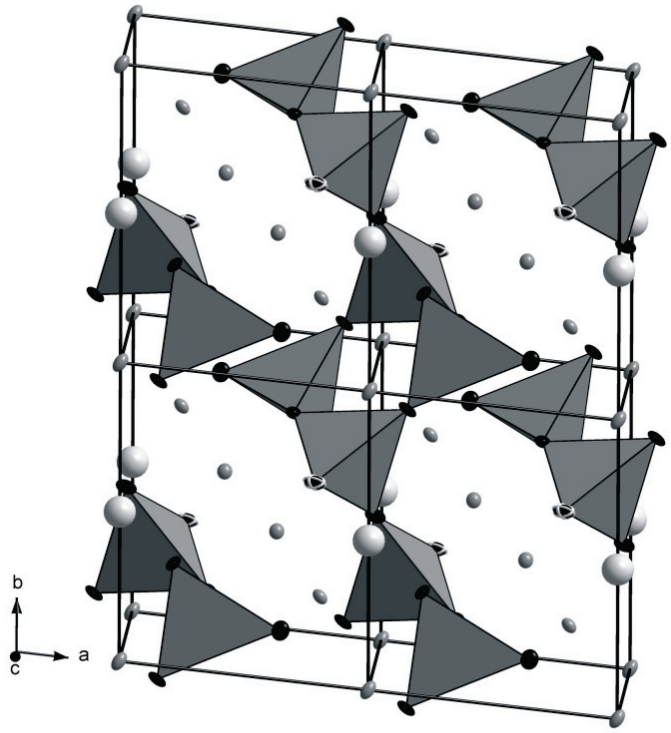

Figure 1. Structure of $LiLn_5Si_4N_{10}O$ with Ln = La, Pr (4 unit cells). Ellipsoids at 90 % probability level. $[SiN_4]$ units are depicted as closed gray tetrahedra, N atoms black, N/O black-white, Ln dark gray and Li^+ ions light gray.

The crystal structure of $LiLa_5Si_4N_{10}O$ is depicted in Figure 1. The silicate substructure consists of loop-branched *dreier* single chains according to the *Liebau* nomenclature.[18] This structural feature has not been identified in (oxo)nitridosilicates so far. However, it is not uncommon for oxosilicates, e.g. $Li_2Mg_2[Si_4O_{11}]$.[19] The distances Si-N range between

1.709(3) and 1.762(3) Å, which is in good agreement with the typical range observed in (oxo)nitridosilicates.[1,10,21] With respect to the sum of the ionic radii (Si-O: 1.64 Å; Si-N: 1.69 Å)[22] we assume that on the remarkably shorter Si-(N/O) bond (1.677(3) Å) oxygen is mainly localized.

Table 1. Crystallographic data of $LiLn_5Si_4N_{10}O$ with Ln = La, Pr.

Formula	$LiLa_5Si_4N_{10}O$	$LiPr_5Si_4N_{10}O$
Formula mass / g · mol^{-1}	969.95	979.95
Crystal system	triclinic	
Space group	$P\bar{1}$ (no. 2)	$P\bar{1}$ (no. 2)
Cell parameters /Å, °	a = 5.7462(11); b = 6.5620(13)	a = 5.6561(11); b = 6.4870(13),
	c = 8.3732(17)	c = 8.2567(17)
	α = 103.54(3); β = 107.77(3)	α = 103.13(3); β = 107.68(3),
	γ = 94.30(3)	γ = 94.42(3)
Cell volume / 10^6 pm^3	V = 288.62(12)	V = 277.57(10)
Formula units / cell	1	
Crystal size / mm^3	0.07 x 0.09 x 0.12	0.04 x 0.02 x 0.02
$\rho_{calcd.}$ / g · cm^{-3}	5.581	5.862
μ / mm^{-1}	18.527	21.966
F(000)	422	432
Diffractometer	Kappa CCD	Stoe IPDS I
Temperature / K	293(2)	293(2)
Radiation, monochromator	Mo-K$_\alpha$, (λ = 71.073 pm), graphite	
Absorption correction	semi-empirical	multi-scan
Min. /max. transmission	0.5503 / 0.9199	0.306 / 0.470
θ range / °	3.1 – 33.7	3.2 – 30.5
Measured reflections	6000	3023
Independent reflections	1315	1173
Observed reflections	1281	1012
Refined parameters	96	95
GoF	1.100	0.926
R indices ($F_o^2 \geq 2\sigma(F_o^2)$)	$R1$ = 0.0165, $wR2$ = 0.0402	$R1$ = 0.0270, $wR2$ = 0.0466
R indices (all data)	$R1$ = 0.0173, $wR2$ = 0.0405[a)]	$R1$ = 0.0212, $wR2$ = 0.0456 [b)]
Max. / min. residual electron density/ eÅ^{-3}	0.93/ -0.74	1.36/ -1.07

a) $w = 1/[\sigma^2(F_o^2) + (0.0023P)^2 + 1.3331P]$ where $P = (F_o^2+2F_c^2)/3$.

b) $w = 1/[\sigma^2(F_o^2) + (0.0244P)^2]$ where $P = (F_o^2+2F_c^2)/3$.

In the crystal structure, there are three crystallographically independent La sites (see Figure 2) at Wyckoff positions 1*a* (La1) and 2*i* (La2 and La3). La1 site is coordinated by six nitrogen atoms and two N/O sites. The other two rare earth sites are coordinated by one N/O site each and six nitrogen atoms (La2), or five nitrogen atoms (La3), respectively. The distances La-(N/O) vary between 2.417(3) and 2.932(1) Å (cf. Table 2) and are in the range observed in other lanthanum containing (oxo)nitridosilicates.[2,23] The sum of the effective ionic radii of La and N/O amounts to 2.48 Å - 2.68 Å for coordination numbers of six to eight and is in good agreement with the distances found in $LiLa_5Si_4N_{10}O$.[22]

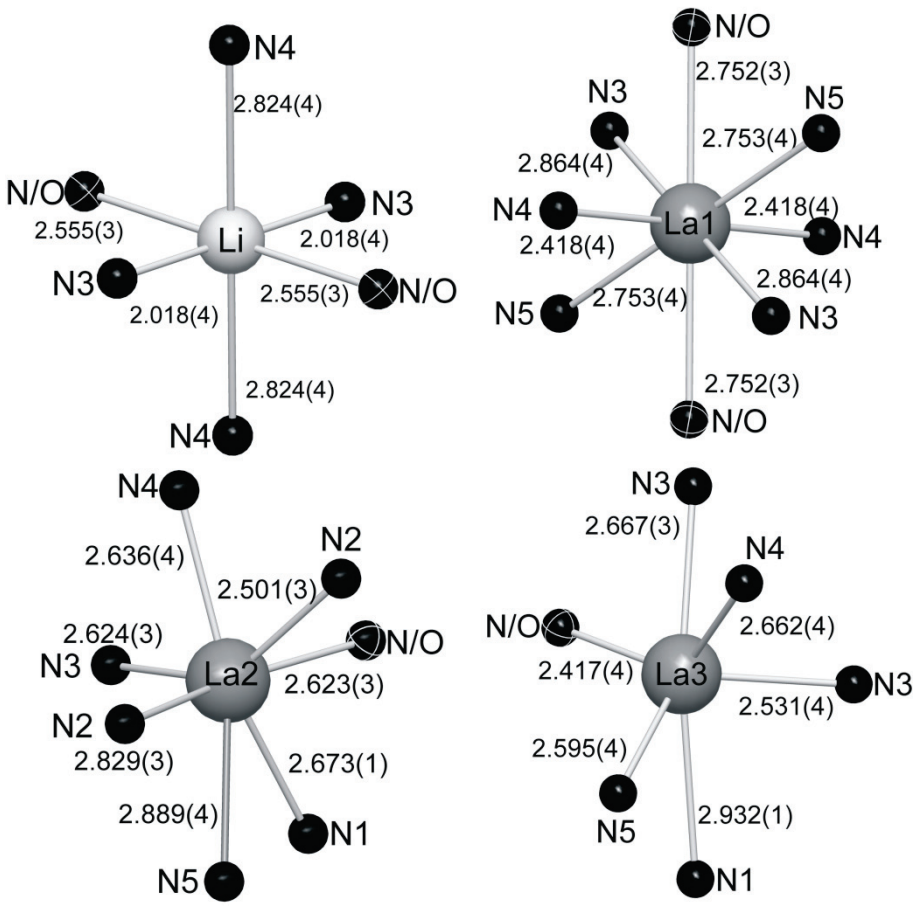

Figure 2. Coordination spheres in $LiLa_5Si_4N_{10}O$ with distances [Å] (standard deviations given in parentheses). N black, mixed occupied N/O black-white, La dark gray and Li light gray.

The lithium position (see Figure 2) exhibits a 4 + 2 coordination sphere made up of four nitrogen and two N/O sites building distorted octahedra. The distances in these octahedra vary

between 2.018(3) and 2.824(4) Å and are in the range of other Li-(N/O) containing compounds and correspond with the sum of the ionic radii.[13,15,16,22,24]

Table 2. Selected interatomic distances [Å] for $LiLa_5Si_4N_{10}O$. Standard deviations are given in parentheses.

La1-N4	2x	2.418(3)	La2-N2		2.501(3)
La1-N/O	2x	2.752(4)	La2-N/O		2.622(3)
La1-N5	2x	2.754(4)	La2-N3		2.624(3)
La1-N3	2x	2.864(4)	La2-N4		2.637(3)
			La2-N1		2.6727(7)
La3-N/O		2.417(3)	La2-N2		2.829(3)
La3-N3		2.531(3)	La2-N5		2.889(4)
La3-N5		2.595(4)			
La3-N4		2.662(4)	Li-N3	2x	2.018(3)
La3-N3		2.667(3)	Li-N/O	2x	2.555(4)
La3-N1		2.932(1)	Li-N4	2x	2.824(4)

3.3.2.2 Solid-state MAS NMR

The ^{7}Li solid-state MAS NMR spectrum of $LiLa_5Si_4N_{10}O$ shows one isotropic intense peak at 0.3 ppm with a full width at half maximum (FWHM) of 8.6 ppm (see Figure 3). This result is in accordance with the crystal structure refinement which exhibits one crystallographic independent lithium site. The chemical shift is slightly below the shift of other lithium containing nitridosilicates (e.g. $LiSi_2N_3$ $\delta = 1.3$ ppm,[24,25] $Li_4Ca_3Si_2N_6$ $\delta = 2.0$ ppm),[14] which exhibit tetrahedral coordination. This can be explained with the octahedral coordination at hand.

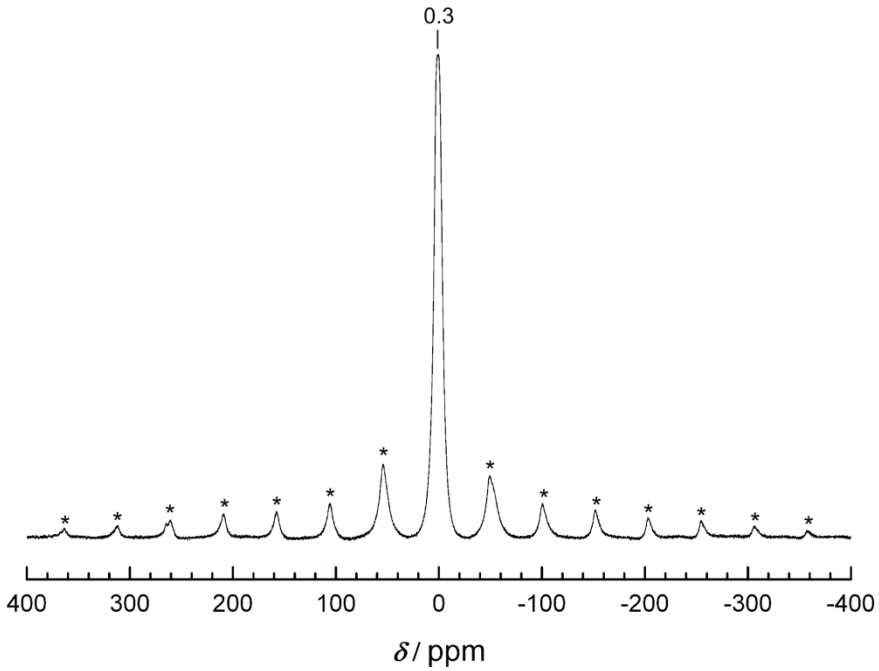

Figure 3. ^{7}Li solid-state MAS NMR of $LiLa_5Si_4N_{10}O$. Rotation bands are indicated by asterisks (rotation frequency 10 kHz).

3.3.2.3 Lattice Energy Calculations According to the MAPLE Concept

Lattice energy calculations (MAPLE Madelung part of lattice energy)[22,26] were performed to corroborate the crystal structure of $LiLa_5Si_4N_{10}O$. Hereby, exclusively electrostatic interactions in an ionic crystal were considered, depending on the charge, distance and coordination spheres of the constituting atoms. The total MAPLE value of the title compound corresponds well with the sum of the total MAPLE values of the constituting binary nitrides and oxides (cf. Table 3). The partial MAPLE values are in the expected ranges.

Table 3. Results of the MAPLE calculations [kJ/mol] for $LiLa_5Si_4N_{10}O$; Δ = difference.[a)]

La^{3+}	3863 - 4320
Si^{4+}	9873; 10167
$N^{[1]\,3-}$	4823; 4768
$N^{[2]\,3-}$	5450 - 5649
$N/O^{1.5-}$	3439
Li^{+}	920
Total MAPLE	114554
Δ	0.31 %
Total MAPLE (1/2 Li_2SiN_2 + 5 LaN + Si_3N_4 + 1/2SiO_2): 114202 kJ/mol	

a) Typical partial MAPLE values [kJ/mol]: La^{3+}: 3500-5000; Si^{4+}: 9000-10200; $N^{[1]\,3-}$: 4300-5000; $N^{[2]\,3-}$: 4600-6000; O^{2-}: 2050-2800 ; Li^{+}: 600-900.

3.3.3 Conclusions

$LiLa_5Si_4N_{10}O$ and its isotypic Pr analogue have been synthesized using lithium flux in weld shut tantalum ampoules at moderate temperatures. These oxonitridosilicates are further examples for the potential of this synthetic approach. By using liquid lithium it is possible to vary the degree of condensation to achieve novel $[SiN_4]$ substructures and, therefore, indirectly the amount of lithium in the resulting structures. Moreover, with the formal substitution of Si-N by Si-O a further extension of the structural possibilities is feasible. The crystal structures of $LiLn_5Si_4N_{10}O$ with Ln = La, Pr reveal a structural feature of loop branched *dreier* single chains of vertex sharing $[SiN_4]$ tetrahedra, which has not been reported for oxonitridosilicates, so far. This further corroborates the importance of the technique of using liquid lithium at moderate temperatures for the search of novel and promising materials.

3.3.4 Experimental Section

3.3.4.1 Synthesis

All manipulations were performed with rigorous exclusion of oxygen and moisture in flame-dried Schlenk-type glassware interfaced to a vacuum line (10^{-3} mbar) or in an argon-filled glove box (Unilab, MBraun, Garching, O_2 < 0.1 ppm, H_2O < 0.1 ppm). Argon (Messer-Griessheim, 5.0) was purified by passage through columns of silica gel (Merck), molecular sieve (Fluka, 4 Å), KOH (Merck, ≥ 85 %), P_4O_{10} (Roth, ≥ 99 %, granulate) and titanium sponge (Johnson Matthey, 99.5 %, grain size ≤ 0.8 cm) at 700 °C. The tantalum tubes were weld shut in an arc furnace under 1 bar purified argon. During this procedure, the crucible holder was water cooled in order to avoid chemical reactions during welding.

For the synthesis of $LiLa_5Si_4N_{10}O$, silicon diimide (23.2 mg, 0.40 mmol; synthesized according to literature),[27] LaF_3 (97.8 mg, 0.49 mmol, Sigma Aldrich, 99.9 %) and LiN_3 (34.5 mg, 0.70 mmol, synthesized according to literature)[28] were mixed in an agate mortar, filled in a tantalum tube and covered with lithium (20 mg, 2.85 mmol, Alfa Aesar, 99.9%) in a glove box. The tantalum ampoule was sealed under argon and heated up in a radio-frequency furnace at 1200 °C within 2 h. The temperature was maintained for 10 h and then cooled down to 600 °C within 30 h. Afterwards the sample was quenched to room temperature by switching off the furnace. The product was obtained as orange crystals.

For the synthesis of $LiPr_5Si_4N_{10}O$ silicon diimide (23.2 mg, 0.40 mmol; synthesized according to literature[27]), PrF_3 (99.2 mg, 0.49 mmol, Sigma Aldrich, 99.9 %) and LiN_3 (34.5 mg, 0.70 mmol, synthesized according to literature)[28] were mixed in an agate mortar, filled in a tantalum tube and covered with lithium (20 mg, 2.85 mmol, Alfa Aesar, 99.9%) in a glove box. The tantalum ampoule was sealed under argon and heated up in a radio-frequency furnace at 1200 °C within 2 h. The temperature was maintained for 10 h and then cooled down to 600 °C within 30 h. Subsequently, the sample was quenched to room temperature by switching off the furnace. $LiPr_5Si_4N_{10}O$ was obtained as few very small red crystals.

3.3.4.2 Chemical Analyses

Scanning electron microscopy was performed on a JEOL JSM-6500F equipped with a field emission gun at an acceleration voltage of 10 kV with a Si/Li EDX detector (Oxford Instruments, model 7418). Samples were prepared by placing single crystals on adhesive conductive pads and subsequently coating them with a thin conductive carbon film. Each EDX spectrum (Oxford Instruments) was recorded with the analyzed area limited onto the

face of one single crystal to avoid the influence of possible contaminating phases. Analysis of three spots per crystallite showed average atomic ratio Ln/Si = 5:4 with Ln = La, Pr which corroborates the composition $LiLn_5Si_4N_{10}O$ with Ln = La, Pr. The determined composition is in accordance to the structure model within the typical error ranges with regard to the fact that lithium cannot be detected by this method (calc. (at%). Ln (Ln = La, Pr) 24, Si 19, N 47, O 5; found (at%) La 24, Si 18, N 53, O 4; Pr 20 Si 15 N 58 O 7).

3.3.4.3 Single Crystal X-ray Analysis

Single crystals of $LiLa_5Si_4N_{10}O$ were isolated under a microscope, which is integrated in a glove box, enclosed in glass capillaries (∅ 0.2 mm), and sealed under argon. Single-crystal X-ray diffraction data were collected at room temperature on a Kappa CCD diffractometer with Mo-K_α radiation (λ = 0.71073 Å, graphite monochromator). The diffraction intensities were scaled using the SCALEPACK software package[29] and a semi-empirical absorption correction was applied. The structure was solved by direct methods after semi-empirical absorption correction. For the structure solution and refinement of $LiLa_5Si_4N_{10}O$ the program package SHELX97 was used.[30,31] Further details of the crystal structure investigation can be obtained from the Fachinformationszentrum Karlsruhe, 76344 Eggenstein-Leopoldshafen, Germany (fax: (+49)7247-808-666; e-mail: crysdata@fiz-karlsruhe.de) on quoting the depository number CSD-423470, the names of the authors and citation of the publication.

3.3.4.4 X-ray Powder Diffraction

X-ray powder diffraction data were collected on a STOE STADI P diffractometer with Ge(111)-monochromatized Mo-$K_{\alpha 1}$ radiation (λ = 0.71073 Å) in Debye-Scherrer geometry (cf. Figure 4). The samples were enclosed in glass capillaries and sealed under argon.

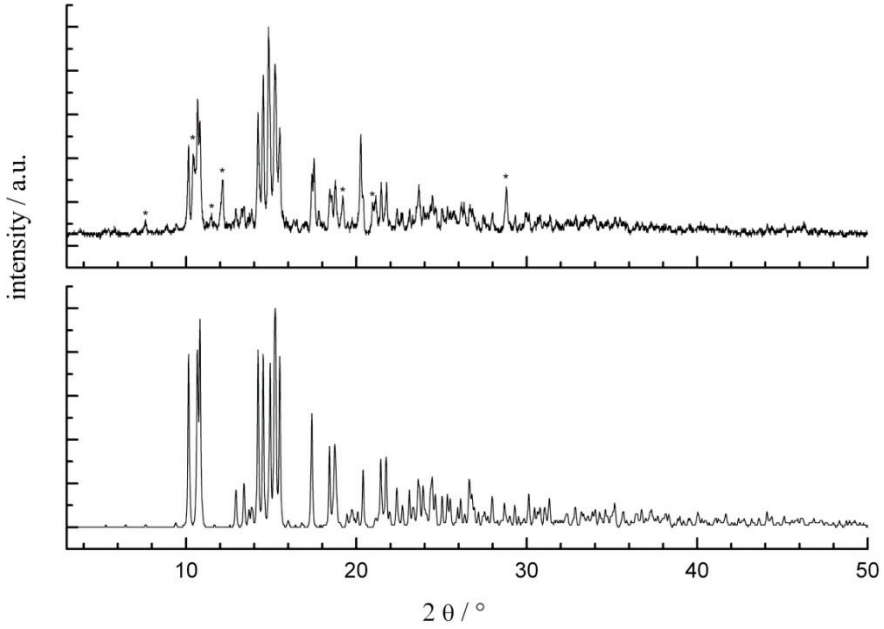

Figure 4. Measured PXRD pattern of $LiLa_5Si_4N_{10}O$ (top, MoKα1 radiation, λ = 71.073 pm) and simulated powder pattern $LiLa_5Si_4N_{10}O$ (below). With asterisks (*) marked peaks belong to an unknown phase.

3.3.4.5 Solid-state MAS NMR

Solid-state NMR experiments were performed on a Bruker Advance DSX 500 spectrometer with an external field of 11.75 T. The ^7Li spectrum was recorded with direct excitation using a commercial 4 mm triple-resonance MAS probe at the frequency 194.415MHz. All experiments were carried out at room temperature in ZrO_2 rotors. The chemical shifts of ^7Li are reported using the frequency ratios published by IUPAC (δ scale relative to 1 % tetramethylsilane (TMS) in $CDCl_3$). The one-dimensional ^7Li NMR spectrum was acquired with a 90° pulse length of 3.0 μs, a recycle delay of 32 s and at a sample spinning frequency of 10 kHz.

3.3.5 References

[1] M. Zeuner, S. Pagano, W. Schnick, *Angew. Chem.* **2011**, *123*, 7898-7920; *Angew. Chem., Int. Ed*. **2011**, *50*, 7754-7775.

[2] W. Schnick, *Angew. Chem.* **1993**, *105*, 846-858; *Angew. Chem., Int. Ed. Engl.* **1993**, *33*, 806-818.

[3] R.-J. Xie, N. Hirosaki, *Sci. Technol. Adv. Mater.* **2007**, *8*, 588-600.

[4] H. A. Höppe, F. Stadler, O. Oeckler, W. Schnick, *Angew. Chem.* **2004**, *116*, 5656-5659; *Angew. Chem,. Int. Ed.* **2004**, *35*, 5540-5542.

[5] Y. Q. Li, G. deWith, H. T. Hintzen, *J. Solid State Chem.* **2008**, *181*, 515-524.

[6] H. A. Höppe, H. Lutz, P. Morys, W. Schnick, A. Seilmeier, *J. Phys. Chem. Solids* **2000**, *61*, 2001-2006.

[7] K. Yamada, K. Kumano, T. Okuda, *Solid State Ionics* **2006**, *177*, 1691-1695.

[8] V. Bachmann, C. Ronda, O. Oeckler, W. Schnick, A. Meijerink, *Chem. Mater* **2009**, *21*, 316-325.

[9] R. Mueller-Mach, G. Mueller, M. R. Krames, H. A. Höppe, F. Stadler, W. Schnick, T. Juestel, P. Schmidt, *Phys. Status Solidi A* **2005**, *202*, 1727-1732.

[10] M. Yamada, T. Naitou, K. Izuno, H. Tamaki, Y. Murazaki, M. Kameshima, T. Mukai, *Jpn. J. Appl. Phys.* **2003**, *42*, L20.

[11] H. Yamane, F. J. DiSalvo, *J. Alloys Compd.* **1996**, *240*, 33-36.

[12] F. Ottinger, R. Nesper, *Z. Anorg. Allg. Chem.* **2005**, *631*, 1597-1602.

[13] S. Pagano, S. Lupart, M. Zeuner, W. Schnick, *Angew. Chem.* **2009**, *121*, 6453-6456; *Angew. Chem., Int. Ed. Engl.* **2009**, *48*, 6335-6338.

[14] S. Pagano, S. Lupart, S. Schmiechen, W. Schnick, *Z. Anorg. Allg. Chem.* **2010**, *636*, 1907-1909.

[15] S. Lupart, S. Pagano, O. Oeckler, W. Schnick, *Eur. J. Inorg. Chem.* **2011**, 2118-2123.

[16] S. Lupart, M. Zeuner, S. Pagano, W. Schnick, *Eur. J. Inorg. Chem.* **2010**, 2636-2641.

[17] S. Lupart, D. Durach, W. Schnick, *Z. Anorg. Allg. Chem.* **2011**, *637*, 1841-1844.

[18] F. Liebau, *Naturwissenschaften* **1962**, *49*, 481-490.

[19] G. Bissert, M. Czank, *Z. Kristallogr.* **1993**, *204*, 129-142.

[20] W. Schnick, *Int. J. Inorg. Mater.* **2001**, *3*, 1267-1272.

[21] Z. A. Gál, P. M. Mallinson, H. J. Orchard, S. J. Clarke, *Inorg. Chem.* **2004**, *43*, 3998-4006.

[22] R. D. Shannon, *Acta Crystallogr., Sect. A: Cryst. Found. Crystallogr.* **1976**, *32*, 751-767.

[23] C. Schmolke, S. Lupart, W. Schnick, *Solid State Sci.* **2009**, *11*, 305-309.

[24] M. Orth, W. Schnick, *Z. Anorg. Allg. Chem.* **1999**, *625*, 1426-1428.

[25] S. Gumann, N. Nestle, V. Liebau-Kunzmann, R. Riedel, *Solid State Nucl. Magn. Reson.* **2007**, *31*, 82-90.

[26] R. Hoppe, *Angew. Chem.* **1966**, *78*, 52-63; *Angew. Chem., Int. Ed.* **1966**, *5*, 95-106.

[27] H. Lange, G. Wötting, G. Winter, *Angew. Chem.* **1991**, *103*, 1606-1625; *Angew. Chem., Int. Ed. Engl.* **1991**, *30*, 1579-1597.

[28] N. Hofman-Bang, *Acta Chem. Scand.* **1957**, *11*, 581-582.

[29] Z. Otwinowski, W. Minor, *Methods Enzymol.* **1997**, *276*, 307-326.

[30] G. M. Sheldrick, *SHELXS-97, Program for the Solution of Crystal Structures,* Universität Göttingen **1997**.

[31] G. M. Sheldrick, *SHELXL-97, Program for the Refinement of Crystal Structures,* Universität Göttingen **1997**.

3.4 $Li_{14}Ln_5[Si_{11}N_{19}O_5]O_2F_2$ with Ln = Ce, Nd – Representatives of a Family of Potential Lithium Ion Conductors

published in

Saskia Lupart, Giuliano Gregori, Joachim Maier and Wolfgang Schnick

J. Am. Chem. Soc. **2012**, *134* (24), 10132-10137
DOI: 10.1021/ja302255d
Copyright © 2012 American Chemical Society
http://pubs.acs.org/doi/abs/10.1021/ja302255d

Abstract. The isotypic layered oxonitridosilicates $Li_{14}Ln_5[Si_{11}N_{19}O_5]O_2F_2$ (Ln = Ce, Nd) have been synthesized using Li as fluxing agent and crystallize in the orthorhombic space group *Pmmn* (Z = 2, $Li_{14}Ce_5[Si_{11}N_{19}O_5]O_2F_2$: a = 17.178(3), b = 7.6500(15), c = 10.116(2) Å, $R1$ = 0.0409, $wR2$ = 0.0896; $Li_{14}Nd_5[Si_{11}N_{19}O_5]O_2F_2$: a = 17.126(2), b = 7.6155(15), c = 10.123(2) Å, $R1$ = 0.0419, $wR2$ = 0.0929). The silicate layers consist of *dreier* and *sechser* rings interconnected via common corners, yielding an unprecedented silicate substructure. A topostructural analysis indicates possible 1D ion migration pathways between five crystallographic independent Li positions. The specific Li-ionic conductivity and its temperature dependence were determined by impedance spectroscopy as well as DC polarization/depolarization measurements. The ionic conductivity is on the order of 10^{-5} S/cm at 300 °C, while the activation energy is about 0.69 eV. Further adjustments of the defect chemistry (e.g., through doping) can make these compounds interesting candidates for novel oxonitridosilicate based ion conductors.

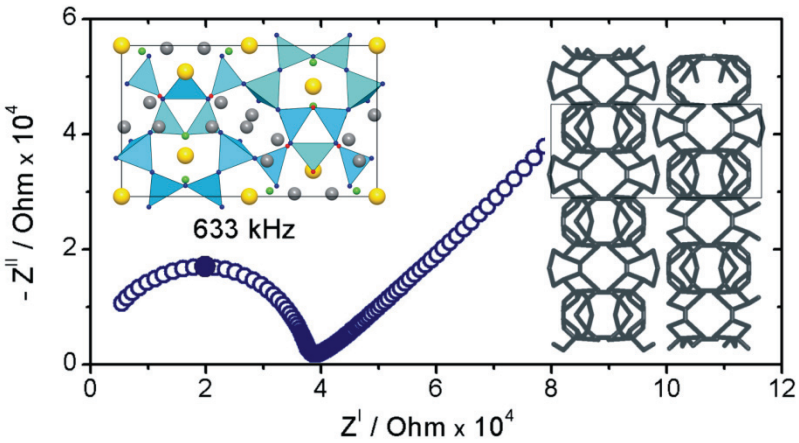

3.4.1 Introduction

As the need for mobile power supply and efficient energy storage has constantly increased in the last decades, rechargeable batteries have become a key technology in modern society.[1-4] In the effort to meet the demand for effective batteries, lithium based electrochemical devices play a major role; however, most make use of organic liquid electrolytes that require relatively stringent safety precautions and hence are rather inapplicable for a large range of applications (e.g., large-scale systems, medical devices).[1] Nonflammable, nonvolatile solid electrolytes have the potential to overcome these problems, but the assortment of materials that combine all of the basic requirements for all-solid-state batteries, i.e. high ionic conductivity at the operating temperature and a high chemical, electrochemical, and thermal stability, is still restricted.[5,6]

Therefore, great effort has been put into the search for new solid electrolytes and a variety of crystalline, glassy, or composite materials have been considered. [1-3,7] Although Li_3N has one of the highest ionic conductivities at room temperature (6 x 10^{-3} S cm^{-1}), novel materials are mostly oxides (e.g., $Li_{2+2x}Zn_{1-x}GeO_4$ (-0.36< x <0.87)[8] or perovskite-related compounds like $La_{0.62}Li_{0.16}TiO_3$)[9] or sulfides (e.g., $Li_{3.25}Ge_{0.25}P_{0.75}S_4$[10] or $Li_{10}GeP_2S_{12}$).[5] Only a few rare exceptions, e.g., $Li_xPO_yN_z$ (x = 2y+3z-5),[11] represent nitrides or oxonitrides. In this context multinary lithium (oxo)nitridosilicates might be interesting candidates for solid-state electrolytes.

Nitridosilicate based ceramics in general exhibit a high chemical stability combined with high decomposition temperatures and high mechanical strength and are often resistant against oxidation and corrosive environments.[12,13] In addition, the ternary phases $LiSi_2N_3$,[14,15] Li_2SiN_2,[15-17] Li_5SiN_3,[18,19] Li_8SiN_4,[15,17] and $Li_{18}Si_3N_{10}$,[17] reported in the quasi-binary system Li_3N-Si_3N_4, all show lithium ion conduction (for example Li_2SiN_2: σ(400 K) = 1 x 10^{-3} S cm^{-1}; Li_8SiN_4: σ(400 K) = 5 x 10^{-2} S cm^{-1}).[15,20,21] These facts lead us to expect perceptible Li ion conduction also in multinary lithium (oxo)nitridosilicates.

In recent years, we have structurally elucidated a number of alkaline earth as well as rare earth (oxo)nitridosilicates: e.g., $LiCa_3Si_2N_5$,[22] $Li_4M_3Si_2N_6$ with M = Ca, Sr,[23] $Li_2Sr_4[Si_2N_5]N$,[24] $Li_5Ln_5Si_4N_{12}$ with Ln = La, Ce,[25] $LiLn_5Si_4N_{10}O$ with Ln = La, Pr,[26] and $Li_{35}Ln_9Si_{30}N_{59}O_2F$ with Ln = Ce, Pr.[27] These compounds not only differ in their nominal amount of lithium in their formula units, but also exhibit different silicate substructures

covering the whole range of dimensionality, i.e., from isolted groups over layered Si-N substructures up to three-dimensional networks.

In this work we report about the synthesis and the structural characterization of a novel layer-like (oxo)nitridosilicate $Li_{14}Nd_5[Si_{11}N_{19}O_5]O_2F_2$ and its isotypic Ce-containing phase. The complementary electrical conduction measurements prove that these compounds are indeed Li ion conductors with a very large ionic transference number. Yet, further adjustments of the defect chemistry of this material (e.g., through aliovalent cation doping) are required to obtain ionic conductivity values which might be interesting for battery applications.

3.4.2 Experimental Section

3.4.2.1 Synthesis

All manipulations were performed with rigorous exclusion of oxygen and moisture in an argon-filled glovebox (Unilab, MBraun, Garching, O_2 < 0.1 ppm, H_2O < 0.1 ppm). The title compounds can be synthesized using two different routes:

Route 1: One route uses tantalum crucibles (wall thickness 0.5 mm, internal diameter 10 mm, length 300 mm), which were arc-welded under a pressure of 1 bar purified argon. The crucible holder was cooled in order to avoid decomposition reactions during welding. Single crystals of $Li_{14}Ln_5[Si_{11}N_{19}O_5]O_2F_2$ with Ln = Ce, Nd were synthesized from 23.6 mg silicon diimide (0.40 mmol, synthesized according to literature),[28] 25 mg LiN_3 (0.52 mmol, synthesized according to literature),[29] 108.4 mg CeF_3 (0.55 mmol, Sigma Aldrich, 99.9 %) for Ln = Ce and 10 mg CeF_3 (0.05 mmol, Sigma Aldrich, 99.9 %) as well as 190 mg $NdBr_3$ (0.50 mmol, Sigma Aldrich, 99.9 %) for Ln = Nd. A 20 mg-portion of Li as fluxing agent were added. After closing, the tantalum crucibles were placed in silica tubes (under Argon) which in turn were positioned in the middle of a tube furnace. The temperature was raised to 1000 °C (5 °C/min), maintained for 24 h, subsequently cooled down to 500 °C (0.5 °C/min) and finally quenched to room temperature.

Route 2: To obtain higher amounts of $Li_{14}Ln_5[Si_{11}N_{19}O_5]O_2F_2$ with Ln = Ce, Nd tungsten crucibles heated in a radio frequency furnace under purified nitrogen were used. 63.8 mg silicon diimide (1.10 mmol, synthesized according to literature),[28] 17 mg Li_2O (0.29 mmol, Alfa Aesar, 99.5 %) and 98.6 mg CeF_3 (0.50 mmol, Sigma Aldrich, 99.9 %) or a mixture of 191.9 mg $NdBr_3$ (0.97 mg, Sigma Aldrich, 99.9 %) and 20 mg CeF_3 (0.10 mg, Sigma Aldrich, 99.9 %) were mixed in an agate mortar, filled in a tungsten crucible, and covered with 20 mg

Li as fluxing agent. The tungsten crucible was placed in a radio frequency furnace and heated within 2 h to 1000 °C. For the Ce-containing compound, the mixture was cooled down over 15 h to 950 °C and subsequently cooled at room temperature within 2 h. The Nd-compound yielded higher purity by maintaining 1000 °C for 15 h, cooling to 800 °C in 1 h, and subsequently quenching the sample to room temperature by switching off the furnace.

3.4.2.2 Chemical Analysis

Scanning electron microscopy was performed using a JEOL JSM 6500F equipped with a field emission gun at an acceleration voltage of 10 kV with a Si/Li EDX detector (Oxford Instruments, model 7418). Samples were prepared by placing single crystals on adhesive conductive pads and subsequently coating them with a thin conductive carbon film. Each EDX spectrum (Oxford Instruments) was recorded with the analyzed area limited onto the face of one single crystal to avoid the influence of possible contaminating phases. Analysis of three spots per crystallite showed an average atomic ratio Ln : Si = 1 : 2.2 which corroborates the composition $Li_{14}Ln_5[Si_{11}N_{19}O_5]O_2F_2$ (Ln = Ce, Nd). For the Nd-containing compound an average of 0.7 % Ce content has been found. The determined composition is within the typical error ranges with regard to the fact that lithium cannot be detected by this method and fluorine could not be detected quantitatively, measured values varied between 0 – 4 atom-% (calcd. (at%):Ln (Ln = Ce, Nd) 9, Si 19, N 33, O 12, F 3; found (at%) Ce 9, Si 20, N 48, O 18; Nd 10, Ce 0.7, Si 22, N 46, O 21).

3.4.2.2 Single Crystal X-ray Analysis

Single-crystal X-ray diffraction data were collected with a Stoe IPDS I (Mo-K_α radiation). The program package SHELX97 was used for structure solution and refinement (see Table 1).[30,31]

Table 1. Crystallographic data of $Li_{14}Ln_5[Si_{11}N_{19}O_5]O_2F_2$ (Ln = Ce, Nd).

	Ln = Ce	Ln = Nd
Formula mass/ g mol^{-1}	1522.94	1543.54
Crystal system	orthorhombic	
Space group	Pmmn	
Cell parameters/ Å	a = 17.178(3) b = 7.6500(15) c = 10.116(2)	a = 17.126(2) b = 7.6155(15) c = 10.123(2)
Cell volume/ 10^6 Å^3	1329.3(5)	1320.3(5)
Formula units/ cell	2	
$\rho_{calc.}$ / g cm^{-3}	3.785	3.883
F(000)	1386	1406
Diffractometer	Stoe IPDS I	
Temperature/ K	293(2)	
Radiation, monochromator	Mo-K$_\alpha$, (λ = 0.71073 Å), graphite	
Absorption correction	semi-empirical	
θ range/ °	2.3 – 30.5	
Measured reflections	10928	10825
Independent reflections	1034	1047
Observed reflections	1684	1589
Refined parameter	144	
GoF	0.876	0.893
R indices [$F_o^2 \geq 2\sigma(F_o^2)$]	$R1$ = 0.0409, $wR2$ = 0.0896	$R1$ = 0.0419, $wR2$ = 0.0929
R indices (all data)	$R1$ = 0.0699, $wR2$ = 0.0971[a]	$R1$ = 0.0678, $wR2$ = 0.1005[b]
Max./min. res. electron density/ eÅ^{-3}	1.67/ -2.97	2.11/ -2.51

[a] $w = [\sigma^2(F_o^2)+(0.0572P)^2]$, in which $P = (F_o^2+2F_c^2)/3$

[b] $w = [\sigma^2(F_o^2)+(0.0574P)^2]$, in which $P = (F_o^2+2F_c^2)/3$

3.4.2.3 X-ray Powder Diffraction

X-ray powder diffraction data were collected with a HUBER G670 diffractometer equipped with an imaging-plate system using Cu-K$_{\alpha 1}$ radiation (Ge monochromator, λ = 1.54051 Å). For temperature-dependent X-ray powder diffraction, a sample of $Li_{14}Nd_5[Si_{11}N_{19}O_5]O_2F_2$ was enclosed in a silica glass capillary with 0.5 mm diameter under argon atmosphere. The data were obtained with a STOE STADI P diffractometer equipped with an imaging plate

system using Mo-$K_{\alpha 1}$ radiation (Ge monochromator, $\lambda = 0.71093$ Å) in Debye-Scherrer geometry using a graphite furnace. Data were collected every 50 °C starting from room temperature up to 900 °C with a heating rate of 5 °C/ min. In this temperature range, the compound undergoes no phase transition or decomposition and therefore it can be assumed that $Li_{14}Nd_5[Si_{11}N_{19}O_5]O_2F_2$ is temperature stable at least until 900 °C.

3.4.2.4 Electrical Conductivity Measurements

For the electrical conductivity measurements, two different sets of samples were prepared: (i) a series of pellets with a diameter of 6 mm and thickness of ~3.5 mm was obtained by uniaxially cold pressing (350 MPa) the $Li_{14}Ln_5[Si_{11}N_{19}O_5]O_2F_2$ powder; (ii) a symmetric cell consisting of the following five layers (containing electron-blocking elements, LiI) was assembled LiAl / LiI / $Li_{14}Ln_5[Si_{11}N_{19}O_5]O_2F_2$ / LiI / LiAl. In this case, the powders were first uniaxially pressed (250 MPa) and subsequently isostatically pressed at 500 MPa for 5 min. The $Li_{14}Ln_5[Si_{11}N_{19}O_5]O_2F_2$ layer had a final diameter of ~5 mm and thickness of about 0.5 mm.

AC measurements were performed using a Novocontrol high resolution dielectric analyzer at frequencies ranging between 1 MHz and 0.01 Hz (AC voltage of 0.3 V, titanium electrodes). DC measurements were carried out by applying a 10 nA current (galvanostatic mode) with a Keithley 220 current source and measuring the voltage response with a Keithley 6514 system electrometer. The impedance spectra were analyzed using the commercial software Z-View by Scribner Ass.

3.4.3 Results and Discussion

3.4.3.1 Synthesis and Crystal Structure

The air and moisture stable compounds $Li_{14}Ln_5[Si_{11}N_{19}O_5]O_2F_2$ with Ln = Ce, Nd were synthesized using liquid lithium as fluxing agent at temperatures around 1000 °C. The title compounds can be synthesized analogously with two different synthetic approaches (see Experimental Section): In closed ampules (tantalum or niobium) with additional LiN_3 in a tube furnace or in "open" tungsten crucibles in a radio frequency furnace with about 1 bar purified dynamic nitrogen atmosphere. However, the results from both synthetic approaches differ slightly from each other: in closed systems (tantalum or niobium ampules) only smaller amounts of the title compounds were accessible and Ta-containing side phases were

unavoidable, whereas in tungsten crucibles, it is possible to obtain larger amounts of the samples, although elemental lithium is used in an open reaction system. In the system Ce-Si-O-N many thermodynamically stable phases exist, which cannot be completely excluded. The Nd phase can only be obtained as single crystals with 0.7 atom-% Ce-content. Due to those reasons listed above, we focused for the physical measurements on the Nd-containing phase, which was synthesized in a radio frequency furnace. To avoid impurities, single crystals of $Li_{14}Nd_5[Si_{11}N_{19}O_5]O_2F_2$ were isolated from the obtained samples for the measurements.

The two isotypic compounds $Li_{14}Ln_5[Si_{11}N_{19}O_5]O_2F_2$ with Ln = Ce, Nd crystallize in the orthorhombic space group *Pmmn* with two formula units per cell (for details see Table 1). Oxygen has been assigned to the Wyckoff positions 2*b*, 4*e*, and 4*f* in the single crystal refinement due to the shortest Si-X distances, which is in accordance with lattice-energy calculations (see Appendix). In order to achieve charge neutrality, three positions are mixed occupied by isolated O- and F-atoms on a ratio O/F = 1:1. The approximate ratio of the heavier elements (Ln : Si) was determined by energy dispersive X-ray microanalysis and confirms the X-ray structure refinement.

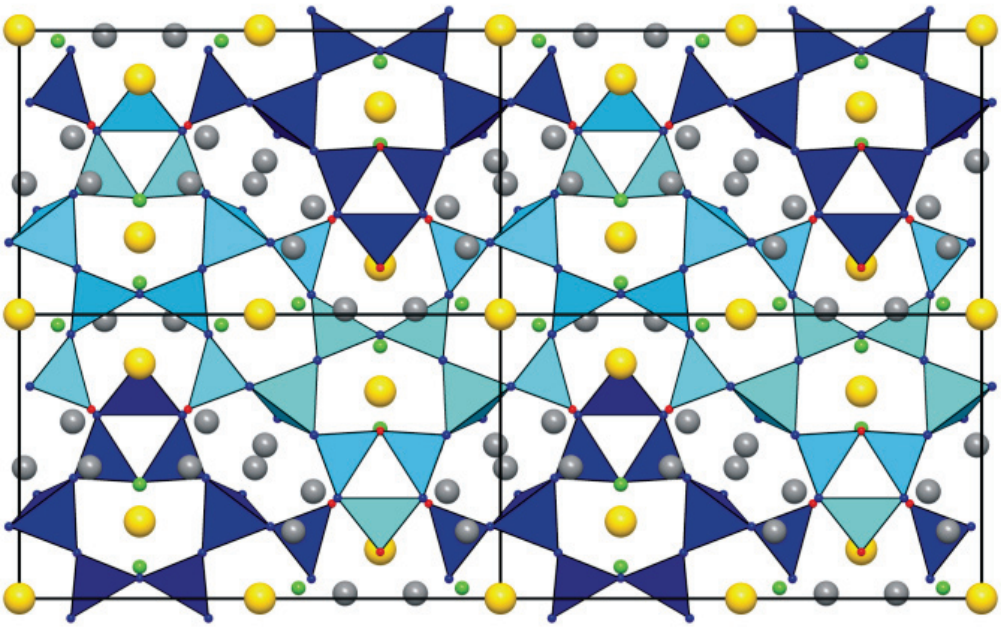

Figure 1. Crystal structure of $Li_{14}Nd_5[Si_{11}N_{19}O_5]O_2F_2$ (Ln = Ce, Nd) viewed along [010]. $[SiX_4]$ tetrahedra (X = N, O) are depicted in blue, with one layer motif highlighted in light blue. (N^{3-} dark blue, O^{2-} red, Ln^{3+} yellow, mixed $O/F^{-1.5}$-positions green, and Li^{+} grey).

The layer silicates $Li_{14}Ln_5[Si_{11}N_{19}O_5]O_2F_2$ with Ln = Ce, Nd consist of *dreier* and *sechser* rings of corner sharing $[SiN_4]$ tetrahedra with an unprecedented topology (cf. Figure 1).[33]

The layers are parallel to [101], and exhibit with κ = 11:24 an uncommonly high degree of condensation, which is usually 2:5 for layer (oxo)silicates. The high degree of condensation can be explained with the topology of the layers, as these layers have a relatively large thickness and the distance to the next layer is rather low. The Si-O distances vary between 1.677(13) – 1.705(8) Å for Ln = Ce and from 1.683(12) to 1.693(7) Å for Ln = Nd, respectively. The Si-N distances are slightly larger with 1.706(9) – 1.778(8) Å and 1.710(14) – 1.771(12) Å for Ln = Ce and Nd. These ranges are in agreement with the sum of the ionic radii (Si-O: 1.64 Å, Si-N: 1.69 Å)[34] and within the values of other oxonitridosilicates.[14,35]

There are three crystallographically independent Ln^{3+} sites which occupy the Wyckoff positions 2a (Ln1), 4e (Ln2), and 4c (Ln3). Ln1 is situated between the layers and exhibits a coordination sphere consisting of four O and three N in a distorted pentagonal bipyramidal arrangement. The other two Ln^{3+} sites are centered in the *sechser* rings of the layers and each is coordinated by eight electronegative atoms. The distances Ln-X (X = N, O, F) in these polyhedra range between 2.335(11) and 2.828(8) Å for Ln = Ce, and 2.320(9) – 2.864(8) Å for Ln = Nd, respectively. The sum of the ionic radii corresponds well with the distances found in the different coordination spheres.[34] Furthermore, other well-investigated (oxo)nitridosilicates exhibit similar distance ranges.[29,36-38]

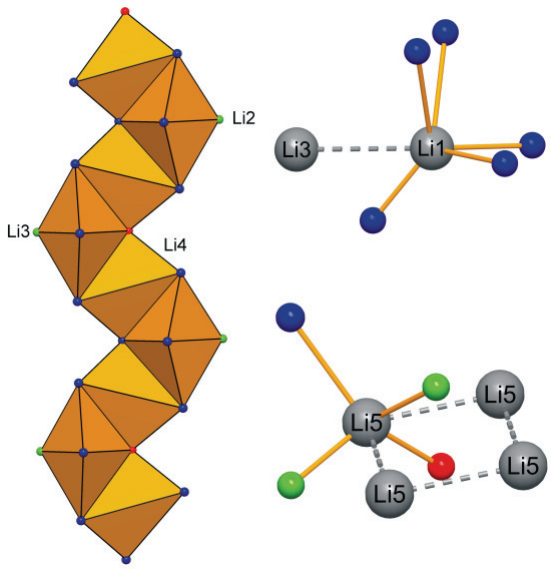

Figure 2. Coordination spheres of the Li^+ sites. Left: Polyhedral strand of alternating distorted tetrahedra and trigonal bipyramides of Li2-Li4. Right: coordination sphere of Li1 and Li5. Nitrogen blue, oxygen red, mixed occupied O/F green and lithium grey.

Four of the five crystallographically independent Li^+ sites in the crystal structure are situated between the layers in the resulting voids in the structure. These Li^+ sites build up double strands along the crystallographic *b*-axis (cf. Figure 2). The coordination spheres of these ions are alternatingly distorted tetrahedra (around Li4) and distorted trigonal bipyramides (around Li2 and Li3) made up from the electronegative atoms in the structure (Figure 2). The polyhedra are interconnected via common edges. Conjoined to Li3, which means to every fourth Li^+ site of a strand is an additional polyhedron centered around Li1 with a pyramidal coordination. In the structure, two strands are always positioned together, with one strand mirror-inverted and staggered to the other, building interlocked pairs (Figure 3). The distances in these polyhedra vary between 1.87(3) and 2.514(15) Å for Ln = Ce and 1.88(3) - 2.494(15) Å for Ln = Nd, respectively, which is in accordance with the sum of the ionic radii and with other Li-containing compounds.[16, 18, 23, 26, 34, 39] The fifth crystallographic Li^+ site (Li5) in the structure (cf. Figure 2) is not interconnected with the Li-strands, but builds isolated $[Li_4X_{13}]^{28.5-}$ units (with X = N,O,F). The coordination of the Li^+ in this building unit is pyramidal. The shortest interatomic Li-Li distances are situated within the strands and exhibit values in the range 2.44(3) – 2.62 Å (cf. Figure 3). In contrast, the lateral attached Li1 exhibit a slightly higher distance to the neighboring Li (Li3) in the strands (2.86(4) Å for Ln = Ce, and 2.79(4) Å for Ln = Nd).

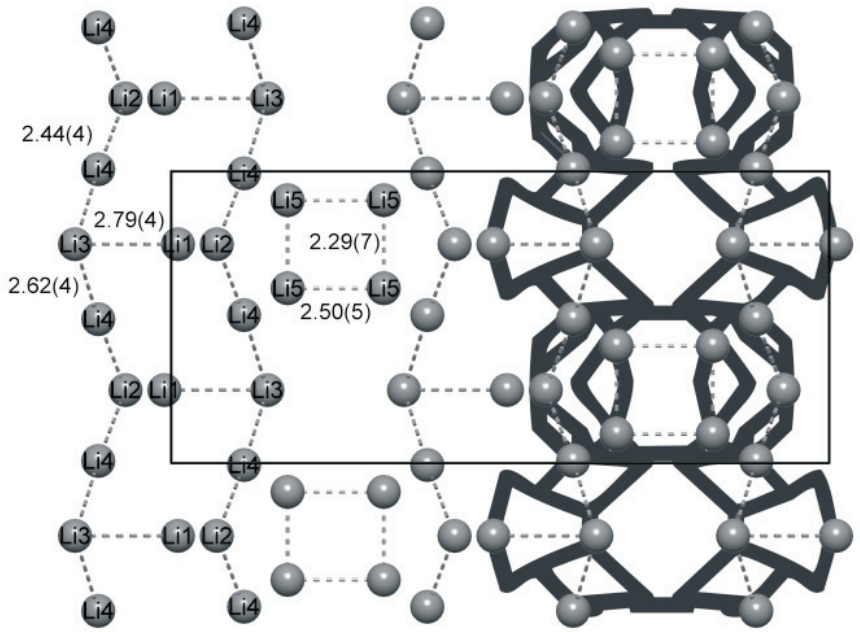

Figure 3. Li^+ positions in the crystal structure (view along [001]) with depicted shortest Li-Li distances in Å (standard deviations in parentheses) and calculated possible Li^+ pathways (dark grey) according to the voids in the structure.

3.4.3.2 Structural Analysis of Possible Lithium Migration Pathways

An analysis concerning voids and migration pathways in the title compounds has been performed. In this context, the program package TOPOS has been employed.[40-42] Hereby, the voids in crystal structures are calculated with the help of Voronoi-Dirichlet polyhedra. The analysis of $Li_{14}Ln_5[Si_{11}N_{19}O_5]O_2F_2$ (Ln = Ce, Nd) on basis of the crystal structure refinement lead to possible 1D migration pathways along the crystallographic *b*-axis shown in Figure 3. A comparison of the shortest distance Li-Li with the pathways calculated due to the voids, which are suitable for lithium migration, shows that these do not coincide. The calculated pathways also include the seemingly isolated positions Li5. Anurova et al. calculated the voids of more than 2000 known compounds containing Li^+ ions with the program TOPOS and all compounds exhibiting infinite lithium pathways are either experimentally proven lithium ion conductors or are promising candidates for lithium ion conductors.[43] According to these calculations, anisotropic lithium ion conductivity is plausible with respect to the structural chemistry of the title compounds.

3.4.3.3 Electrical Conductivity Measurements

Figure 4 shows the Nyquist plot of the impedance spectrum acquired from the Ti/ $Li_{14}Ln_5[Si_{11}N_{19}O_5]O_2F_2$ / Ti cell (the sample was kept at 300°C for 20 hours). One high frequency contribution (which can be fitted with an RQ equivalent circuit, R being the resistance and Q a constant phase element defined as $C = (R^{1-n}Q)^{1/n}$, where C is the capacitance and *n* an additional fitting parameter) followed by a Warburg behavior can be clearly recognized. The conductivity associated with the high frequency semicircle is on the order of 510^{-5} S/cm at 300 °C while its capacitance value is ~6 pF ($\square$ ~ 80). Notably, the appearance of a Warburg behavior in the presence of Ti electrodes indicates the occurrence of ionic diffusion. Impedance spectra were recorded during cooling every 20 K and upon a dwell time of 1 h at each step. Figure 5 illustrates the corresponding Arrhenius plot obtained after fitting the high frequency contribution: The activation energy is 0.69 eV. From these data, it is possible to extrapolate the electrical conductivity at room temperature, which is on the order of $1.7 \cdot 10^{-10}$ S/cm. It is worth noting that additional tests were also performed with platinum electrodes and very similar values of conductivity as well as activation energy were obtained. The black triangle symbol in Figure 5 corresponds to a measurement performed at the end of all AC and DC measurements (see below). The sample exhibits only a minor degradation of the conduction properties.

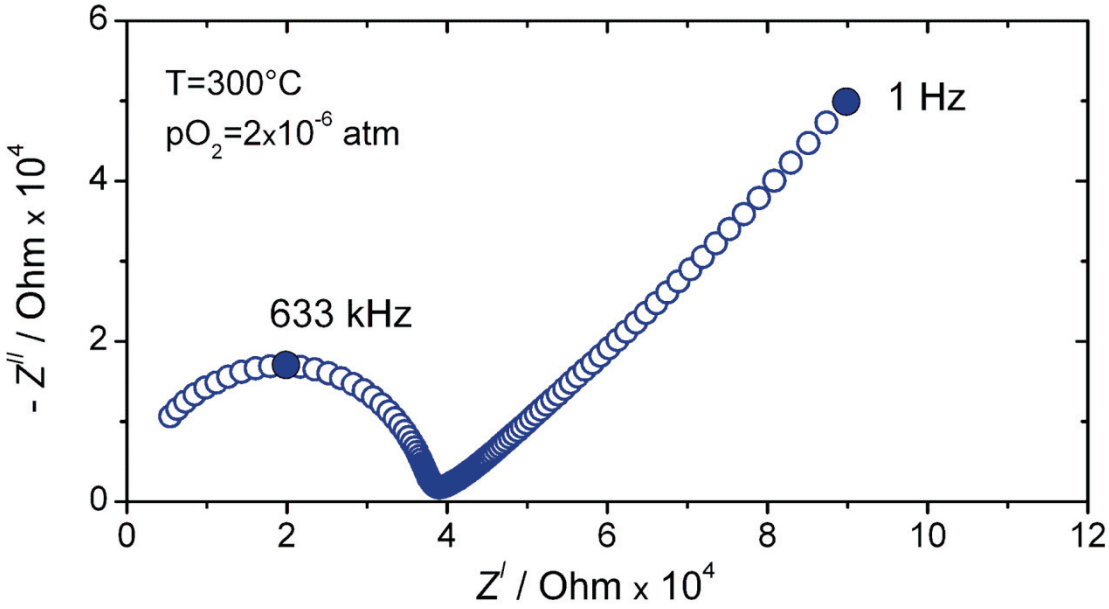

Figure 4. Impedance Nyquist plot of a spectrum collected from the Ti/ $Li_{14}Nd_5[Si_{11}N_{19}O_5]O_2F_2$ / Ti cell.

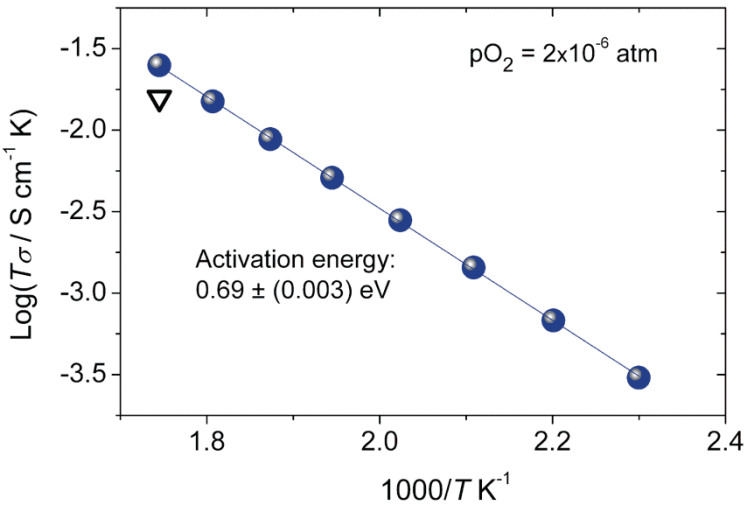

Figure 5. Arrhenius diagram obtained from the impedance spectroscopy measurements carried out with titanium electrodes.

DC polarization/depolarization measurements were also performed on the same Ti/ $Li_{14}Ln_5[Si_{11}N_{19}O_5]O_2F_2$ / Ti cell. As shown in Figure 6(a), the change of the potential U upon the application of a DC current of 10 nA is not instantaneous, but it rather exhibits the occurrence of an evident polarization process, which confirms the ionic character of the

electrical conduction. If one compares the DC resistance at the plateau with the AC resistance values of the high frequency contribution of the impedance spectra (Figure 6(b)) then the ionic transference number (> 0.99 at 300°C) can be estimated.

In order to verify whether the ionic conductivity was indeed due to the Li ion migration the second cell was prepared so as to block the electron transport and let lithium ions migrate: LiAl / LiI / $Li_{14}Ln_5[Si_{11}N_{19}O_5]O_2F_2$ / LiI / LiAl.

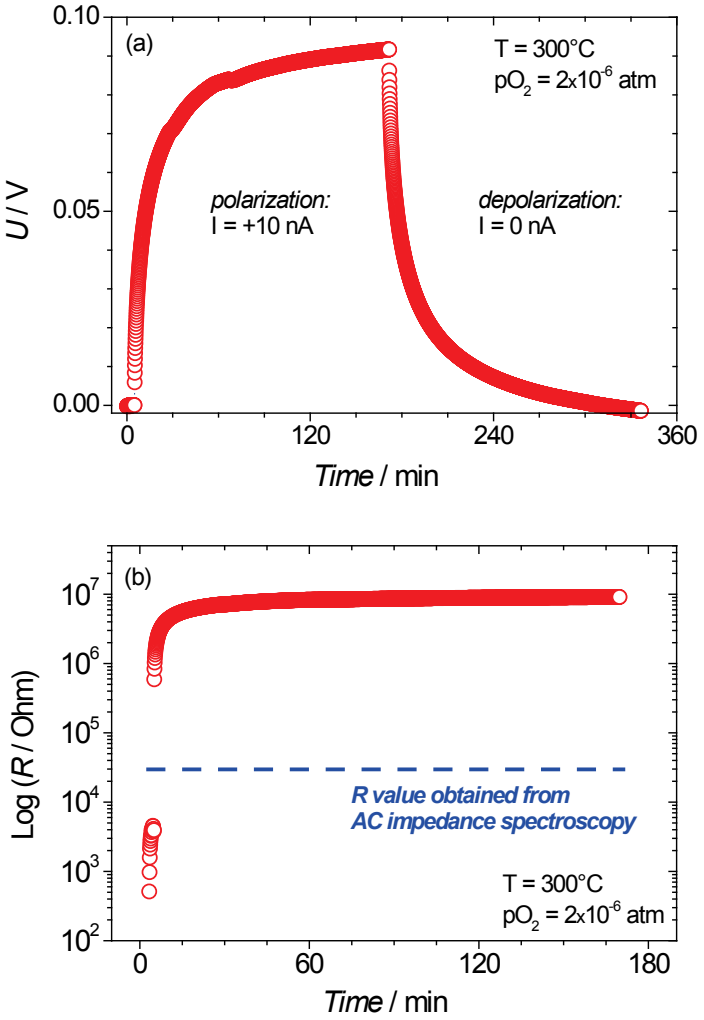

Figure 6. DC polarization/depolarization measurements: (a) polarization voltage as function of time for an applied current of 10 nA. (b) Resistance values obtained from (a); the AC resistance (cf. Figure 5) is shown for comparison.

The results of the polarization/depolarization measurement performed on the cell with electron-blocking elements are shown in Figure 7. Upon switching on a DC current of 10 nA, an instantaneous change of the potential U was recorded. Only a minor deviation from the

ideal behavior was detected at the beginning of the polarization test. An analogous behavior characterizes the depolarization process when the current was turned off.

The resistance values obtained from the voltage plateau correspond to a conductivity on the order of $2.4 \cdot 10^{-10}$ S/cm in very good agreement with the conductivity values extrapolated from the data of Figure 6.

AC impedance spectra were also acquired from this cell. In this case, two semicircles could be recognized. As the high frequency contribution exhibited a resistance that was ~ 500 times lower than the second one, one can safely assign it to the LiI elements. The second semicircle, whose conductivity was equal to $\sim 6 \cdot 10^{-10}$ S/cm could be ascribed to the $Li_{14}Ln_5[Si_{11}N_{19}O_5]O_2F_2$ layer.

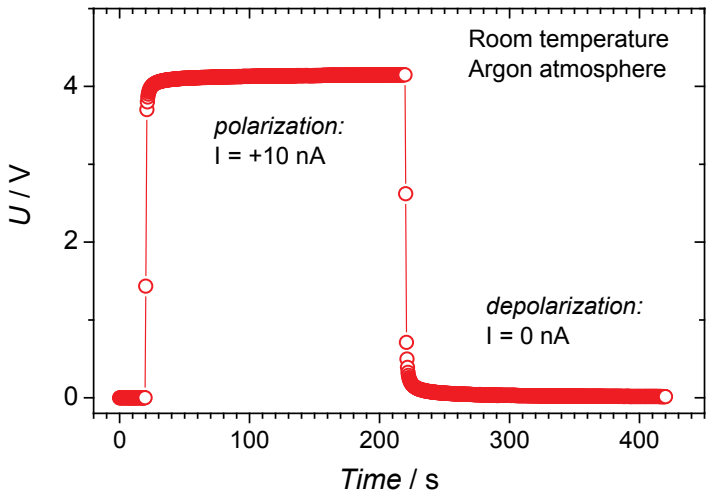

Figure 7. Time dependence of DC polarization and depolarization voltage for the LiAl / LiI / $Li_{14}Ln_5[Si_{11}N_{19}O_5]O_2F_2$ / LiI / LiAl cell.

Although such values of lithium ion conductivity are rather low compared with other solid-state electrolytes,[3] it is important to emphasize that the samples investigated here were simply cold pressed and not sintered. Therefore, one can expect the ionic conduction to improve upon the adjustment of the sintering conditions. More importantly, it is worth noting that the stoichiometry of $Li_{14}Ln_5[Si_{11}N_{19}O_5]O_2F_2$ has not been optimized yet as far as the ion transport properties are concerned. In the light of the unique structure of the phases considered here (the Li^+ sites create double strands along the crystallographic *b*-axis, cf. Figures 2 and 3), one can expect a significantly enhanced conductivity (within these strands) upon doping with aliovalent cations. In this context, it is important to recall that doping

$LiSi_2N_3$ with Ca^{2+} resulted in an ionic conductivity enhancement up to 4 orders of magnitude, while the activation energy decreased from 0.69 eV (undoped) down to 0.22 eV.[43]

In summary, the high chemical (resistivity against air, moisture, and acids) and thermal (up to 900 °C measured) stability – characteristic for most (oxo)nitridosilicates[12] - of $Li_{14}Ln_5[Si_{11}N_{19}O_5]O_2F_2$ with Ln = Ce, Nd combined with the lithium ion conductivity makes this material interesting for future research.

3.4.4 Conclusion

In this contribution, we presented the novel oxonitridosilicate $Li_{14}Nd_5[Si_{11}N_{19}O_5]O_2F_2$ and the isotypic Ce-containing phase. The compounds exhibit an unprecedented structure with a silicate substructure consisting of *dreier* and *sechser* rings of corner sharing tetraheda building layers. Structural analysis performed using the program TOPOS predicts lithium ion migration along the preferential crystallographic *b*-axis. Electrical conductivity measurements (DC as well as AC impedance spectroscopy) confirm the ionic character of the electrical transport (the ionic transference number is larger than 0.99 at 300 °C). The lithium ion conductivity is on the order of $5 \cdot 10^{-5}$ S/cm at 300 °C with an activation energy of 0.69 eV.

These results indicate that these undoped (oxo)nitridosilicates, a class of materials or which a plethora of different phases has already been structurally elucidated, represent a family of potential lithium ion conductors, whose defect chemistry needs however to be optimized (e.g., through aliovalent cations doping).

3.4.5 References

[1] J. F. M. Oudenhoven, L. Baggetto, P. H. L. Notten, *Adv. Energy Mater.* **2011**, *1*, 10-33.

[2] M. S. Whittingham, *Chem. Rev.* **2004**, *104*, 4271-4301.

[3] M. Park, X. Zhang, M. Chung, G. B. Less, A. M. Sastry, *J. Power Sources* **2010**, *195*, 7904-7929.

[4] M. Armand, J.-M. Tarascon, *Nature* **2008**, *451*, 652-657.

[5] N. Kamaya, K. Homma, Y. Yamakawa, M. Hirayama, R. Kanno, M. Yonemura, T. Kamiyama, Y. Kato, S. Hama, K. Kawamoto, A. Mtsui, *Nat. Mater.* **2011**, *10*, 682-686.

[6] C. Masquelier, *Nat. Mater.* **2011**, *10*, 649-650.

[7] A. D. Robertson, A. R. West, A. G. Ritchie, *Solid State Ionics* **1997**, *104*, 1-11.

[8] P. G. Bruce, A. R. West, *J. Solid State Chem.* **1982**, *44*, 354-365.

[9] M. Yashima, M. Itoh, Y. Inaguma, Y. Morii, *J. Am. Chem. Soc.* **2005**, *127*, 3491-3495.

[10] R. Kanno, T. Hata, Y. Kawamoto, M. Irie, *Solid State Ionics* **2000**, *130*, 97-104.

[11] Y. A. Du, N. A. W. Holzwarth, *Phys. Rev. B* **2010**, *81*, 184106/184101-184106/184115.

[12] M. Zeuner, S. Pagano, W. Schnick, *Angew. Chem.* **2011**, *123*, 7898-7920; *Angew. Chem. Int. Ed.* **2011**, *50*, 7754-7775.

[13] W. Schnick, *Angew. Chem.* **1993**, *105*, 846-858; *Angew. Chem., Int. Ed. Engl.* **1993**, *33*, 806-818.

[14] M. Orth, W. Schnick, *Z. Anorg. Allg. Chem.* **1999**, *625*, 1426-1428.

[15] J. Lang, J.-P. Charlot, *Rev. Chim. Miner.* **1970**, *7*, 121-131.

[16] S. Pagano, M. Zeuner, S. Hug, *Eur. J. Inorg. Chem.* **2009**, 1579-1584.

[17] H. Yamane, S. Kikkawa, M. Koizumi, *Solid State Ionics* **1987**, *25*, 183-191.

[18] R. Juza, H. H. Weber, E. Meyer-Simon, *Z. Anorg. Allg. Chem.* **1953**, *273*, 48-64.

[19] A. T. Dadd, P. Hubberstey, *J. Chem. Soc. Dalton Trans.* **1982**, 2175-2179.

[20] H. Hillebrecht, J. Cruda, L. Schröder, H. G. v. Schnering, *Z. Kristallogr. Suppl.* **1993**, *6*, 80.

[21] M. S. Bhamra, D. J. Fray, *J. Mater. Sci.* **1995**, *30*, 5381-5388.

[22] S. Pagano, S. Lupart, M. Zeuner, W. Schnick, *Angew. Chem.* **2009**, *121*, 6453-6456; *Angew. Chem., Int. Ed. Engl.* **2009**, *48*, 6335-6338.

[23] S. Pagano, S. Lupart, S. Schmiechen, W. Schnick, *Z. Anorg. Allg. Chem.* **2010**, *636*, 1907-1909.

[24] S. Lupart, S. Pagano, O. Oeckler, W. Schnick, *Eur. J. Inorg. Chem.* **2011**, 2118-2123.

[25] S. Lupart, M. Zeuner, S. Pagano, W. Schnick, *Eur. J. Inorg. Chem.* **2010**, 2636-2641.

[26] S. Lupart, W. Schnick, *Z. Anorg. Allg. Chem.* **2011**, *638*, 94-97.

[27] S. Lupart, D. Durach, W. Schnick, *Z. Anorg. Allg. Chem.* **2011**, *637*, 1841-1844.

[28] H. Lange, G. Wötting, G. Winter, *Angew. Chem.* **1991**, *103*, 1606-1625; *Angew. Chem., Int. Ed. Engl.* **1991**, *30*, 1579-1597.

[29] N. Hofman-Bang, *Acta Chem. Scand.* **1957**, *11*, 581-582.

[30] G. M. Sheldrick, *Acta Crystallogr. A* **2008**, *64*, 112-122.

[31] Further details of the crystal structure investigation can be obtained from the Fachinformations-Zentrum Karlsruhe, 76344 Eggenstein-Leopoldshafen, Germany (fax: (+49)7247-808-666; e-mail: crysdata@fiz-karlsruhe.de) on quoting the depository numbers CSD-424264 for Ln = Ce, and CSD-424265 for Ln = Nd, the names of the authors and citation of the publication.

[32] The terms *dreier* and *sechser* rings were coined by Liebau and are derived from the German words "drei" (three) and "sechs" (six); however, for example a *dreier* ring is not a three-membered ring, but a six-membered ring comprising *three* tetrahedra centers.

[33] R. D. Shannon, *Acta Crystallogr., Sect. A: Cryst. Found. Crystallogr.* **1976**, *32*, 751-767.

[34] W. Schnick, H. Huppertz, *Chem. Eur. J.* **1997**, *3*, 679-683.

[35] M. Woike, W. Jeitschko, *Inorg. Chem.* **1995**, *34*, 5105-5108.

[36] H. Huppertz, W. Schnick, *Angew. Chem.* **1997**, *109*, 2765-2767; *Angew. Chem., Int. Ed.* **1997**, *36*, 2651-2652.

[37] C. Schmolke, D. Bichler, D. Johrendt, W. Schnick, *Solid State Sci.* **2009**, *11*, 389-394.

[38] M. Zeuner, S. Pagano, S. Hug, P. Pust, S. Schmiechen, C. Scheu, W. Schnick, *Eur. J. Inorg. Chem.* **2010**, 4945-4951.

[39] V. A. Blatov, *Acta Crystallogr., Sect. A: Cryst. Found. Crystallogr.* **2000**, *56*, 178-188.

[40] V. A. Blatov, A. P. Shevchenko, V. N. Serezhkin, *J. Appl. Crystallogr.* **2000**, *32*, 377.

[41] V. A. Blatov, *IUCr Comp. Comm. Newsletter* **2006**, *7*, 4-38.

[42] N. A. Anurova, V. A. Blatov, G. D. Ilyushin, O. A. Blatova, A. K. Ivanov-Schitz, L. N. Dem'yanets, *Solid State Ionics* **2008**, *179*, 2248-2254.

[43] E. Narimatsu, Y. Yamamoto, T. Takeda, T. Nishimura, N. Hirosaki, *J. Mater. Res.* **2011**, *26*, 1133-1142.

3.5 $Li_{35}Ln_9[Si_{30}N_{59}]O_2F$ with Ln = Ce, Pr - Highly Condensed Nitridosilicates

published in Saskia Lupart, Dajana Durach, and Wolfgang Schnick

Z. Anorg. Allg. Chem. **2011**, *637* (12), 1841-1844
DOI: 10.1002/zaac.201100171
Copyright © 2011 WILEY-VCH Verlag GmbH & Co. KGaA, Weinheim
http://onlinelibrary.wiley.com/doi/10.1002/zaac.201100171/abstract

Abstract. The isotypic nitridosilicates $Li_{35}Ln_9Si_{30}N_{59}O_2F$ with *Ln* = Ce, Pr were synthesized by reaction of LnF_3 and LiN_3 with $Si(NH)_2$ in liquid lithium flux in weld shut tantalum ampoules. The crystal structures of the isotypic compounds have been solved and refined on the basis of single-crystal X-ray diffraction ($P\bar{3}c1$ (no. 165), Z = 2; $Li_{35}Ce_9Si_{30}N_{59}O_2F$:, a = 1479.9(2), c = 1538.3(3) pm, $R1$ = 0.0526, 1671 data, 175 parameters; $Li_{35}Pr_9Si_{30}N_{59}O_2F$: a = 1477.3(2), c = 1533.9(3) pm, $R1$ = 0.0441, 1331 data, 175 parameters). The silicate substructure represents a 3D network of all side corner sharing SiN_4-tetrahedra. At one discrete and not condensed mixed anion position an atomic ratio O : F = 2 : 1 is assumed in order to achieve charge neutrality. With an atomic ratio Si : N = 30 : 59, the degree of condensation of the silicate substructure is slightly above κ = ½. Accordingly, there are triply crosslinking $N^{[3]}$ atoms in the silicate substructure. The obtained structures prove that by employing the lithium flux technique not only nitridosilicates with a low degree of condensation can be obtained by using rather mild reaction conditions at low temperatures. Lattice energy calculations (MAPLE) and EDX measurements confirmed the electrostatic bonding interactions and the chemical composition.

3.5.1 Introduction

Recently, we reported about a new synthetical approach to quaternary nitridosilicates[1] employing liquid lithium as fluxing agent in weld shut tantalum ampoules. The advantage of this method stems from the ability of lithium to dissolve various metals as well as silicon and nitrogen. The use of lithium fluxes allows establishing lower reactions temperatures (about 900 °C) compared to the classical high-temperature approaches that have been utilized for the synthesis of nitridosilicates above 1500 °C.[2-4] Accordingly, less condensed nitridosilicates can be obtained, such as the isotyopic compounds $Li_4M_3Si_2N_6$ with M = Ca, Sr, which exhibit discrete bow-tie units of edge-sharing SiN_4-tetrahedra.[5] Furthermore, by changing of the reaction temperature and particularly the nitrogen pressure inside the ampoule by varying the content of LiN_3, we have synthesized new quaternary alkaline earth nitridosilicates with dimensionality of the silicate substructure varying from 0D to 3D.[1,6] This promising route can also be extended to rare earth elements, e. g. the isotypic compounds $Li_5Ln_5Si_4N_{12}$ with Ln = La, Ce were synthesized starting from the respective metal chlorides.[7] In this contribution, we report on synthesis and structural features of $Li_{35}Ln_9Si_{30}N_{59}O_2F$ with Ln = Ce, Pr which exhibit a 3D nitridosilicate network with exclusively corner sharing tetrahedra. Despite the moderate reaction temperature, the silicate substructure contains triply bridging nitrogen $N^{[3]}$ ions which proves that this synthetic route provides access to highly condensed nitridosilicates as well.[8]

3.5.2 Results and Discussion

3.5.2.1 Crystal structure description

Table 1. Crystallographic data of $Li_{35}Ln_9Si_{30}N_{59}O_2F$ with Ln = Ce, Pr.

Formula	$Li_{35}Ce_9Si_{30}N_{59}O_2F$	$Li_{35}Pr_9Si_{30}N_{59}O_2F$
Formula mass / g · mol^{-1}	3224.27	3231.38
Crystal system	trigonal	
Space group	$P\,\bar{3}c1$ (no. 165)	
Cell parameters / pm, °	a = 1479.9(2) c = 1538.3(3)	a = 1477.3(2) c = 1533.9(3)
Cell volume / 10^6 pm^3	V = 2917.8(8)	V = 2899.0(8)
Formula units / cell	2	
Crystal size / mm^3	0.03 x 0.04 x 0.05	0.02 x 0.03 x 0.02
$\rho_{calcd.}$ / g · cm^{-3}	3.670	3.702
μ / mm^{-1}	7.578	8.124
F(000)	2970	2988
Diffractometer	Stoe IPDS 1	
Temperature / K	293(2)	
Radiation, monochromator	Mo-K$_\alpha$, (λ = 71.073 pm), graphite	
Absorption correction	multi-scan[9]	
Min. /max. transmission	0.351; 0.444	0.588; 0.674
θ range / °	2.3 – 30.5	2.3 – 30.5
Measured reflections	25182	19697
Independent reflections	2460	1898
Observed reflections	1671	1331
Refined parameters	175	175
GoF	0.953	0.940
R indices ($F_o^2 \geq 2\sigma(F_o^2)$)	$R1$ = 0.0526 $wR2$ = 0.1300	$R1$ = 0.0441 $wR2$ = 0.0992
R indices (all data)	$R1$ = 0.0807 $wR2$ = 0.1406[a)]	$R1$ = 0.0722 $wR2$ = 0.1071[b)]
Max. / min. residual electron density/ eÅ^{-3}	3.40/ -3.75	2.57/ -2.55

a) $w = 1/[\sigma^2(F_o^2) + (0.0929\,P)^2]^{-1}$ where $P = (F_o^2 + 2\,F_c^2)/3$.
b) $w = 1/[\sigma^2(F_o^2) + (0.0646\,P)^2]^{-1}$ where $P = (F_o^2 + 2\,F_c^2)/3$.

The compounds $Li_{35}Ln_9Si_{30}N_{59}O_2F$ with Ln = Ce, Pr can be obtained as few single crystals by the reaction of LnF_3, $Si(NH)_2$ and an excess of LiN_3 in liquid lithium as flux in weld shut

tantalum ampoules at temperatures around 1200 °C. The oxygen content originates probably due to impurities of the rare earth fluorides employed or the tantalum ampoules. Both compounds are sensitive against air and moisture and were handled under inert gas atmosphere. The title compounds crystallize in the trigonal space group $P\,\bar{3}c1$ with two formula units per unit cell (for details see Table 1 and Appendix 6.4). All atoms except the lithium and the mixed occupied position were refined anisotropically. For crystal structure refinement, the atomic ratio O:F has been fixed at a value of 2:1 in order to provide charge neutrality. This O/F-content has been corroborated semiquantitatively by EDX measurements. However, fluorine is at the border of the detection limit and its signal is overlapping with one emission line of cerium. Fluorine can be detected in the EDX-measurements, however, cannot be fitted in the spectra.

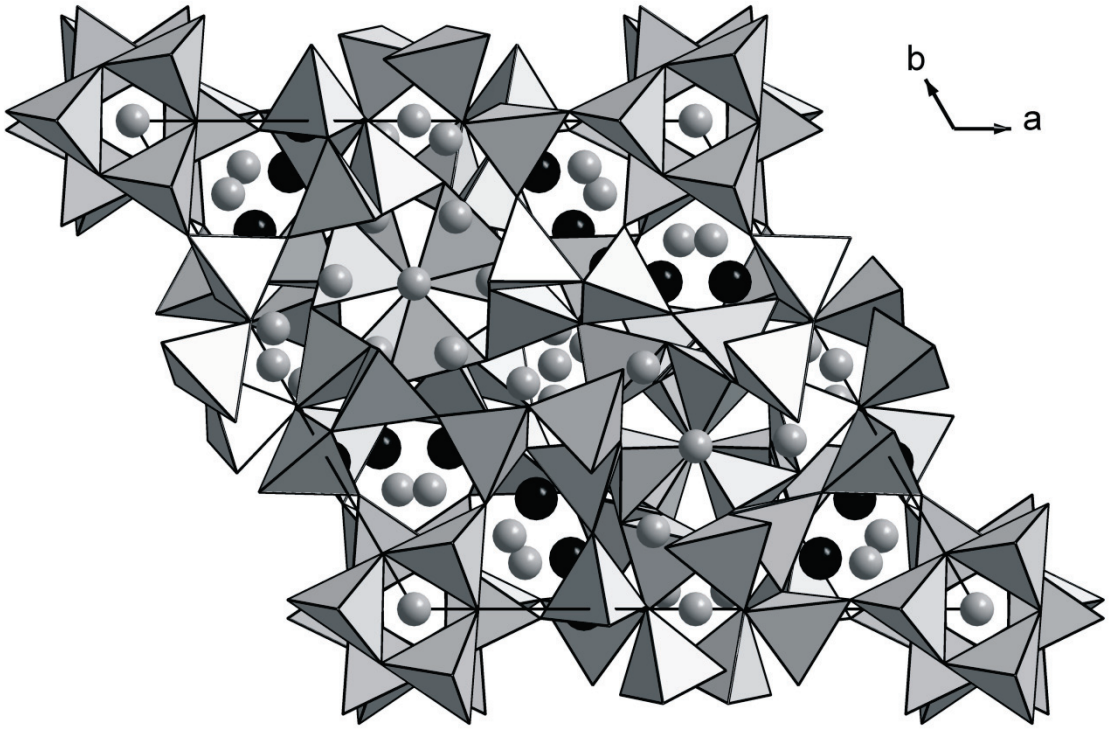

Figure 1. Unit cell of $Li_{35}Ln_9Si_{30}N_{59}O_2F$ with Ln = Ce, Pr, view along [001]. SiN_4-tetrahedra are depicted as closed gray polyhedra, Ln ions black and Li ions gray.

The unit cell of $Li_{35}Ln_9Si_{30}N_{59}O_2F$ with *Ln* = Ce, Pr is depicted in Figure 1. The nitridosilicate substructure consists of all corner sharing SiN_4-tetrahedra with a degree of condensation $\kappa = 30 : 59$, resulting in a 3D network including triply bridging $N^{[3]}$ (cf. Figure 2a). The

structural motif of triply bridging $N^{[3]}$ is typical for highly condensed nitridosilicates with $\kappa > ½$ and it has also been observed in $M_2Si_5N_8$ (M = Sr, Ba),[10] $Ln_3Si_6N_{11}$ (Ln = La, Ce, Pr, Nd, Sm)[11] and $Sr_{10}Sm_6Si_{30}Al_6O_7N_{54}$,[12] which were all synthesized at reaction temperatures ≥ 1500 °C. Another structural motif in the SiN_4 network of $Li_{35}Ln_9Si_{30}N_{59}O_2F$ with Ln = Ce, Pr are double *dreier* rings, which are stacked along [001] (black tetrahedra, Figure 2b). The residual tetrahedra (depicted in light gray in Figure 2c) complete an all-corner sharing nitridosilicate network. The distances Si-N range between 170.6(2) and 177.5(2) pm for Ln = Ce and 170.5(2) – 177.9(2) pm for Ln = Pr, respectively. These values are in good accordance with other nitridosilicates.[2,4,10,13]

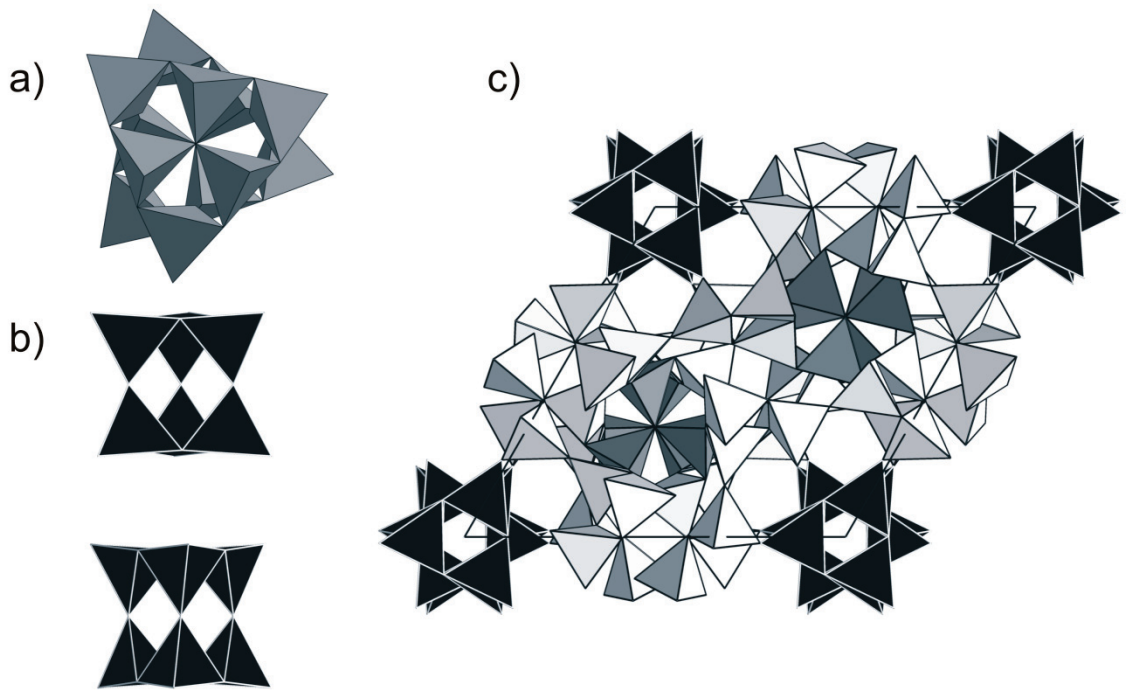

Figure 2. Nitridosilicate substructure: a) $[Si_6N_{11.5}]^{10-}$ units with triply bridging $N^{[3]}$ (dark grey tetrahedra); b) double *dreier* rings (black tetrahedra); c) unit cell.

There are two crystallographically independent Ln^{3+} positions (Ln = Ce, Pr) which occupy the Wyckoff positions 6*f* (Ln1) and 12*g* (Ln2). The Ln1 positions are surrounded by seven nitrogen atoms with distances Ln1-N ranging between 244.8(11) and 266.3(9) pm for Ln = Ce and 243.3(11) – 265.4(8) pm for Ln = Pr, respectively. These values correspond well with the

sum of the ionic radii according to *Shannon* (253 pm for *Ln* = Ce, 259 pm for *Ln* = Pr)[14] and literature data of other cerium or praseodymium containing nitridosilicates.[10,15,16] The positions *Ln*2 are coordinated by six nitrogen atoms and one site occupied by both O and F. The distances *Ln*2-N range between 247.4(8) and 284.7(8) pm for *Ln* = Ce and 246.1(8) – 284.5(8) pm for *Ln* = Pr, respectively, and are also in good accordance with the sum of the ionic radii. The distance *Ln*-O/F amounts to 219.4(2) pm for *Ln* = Ce and 218.37(9) pm for *Ln* = Pr and is slightly shorter than the sum of the ionic radii (Ce-O: 243 pm, Ce-F: 237 pm, Pr-O: 249 pm, Pr-F: 243 pm).[14] However, this distance is in good accordance with a number of fluorides and oxides of Ce and Pr, respectively, e.g. Ln_2O_3 (*Ln* = Ce, Pr),[17] CeF_4[18] or Cs_3PrF_6.[19]

At one discrete mixed anion position which does not belong to the silicate substructure an atomic ratio O : F = 2 : 1 was assumed in order to achieve charge neutrality. This site is surrounded by two Ln^{3+} ions and one Li^+ ion resulting in a T-shaped coordination sphere. Such a coordination sphere has not been reported for silicates as yet, however it seems not uncommon for other compound classes, e.g. in $Li[AuF_4]$ or $Pr_4(SeO_3)_2SeO_4F_6$.[20,21] In the second coordination sphere the O/F position is coordinated by two additional Li^+ ions.

There are nine crystallographically independent Li^+ sites. Three of the latter exhibit distorted tetrahedral coordination made up of nitrogen atoms. Another four Li^+ ions are coordinated by five atoms (nitrogen and O/F). The remaining Li^+ sites are surrounded by six nitrogen atoms forming distorted octahedra. The distances within these coordination spheres range from 199(2) to 273(2) pm for *Ln* = Ce and 195(2) – 273(2) pm for *Ln* = Pr, respectively. These distances are in accordance with the sum of the effective ionic radii (205 - 212 pm)[14,22,23] and with other previously reported lithium nitridosilicates.[1,7,24]

3.5.2.2 Lattice Energy Calculations According to the MAPLE Concept

Lattice energy calculations (MAPLE: Madelung part of lattice energy)[14,25,26] were performed to prove the electrostatic consistency of the crystal structure and especially to substantiate the mixed occupied O/F position. Within the MAPLE calculations, exclusively electrostatic interactions in an ionic crystal are considered, depending on the charge, distance and coordination spheres of the constituting atoms. The calculated partial MAPLE values of the crystallographically independent atoms are in agreement with typical ranges of partial

MAPLE values of comparable compounds in literature (cf. Table 2) Moreover, the total MAPLE sums correspond well with the sum of the total MAPLE values of the formally constituting compounds. A distribution of O^{2-} or F^- has no great influence on the MAPLE sum, partially occupation of nitrogen on the isolated position lead to poorer partial MAPLE values. Therefore, it is assumed, that O^{2-} as well as F^- are mainly located at the distinct O/F position and not distributed on the nitridosilicate network. MAPLE calculations support the fluorine content in the crystal structure, as well.

Table 2. Results of the MAPLE calculations [kJ/mol] for $Li_{35}Ln_9Si_{30}N_{59}O_2F$ (*Ln* = Ce, Pr); Δ = difference.[a]

	Ce	Pr
Ln^{3+}	3832; 3881	3915 – 4142
Si^{4+}	9533 – 10062	9467 – 10050
$N^{[2]\,3-}$	5294 – 5802	5373 - 5679
$N^{[3]\,3-}$	6086	6162
O/F	1433	1390
Li^+	569 - 791	505 - 743
Total MAPLE	681404	682338
Δ	0.05 %	0.37 %
Total MAPLE (10 Si_3N_4 + 2 Li_2O + LiF + 10 Li_3N + 9 *Ln*N)		
Ln = Ce: 681767 kJ/mol; *Ln* = Pr: 679783 kJ/mol		

[a] Typical partial MAPLE values [kJ/mol]: Ce^{3+}: 3800 - 4800; Pr^{3+}: 3800 – 4500; Si^{4+}: 9000 – 10200; $N^{[2]3-}$: 4600 – 6000; $N^{[3]3-}$:5200 – 6300; $O/F^{1.5-}$: 1225 – 1700; Li^+: 550 -860.

3.5.3 Conclusions

In this contribution, we report on two new isotypic nitridosilicates, namely $Li_{35}Ln_9Si_{30}N_{59}O_2F$ (*Ln* = Ce, Pr), which exhibit highly condensed SiN_4 frameworks including a triply bridging $N^{[3]}$ position. The compounds were synthesized by using lithium melts in tantalum ampoules at moderate temperatures. It has been demonstrated, that this synthetic approach cannot only lead to new less condensed nitridosilicates with interesting structural features but can also be applied to the synthesis of highly condensed structures. Therefore, the lithium flux method

seems to provide access to new structures, which can exhibit interesting structural as well as applicable characteristics.

3.5.4 Experimental Section

3.5.4.1 Syntheses

All manipulations were performed with rigorous exclusion of oxygen and moisture in flame-dried Schlenk-type glassware on a Schlenk line interfaced to a vacuum (10^{-3} mbar) line or in an argon-filled glove box (Unilab, MBraun, Garching, O_2 < 0.1 ppm, H_2O < 0.1 ppm). Li_3N was purchased from Alfa Aesar (99.4 %), Ca and Sr from Sigma-Aldrich (99.99 %) and $Si(NH)_2$ was synthesized according to the literature.[27]

For the reactions, tantalum crucibles (wall thickness 0.5 mm, internal diameter 10 mm, length 300 mm) were arc-welded under a pressure of 1 bar purified argon. The crucible holder was water cooled in order to avoid decomposition reactions during welding.

Single crystals of $Li_{35}Ce_9Si_{30}N_{59}O_2F$ were synthesized starting from 24.4 mg LiN_3 (0.50 mmol), 23.2 mg $Si(NH)_2$ (0.40 mmol), 98.6 mg CeF_3 (0.50 mmol, sigma aldrich, 99.99 %) and 20 mg Li (1.44 mmol) in closed tantalum ampoules. The ampoules were heated up in a radio-frequency furnace within 2 h at 1250 °C, kept at this temperature for 10 h and then cooled down at 700 °C in 30 h and finally quenched to room temperature by switching off the furnace.

Single crystals of $Li_{35}Pr_9Si_{30}N_{59}O_2F$ were synthesized from 24.5 mg LiN_3 (0.50 mmol), 23.2 mg $Si(NH)_2$ (0.40 mmol), 98.8 mg PrF_3 (0.50 mmol, sigma aldrich, 99.99 %) and 10 mg Li (1.44 mmol) as fluxing agent in closed tantalum crucibles. These were heated up with a radio-frequency furnace at 1200 °C within 2 h. The temperature was maintained for 9 h and then cooled down within 60 h at 600 °C. Afterwards the sample was quenched to room temperature by switching off the furnace.

3.5.4.2 X-ray Diffraction

By inspection under a microscope integrated in a glove box, single crystals of the title compounds were isolated and enclosed in glass capillaries. Single-crystal X-ray diffraction data were collected with a Stoe IPDS 1 ($Mo_{K\alpha}$ radiation). The program package SHELX97[28]

was used for structure solution and refinement. Further details of the crystal structure investigations can be obtained from the Fachinformationszentrum Karlsruhe, 76344 Eggenstein-Leopoldshafen, Germany (fax: (+49)7247-808-666; e-mail: crysdata@fiz-karlsruhe.de) on quoting the depository number CSD-422895 for *Ln* = Ce and CSD-422896 for *Ln* = Pr.

3.5.4.3 Microanalysis

EDX spectra of selected crystals were obtained using a JSM 6500F scanning electron microscope (JEOL) equipped with an EDX detector 7418 (Oxford Instruments). The approximate ratio Ce : Si was found to be 1 : 3.5 for $Li_{35}Ce_9Si_{30}N_{59}O_2F$ and Pr : Si was found to be 1 : 3.4 for $Li_{35}Pr_9Si_{30}N_{59}O_2F$. Fluorine could not be detected quantitatively, measured values varied in the range 0 – 3 atom%.

3.5.5 References

[1] S. Pagano, S. Lupart, M. Zeuner, W. Schnick, *Angew. Chem.* **2009**, *121*, 6453-6456; *Angew. Chem., Int. Ed. Engl.* **2009**, 6*448*, 6335-6338.

[2] M. Zeuner, S. Pagano, W. Schnick, *Angew. Chem.* **2011**, *123*, 7898-7920; *Angew. Chem. Int. Ed.* **2011**, *50* 7754-7775.

[3] W. Schnick, H. Huppertz, *Chem. Eur. J.* **1997**, *3*, 679-683.

[4] W. Schnick, *Angew. Chem.* **1993**, *105*, 846-858; *Angew. Chem., Int. Ed. Engl.* **1993**, *33*, 806-818.

[5] S. Pagano, S. Lupart, S. Schmiechen, W. Schnick, *Z. Anorg. Allg. Chem.* **2010**, *636*, 1907-1909.

[6] M. Zeuner, S. Pagano, S. Hug, P. Pust, S. Schmiechen, C. Scheu, W. Schnick, *Eur. J. Inorg. Chem.* **2010**, 4945-4951.

[7] S. Lupart, M. Zeuner, S. Pagano, W. Schnick, *Eur. J. Inorg. Chem.* **2010**, 2636-2641.

[8] Superscripted numbers specify connectedness: number of directly connected silicon atoms.

[9] *X.PREP*, Bruker-AXS, Madison, Wisconsin, USA, **1996**.

[10] T. Schlieper, W. Milius, W. Schnick, *Z. Anorg. Allg. Chem.* **1995**, *621*, 1380-1384.

[11] M. Woike, W. Jeitschko, *Inorg. Chem.* **1995**, *34*, 5105-5108.

[12] R. Lauterbach, W. Schnick, *Solid State Sci.* **2000**, *2*, 463-472.

[13] H. Huppertz, W. Schnick, *Z. Anorg. Allg. Chem.* **1997**, *623*, 212-217.

[14] R. D. Shannon, *Acta Crystallogr., Sect. A: Cryst. Found. Crystallogr.* **1976**, *32*, 751-767.

[15] C. Schmolke, D. Bichler, D. Johrendt, W. Schnick, *Solid State Sci.* **2009**, *11*, 389-394.

[16] S. Lupart, W. Schnick, *Acta Crystallogr., Sect. E* **2009**, *65*, i43.

[17] W. H. Zachariasen, *Z. Phys. Chem.* **1926**, *123*, 134-150.

[18] W. H. Zachariasen, *Acta Crystallogr.* **1949**, *2*, 388-390.

[19] G. A. Bukhalova, N. A. Litovskaya, V. A. Lyutsedarskii, *Neorg. Mater.* **1969**, *5*, 510 - 514.

[20] U. Engelmann, B. G. Müller, *Z. Anorg. Allg. Chem.* **1991**, *598/599*, 103-110.

[21] I. Krügermann, M. S. Wickleder, *Z. Anorg. Allg. Chem.* **2002**, *628*, 147-151.

[22] J. C. Slater, *J. Chem. Phys.* **1964**, *41*, 3199-3204.

[23] W. H. Baur, *Crystallogr. Rev.* **1987**, *1*, 59-83.

[24] S. Pagano, M. Zeuner, S. Hug, *Eur. J. Inorg. Chem.* **2009**, 1579-1584.

[25] R. Hoppe, *Angew. Chem.* **1966**, *78*, 52-63; *Angew. Chem. Int. Ed.* **1966**, *5*, 95-106.

[26] R. Hübenthal, Vers. 4 ed., Universität Gießen, **1993**.

[27] H. Lange, G. Wötting, G. Winter, *Angew. Chem*. **1991**, *103*, 1606-1625; *Angew. Chem. Int. Ed. Engl*. **1991**, *30*, 1579-1597.

[28] G. M. Sheldrick, *Acta Crystallogr, Sect.. A* **2008**, *64*, 112-122.

4 Outlook

Lithium (oxo)nitridosilicates of variable dimensionality are interesting compounds not only from a structural point of view but also as they might be an intriguing alternative to known Li^+ ion conductors. In the course of this work various synthetic approaches were successfully used to obtain new members of this class of materials.

A prominent role in the search for novel alkaline earth lithium nitridosilicates can be attributed to a synthetic approach utilizing liquid lithium as fluxing agent in closed tantalum or niobium ampoules (Chapter 2). Not only did this preparative technique yield the band-type nitridosilicate $LiCa_3Si_2N_5$,[1] but also the nitridosilicate nitride $Li_2Sr_4[Si_2N_5]N$ that exhibits the remarkable structural feature of isolated nitride ions.[2] Furthermore, this synthetic route could also be extended to rare-earth elements (Chapter 3), whereupon the first representatives of lanthanide (La-Nd) containing lithium (oxo)nitridosilicates, i.e. $Li_5Ln_5Si_4N_{12}$ (Ln = La, Ce)[3] and $LiLn_5Si_4N_{10}O$ (Ln = La, Pr)[4] were found and structurally elucidated. In contrast to the alkaline-earth lithium nitridosilicates, for lanthanide lithium nitridosilicates the respective halogenides have been used as starting materials as from the elemental metals no crystalline phases were obtained. These examples further corroborate that the possibilities of this synthetic route are enormous. It surely would be interesting to further extent this preparative approach for example by alteration of the starting materials or by adding additional components which might be incorporated into new compounds or act as catalyst for the formation of novel phases.

Although the use of closed tantalum or niobium ampoules has manifold advantages, it also features several intrinsic disadvantages. The procedure of arc welding which has been used to close the ampoules, can lead to rather high uncontrollable temperatures inside even if the sample holder is cooled. This fact is underlined by the formation of silicide nitride $(Ce_{0.5}Si)(Ce_{1.5}TaN_3)$ (*Cmcm*; $a = 4.1073(8)$, $b = 27.069(6)$, $c = 4.0050(8)$ Å; $R1 = 0.0248$; $wR2 = 0.0534$), which has been obtained by arc welding a tantalum ampoule starting from silicon diimide, $CeCl_3$ and LiN_3 (Figure 4.2a). The formation of this compound shows that the temperatures of the ampoule and in the reaction mixture can at least locally be extreme, and even silicon might be reduced to form a silicide. In addition, the volume of samples which can be obtained in closed ampoules is restricted by the size of the latter. Especially, if the properties of new compounds need to be measured, the small amount of material accessible is

a serious problem for many characterization techniques. In such cases, larger, however, inert reaction vessels are desirable. First experiments performed in the course of this work did show that for example Li_2SiN_2 can also be synthesized in graphitized silica glass ampoules which might provide an alternative to metallic ampoules with respect to the preparation of novel lithium nitridosilicates. Larger reaction volumes are accessible which simultaneously allows one to obtain larger sample amounts and also opens new possibilities to adjust the reaction conditions: different pressure conditions can be realized and temperatures remain controllable during the complete preparation as the silica glass ampoules can be conveniently closed without arc welding.

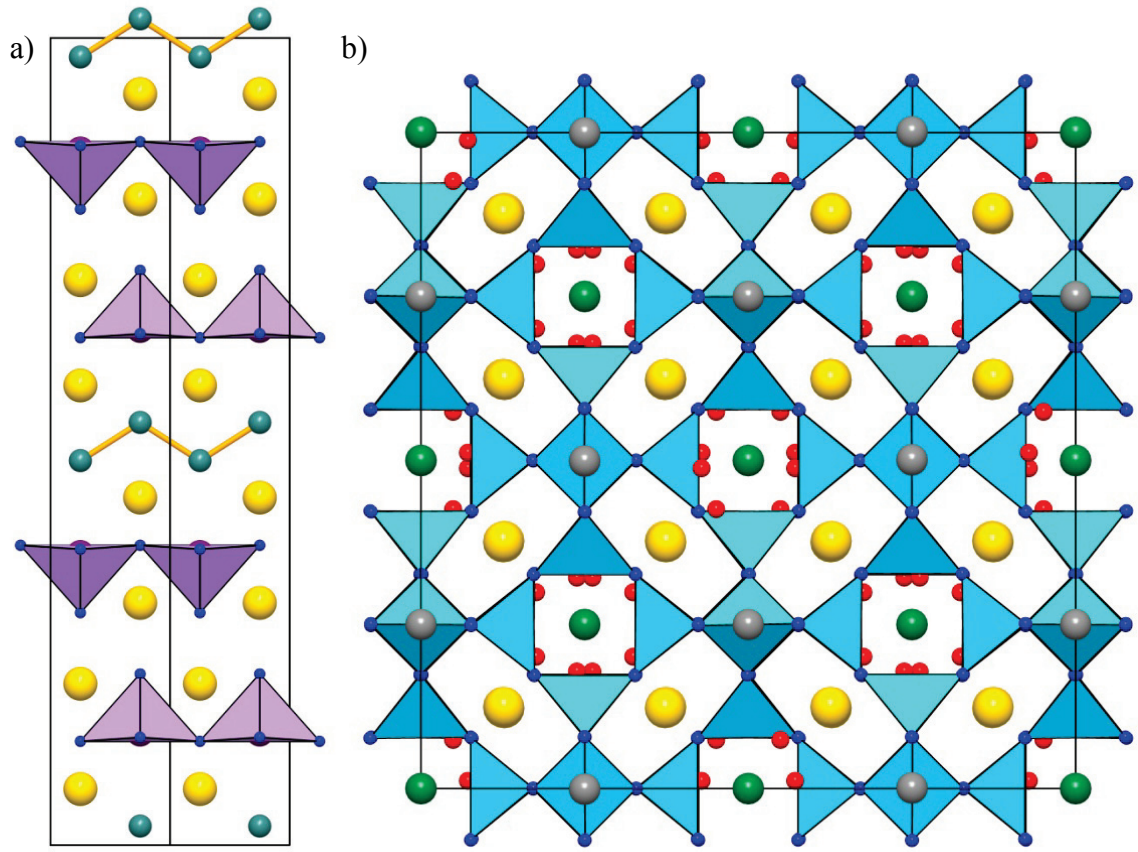

Figure 4.1 a) Crystal structure of $(Ce_{0.5}Si)(Ce_{1.5}TaN_3)$, b) Crystal structure of the sodalite-like "$Li_xW_yCe_{10-y}Si_{12}N_{24}O_8$" (Ce: yellow, Ta: lilac; Si: dark green, W: light green, N: blue, O: red, Li: gray and SiN_4 tetrahedra light blue).

A further way to avoid the disadvantages of tantalum ampoules is the transfer of lithium flux techniques to open systems. However, it was not possible in earlier works to synthesize single crystals of multinary lithium nitridosilicates in a tungsten crucible with or without lithium

flux. Although, *Zeuner* was able to synthesize $Li_2SrSi_2N_4$ in a tungsten crucible heated by a radio-frequency furnace, neither single crystals were obtained, nor was it possible to substitute Sr by Ca to obtain higher amounts of the corresponding Ca-phase.[5]

In contrast, in this work, single crystals of multinary lithium rare-earth (oxo)nitridosilicates were obtained in a radio-frequency furnace in open systems. Remarkably for these syntheses in the open tungsten crucible is that only about 25 % of lithium flux is necessary compared to the syntheses of the same compounds in tantalum ampoules. With higher amounts of lithium flux almost no crystalline products could be observed. This indicates that the tungsten crucible itself might be acting as a catalyst for the activation of lithium. This assumption is corroborated by the several W-containing side-phases, which often occur and the formation of a novel (oxo)nitridosilicate crystallizing in the sodalite structure-type with 5-8 atom% tungsten according to EDX measurements. The crystal structure of this compound is not unequivocally solved, as it shows superstructure reflections resulting in a pseudo-cubic cell with a = 18.55 Å (compared to $a \approx 9$ Å for the typical sodalite structure-type) and twinning.[6] However, as the metric is pseudo-cubic the correct twinning law is not easily found. The best structure solution is in space group $I4_1/acd$ with a twinning law 010 001 100 taken three twin domains into account. In Figure 4.2b the preliminary crystal structure is shown solved by a combination of single-crystal structure solution and Rietveld refinement leading to a tentative sum formula of "$Li_xW_yCe_{10-y}Si_{12}N_{24}O_8$" with $y < 4$, which is in accordance with EDX measurements with respect to the heavy elements. Recently, it was also possible to synthesize the isotypic lanthanum containing phase, which exhibits however, the same twinning problems and a similar superstructure.

Synthesis in open systems is not only an interesting possibility to find novel compounds but also gives the opportunity to obtain larger amounts of oxonitridosilicates, which is often necessary to measure their materials properties. For example, the lithium ion conductor $Li_{14}Nd_5[Si_{11}N_{19}O_5]O_2F_2$ could be synthesized in both tantalum and tungsten crucibles, respectively. The latter approach did allow to obtain samples suitable to determine the Li^+ ion conductivity of this phase, which amounts to 5 10^{-5} S/cm at 300 °C, a promising value for a not-optimized Li^+ ion conductor. In future experiments, it may be interesting to sinter the material to reduce the influence of the grain boundaries on the conductivity. Moreover, doping of $Li_{14}Nd_5[Si_{11}N_{19}O_5]O_2F_2$ should allow to introduce additional defects which may increase the conductivity significantly, as has already been shown for various Li^+ ion conductors.[7,8]

In this work it could be demonstrated that (oxo)nitridosilicates are indeed a compound class with potential for Li^+ ion conduction. Therefore, future research should focus on the investigation of novel lithium (oxo)nitridosilicates as possible Li^+ ion conductors and doping of known nitridic Li^+ ion conductors, e.g. Li_2SiN_2 which already exhibits a lithium conductivity of 1 10^{-5} S/cm at 400 K without doping.[9]

[1] S. Pagano, S. Lupart, M. Zeuner, W. Schnick, *Angew. Chem.* **2009**, *121*, 6453-6456; *Angew. Chem., Int. Ed. Engl.* **2009**, *48*, 6335-6338.

[2] S. Lupart, S. Pagano, O. Oeckler, W. Schnick, *Eur. J. Inorg. Chem.* **2011**, 2118-2123.

[3] S. Lupart, M. Zeuner, S. Pagano, W. Schnick, *Eur. J. Inorg. Chem.* **2010**, 2636-2641.

[4] S. Lupart, W. Schnick, *Z. Anorg. Allg. Chem.* **2011**, (in press).

[5] M. Zeuner, *Dissertation*, **2009**, LMU München.

[6] P. Villars, K. Cenzual, *Pearson's Crystal Data – Crystal Structure Database for Inorganic Compounds*, Release **2009/10**, ASM International, Materials Park, Ohio, USA.

[7] M. Park, X. Zhang, M. Chung, G. B. Less, A. M. Sastry, *J. Power Sources* **2010**, *195*, 7904-7929,.

[8] E. Narimatsu, Y. Yamamoto, T. Takeda, T. Nishimura, N. Hirosaki, *J. Mater. Res.* **2011**, *26*, 1133-1142.

[9] M. S. Bhamra, D. J. Fray, *J. Mater. Sci.* **1995**, *30*, 5381-5388.

5 Summary

5.1 Tuning the Dimensionality in Lithium Melts: The ability of lithium to dissolve various metals, e.g. Ca and Sr, and especially silicon and nitrogen at low temperatures, gives access to a novel synthetic approach for the syntheses of lithium nitridosilicates. As the reaction temperature can be lowered to about 900 °C, this allows to obtain also low condensed silicate substructures. The dimensionality can be tuned by the amount of Li : Li_3N : LiN_3. In this course several lithium nitridosilicates could be structurally elucidated: 0D group-like silicate $Li_4Ca_3Si_2N_6$ (0D), chain-type $LiCa_3Si_2N_5$ (1D) and up to zeolite-like structures as observed in $Li_2Sr_4Si_4N_8O$ (3D).

5.2 $Li_4Ca_3Si_2N_6$ and $Li_4Sr_3Si_2N_6$ – Quaternary Lithium Nitridosilicates with Isolated $[Si_2N_6]^{10-}$ Ions: The compound $Li_4Ca_3Si_2N_6$ ($C2/m$, Z = 2, a = 5.7873(12), b = 9.7045(19), c = 5.9771(12), β = 90.45(3), $R1$ = 0.0219, $wR2$ = 0.0566) is isotypic to the nitridogermanate $Li_4Sr_3Ge_2N_6$. The structure consists of bow-tie $[Si_2N_6]^{10-}$ units. The angles and distances significantly deviate from the ideal tetrahedral angles and the "normal" distances Si-N. The deviations of the interatomic distances and angles in the vertex-sharing $[SiN_4]$ tetrahedral are strongly correlated to the size of the counter-ions and the Lewis acidity thereof, as a higher acidity of the counterions leads to a displacement of the nitrogen atoms towards them. This seems not surprising, as solid-state structures are always three-dimensional and only the isolated silicate substructure can formally be described as zero-dimensional and therefore, all interactions have to be taken into account.

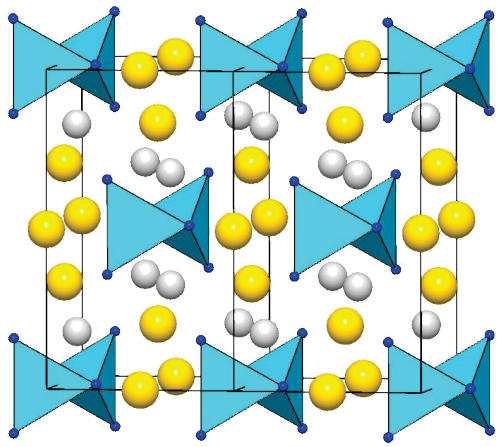

5.3 $LiCa_3Si_2N_5$ – A Lithium Nitridosilicates with $[Si_2N_5]^{7-}$ Double-Chains: The lithium nitridosilicate $LiCa_3Si_2N_5$ was synthesized starting from calcium, silicon diimide and Li_3N in weld shut tantalum ampoules at 900 °C. Single crystals of $LiCa_3Si_2N_5$ were obtained by adding lithium as fluxing agent to the reaction mixture. $LiCa_3Si_2N_5$ crystallizes in the monoclinic space group $C2/c$ (Z = 8, a = 5.145(2), b = 20.380(4), c = 10.357(2) Å, β = 91.24(3), $R1$ = 0.0443, $wR2$ = 0.1120) with an unprecedented silicate substructure of double-chains of edge-sharing $[SiN_4]$ tetrahedra. The Li^+ ions in the structure are situated as

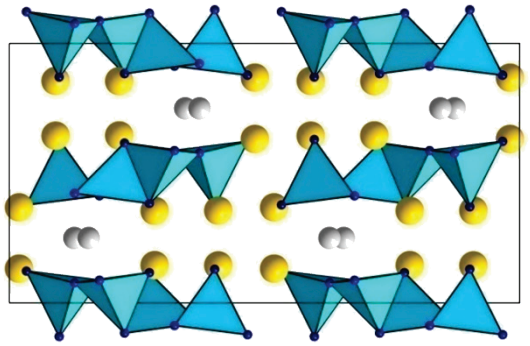

strands along the crystallographic *a*-axis. Therefore, this compound might be interesting for Li^+ ion conductivity measurements. However, as the compound is not only air and moisture sensitive but also metastable, phase pure samples have not been obtained, yet.

5.3 $Li_2Sr_4[Si_2N_5]N$ – A Layered Lithium Nitridosilicate Nitride: By adding CsI to the reaction of Sr, silicon diimide and LiN_3 in lithium flux in closed ampoules the compound $Li_2Sr_4[Si_2N_5]N$ was obtained as single crystals. The layered lithium nitridosilicate nitride can be derived from the apophyllite structure type and crystallizes in the tetragonal space group, $I\bar{4}m2$ (Z = 4, a = 7.5146(11), c = 15.089(3) Å, $R1$ = 0.0499, $wR2$ = 0.1364). Nitridosilicate nitrides have not been observed, yet, but isolated N^{3-} positions are not uncommon, as they occur e.g. in nitridogermanates and nitridogallates. For a further corroboration of the existence of discrete N^{3-} positions MAPLE (Madelung part of lattice energy) and density functional calculations have been performed. As the isolated N^{3-} position (Wyckoff site 8*i*) is only half occupied, several subgroups with only full occupied positions had to be taken into account for MAPLE and DFT calculations. Thereby the model (*Imm*2, (**a**, 3**b**, **c**)) with the highest dispersion between the defect sites is energetically favored.

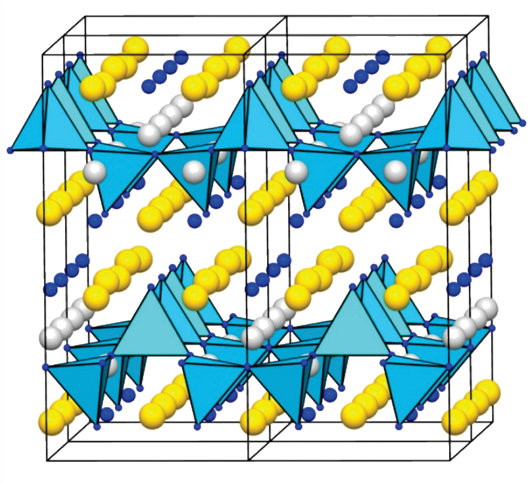

5.4 Chain-Type Lithium Rare-Earth Nitridosilicates – $Li_5Ln_5Si_4N_{12}$ with Ln = La, Ce: With the formation of the isotypic nitridosilicates $Li_5Ln_5Si_4N_{12}$ (Ln = La, Ce) synthesized starting from the according chlorides in lithium melts, it could be shown, that the synthetic route using liquid lithium could be extended to rare-earth elements. The compounds $Li_5Ln_5Si_4N_{12}$ with Ln = La, Ce ($Li_5Ce_5Si_4N_{12}$: $P\bar{4}b2$, Z = 2, a = 10.9778(16), c = 5.5143(11), $R1$ = 0.0294, $wR2$ = 0.0749; $Li_5La_5Si_4N_{12}$ (has been investigated together with *Zeuner*): $Li_5La_5Si_4N_{12}$: $P\bar{4}b2$, Z = 2, a = 11.428(16), c = 5.5730(11), $R1$ = 0.0482, $wR2$ = 0.1278) comprise *zweier* single chains of vertex-sharing $[SiN_4]$ tetrahedra, which is in agreement with the condensation degree κ = 1 : 3. Single *zweier* chains, which are not branched, are seldom for nitridosilicates and only occur in the recently described Eu_2SiN_3, which comprises

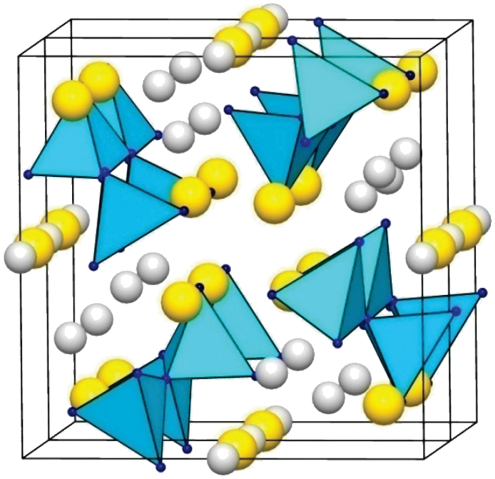

europium in the oxidation states +II and +III. The Li^+ ions in $Li_5Ln_5Si_4N_{12}$ (Ln = La, Ce) build $[Li_5N_{10}]^{25-}$ units, which are not connected with each other. The ^7Li solid-state MAS-NMR of $Li_5La_5Si_4N_{12}$ has also been investigated in this work. Although there are two crystallographic independent Li^+ sites in the crystal structure, in the NMR only one signal can be detected. This is due to the bad resolution of ^7Li-NMR, which could also be observed for the lithium alkaline-earth nitridosilicates.

5.5 $LiLa_5Si_4N_{10}O$ and $LiPr_5Si_4N_{10}O$ – Chain Type Oxonitridosilicates: Loop branched *dreier* single chains could be observed in the isotypic compounds $LiLn_5Si_4N_{10}O$ with Ln = La, Pr (Chapter 3.4) ($LiLa_5Si_4N_{10}O$: $P\bar{1}$, Z = 1, a = 5.7462(11), b = 6.5620(13), c = 8.3732(17), α = 103.54(3); β = 107.77(3), γ = 94.30(3), $R1$ = 0.0165, $wR2$ = 0.0402; $LiPr_5Si_4N_{10}O$: $P\bar{1}$, Z = 1, a = 5.6561(11), b = 6.4870(13), c = 8.2567(17), α = 103.13(3); β = 107.68(3), γ = 94.42(3), $R1$ = 0.0270, $wR2$ = 0.0466). The ^7Li solid-state MAS NMR of the La-containing compound exhibits one peak at 0.3 ppm, which confirms the single Li^+ position with octahedral coordination. For both compounds MAPLE calculations have been performed which corroborate the crystal structure. The existence of these two oxonitridosilicates proves that also oxonitridosilicates can be synthesized in liquid lithium. Compared to the zeolite-like $Li_2Sr_4Si_4N_8O$, where oxygen is only incorporated as Li_2O in channels along [001] and is not part in the silicon network, this is no matter of course.

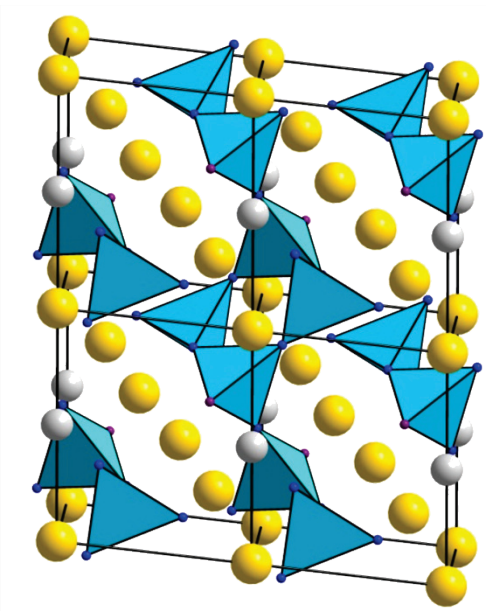

5.6 $Li_{14}Ln_5[Si_{11}N_{19}O_5]O_2F_2$ with Ln = Ce, Nd – Representatives of a Novel Family of Lithium Ion Conductors: The isotypic oxonitridosilicates $Li_{14}Ln_5[Si_{11}N_{19}O_5]O_2F_2$ with Ln = Ce, Nd [$Li_{14}Ce_5[Si_{11}N_{19}O_5]O_2F_2$: *Pmmn*, Z = 2, *a* = 17.178(3), *b* = 7.6500(15), *c* = 10.116(2), *R*1 = 0.0409, *wR*2 = 0.0896; $Li_{14}Nd_5[Si_{11}N_{19}O_5]O_2F_2$: *Pmmn*, Z = 2, *a* = 17.126(2), *b* = 7.6155(15), *c* = 10.123(2), *R*1 = 0.0419, *wR*2 = 0.0929] are layer silicates with a novel topology. The Li^+ sites are mainly situated in strands along [010] with short Li-Li distances. An analysis of possible ion pathways with TOPOS revealed channels in the direction of the crystallographic *b*-axis, as well. The compounds show a high thermal (at least up to 900 °C) and chemical resistivity (resistance against air, water and acids). The specific lithium ion conductivity of $Li_{14}Nd_5[Si_{11}N_{19}O_5]O_2F_2$ and its temperature dependence were determined by impedance spectroscopy. Measurements with a LiAl/ LiI/ $Li_{14}Nd_5[Si_{11}N_{19}O_5]O_2F_2$/ LiI/ LiAl cell were performed, to prove that Li^+ is the conducting species. The conductivity at 300 °C is 5 10^{-5} S/cm with an activation energy of 0.69 eV.

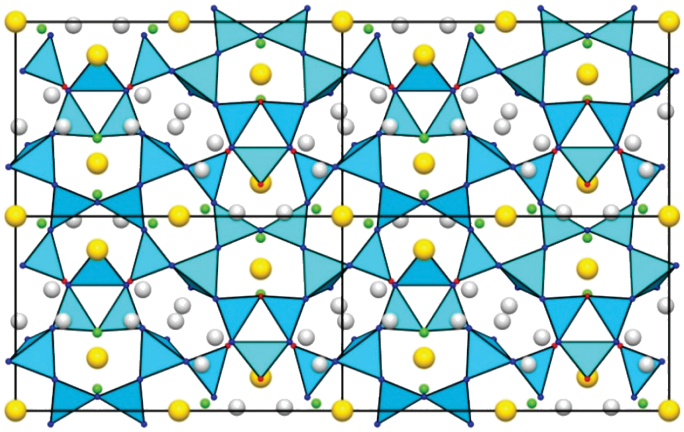

5.7 $Li_{35}Ln_9Si_{30}N_{59}O_2F$ with Ln = Ce, Pr - Highly Condensed Nitridosilicates: The three dimensional nitridosilicates $Li_{35}Ln_9Si_{30}N_{59}O_2F$ with Ln = Ce, Pr ($Li_{35}Ce_9Si_{30}N_{59}O_2F$: $P\bar{3}c1$, Z = 2, *a* = 14.799(2), *c* = 15.383(3), *R*1 = 0.0526, *wR*2 = 0.1300; $Li_{35}Pr_9Si_{30}N_{59}O_2F$: $P\bar{3}c1$, Z = 2, *a* = 14.773(2), *c* = 15.339(3), *R*1 = 0.0441, *wR*2 = 0.0992) exhibit an all corner sharing [SiN_4] network including triply bridging nitrogen positions ($N^{[3]}$). Whereas, other (oxo)nitridosilicates with triply bridging nitrogen atoms were all synthesized at high temperatures (≥ 1500 °C), the compounds $Li_{35}Ln_9Si_{30}N_{59}O_2F$ (Ln = Ce, Pr) were synthesized at about 1200 °C. Therefore, also with low

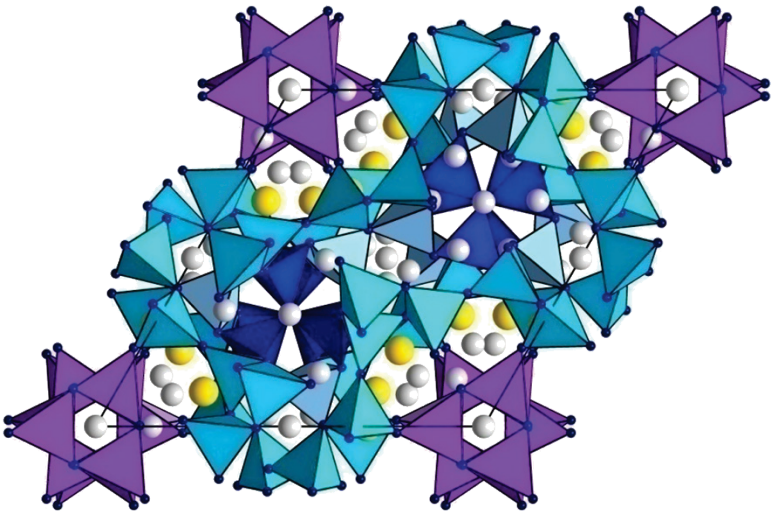

reaction temperatures also highly condensed silicate substructures can be achieved. The oxygen and fluorine in the crystal structure are not connected to the $[SiN_4]$ network but build isolated mixed occupied sites with a T-shaped coordination built up from Li and Ln (Ln = Ce, Pr). Lattice energy calculations (MAPLE) and EDX measurements confirmed the electrostatic bonding interactions and the chemical composition.

6 Appendix

6.1 Supporting Information for Chapter 2.2

Sandro Pagano, Saskia Lupart, Martin Zeuner, and Wolfgang Schnick *Angew. Chem.* **2009**, *121*, 6453-6456; *Angew. Chem. Int. Ed.* **2009**, *48*, 6335-6338.

Table S1: Information about the data collection and selected crystallographical details on the single-crystal investigations and Rietveld refinement of $Li_4Ca_3Si_2N_5$.

Diffractometer	IPDS1, Stoe & Cie	STADI P, Stoe & Cie
Radiation, wavelength [Å]	λ = 0.71073 Mo-$K_{\alpha 1}$	λ = 1.540596 Cu-$K_{\alpha 1}$
Monochromator	Graphite	Curved Ge single crystal
Temperature [K]	T = 294(2)	T = 294(2)
Measuring mode	φ-scans 0° ≤ φ ≤ 180°, Δφ = 1.8	Debye-Scherrer geom., capillary (0.2mm)
Data Range	2.3° ≤ υ ≤ 30.5°	10.0° ≤υ ≤ 70°
Corrections	multi-scan	
Software	SHELXS-97, SHELXL-97	TOPAS
Crystal shape	block	
Crystal dimensions [mm^3]	0.02 x 0.05 x 0.08	
Crystal color	colorless	
Formula per unit cell	Z = 2	
Space group	$C2/m$	
Lattice constants [Å]	a = 5.7873(12) b = 9.7045(19) c = 5.9771(12) β = 90.45(3)	a = 5.7983(5) b = 9.7222(7) c = 5.9885(5) β = 90.383(5)
Volume [Å^3]	V = 335.68(12)	337.79(6)
Crystallograph. Density [g/cm^3]	ρ = 2.852	
Absorption coefficient [mm^{-1}]	μ = 2.751	
Min. / max. transmission	0.73 / 0.95	
R values	R_{int}, $R(\sigma)$ = 0.0398, 0.0281 $R1$ ($F_o^2 \geq 2\sigma$ (F_o^2)) = 0.0219 $R1$ (all data) = 0.0252 $wR2$ ($F_o^2 \geq 2\sigma$ (F_o^2)) = 0.0566 $wR2$ (all data) = 0.0572	R_p = 0.0908 R_p (background) = 0.3860 wR_p = 0.1178 wR_p (background) = 0.3399 R_F^2 = 0.0248
GoF	1.117	1.015
Resid. electron density [e/Å^3]	-0.457, 0.512	
Parameters	40	
Nr. of data (obs. / unique)	1787/505	85

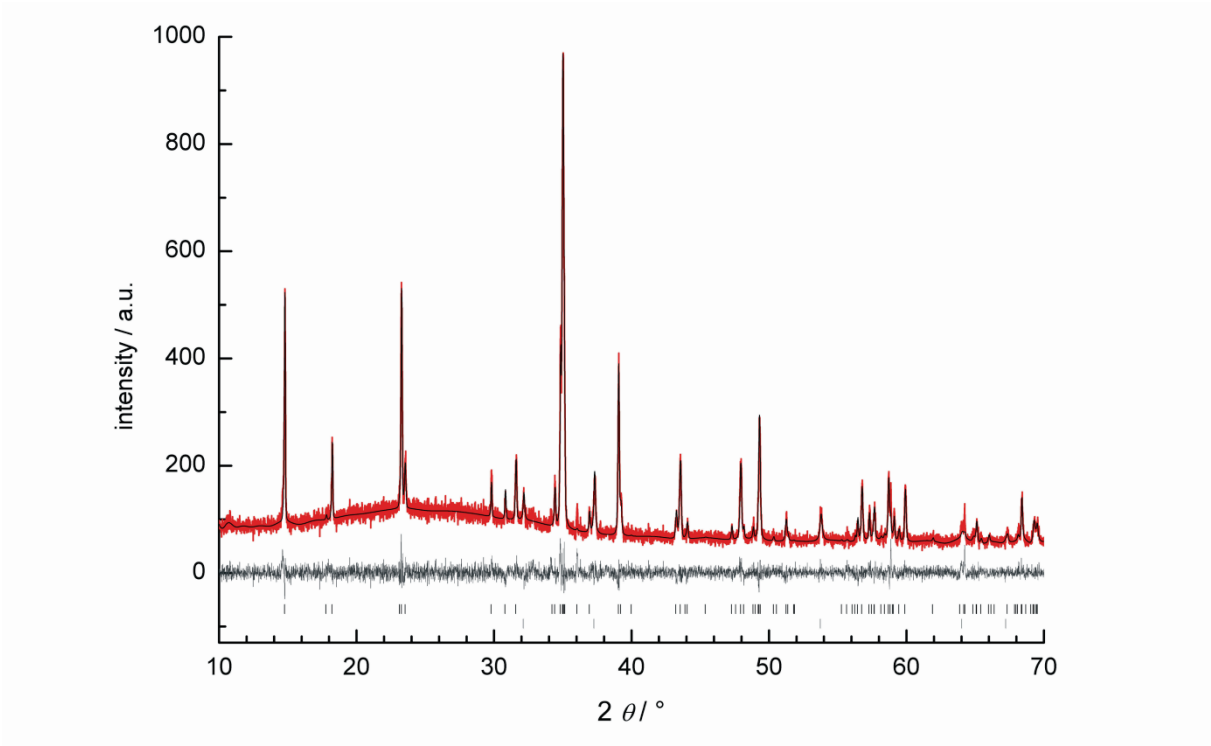

Figure S1. Final Rietveld refinement plot for $Li_4Ca_3Si_2N_6$ (**I**). Observed (red line), calculated (black line) and difference profile of the X-ray powder diffraction are plotted on the same scale. Bragg peaks are indicated by vertical lines for I (above) and CaO (below). The molar ratio of **I** to CaO was determined to be 5.5 % CaO and 94.5 % **I**.

Table S2: Information about the data collection and selected crystallographical details on the single-crystal investigations and Rietveld refinement of $LiCa_3Si_2N_5$.

Diffractometer	IPDS1, Stoe & Cie	STADI P, Stoe & Cie
Radiation, wavelength [Å]	λ = 0.71073 Mo-$K_{\alpha 1}$	λ = 0.71073 Mo-$K_{\alpha 1}$
Monochromator	Graphite	Curved Ge single crystal
Temperature [K]	T = 140(2)	T = 294(2)
Measuring mode	φ-scans $0° \leq \varphi \leq 180°$ $\Delta\varphi = 1.8$	
Data Range	$3.9° \leq \upsilon \leq 27.5°$	$5° \leq \upsilon \leq 50°$
Corrections	Lorentz, polarisation, absorption (numerical)	
Software	SHELXS-97, SHELXL-97	TOPAS
Crystal shape	block	
Crystal dimensions [mm^3]	0.04 x 0.06 x 0.09	
Crystal color	colorless	
Formula per unit cell	Z = 8	
Space group	$C2/c$	
Lattice constants [Å]	a = 5.1454(10) b = 20.380(4) c = 10.357(2) β = 91.24(3)	a = 5.1531(4) b = 20.412(2) c = 10.400(8) β = 91.02(6)
Volume [$Å^3$]	V = 1085.8(4)	V = 1093.7(2)
Crystallograph. Density [g/cm^3]	ρ = 3.100	
Absorption coefficient [mm^{-1}]	μ = 3.382	
Min. / max. transmission	0.64 / 0.75	
Twinlaw	100 0-10 00-1	
BASF	0.0414	
R values	R_{int}, $R(\sigma)$ = 0.0529, 0.0214 $R1$ ($F_o^2 \geq 2\sigma$ (F_o^2)) = 0.0442 $R1$ (all data) = 0.0751 $wR2$ ($F_o^2 \geq 2\sigma$ (F_o^2)) = 0.1084 $wR2$ (all data) = 0.1222	R_p = 0.0836 R_p (background) = 0.3051 wR_p = 0.1068 wR_p (background) = 0.2948 R_F^2 = 0.0326
GoF	1.135	1.252
Resid. electron density [$e/Å^3$]	-0.677, 1.182	
Parameters	96	85
Nr. of data (obs. / unique)	4447 / 1244	1001

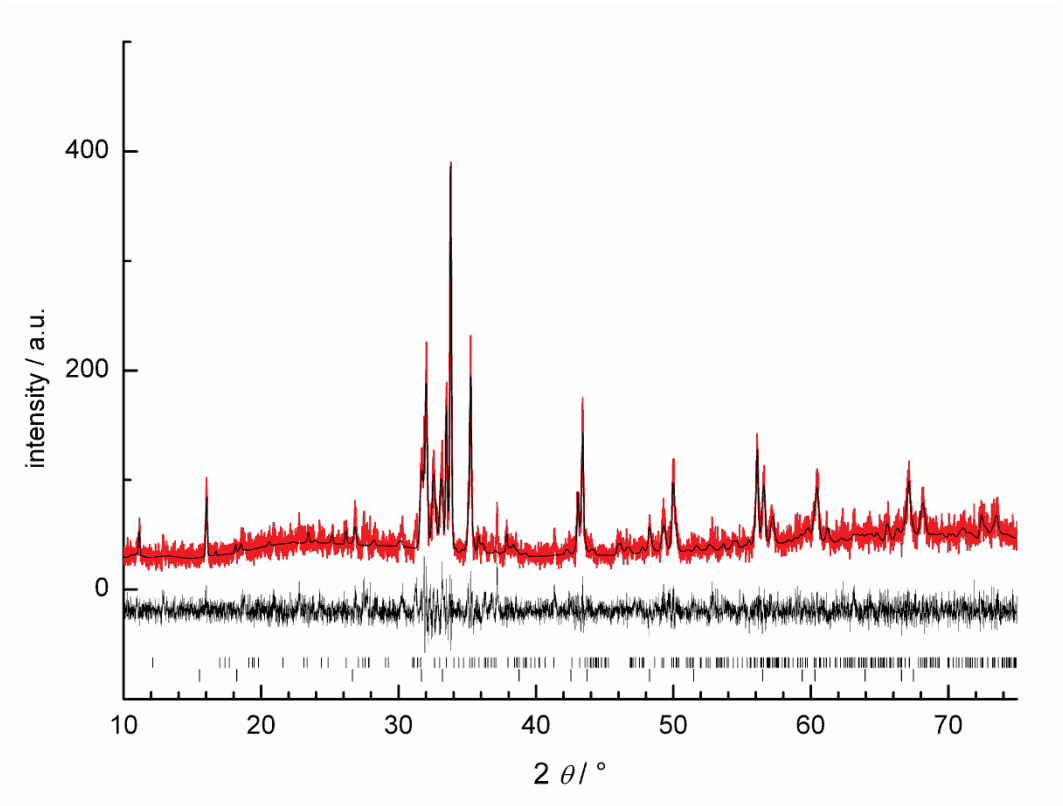

Figure S3. Final Rietveld refinement plot for $LiCa_3Si_2N_5$ (**II**). Observed (red line), calculated (black line) and difference profile of the X-ray powder diffraction are plotted on the same scale. Bragg peaks are indicated by vertical lines for I (above) and CaO (below). The molar ratio of **II** to CaO was determind to be 3.9 % CaO and 96.1 % **II**.

6.2 Supporting Information for Chapter 3.3

Saskia Lupart and Wolfgang Schnick, *Z. Anorg. Allg. Chem.* **2011**, *638*, 94-97.

Table S1. Atomic coordinates and equivalent displacement parameters [Å^2] for $LiLa_5Si_4N_{10}O$.

	s.o.f.	*x*	*y*	*z*	U_{iso}*/U_{eq}
La1		0.5000	½	½	0.01168(10)
La2		0.71540(4)	1.27195(4)	0.87509(3)	0.00983(9)
La3		0.08924(4)	0.85354(4)	0.66903(3)	0.01017(9)
Si1		0.82792(18)	1.64276(16)	0.25902(13)	0.0071(2)
Si2		0.62292(19)	0.79100(16)	0.90609(13)	0.0067(2)
N1		½	0	0	0.0123(9)
N2		0.8282(6)	1.7048(5)	0.0654(4)	0.0107(6)
N3		0.7064(6)	0.8246(5)	0.3833(4)	0.0105(6)
N4		0.1303(6)	1.6374(6)	0.3699(4)	0.0130(7)
N5		0.3661(6)	0.5950(5)	0.7947(5)	0.0138(7)
N6	½	0.7282(6)	0.8668(5)	0.7596(4)	0.0177(7)
O	½	0.7282(6)	0.8668(5)	0.7596(4)	0.0177(7)
Li		½	0	½	0.044(4)*

Table S2. Atomic displacement parameters [Å^2] for $LiLa_5Si_4N_{10}O$.

	U_{11}	U_{22}	U_{33}	U_{12}	U_{13}	U_{23}
La1	0.00984(16)	0.01635(18)	0.01056(17)	0.00649(12)	0.00401(12)	0.00467(13)
La2	0.00899(12)	0.01099(13)	0.00913(13)	−0.00014(8)	0.00321(9)	0.00228(9)
La3	0.00923(13)	0.01179(13)	0.00939(13)	0.00282(8)	0.00279(9)	0.00271(9)
Si1	0.0063(5)	0.0070(5)	0.0073(5)	0.0012(4)	0.0019(4)	0.0012(4)
Si2	0.0073(5)	0.0059(5)	0.0070(5)	0.0011(4)	0.0027(4)	0.0011(4)
N1	0.016(2)	0.010(2)	0.015(2)	0.0064(18)	0.0100(19)	0.0032(19)
N2	0.0117(15)	0.0123(17)	0.0078(14)	0.0029(13)	0.0023(12)	0.0035(13)
N3	0.0093(15)	0.0098(16)	0.0122(16)	0.0020(12)	0.0046(13)	0.0010(13)
N4	0.0093(15)	0.0234(19)	0.0077(15)	0.0049(13)	0.0035(12)	0.0054(14)
N5	0.0136(16)	0.0087(16)	0.0148(17)	−0.0040(13)	0.0017(13)	0.0008(13)
N6	0.0229(17)	0.0127(16)	0.0219(17)	−0.0006(13)	0.0156(14)	0.0030(13)
O	0.0229(17)	0.0127(16)	0.0219(17)	−0.0006(13)	0.0156(14)	0.0030(13)

Table S3. Atomic coordinates and equivalent displacement parameters [Å^2] for $LiPr_5Si_4N_{10}O$.

	s.o.f.	*x*	*y*	*z*	U_{iso}*/U_{eq}
Pr1		0	0	0	0.01388(12)
Pr2		0.21391(6)	0.77057(5)	0.37368(5)	0.01067(10)
Pr3		0.58789(6)	0.35239(5)	1.16550(5)	0.01155(10)
Si1		0.3320(3)	1.1417(2)	-0.2417(2)	0.0073(3)
Si2		0.1234(3)	0.2902(2)	0.4040(2)	0.0070(3)
N1		0	½	½	0.0150(15)
N2		0.3326(9)	1.1980(7)	-0.4382(7)	0.0121(10)
N3		0.2087(9)	0.3271(7)	0.8808(7)	0.0109(10)
N4		0.639(1)	1.1418(9)	-0.1275(8)	0.0155(11)
N5		-0.1386(10)	0.0967(8)	0.2912(7)	0.0161(12)
N6	½	0.2306(9)	0.3709(7)	0.2564(7)	0.0165(10)
O	½	0.2306(9)	0.3709(7)	0.2564(7)	0.0165(10)
Li		0	½	0	0.027(4)*

Table S4. Atomic displacement parameters [Å^2] for $LiPr_5Si_4N_{10}O$.

	U_{11}	U_{22}	U_{33}	U_{12}	U_{13}	U_{23}
Pr1	0.0102(2)	0.0216(2)	0.0118(3)	0.00934(18)	0.00359(17)	0.00613(19)
Pr2	0.00813(17)	0.01298(16)	0.0101(2)	-0.00045(12)	0.00282(12)	0.00258(12)
Pr3	0.00883(17)	0.01553(17)	0.0100(2)	0.00318(12)	0.00243(12)	0.00318(13)
Si1	0.0056(7)	0.0084(6)	0.0072(9)	0.0008(5)	0.0017(5)	0.0012(6)
Si2	0.0055(7)	0.0074(6)	0.0076(9)	0.0011(5)	0.0019(5)	0.0014(5)
N1	0.017(4)	0.015(3)	0.015(4)	0.002(3)	0.006(3)	0.006(3)
N2	0.009(2)	0.012(2)	0.015(3)	0.0007(18)	0.0037(18)	0.0029(19)
N3	0.010(2)	0.011(2)	0.011(3)	0.0067(18)	0.0026(18)	0.0019(19)
N4	0.011(3)	0.024(3)	0.012(3)	0.005(2)	0.005(2)	0.006(2)
N5	0.012(2)	0.015(2)	0.017(3)	-0.002(2)	0.000(2)	0.005(2)
N6	0.019(2)	0.016(2)	0.020(3)	0.0057(18)	0.012(2)	0.0061(19)
O	0.019(2)	0.016(2)	0.020(3)	0.0057(18)	0.012(2)	0.0061(19)

6.3 Supporting Information for Chapter 3.4

Table S1. Atomic coordinates and equivalent displacement parameters [Å^2] for $Li_{14}Ce_5[Si_{11}N_{19}O_5]O_2F_2$.

	Wyck.	*s.o.f.*	*x*	*y*	*z*	U_{iso}*/U_{eq}
Ce1	2*a*		¾	-¼	1.17927(14)	0.0264(3)
Ce2	4*e*		¾	0.00139(14)	0.72928(7)	0.01576(18)
Ce3	4*c*		½	0	1.00000	0.01362(17)
Si1	2*b*		¾	¼	0.2643(5)	0.0143(11)
Si2	4*f*		0.6592(2)	¼	0.5240(4)	0.0127(8)
Si3	4*f*		0.64875(19)	-¼	0.9167(3)	0.0113(8)
Si4	8*g*		0.56198(13)	-0.0462(3)	0.6946(2)	0.0105(5)
Si5	4*f*		0.5723(2)	-¼	1.2307(4)	0.0132(8)
N1	8*g*		0.3798(4)	0.0591(10)	0.1610(7)	0.0094(15)
N2	4*f*		0.5385(6)	-¼	0.6362(11)	0.013(2)
N3	2*a*		1/4	¼	0.0739(15)	0.011(3)
N4	4*f*		0.6079(6)	-¼	1.0704(12)	0.013(2)
N5	4*f*		0.6634(6)	¼	0.3549(11)	0.013(3)
N6	8*g*		0.6142(4)	0.0623(12)	0.5774(8)	0.0189(19)
N7	8*g*		0.4790(5)	0.0604(14)	-0.2536(8)	0.021(2)
O1	2*b*		¼	-¼	-0.5912(15)	0.024(4)
O2	4*f*		0.3513(6)	¼	-0.3335(10)	0.026(3)
O3	4*e*		¾	0.0779(16)	0.1611(10)	0.023(2)
O1O	2*b*	½	¾	¼	0.8845(15)	0.028(4)
F1F	2*b*	½	¾	¼	0.8845(15)	0.028(4)
O2O	4*f*	½	0.5821(5)	¼	0.0373(10)	0.022(2)
F2F	4*f*	½	0.5821(5)	¼	0.0373(10)	0.022(2)
O3O	2*a*	½	¼	¼	-0.5963(14)	0.028(4)
F3F	2*a*	½	¼	¼	-0.5963(14)	0.028(4)
Li1	4*f*		0.5120(15)	¼	-0.457(3)	0.028(6)*
Li2	4*f*		0.5676(18)	¼	0.238(3)	0.033(7)*
Li3	4*f*		0.3516(18)	¼	-0.531(3)	0.035(7)*
Li4	8*g*		0.3880(11)	-0.004(4)	-0.3750(19)	0.033(4)*
Li5	8*g*		0.3260(16)	-0.099(5)	-0.021(3)	0.059(7)*

Table S2. Atomic displacement parameters [Å^2] for $Li_{14}Ce_5[Si_{11}N_{19}O_5]O_2F_2$.

	U_{11}	U_{22}	U_{33}	U_{12}	U_{13}	U_{23}
Ce1	0.0172(6)	0.0368(10)	0.0220(7)	0	0	0
Ce2	0.0100(3)	0.0130(4)	0.0174(3)	0	0	0.0048(4)
Ce3	0.0135(3)	0.0093(4)	0.0116(3)	0.0001(3)	0.0007(2)	-0.0003(3)
Si1	0.016(2)	0.011(3)	0.013(3)	0	0	0
Si2	0.0102(15)	0.011(2)	0.0125(19)	0	-0.0012(12)	0
Si3	0.0108(15)	0.010(2)	0.0079(17)	0	0.0011(12)	0
Si4	0.0081(9)	0.0070(15)	0.0089(11)	-0.0006(8)	0.0006(8)	-0.0005(8)
Si5	0.0097(16)	0.013(2)	0.0091(17)	0	-0.0011(12)	0
N1	0.014(3)	0.004(4)	0.009(3)	-0.001(3)	0.003(3)	0.001(3)
N2	0.009(5)	0.012(7)	0.013(5)	0	-0.005(4)	0
N3	0.010(7)	0.028(12)	0.005(8)	0	0	0
N4	0.007(5)	0.015(7)	0.020(6)	0	0.001(4)	0
N5	0.009(5)	0.007(7)	0.013(6)	0	0.000(4)	0
N6	0.016(4)	0.014(5)	0.023(4)	-0.002(3)	-0.006(3)	0.008(3)
N7	0.015(4)	0.036(7)	0.016(4)	0.004(4)	-0.001(3)	-0.005(4)
O1	0.022(7)	0.010(9)	0.024(8)	0	0	0
O2	0.030(6)	0.034(8)	0.009(5)	0	0.005(4)	0
O3	0.015(4)	0.026(7)	0.026(6)	0	0	-0.001(5)
O1O	0.041(8)	0.013(9)	0.029(8)	0	0	0
F1F	0.041(8)	0.013(9)	0.029(8)	0	0	0
O2O	0.011(4)	0.019(6)	0.031(5)	0	0.000(4)	0
F2F	0.011(4)	0.019(6)	0.031(5)	0	0.000(4)	0
O3O	0.020(7)	0.031(10)	0.021(7)	0	0	0
F3F	0.020(7)	0.031(10)	0.021(7)	0	0	0

Table S3. Atomic coordinates and equivalent displacement parameters [Å^2] for $Li_{14}Nd_5[Si_{11}N_{19}O_5]O_2F_2$.

	Wyck.	*s.o.f.*	*x*	*y*	*z*	U_{iso}*/U_{eq}
Nd1	2*a*		¾	-¼	1.17304(13)	0.0269(3)
Nd2	4*e*		¾	0.00036(15)	0.72903(7)	0.0199(2)
Nd3	4*c*		½	0	1.00000	0.0183(2)
Si1	2*b*		¾	¼	0.2639(6)	0.0177(11)
Si2	4*f*		0.6593(2)	¼	0.5239(4)	0.0184(8)
Si3	4*f*		0.6485(2)	-¼	0.9157(4)	0.0162(8)
Si4	8*g*		0.56174(14)	-0.0469(4)	0.6961(3)	0.0157(6)
Si5	4*f*		0.5725(2)	-¼	1.2298(4)	0.0165(8)
N1	8*g*		0.3803(4)	0.0574(12)	0.1615(8)	0.0191(17)
N2	4*f*		0.5368(7)	-¼	0.6339(12)	0.020(3)
N3	2*a*		¼	¼	0.0721(18)	0.021(4)
N4	4*f*		0.6070(7)	-¼	1.0693(13)	0.024(3)
N5	4*f*		0.6613(7)	¼	0.3537(12)	0.015(2)
N6	8*g*		0.6124(5)	0.0639(13)	0.5757(9)	0.024(2)
N7	8*g*		0.4783(5)	0.0587(15)	-0.2533(9)	0.027(2)
O1	2*b*		¼	-¼	-0.5903(15)	0.027(4)
O2	4*f*		0.3506(6)	¼	-0.3342(11)	0.027(2)
O3	4*e*		¾	0.0731(15)	0.1642(11)	0.022(2)
O1O	2*b*	½	¾	¼	0.8884(16)	0.034(4)
F1F	2*b*	½	¾	¼	0.8884(16)	0.034(4)
O2O	4*f*	½	0.5800(5)	¼	0.0371(10)	0.028(2)
F2F	4*f*	½	0.5800(5)	¼	0.0371(10)	0.028(2)
O3O	2*a*	½	¼	¼	-0.5985(15)	0.025(3)
F3F	2*a*	½	¼	¼	-0.5985(15)	0.025(3)
Li1	4*f*		0.5103(16)	¼	-0.460(3)	0.032(6)*
Li2	4*f*		0.5694(18)	¼	0.236(3)	0.035(7)*
Li3	4*f*		0.3539(19)	¼	-0.538(4)	0.041(8)*
Li4	8*g*		0.3892(13)	-0.007(4)	-0.377(2)	0.045(5)*
Li5	8*g*		0.3231(15)	-0.099(5)	-0.018(3)	0.051(6)*

Table S4. Atomic displacement parameters [Å^2] for $Li_{14}Nd_5[Si_{11}N_{19}O_5]O_2F_2$.

	U_{11}	U_{22}	U_{33}	U_{12}	U_{13}	U_{23}
Nd1	0.0201(5)	0.0357(9)	0.0250(6)	0	0	0
Nd2	0.0168(3)	0.0172(4)	0.0257(4)	0	0	0.0033(3)
Nd3	0.0196(3)	0.0166(4)	0.0185(3)	-0.0005(3)	0.0009(2)	-0.0009(3)
Si1	0.017(2)	0.018(3)	0.018(3)	0	0	0
Si2	0.0185(17)	0.019(2)	0.0180(19)	0	0.0004(13)	0
Si3	0.0137(15)	0.018(2)	0.0170(18)	0	0.0012(12)	0
Si4	0.0155(10)	0.0137(16)	0.0179(12)	-0.0005(9)	0.0003(9)	-0.0007(9)
Si5	0.0154(16)	0.019(2)	0.0153(17)	0	-0.0009(12)	0
N1	0.020(3)	0.014(5)	0.023(4)	0.002(3)	-0.006(3)	0.001(3)
N2	0.024(5)	0.015(7)	0.021(6)	0	0.003(4)	0
N3	0.021(7)	0.019(11)	0.023(9)	0	0	0
N4	0.020(5)	0.023(8)	0.028(7)	0	0.002(5)	0
N5	0.020(5)	0.009(7)	0.016(6)	0	0.000(4)	0
N6	0.029(4)	0.023(6)	0.022(4)	-0.003(3)	-0.004(3)	0.010(3)
N7	0.014(4)	0.038(7)	0.029(4)	0.009(4)	-0.004(3)	-0.007(4)
O1	0.044(9)	0.024(11)	0.014(7)	0	0	0
O2	0.032(5)	0.031(8)	0.017(5)	0	-0.008(4)	0
O3	0.013(4)	0.025(7)	0.029(5)	0	0	-0.006(4)
O1O	0.029(7)	0.041(11)	0.032(8)	0	0	0
F1F	0.029(7)	0.041(11)	0.032(8)	0	0	0
O2O	0.024(4)	0.036(7)	0.024(5)	0	0.008(4)	0
F2F	0.024(4)	0.036(7)	0.024(5)	0	0.008(4)	0
O3O	0.009(5)	0.033(10)	0.032(8)	0	0	0
F3F	0.009(5)	0.033(10)	0.032(8)	0	0	0

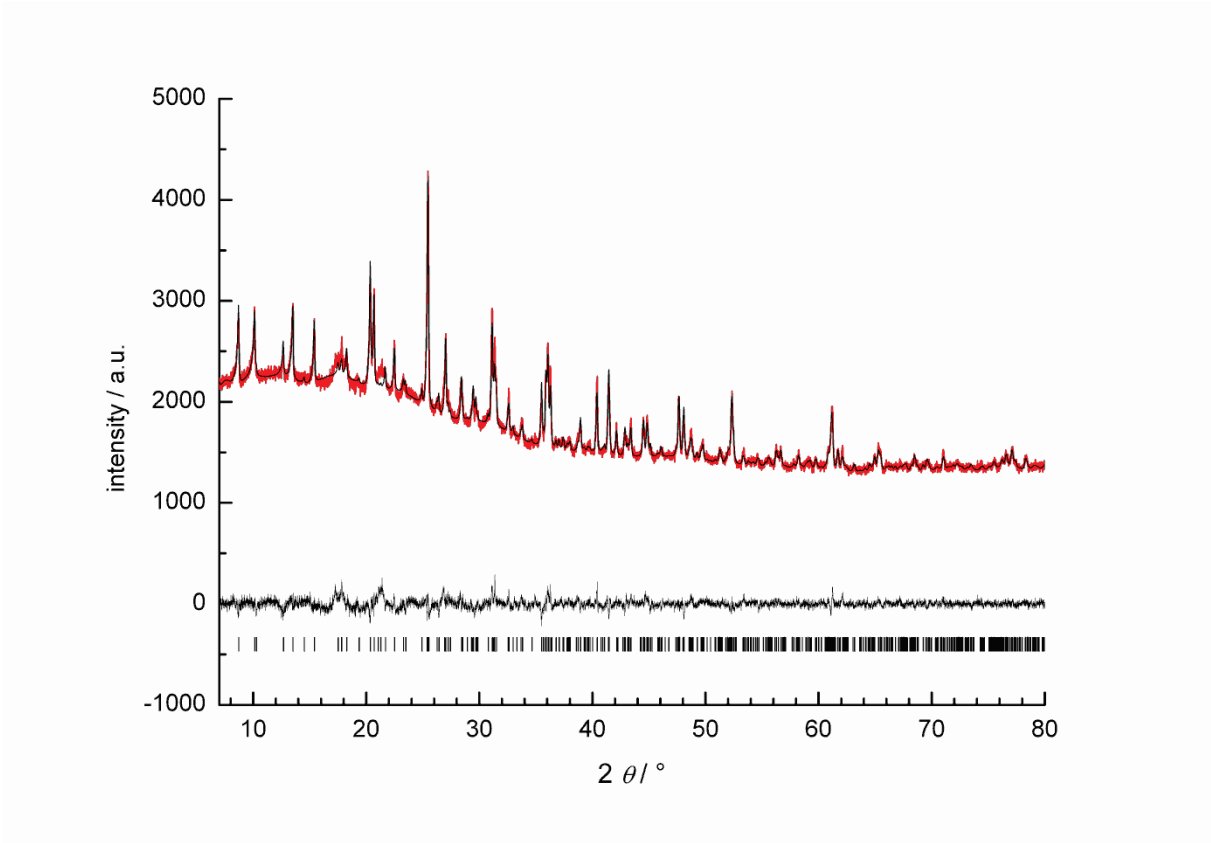

Figure S1. Rietveld plot of the bulk sample of $Li_{14}Nd_5[Si_{11}N_{19}O_5]O_2F_2$.

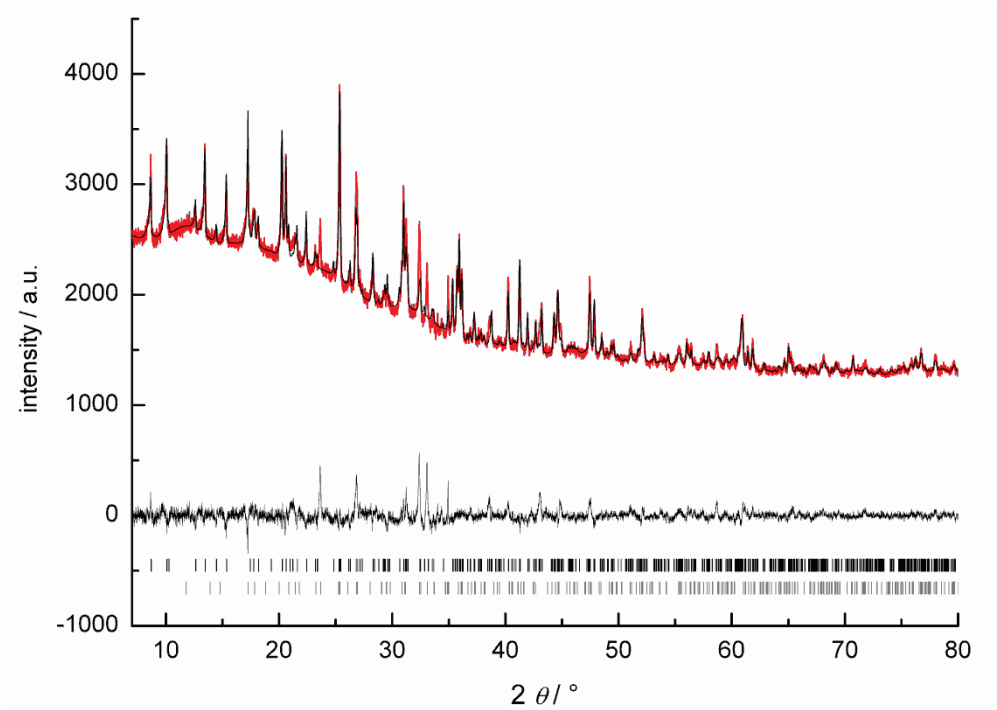

Figure S2. Rietveld plot of $Li_{14}Ce_5[Si_{11}N_{19}O_5]O_2F_2$ (black tick marks).Side phase: Li_2SiN_2 (grey tick marks), residual unindexed peaks belong to unknown side phases.

Lattice energy calculations according to the MAPLE concept

Lattice energy calculations (MAPLE: Madelung part of lattice energy)[1-4] were performed to prove the electrostatic consistency of the crystal structure and especially to analyze the distribution of oxygen in the structure. The program computes electrostatic interactions in an ionic crystal, depending on the charge, distance and coordination spheres of the constituting atoms. The total MAPLE values of the title compounds correspond well with the sum of the total MAPLE values of the constituting binary oxides and nitrides (cf. Table S6). The partial MAPLE values are in the expected ranges. During the calculations possible other oxygen distributions were taken into account. Mixed occupied N/O positions as well as other N/O distributions lead to a significant worsening of the total MAPLE values (deviation > 2 %). Therefore, it can be assumed that oxygen is mainly situated on the positions assigned in the crystal structure refinement. However, a minor disorder or even a slightly higher oxygen content, which would possibly lead to voids in the cation structure, can not be excluded. Neutron powder diffraction experiments of similar systems show that oxygen and nitrogen are distributed mainly statistically in the silicate network.[5]

Table S5. Results of the MAPLE calculations [kJ/mol] for $Li_{14}Ln_5[Si_{11}N_{19}O_5]O_2F_2$ with Ln = Ce, Nd; Δ = difference.[a]

	Ce	Nd
Ln^{3+}	3747 – 3932	3523 – 3873
Si^{4+}	9264 – 10178	9190 – 10095
N^{3-}	5357 – 5626	5214 – 5735
O^{2-}	2488 – 3293	2523 – 3315
$O/F^{1.5-}$	1183 – 1268	1231 – 1369
Li^{+}	643 – 754	615 – 808
Total MAPLE	259172	256485
Δ	0.3 %	0.8 %
Total MAPLE ($3\ Si_3N_4 + 2\ SiO_2 + 2\ LiF + 4\ Li_3N + 3\ LnN + Ln_2O_3$)		
Ln = Ce: 259879 kJ/mol; Ln = Nd: 258682 kJ/mol		

[a] Typical MAPLE values [kJ/mol]: Ln^{3+}: 3500 – 5100; Si^{4+}: 9000 – 10200; N^{3-}: 4300 – 6200; O^{2-}: 2000- 2800; F^{-}: 450 – 600; Li^{+}: 600 – 860.[6]

[1] R. D. Shannon, *Acta Crystallogr., Sect. A: Cryst. Found. Crystallogr.* **1976**, *32*, 751-767.

[2] R. Hübenthal, Vers. 4 ed., Universität Gießen, **1993**.

[3] R. Hoppe, *Angew. Chem.* **1966**, *78*, 52-63; *Angew. Chem., Int. Ed.* **1966**, **196***5*, **19**95-**1**106.

[4] R. Hoppe, *Angew. Chem.* **1970**, *82*, 7-16; *Angew. Chem. Int. Ed.* **1970**, **197***9*, **19**25-**19**34.

[5] A. Lieb, M. T. Weller, P. F. Henry, R. Niewa, R. Pöttgen, R.-D. Hoffmann, H. E. Höfer, W. Schnick, *J. Solid State Chem.* **2005**, *178*, 976-988.

[6] M. Zeuner, S. Pagano, W. Schnick, *Angew. Chem.* **2011**, *123*, 7898-7920; *Angew. Chem. Int. Ed*. **2011**, 78*50*, 7754-7775.

6.4 Supporting Information for Chapter 3.5

Saskia Lupart, Dajana Durach, and Wolfgang Schnick, *Z. Anorg. Allg. Chem.* **2011**, *637*, 1841-1844.

Table S1. Atomic coordinates and equivalent displacement parameters [Å^2] for $Li_{35}Ce_9Si_{30}N_{59}O_2F$.

	Wyck.	*s.o.f*	*x*	*y*	*z*	U_{iso}*/U_{eq}
Ce1	6*f*		0.69876(5)	0	1/4	0.0122(2)
Ce2	12*g*		0.66969(6)	−0.22607(5)	0.36291(4)	0.0226(2)
Si1	12*g*		0.8857(2)	0.0021(2)	0.13856(15)	0.0080(5)
Si2	12*g*		0.6207(2)	0.1265(2)	0.14297(16)	0.0073(4)
Si3	12*g*		0.46227(19)	−0.30667(19)	0.24812(16)	0.0070(4)
Si4	12*g*		0.68904(19)	0.0264(2)	0.45018(16)	0.0077(5)
Si5	12*g*		0.5418(2)	−0.2909(2)	0.04390(15)	0.0068(4)
N1	12*g*		0.6354(6)	−0.0352(6)	0.5482(5)	0.0091(14)
N2	12*g*		0.8864(6)	−0.1111(6)	0.1086(5)	0.0098(14)
N3	4*d*		1/3	−1/3	0.2707(8)	0.008(2)
N4	12*g*		0.5875(6)	0.0031(6)	0.3772(5)	0.0077(14)
N5	12*g*		0.4890(6)	−0.3841(6)	0.3158(5)	0.0111(15)
N6	12*g*		0.6553(7)	0.1954(6)	0.0452(5)	0.0104(15)
N7	12*g*		0.7221(6)	0.1766(6)	0.2220(5)	0.0100(15)
N8	6*f*		0.8646(8)	0	¼	0.010(2)
N9	12*g*		0.6028(7)	−0.1572(7)	0.0291(6)	0.0143(17)
N10	12*g*		0.7861(7)	0.0174(8)	0.0946(5)	0.0157(17)
N11	12*g*		0.4691(6)	−0.3287(6)	0.1392(5)	0.0080(14)
O1	6*f*	2/3	0.7307(12)	−0.2693(12)	¼	0.052(4)*
F1	6*f*	1/3	0.7307(12)	−0.2693(12)	¼	0.052(4)*
Li1	2*b*		0	0	0	0.017(8)*
Li2	6*f*		0.8590(16)	−0.1410(16)	¼	0.013(5)*
Li3	12*g*		0.6544(16)	0.1587(16)	0.3622(13)	0.021(4)*
Li4	4*d*		1/3	-1/3	0.098(2)	0.015 (6)*
Li5	12*g*		0.5199(17)	0.1926(16)	0.0502(13)	0.023(4)*
Li6	4*d*		1/3	-1/3	0.408(2)	0.019(6)*
Li7	12*g*		0.5735(18)	−0.4636(18)	0.3311(15)	0.028(4)*
Li8	6*e*		½	0	½	0.032(7)*
Li9	12*g*		0.757(3)	−0.148(3)	0.027(2)	0.055(8)*

Table S2. Atomic displacement parameters [Å^2] for $Li_{35}Ce_9Si_{30}N_{59}O_2F$.

	U^{11}	U^{22}	U^{33}	U^{12}	U^{13}	U^{23}
Ce1	0.0115(3)	0.0191(4)	0.0084(3)	0.0096(2)	−0.00052(13)	−0.0010(3)
Ce2	0.0235(3)	0.0220(3)	0.0217(3)	0.0109(3)	−0.0011(2)	0.0013(2)
Si1	0.0079(11)	0.0082(11)	0.0083(10)	0.0044(9)	−0.0011(9)	−0.0004(8)
Si2	0.0066(11)	0.0069(11)	0.0081(10)	0.0031(9)	−0.0012(8)	−0.0019(8)
Si3	0.0073(11)	0.0059(11)	0.0076(10)	0.0031(9)	0.0002(8)	0.0001(8)
Si4	0.0066(11)	0.0068(11)	0.0093(11)	0.0031(9)	−0.0010(8)	−0.0004(8)
Si5	0.0070(11)	0.0076(11)	0.0071(10)	0.0046(9)	0.0017(8)	−0.0010(8)
N1	0.008(3)	0.012(4)	0.006(3)	0.004(3)	0.001(3)	−0.001(3)
N2	0.010(4)	0.005(3)	0.014(4)	0.004(3)	−0.005(3)	−0.002(3)
N3	0.010(4)	0.010(4)	0.003(5)	0.0050(19)	0.000	0.000
N4	0.007(3)	0.008(3)	0.006(3)	0.002(3)	0.000(3)	0.001(3)
N5	0.010(4)	0.008(3)	0.009(3)	0.000(3)	−0.002(3)	0.001(3)
N6	0.015(4)	0.009(4)	0.007(3)	0.007(3)	0.004(3)	0.001(3)
N7	0.008(4)	0.008(3)	0.010(3)	0.001(3)	−0.001(3)	−0.002(3)
N8	0.010(4)	0.013(5)	0.006(5)	0.006(3)	0.0010(19)	0.002(4)
N9	0.013(4)	0.009(4)	0.023(4)	0.006(3)	0.004(3)	0.004(3)
N10	0.011(4)	0.027(5)	0.011(4)	0.011(4)	−0.003(3)	−0.004(3)
N11	0.012(4)	0.008(3)	0.006(3)	0.006(3)	−0.001(3)	−0.002(2)

Table S3. Atomic coordinates and equivalent displacement parameters [Å^2] for $Li_{35}Pr_9Si_{30}N_{59}O_2F$.

	Wyck.	*s.o.f*	*x*	*y*	*z*	U_{iso}*/U_{eq}
Pr1	6*f*		0	0.30135(5)	1/4	0.0104(2)
Pr2	12*g*		0.22627(5)	0.33003(6)	0.13718(4)	0.0206 2)
Si1	12*g*		0.0022(2)	0.1170(2)	0.13864(17)	0.0065(5)
Si2	12*g*		-0.1263(2)	0.3798(2)	0.35720(17)	0.0067(5)
Si3	12*g*		-0.0266(2)	0.3106(2)	0.04990(16)	0.0047(5)
Si4	12*g*		0.3060(2)	0.5370(2)	0.25176(17)	0.0067(5)
Si5	12*g*		0.2904(2)	0.4579(2)	0.45593(16)	0.0061(5)
N1	6*f*		0	0.1367(8)	1/4	0.010(3)
N2	12*g*		0.0031(7)	0.4142(7)	0.3759(5)	0.0082(16)
N3	12*g*		-0.1950(7)	0.3450(7)	0.4560(6)	0.0103(17)
N4	12*g*		0.1758(7)	0.4542(7)	0.2220(5)	0.0088(16)
N5	4*d*		1/3	2/3	0.2295(8)	0.005(3)
N6	12*g*		0.0175(8)	0.2320(7)	0.0952(6)	0.0140(18)
N7	12*g*		0.1128(7)	0.1090(7)	0.1094(5)	0.0080(16)
N8	12*g*		0.3836(7)	0.5111(7)	0.1844(5)	0.0092(16)
N9	12*g*		0.3299(7)	0.3648(7)	0.4518(5)	0.0088(16)
N10	12*g*		0.3282(7)	0.5304(7)	0.3607(6)	0.0119(18)
N11	12*g*		-0.1569(7)	0.2399(7)	0.0267(6)	0.0122(18)
O1	6*f*	2/3	0.2704(11)	0.2704(11)	1/4	0.045(4)*
F1	6*f*	1/3	0.2704(11)	0.2704(11)	1/4	0.045(4)*
Li1	4*d*		1/3	2/3	0.404(2)	0.011(6)*
Li2	2*b*		0	0	0	0.012(8)*
Li3	6*f*		0.1416(18)	0.1416(18)	1/4	0.015(5)*
Li4	12*g*		-0.1937(16)	0.4770(16)	0.4513(13)	0.019(4)*
Li5	6*e*		0	1/2	1/2	0.031(7)*
Li6	4*d*		-1/3	1/3	0.411(2)	0.019(7)*
Li7	12*g*		0.4646(19)	0.4262(18)	0.1673(15)	0.026(5)*
Li8	12*g*		0.243(3)	0.153(3)	0.027(2)	0.049(7)*
Li9	12*g*		0.1583(15)	0.5041(15)	0.3607(13)	0.017(4)*

Table S4. Atomic displacement parameters [Å^2] for $Li_{35}Pr_9Si_{30}N_{59}O_2F$.

	U_{11}	U_{22}	U_{33}	U_{12}	U_{13}	U_{23}
Pr1	0.0158(4)	0.0096(3)	0.0077(4)	0.0079(2)	-0.0007(3)	-0.00036(15)
Pr2	0.0193(4)	0.0218(4)	0.0201(3)	0.0099(3)	0.0008(3)	-0.0009(2)
Si1	0.0066(12)	0.0059(12)	0.0071(12)	0.0031(11)	0.0007(9)	0.0005(10)
Si2	0.0055(12)	0.0067(12)	0.0079(12)	0.003(1)	0.0006(9)	0.0000(9)
Si3	0.0029(12)	0.0024(12)	0.0073(12)	0.0002(10)	-0.0005(9)	0.0000(9)
Si4	0.0053(12)	0.0083(13)	0.0059(11)	0.003(1)	0.0005(9)	0.0009(10)
Si5	0.0060(12)	0.0072(12)	0.0062(12)	0.0041(10)	0.0005(9)	0.0010(9)
N1	0.017(6)	0.009(4)	0.007(6)	0.009(3)	0.001(5)	0.000(2)
N2	0.005(4)	0.013(4)	0.006(4)	0.004(3)	0.000(3)	0.001(3)
N3	0.011(4)	0.010(4)	0.013(4)	0.008(4)	0.001(3)	0.002(3)
N4	0.006(4)	0.011(4)	0.008(4)	0.003(3)	0.000(3)	0.000(3)
N5	0.008(4)	0.008(4)	0.001(6)	0.004(2)	0.00000	0.00000
N6	0.021(5)	0.015(5)	0.012(4)	0.013(4)	0.001(4)	0.001(3)
N7	0.008(4)	0.009(4)	0.009(4)	0.006(3)	0.005(3)	0.001(3)
N8	0.008(4)	0.010(4)	0.010(4)	0.004(3)	-0.001(3)	0.000(3)
N9	0.008(4)	0.011(4)	0.007(4)	0.005(4)	0.001(3)	0.003(3)
N10	0.011(4)	0.018(5)	0.011(4)	0.011(4)	-0.001(3)	-0.004(3)
N11	0.009(4)	0.006(4)	0.019(5)	0.002(4)	0.002(3)	0.001(3)

7 Publications

Major results of this thesis were published in scientific journals by way of the following publications. References of publications, which are not included in this work, as well as oral and poster presentations are included separately below. Furthermore, the details of the crystal structure investigations of the characterized compounds may be obtained by quoting the depository numbers (Fachinformationszentrum Karlsruhe, 76344 Eggenstein-Leopoldshafen, Germany (fax: (+49)7247-808-666; e-mail: crysdata@fiz-karlsruhe.de).

A Published as part of this thesis:

1. **Tuning the Dimensionality of Nitridosilicates in Lithium Melts.**
   S. Pagano, S. Lupart, M. Zeuner, W. Schnick
   Angew. Chem. **2009**, *121*, 6453-6456; *Angew. Chem. Int. Ed.* **2009**, *48*, 6335-6338.

2. **$Li_4Ca_3Si_2N_6$ and $Li_4Sr_3Si_2N_6$ – Quaternary Lithium Nitridosilicates with Isolated $[Si_2N_6]^{10-}$ Ions**
   Sandro Pagano, Saskia Lupart, Sebastian Schmiechen, and Wolfgang Schnick
   Z. Anorg. Allg. Chem. **2010**, *636*, 1907-1909.

3. **Chain-Type Lithium Rare-Earth Nitridosilicates – $Li_5Ln_5Si_4N_{12}$ with Ln = La, Ce**
   Saskia Lupart, Martin Zeuner, Sandro Pagano, and Wolfgang Schnick
   Eur. J. Inorg. Chem. **2010**, 2636-2641.

4. **$Li_2Sr_4[Si_2N_5]N$ – A Layered Lithium Nitridosilicate Nitride**
   Saskia Lupart, Sandro Pagano, Oliver Oeckler, and Wolfgang Schnick
   Eur. J. Inorg. Chem. **2011**, 2118-2123.

5. **$Li_{35}Ln_9Si_{30}N_{59}O_2F$ with Ln = Ce, Pr - Highly Condensed Nitridosilicates**
   Saskia Lupart, Dajana Durach, and Wolfgang Schnick
   Z. Anorg. Allg. Chem. **2011**, *637*, 1841-1844.

6. **$LiLa_5Si_4N_{10}O$ and $LiPr_5Si_4N_{10}O$ – Chain Type Oxonitridosilicates**
   Saskia Lupart and Wolfgang Schnick
   Z. Anorg. Allg. Chem. **2012**, *638*, 94-97.

7. **$Li_{14}Ln_5[Si_{11}N_{19}O_5]O_2F_2$ with Ln = Ce, Nd – Representatives of a Family of Potential Lithium Ion Conductors**
   Saskia Lupart, Giuliano Gregori, Joachim Maier, and Wolfgang Schnick
   J. Am. Chem. Soc. **2012**, *134*, 10132-10137.

8. **$LiCa_3Si_2N_5$ – A Lithium Nitridosilicate with $[Si_2N_5]^{7-}$ double-chains**
   Saskia Lupart and Wolfgang Schnick
   Z. Anorg. Allg. Chem. **2012**, (in print).

B Other publications:

$La_{16}[Si_8N_{22}][SiON_3]_2$ - a nitridosilicate with isolated, corner-sharingand edge-sharing tetrahedra.
C. Schmolke, S. Lupart, W. Schnick
Solid State Sci. **2009**, *11*, 305-309.

$Ln_3[SiON_3]O$ (Ln = La, Ce, Pr) – Three Oxonitridosilicate Oxides with Crystal Structures Derived from the Anti-Perovskite Structure Type.
J.A. Kechele, C. Schmolke, S. Lupart, W. Schnick
Z. Anorg. Allg. Chem. **2009**, *636*, 176-182.

$Pr_5Si_3N_9$.
S. Lupart, W. Schnick
Acta Crystallogr. **2009**, *E65*, i43.

C Conference contributions:

Gute Laune bei Nitridosilicaten durch ^{7}Li (talk)
S. Pagano, S. Lupart, W. Schnick
Hemdsärmelkolloquium, Marburg, 5.-7.3.09

Tuning the Dimensionality of Nitridosilicates in Lithium Melts (poster)
S. Pagano, S. Lupart, M. Zeuner, W. Schnick
12th European Conference on Solid State Chemistry, Münster, 20.23.9.09

Neue Nitridosilicate aus Lithium-Schmelzen (talk)
S. Lupart, S. Pagano, M. Zeuner, W. Schnick
Hirschegg-Seminar, Hirschegg (Austria), 4.-6.3.10

Neue Nitridosilicate aus Lithium-Schmelzen (poster)
S. Lupart, S. Pagano, M. Zeuner, W. Schnick
15th Conference of GDCh Division for Solid State Chemistry and Material Research, Berlin, 20.-22.9.10

Lithium-(oxo)nitridosilicates as potential Li^+ ionic conductors (talk)
S. Lupart, W. Schnick
Max-Planck-Institute, Group of Prof. Maier, Stuttgart, 31.08.11

D Depository numbers of the single crystal data

$LiCa_3Si_2N_5$	CSD-420676
$Li_4Ca_3Si_2N_6$	CSD-420675
$Li_2Sr_4[Si_2N_5]N$	CSD-422596
$Li_5La_5Si_4N_{12}$	CSD-421528
$Li_5Ce_5Si_4N_{12}$	CSD-421527
$LiLa_5Si_4N_{10}O$	CSD-423470
$Li_{14}Ce_5[Si_{11}N_{19}O_5]O_2F_2$	CSD-424264
$Li_{14}Ce_5[Si_{11}N_{19}O_5]O_2F_2$	CSD-424265
$Li_{35}Ce_9Si_{30}N_{59}O_2F$	CSD-422895
$Li_{35}Ce_9Si_{30}N_{59}O_2F$	CSD-422896

8 Curriculum Vitae

Saskia Lupart

25. September 1983	Geboren in Augsburg
	Staatsangehörigkeit: Deutsch; Familienstand: ledig
1990 – 1992	Grund- und Hauptschule Kirchheim, bei München
1992 – 1994	Grund- und Parkschule Göggingen West, Augsburg
1994 – 2003	Gymnasium bei St. Anna, Augsburg
Mai 2003	Allgemeine Hochschulreife
Okt. 2003 – Apr. 2007	Studium (Bachelor of Science Chemie/ Biochemie) an der Ludwig-Maximilians-Universität München
Apr. 2007 – Nov. 2008	Studium (Master of Science Chemie) an der Ludwig-Maximilians-Universität München
Mai 2008 – Nov. 2008	Masterarbeit an der Ludwig-Maximilians-Universität München bei Prof. Dr. Wolfgang Schnick mit dem Thema: „Lithium Calciumnitridosilicate“ (ausgezeichnet mit dem Römer-Preis der Dr. Klaus Römer-Stiftung)
Nov. 2008	Master of Science Chemistry an der Ludwig-Maximilians-Universität München
seit 1. Jan. 2009	Anstellung als wissenschaftliche Mitarbeiterin in der Arbeitsgruppe von Prof. Dr. Wolfgang Schnick am Lehrstuhl für anorganische Festkörperchemie (Ludwig-Maximilians-Universität München) mit dem Ziel einer Promotion über das Thema: „Syntheses of Multinary Lithium (Oxo)nitridosilicates“